2017

Studies of spontaneous combustion of coal in Shendong underground mines and surface stockpiles

Jian Zhang
University of Wollongong

UNIVERSITY
OF WOLLONGONG
AUSTRALIA

Faculty of Engineering & Information Sciences

School of Civil, Mining and Environmental Engineering

Studies of spontaneous combustion of coal in Shendong underground mines and surface stockpiles

Jian Zhang

This thesis is presented in fulfilment of the requirement for the Award of the Degree of Doctor of Philosophy of University of Wollongong

May 2017

AFFIRMATION

I, Jian Zhang, declare that this thesis, submitted in fulfilment of the requirements for the award of Doctor of Philosophy, in School of Civil, Mining and Environmental Engineering, University of Wollongong, is wholly my own work unless otherwise referenced or acknowledged. The thesis was completed under the supervision of Associate Professor Ting Ren and Dr. Jan Nemcik, and has not been submitted for qualifications at any other academic institution.

Jian Zhang
5/May/2017

PUBLICATIONS

1. **Jian Zhang**, Yuntao Liang, Ting Ren, Zhongwei Wang and Gongda Wang (2016). "Transient CFD modelling of low-temperature spontaneous heating behaviour in multiple coal stockpiles with wind forced convection." ***Fuel Processing Technology*** 149: 55-74.
2. **Jian Zhang**, Ting Ren, Yuntao Liang and Zhongwei Wang (2016). "A review on numerical solutions to self-heating of coal stockpile: Mechanism, theoretical basis, and variable study." ***Fuel*** 182: 80-109.
3. Yuntao Liang, **Jian Zhang**, Ting Ren, Zhongwei Wang, Shuanglin Song (2016). "Application of ventilation simulation to spontaneous combustioncontrol in underground coal mine: A case study in Bulianta colliery."***International Journal of Mining Science and Technology***. (Accepted manuscript, IJMST-D-16-00130)
4. **Jian Zhang**, Ting Ren, Yuntao Liang, Quanbing Luo, Shuanglin Song (2016). "Kinetics and exothermicity analysis of low temperature oxidation of coals with pre-heating histories: A DSC study"***Proceedings of 9th International Symposium on Green Mining***.
5. Quanbing Luo, Ting Ren, Dong Liang, **Jian Zhang**, and Hao Shen, A study on the thermal decomposition temperature (TDT) and critical ambient temperature (CAT) of cotton. ***Journal of Thermal Analysis and Calorimetry***, 2017: p. 1-9.
6. Ting Ren, Zhongwei Wang, Yuanping Cheng, **Jian Zhang** and Frank Hungerford (2015). Modelling of gas and ventilation flow characteristics at an underground in-seam drilling site. ***32nd Annual International Pittsburgh Coal Conference****: Coal-Energy, Environment and Sustainable Development, IPCC 2015*.
7. Gongda Wang, Ting Ren, Qingxin Qi, Jia Lin, Qingquan Liu, and **Jian Zhang**, Determining the diffusion coefficient of gas diffusion in coal: Development of numerical solution.***Fuel***, 2017. 196: p. 47-58.

ACKNOWLEDGEMENTS

I would like to express my deepest gratitude to my supervisors, Associate Professor Ting Ren and Dr. Jan Nemcik, for theirinvaluable guidance and critical advice as well as consistent support throughout the study. Besides my academic research, Associate Professor Ren's considerate care in life also makes me enjoy my stay in Australia.

I am highly grateful to the scholarship from the University of Wollongong and the Shenhua Group Innovative Technology Research Fund (SHGF-13-07) for providing me tuition fee and living allowance, respectively.

I also feel indebted to the following staff and organisations:

- Dr.Yuntao Liang, Mr. Shuanglin Song, Mr. Wei Wang and other staff from CCRI Shenyang for consistent support and data collection in Shenhua research project;
- Mr. Yong Zhou, Mr. Zhanguo Zhang, Mr. Gang Wang and other staff from Shenhua Group for assisting field work and visit in Shendong coal mines;
- Mr. Andy Chen and Mr. James Grebert from Austar coal mine for providing field visit and information collection;
- Dr. David Fletcher from University of Sydney for providing CFD package training and helping me correcting numerical solutions to self-heating issues in coal mass;
- Technical staff in the School of CME, especially Mr. Alan Grant, Mr. Duncan Best, and Mr. Richard Gasser for their assistances of laboratory work.

I would also like to extend my gratitude to all my colleagues and friends, especially Dr. Chen Cao, Dr. Lei Zhang, Dr. Zhongwei Wang, Dr. Gongda Wang, Dr. Brian Plush, Dr.Gaofeng Wang, Dr.Frank Hungerford, Mr. Patrick Booth, Mr. Andy Liu and Mr. Jia Lin for their friendly support and motivation during my study.

Finally, I would like to thank my family for their consistent encouragement and support. This study would not have been completed without their care, love and encouragement.

ABSTRACT

Spontaneous combustion of coal is a hazard that is likely to occur during coal mining, storage, transport, and utilisation under favourable circumstances. Due to a variety of geological and operational reasons, spontaneous combustion has occurred and become a major threat to mining operations and coal reserve recovery in Shendong coal mines. With the support of Shenhua Mining Group, a collaborative research project with China Coal Research Institute Shenyang was initiated in 2013 to gain a better understanding of the causes of the hazard and eventually develop new cost-effective technologies for the control of the hazard in these mines. Relevant literature review was conducted to understand the mechanism of self-heating and low temperature oxidation of coal. A review of the experimental methods for coal oxidation testing was also accomplished. Current spontaneous combustion detection techniques and control practices in underground coal mines were briefly examined. Spontaneous combustion in Shendong coal mines has its own features and therefore a critical investigation was conducted. Key features of mining in Shendong coalfield were identified and associated spontaneous combustion problems were then critically investigated.

To differentiate oxidation behaviour of fresh, flooded, and oxidised Shendong coals, experimental studies including ignition temperature determination, gas evolution, and adiabatic oxidation tests were conducted. It was found that ignition temperatures of all coal samples were all below 300^{o}C, little difference was observed between fresh coals and flooded coals, and an appreciable reduction in ignition temperature of the oxidised coals was reported. Gas evolution tests indicated less CO_x gases (CO and CO_2) were produced for all oxidised coals than that for fresh coals and flooded coals. Fresh coals tend to liberate more CO_x gases than flooded coals at low temperature while with coal temperature exceeding a critical value, the trend was reversed. A similar pattern of methane evolution was observed for fresh and flooded coals while ethylene evolution of flooded coal samples was higher than that of fresh coals across the whole tests. A new adiabatic oxidation rig has been designed, assembled and commissioned at the University of Wollongong. The system consists of a reaction vessel and four coil-heaters immersed in an oil bath with automatic

temperature control and data logger, allowing the tracking of temperature rise resulting from ‘adiabatic oxidation’ of coal sample. Testing results indicated all coals have medium to high risk of heating while the flooded coals even present a higher risk.

Based on real on-site conditions, a three-dimensional CFD model was developed to study heating evolution in a ‘U’ shape Shendong longwall goaf. After the base model (1000m) was validated and calibrated, two more models (500m model and 1000m model with air leakage) were studied. Both steady state and transient simulations were conducted to study the flow dynamics of air velocity, oxygen ingress, dispersion of gaseous products and heating evolution in the longwall goaf. Proactive and reactive inertisation plans using nitrogen to suppress the onset and development of goaf heatings were studied. The results showed that airflow leakage into goaf is a major driver to the development of heatings. To study the problem more critically, ventilation network simulation was used to conduct a case study in Bulianta colliery. Two solutions were proposed to minimize the pressure differential between the longwall face and surface. Isolating and pressurising active longwall panel can mitigate the problem and the pressure differential can be controlled by adjusting the auxiliary fan and resistance of ventilation regulator(s). A Force-Exhaust mine ventilation system can also be used to reduce pressure drops with the neutral point being located in any position along the ventilation network.

The spontaneous combustion CFD model was also employed to study the low-temperature self-heating behaviour of coal in multiple stockpiles under different prevailing wind conditions. The steady wind flow field indicates a wake region is induced on the leeward side of each coal stockpile. Pressure coefficient drops as the wind stream encounters or leaves a stockpile. Heating develops and migrates towards deep regions in each of these stockpiles which are loosely compacted under higher wind velocity conditions. Wind velocity and porosity of stockpile have significant influences on heating behaviour of the stockpiles and the transport pattern of gaseous products liberated by coal oxidation. This study has practical reference to the coal industry especially where multiple coal stockpiles need to be constructed.

TABLE OF CONTENT

LIST OF FIGURES

LIST OF TABLES

LIST OF SYMBOLS AND ABBREVIATIONS

Symbols

A	Arrhenius pre-exponential factor	$(kmol/m^3)^{1-n}s^{-1}$
a	Empirical constant in Elovich equation	
C	Gas concentration	$kmol\ m^{-3}$
C_p	Specific heat capacity	$J\ kg^{-1}\ K^{-1}$
C_{Pr}	Pressure coefficient	
D	Diffusion coefficient of specie in the gas	$m^2\ s^{-1}$
d	Diameter of coal particle	m
E	Apparent activation energy	$kJ\ mol^{-1}$
G	Specific porous media surface area	m^{-1}
g	Gravitational acceleration	$m\ s^{-2}$
h	Heat transfer coefficient	$W\ m^{-2}\ K^{-1}$
k	Permeability of the coal matrix	m^{-2}
n	Apparent reaction order	
P	Pressure	Pa
q	Amount of oxygen taken up per unit	
R	Universe gas constant	$kJ\ mol^{-1}\ K$
Ra	Radius of coal particle	m
r	Consumption rate of oxygen	$kmol\ m^{-3}\ s^{-1}$
r_m	Rate of drying or wetting	$kmol\ m^{-3}\ s^{-1}$
ř	Radial coordinate	m
S	Source term	
T	Temperature	K
t	Time	s
U	Gas superficial velocity	$m\ s^{-1}$
u	Velocity componentin x direction	$m\ s^{-1}$
V	Free stream velocity	$m\ s^{-1}$
v	Velocity componentin y direction	$m\ s^{-1}$
w	Velocity componentin z direction	$m\ s^{-1}$
x	Longitudinal coordinate	m
y	Transverse coordinate	m
z	Axial coordinate	m

Greek letters

α	Empirical constant in Elovich equation	
β	Thermal expansion coefficient	K^{-1}
ΔH	Heat of coal oxidation	$kJ\ mol^{-1}\ O_2$
ΔH_m	Heat of evaporation or condensation	$kJ\ mol^{-1}$
ε	Porosity	
λ	Thermal conductivity	$W\ m^{-1}\ K^{-1}$
μ	Gas viscosity	$kg\ m\ s^{-2}$
ρ	Density	$kg\ m^{-3}$
ψ	Stream function	$kg\ m^{-1}\ s^{-1}$

Subscripts

am	Ambient
b	Bulk coal

c	Coal
e	Effective
g	Gas
m	Moisture
o	Oxygen
r	Reference

Abbreviations

ACARP	Australian Coal Association Research Program
AFC	Armoured Face Conveyor
AFM	Atomic Force Microscopy
AMSA	Advanced Membrane Supply Approach
CCRI	China Coal Research Institute
CFD	Computational Fluid Dynamics
CRM	Cook Resource Mining
DTG	Differential Thermogravimetric
FTIR	Fourier Transform Infrared spectroscopy
GAG	GorniczyAgregatGasniczy
GC	Gas Chromatograph
GCP	Gaseous Combustion Products
IR	Infrared Spectroscopy
ISCP	Intrinsic Spontaneous Combustion Propensity
LPG	Liquefied Petroleum Gas
LW	Longwall
MSNG	Membrane Separation Nitrogen Generator
MTA	Mining Technologies Australia
PLC	Programmable Logic Controllor
PPC	Positive Pressure Chamber
PSA	Pressure Swing Adsorption
QMRS	Queensland Mines Rescue Service
SBC	South Blackwater Coal
SEM	Scanning Electron Microscopy
SIMS	Secondary Ion Mass Spectrometry
Sponcom	Spontaneous Combustion
TARPs	Trigger, Action, Response, Plans
TB	Tomlison Boiler
TBS	Tube bundle system
TCD	Thermal Conductivity Detector
TGA	Thermogravimetric Analysis
TS	Telemetric system
UCS	Uniaxial Compressive Strength
UDF	User Defined Function
X-Ray	X-Radiation
XPS	X-ray Photoelectron Spectroscopy
13^{C} NMR	13^{C} Nuclear Magnetic Resonance

1 GENERAL INTRODUCTION

1.1 Background

Coal is a flammable black soft rock which is formed from the remains of plants millions years' ago after a range of coalification processes. Within different conditions of coalification coal ends with a verity of types/ranks such as peat, lignite, bituminous and anthracite. Coal has been used as an energy resource, primarily burned for the generation of electricity and/or heat, and also used for other industrial purposes. Besides being utilised as a solid fuel, coal can also be converted to liquid and gaseous phase for broader utilisations. Coal is the largest source of energy for the generation of electricity, and yet one of the largest anthropogenic contributors to greenhouse effect gas emission. Coal is mined commercially in over 50 countries and its production in 2015 of several top mining nations is shown in Figure 1.1. It is obvious both China and Australia are important contributors to global coal production. Figure 1.2 shows the trend of global coal production from 2000 to 2012. It can be seen that global coal production has been growing gradually, which implies the significance of coal is currently unlikely to be replaced in spite of strong criticism of severe damage to environment caused by coal utilisation.

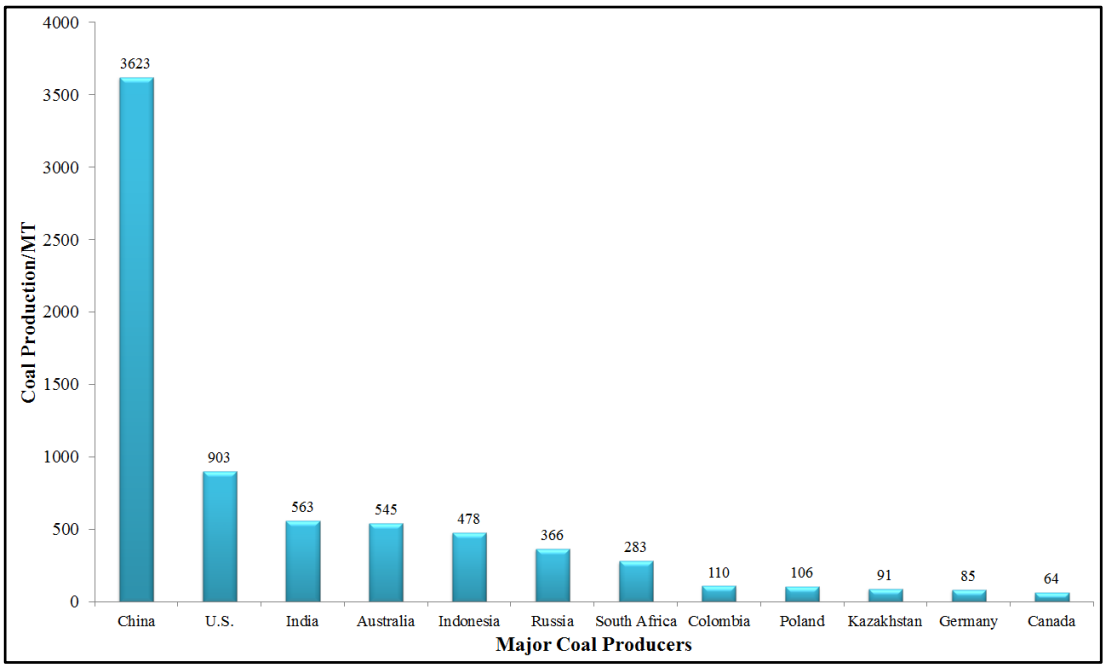

Figure 1.1 Coal production of major coal mining nations in 2015 [1]

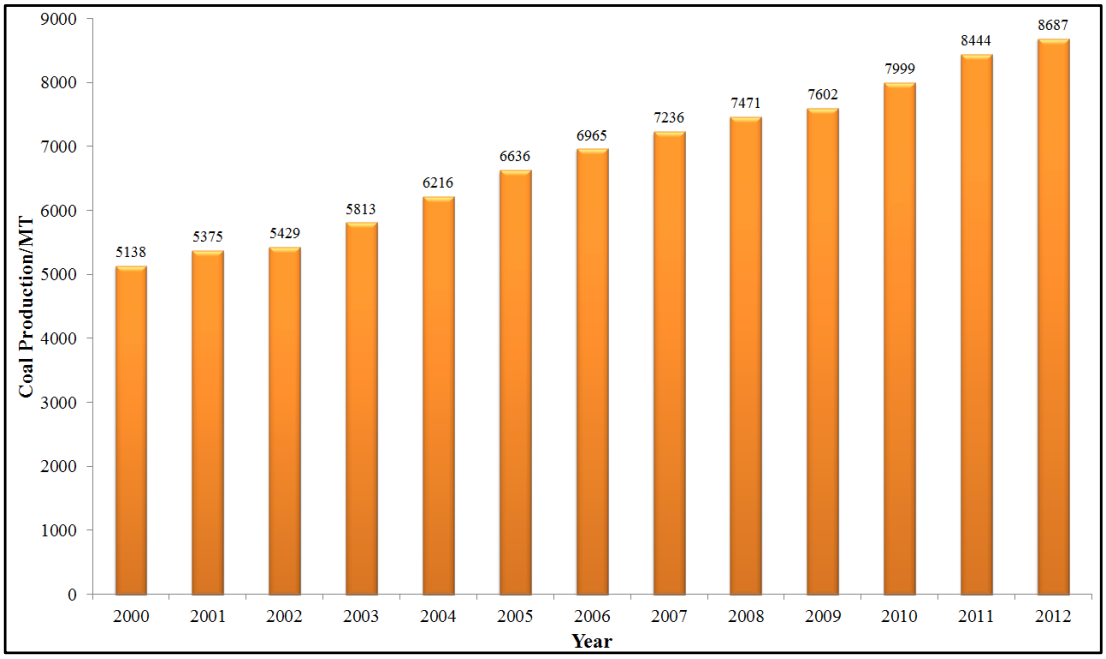

Figure 1.2 Global coal production from 2000 to 2012 [2]

Apart from a number of environmental impacts, there are many hazards involved in the processes of coal mining and coal utilization. For instance, slope failures and vehicle collisions can place miner's life into jeopardy in open cut coal mining operations and meanwhile mine fires, gas issues including excessive presence in airflow stream, gas outburst, and gas explosion, roof collapse, rock/coal burst, and water inrush pose great threats to working crew in underground coal mining operations. Among the underground coal mining hazards a persistent one is mine fire which is often caused by spontaneous heating of coal. If the heating develops to an open fire, a term "spontaneous combustion" is used to describe such a phenomenon. Coal in all ranks, as a carbonaceous material, is able to be oxidised at low temperature with presence of oxygen rich air [3-21]. The interaction of coal with oxygen at low temperature is exothermic as a whole although some reaction sequences could be endothermic [17, 22]. It is widely recognised that low temperature oxidation is the main source of heat leading to spontaneous ignition of coal mass. Other exothermic processes like microbial metabolism, interaction of coal with water, and oxidation of pyrite can also contribute to self-heating of coal mass [23].

The hazard exists when, in underground confined areas like a longwall goaf, the rate of heat accumulation due to oxidation surpasses the rate of cooling by ventilation or

environment. The excessive heat is, to a considerable extent, stored in the coal by virtue of its poor thermal conductivity and results in a net increment of temperature and also the reaction rate of coal oxidation. Once the temperature of a coal mass reaches a critical value at which thermal runaway occurs, a fire ensues if not averted with appropriate remedies [24-26]. A review of Australian coal mining history indicates that more than 125 fire incidents have been recorded in New South Wales whilst at least 68 incidents have been reported in Queensland from 1960 to 1991 and most of them occurred in underground workings [27]. From 1990 to 1999, approximately 17% of the 87 total reported fires for U.S. underground coal mines were caused by self-heating [28]. In India, 75% of the coal mine fires occurs due to spontaneous combustion [29]. In China, more than 50% of coal mines have had self-heating incidents and there are estimated to be 360 fire incidents each year caused by the spontaneous combustion within only several key coal mines [30]. A third of the 254 mine fires reported during the period from 1970 to 1990 was caused by spontaneous combustion of coal in South Africa [31].

Self-heating on a coal stockpile is also likely to occur if the heat generated by coal oxidation and other mechanisms is not adequately dissipated to the surroundings via conduction, convection, and radiation. Such incidents are likely to take place in long term storage stockpiles of thermal power station, surface coal mining spoils, and transportation in cargo ship or train over large distances [26, 32-37]. Spontaneous ignition and smouldering of coal stockpile burns the valuable fossil asset and poses a great threat to coal producers and users. In addition, serious and extensive oxidation of coal can also cause loss of its calorific value and coking property [38-40]. More recently, the liberation of large amounts of greenhouse gases, toxic gases, such as CO and NO_x, hazardous substances (arsenic, selenium, mercury), and lead from spontaneous combustion and low temperature oxidation of large-scale coal mass has raised considerable concerns from global communities [41-45].

Shendong coalfield is the largest coalfield and the most important energy supplier in China. Within the coalfield, a number of large underground coal mines with annual production over five million tonnes of coal are being operated. Due to market demand and advancement of mining technology, the production rates of Shendong

coal mines have significantly improved since 2000. Meanwhile, coal spontaneous combustion has gradually become a major hazard with increasing mining intensity and insufficient mitigation strategies. The reported heating incidents rapidly increased after 2000 and culminated with a serious fire incident in Bulianta coal mine in 2012. Spontaneous combustion in Shendong coal mines is complicated due to a variety of on-site conditions such as multiple coal seam extraction, large panel and high mining height, and high proneness of coal to self-heating. To mitigate such an intractable problem, a joint project "***key technologies for the prevention and control of fires in coal mines extracting multiple seams liable to spontaneous heating***" was initiated in collaboration between three parties: Shenhua Group, Shenyang Branch of CCRI (China Coal Research Institute), and University of Wollongong. The project covers a range of related research works including detailed investigation of heating incidents, computational fluid dynamics (CFD) modelling, ventilation network simulation and geotechnical modelling, experimental studies of Shendong coals, and the development of innovative mine fire monitoring, detection and control techniques. This thesis presents part of the research outcome of this project. Furthermore, the developed spontaneous combustion CFD model was extended to study heating problem in surface coal stockpiles and possibly contribute to research effort in coal spontaneous combustion in other areas.

1.2 Problem statement

Shendong coal mines have been plagued by spontaneous combustion for years and yet, there is still no in-depth investigation of spontaneous combustion problem in Shendong coal mines. A correct diagnosis is likely to significantly facilitate the hazard management while unclear information may mislead the mitigation of the hazard. Many Shendong coal mines are operating multiple-seam extraction and residual coal in the upper longwall goafs were often flooded or oxidised. If the flooded or oxidised coals were exposed to contact with oxygen again, it has been observed to exhibit different heating behaviour compared with fresh coals. Experimental studies have been conducted to attempt to establish more convincing relationships [46-49]. However, the testing results are inconsistent and comprehensive information including low temperature oxidation kinetics, gaseous products evolution, and produced heat is rarely reported. This knowledge is

important to provide fundamentals to spontaneous combustion control in multiple coal seams mining operations like Shendong coal mines. Therefore a comprehensive study of the heating characteristics of different Shendong coal samples is required.

Shendong coal mines are often operated under shallow cover and as a result, mining induced cracks are likely to propagate to surface and to induce airflow ingress into sealed areas such as longwall goafs. The root cause of the airflow leakage is the presence of differential pressure between longwall face and surface. At mine site the cracks are often sealed and yet the effectiveness of the control measure is compromised because many concealed cracks can still draw airflow into goafs. The ultimate treatment to the problem is to eliminate the differential pressure but few practices were exercised to quantify and minimise the differential pressure. Thus solutions to minimising air leakage from this viewpoint are promising and worthy of more research. For a long time it also has been known gas leakage into goaf can cause a variety of problems including noxious gas ingress into longwall face, spontaneous combustion of residual coal, and formation of explosive gas mixture. The severity of these problems is difficult to be assessed because the leakage derives from multiple sources such as longwall airflow behind chocks, mining induced cracks, adjacent goaf, and poorly constructed seals. Hence gas flow pattern and heating behaviour of residual coal in goaf under influence of air leakage must be studied.

Many studies were conducted to investigate heating problem in coal stockpiles [50-64]. Most previous research only focused on temperature rising profiles of a single coal stockpile. Gas emission from low temperature oxidation of stockpiled coal recently has raised considerable environmental concerns [41-45]. Therefore dispersion of gaseous products liberated from oxidation stockpiled coal needs more research. Many models were treated in equilibrium thermal approach in which there is no heat interaction between fluid gas and solid coal and clearly, this approach is not close to reality. Previous solutions to self-heating of coal stockpile usually only deal with a single coal stockpile scenario but practically, multiple stockpiles are probably required to be stacked in storage yard of a coal mine or a port to increase storage capacity. Heating behavior and interactions of coal stockpiles constructed in

adjacent can be also a research direction. Especially coal operators may need such information to facilitate strategic management of multiple coal stockpiles.

1.3 Research objectives

The main aim of the work is to provide more insights and better solutions to sponcom problems in Shendong coal mines. Beyond that sponcom in surface coal stockpiles will also be studied to obtain more understandings. Major objectives of this thesis are:

- To collate information and conduct critical analysis of spontaneous combustion problem in Shendong coal mines and thus provide a basis for strategic management of the hazard in Shendong coal mines;
- To study the heating characteristics of fresh, flooded, and oxidised Shendong coal samples and their oxidation kinetics, gas evolution, and heat generation;
- To develop a computational model to understand the flow dynamics of gas flow pattern, heating development, and goaf inertisation options for typical Shendong longwall mines;
- To develop a solution to minimise air leakage from surface through mining induced cracks in Shendong coal mines from a viewpoint of minimising ventilation pressure differential between surface and the longwall face;
- To establish non-equilibrium thermal model to better understand the heating process and gas emission from low temperature oxidation of coal in stockpiles.

1.4 Research timeframe

A range of research activities have been conducted during the course of this study, as summarised in Table 1.1.

Table 1.1 Main research activities and time frame

Task	2013	2014		2015		2016		2017
	S2	S1	S2	S1	S2	S1	S2	S1
Literature review of fundamentals of self-heating of coal and associated theory on heat and mass transfer;								
A survey of experimental study and numerical modelling of self-heating and oxidation of coal;								
Information collection on general knowledge of current coal mine fire detection, prevention, and control practices;								
A detailed review of design, operation, and results interpretation of adiabatic coal heating test apparatus;								
Coal mine (Australia and China) sites visit and information collection;								
An investigation of spontaneous combustion problems in Shendong coal mines and report draft;								
Multiple experimental tests (ignition temperature test, gas evolution test, DSC test and associated works including coal sample collection, preparation, and proximate & ultimate tests) of Shendong coal samples in CCRI (China Coal Research Institute) laboratory;								
Design and assembly of adiabatic coal heating testing rig;								
Adiabatic heating tests of Shendong coal samples;								
Ventsim modelling of Bulianta coal mine to find a possible mitigation to air leakage into goaf;								
CFD modelling on gas flow pattern, heating evolution, and generation of spontaneous combustion gases in goaf of Bulianta coal mine;								
CFD modelling on low temperature heating process and dispersion of gaseous products of multiple coal stockpiles constructed in adjacent under forced convection;								
Thesis writing, proof reading, and examination.								

***S1-First academic session, S2-Second academic session**

1.5 Thesis outline

The thesis is presented in eight chapters.

Chapter One is a general introduction in which brief background knowledge, problem statement, research objectives, research programme, and outline of the thesis are provided.

Chapter Two provides a critical literature review which incorporates a variety of aspects of spontaneous combustion of coal including mechanism and development of the hazard, thermodynamics and mass transport of self-heating of coal mass, low temperature coal oxidation kinetics, numerical modelling and associated theoretical basis, experimental methods of coal spontaneous combustion, practical detection, prevention, and control of the hazard.

Chapter Three presents a critical investigation of spontaneous combustion issues in Shendong coal mines. In this investigation detailed information and main contributors to spontaneous combustion in Shendong coal mines are provided and analysed.

Chapter Four presents the results of laboratory tests of Shendong coals. The main purpose of these tests is to distinguish different behaviour of spontaneous combustion of fresh, oxidised, and flooded coal samples. These tests include proximate and ultimate analysis, ignition temperature determination tests, low temperature adiabatic tests, gas evolution tests, and DSC tests.

Chapter Five describes the development of a CFD model to investigate the gas flow patterns and heating development in Shendong coal mine goaf with and without influence of gas leakage. Options of goaf inertisation of heating development are presented.

Chapter Six addresses air leakage problem due to the presence of pressure differential between longwall face and surface by application of ventilation simulation based on the real mine plan map of Bulianta coal mine. Two solutions, namely pressurising longwall goaf and use of a combination of forcing and exhaust ventilation system, are proposed to mitigate the airflow leakage problem.

Chapter Seven extends the CFD model to study spontaneous combustion in multiple coal stockpiles constructed in vicinity under forced convection. Parametric studies including wind velocity, geometry of stockpile, and porosity are conducted to explain the causes of heating in coal stockpiles. The dispersion of gaseous products liberated from low temperature coal oxidation is also investigated.

Chapter Eight provides a summary of the main conclusions from this study and recommendations for future work.

2 BASICS OF SPONTANEOUS COMBUSTION OF COAL

2.1 Fundamentals of coal self-heating and oxidation kinetics

2.1.1 Mechanistic understanding of the hazard

The mechanistic understanding of coal heating is given based on a surface coal stockpile. Analogous to many other biological and chemical porous reactors, a coal stockpile is essentially a coal mass consisting of heterogeneous distribution of porous coal particles and gaseous species like oxygen, water vapour, and gaseous product liberated by oxidation reaction transporting in the inter-particle channels and the microstructures of coal particles [65, 66]. Figure 2.1 provides a schematic illustration of the process and main features of self-heating in a coal stockpile. Very briefly, phenomenon of self-heating is possible to occur if the heat generated by coal oxidation and other exothermic processes exceed the heat dissipated to the surroundings by conduction, convection, and radiation. The air inside of stockpile can be constantly replaced and replenished through advective motion caused by forced or natural convection caused by presence of pressure gradient and diffusive motion caused by oxygen consumption of coal which results concentration of oxygen in stockpile is lower than that of ambient atmosphere. The heat can be continuously produced if air supply is not eliminated. Interaction of coal with oxygen including coal oxidation and oxygen adsorption at low temperature is exothermic as a whole although it could be endothermic at some steps [17, 22].The thermal effect of moisture might not be ignored at the initial stage of coal self-heating but heat generated by coal oxidation will dominate with progressive drying of coal. Therefore it is safe to argue that the major heat generation mechanism responsible for self-heating is still coal oxidation [33]. The heat of reaction during oxidation of lignite increased from approximately 313kJ per mole oxygen absorbed at 20^{o}C to 376 kJ per mole oxygen at 90 ^{o}C [50]. Kaji *et al.* [9] measured the rates of heat liberation and oxygen consumption due to coal oxidation in the temperature range 20-170^{o}C using coals ranging from subbituminous to anthracite and 75-90kcal (i.e. 300-379kJ) heat evolved per mole of oxygen at steady state was reported. The generated heat is transported out of the stockpile by conduction through coal mass, convection through wind, and radiation. If the rate of heat generation is greater than

the rate at which heat can be dissipated to the external environment, the excessive heat will be stored in coal matrix and results in a temperature rise. The higher temperature would cause a more drastic reaction taking place, and if no controls are exercised, a fire is very likely to outbreak. Considering the factors that weathering coal particles at surface of coal stockpile are relatively inert in terms of oxidative reaction with long period of exposure to the ambient atmosphere and convective and conductive heat dissipation is stronger than heat production at surface area, the self-heating zone normally may reside at a few meters deep to stockpile surface, refer Figure 2.1. Besides the features described above, self-heating process of coal stockpile is also affected by local meteorological conditions through wind, rain/shower, varying ambient temperature and solar radiation. Water vapour is transported either into or away from the stockpile, depending on the relative ambient humidity and the equilibrium relative humidity within the coal for a given coal water content [33, 67-69]. Moisture has an impact on the process through both chemical and physical ways albeit the effects exhibited in chemical ways have not been fully grasped.

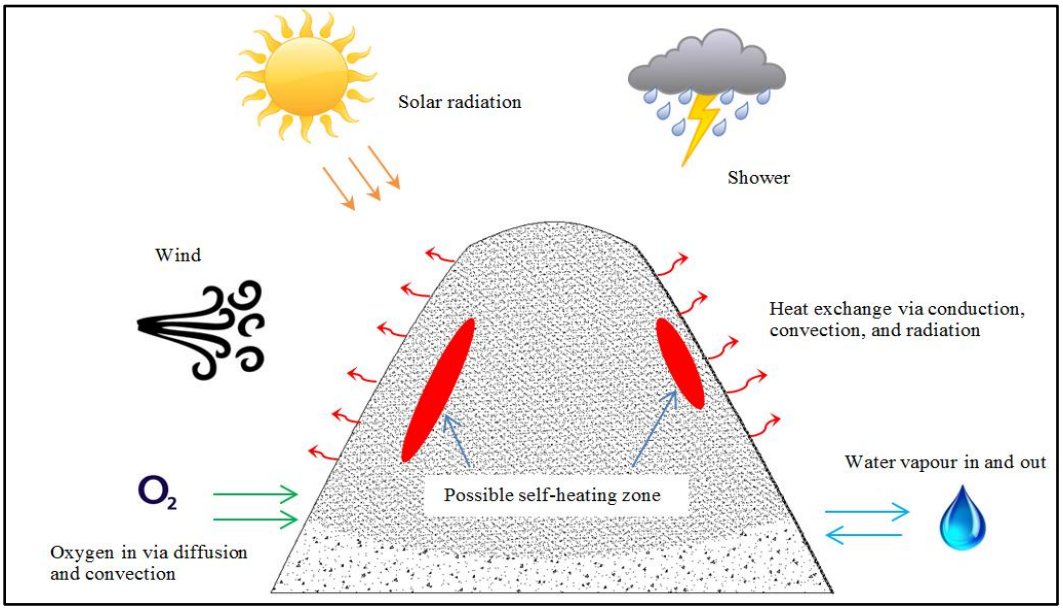

Figure 2.1 Schematic process and main feature of coal stockpile self-heating [37]

To be more realistic to describe heat interaction inside a coal stockpile, heat transfer between coal particles should be treated in a non-equilibrium thermal approach because temperature differentials between air transported from ambient and coal particles could be substantially high. In other words, a stockpile should not be treated

as a non-porous body and convective heat loss which takes place in the interior of stockpile ought to be featured. If the temperature differential between the solid coal particle and gas is important in the thermal behaviour, it is necessary to represent the energy stored in each individual phase as well as the exchange of thermal energy between them [70, 71]. Figure 2.2 is a close-up schematic illustration of intra-and inner-particle heat and mass transfer process. Heat conduction can occur between gas-to-gas, gas-to-coal, and coal-to-coal where effective solid conductance is introduced because of narrow clearance existing between coal particles which further reduce the thermal conductivity of coal. It is assumed that the porous coal stockpile may be treated as homogeneous so that conduction can be modelled by a single effective thermal conductivity [55]. Effective thermal conductivity λ_e is often given by Equation 2.1 [24, 26, 66, 72], other solutions for effective thermal conductivity can be found in the literatures [59, 64, 73],

$$\lambda_e = \varepsilon\lambda_g + (1-\varepsilon)\lambda_c \tag{2.1}$$

The low thermal conductivity of coal is the main reason why thermal energy can be well contained in the deep stockpile. Heat convection occurs between gas to coal and the efficiency of heat convection is mainly determined by velocity of gas advection stream within narrow connected channels between coal particles. Whilst heat radiation could be a major contributor in the surface of stockpile because of solar energy it absorbed but in deep stockpile heat radiation can be negligible [74]. Another efficient heat transfer mechanism is interaction of coal with moisture in which the vaporisation and diffusion of water from a hot region, followed by condensation in a cooler region, is accompanied by a considerably higher effective rate of heat transfer than that which can occur by conduction alone [75]. The interaction of coal with water proceeds much quicker than with oxygen molecule and that leads to the conclusion thatinteraction of coal with moisture is an efficient heat transfer mechanism especially at temperature range 80~90^{o}C. Air transported into coal stockpile via convection and diffusion. Convective flow in both natural and forced ways is pressure-driven flow and diffusive motion is caused by gas concentration gradients because neither oxygen is consumed nor gaseous products are produced at an equal rate everywhere. Convective flow is the primary driver in micro-scale flow, even very small pressure gradients will cause larger flux than flux generated by very steep concentration gradients [76]. Air convection mainly occurs

in inter-particle channels and diffusion mainly occurs in inner pores of coal particle and in deep region of coal stockpile where convective flow is very weak. Irrespective of complex pore structure of coal, many numerical solutions adopted a global surface reaction mechanism so detailed transport mechanism like gas diffusion into inner pores is normally disregarded.

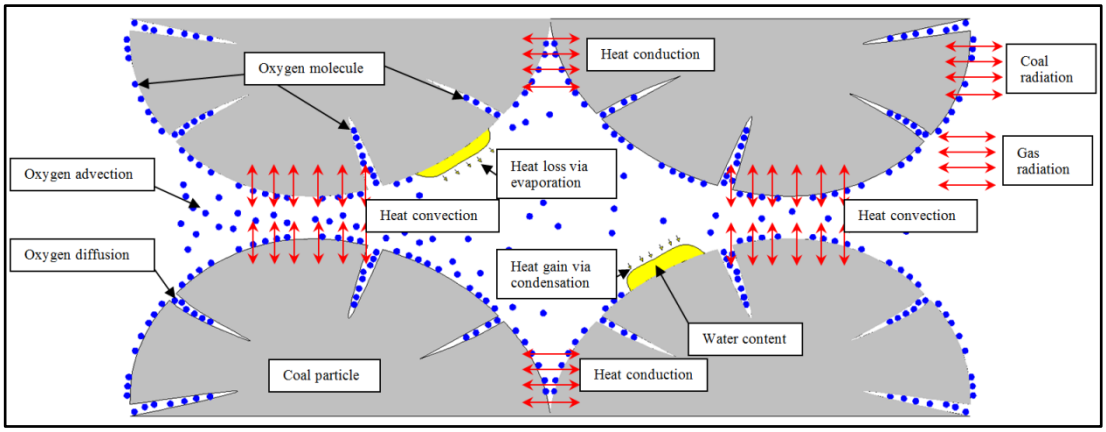

Figure 2.2 A schematic view of heat and mass transfer between coal particles

2.1.2 A brief study of coal oxidation kinetics

To define oxygen consumption rate of coal on a quantitative basis for numerical solution, the nature and chemical kinetics of low temperature coal oxidation must be well studied. Mechanism of low-temperature coal oxidation has been investigated by many studies but complete understanding has never been obtained because of complex pore structure and chemical composition of coal [6, 11, 17-20, 22, 33, 40, 77-92]. Despite of the incomplete understanding of the mechanism and kinetics of coal oxidation, overall reaction paths have reached a general consensus. Very briefly two parallel interaction sequences exist: direct burn-off and adsorption sequence. The burn-off reaction resembles direct combustion of solid fuels which is strongly dependent on temperature. The burn-off reaction sequence is likely to occur at specific sites in a coal's aromatic or aliphatic structure, resulting in the direct formation of gaseous products including CO, CO_2, and H_2O [10, 11, 17, 84, 89, 93]. The adsorption sequence includes: (i) reversible physical adsorption; (ii) irreversible chemisorption of oxygen on the surfaces of pores and the formation of intermediate coal-oxygen complexes including peroxygen, hydroperoxide and hydroxyl species; (iii) the degradation of unstable solid coal-oxygen complexes to gaseous products and formation of stable solid compounds, e.g. carbonyl or carboxyl containing species; (iv) the decomposition of stable compounds and the exposure of new active

sites for oxidation [17, 79], refer Figure 2.3 which is a very representative chart of interaction of coal with oxygen at low temperature.More kinetic models were summarized in a review work undertaken by Wang *et al.* [17] and the compilation is further cited in this work to describe a more realistic picture of kinetic models of coal oxidation, refer Table 2.1.

Table 2.1 Comparisons of kinetic models developed by various investigators [17]

Reference	Temperature range (^{o}C)	Reaction mechanism	Model features
[88, 89]	200~225	➢ Direct burn-off reaction coal+O_2→CO_2, CO, H_2O ➢ Sorption sequence coal+O_2→complex↔CO_2, CO, H_2O	❖ Prediction of oxygen consumption and gaseous products (CO_2, CO and H_2O), ❖ Analytical solutions for the reaction rates, as a sum of constant and exponential decay terms, ❖ Stoichiometric correlation between the reactants and the gaseous products
[84, 85]	150~160	➢ Direct burn-off reaction coal+O_2→CO_2, CO ➢ Sorption sequence coal+O_2↔physisorbed O_2→chemisorbed O_2→CO_2, CO ➢ Separate water production coal + O_2→H_2O	❖ Prediction of oxygen consumption, gaseous products (CO_2, CO and H_2O) and solid intermediates, ❖ Site conservation among various active sites, ❖ Numerical solution of the model
[10, 11]	25~95	➢ Direct burn-off reaction coal +O_2→CO_2 ➢ Sorption sequence coal+O_2→oxycoal →CO_2	❖ Prediction of oxygen consumed and carbon dioxide produced, ❖ Conserved active sites and exponential decay in the active sites for oxygen adsorption, ❖ Analytical solutions for the rates
[79]	60~90	➢ Direct burn-off reaction coal+O_2→CO_2, CO, others ➢ Sorption sequence coal+O_2→carboxyl+carbonyl +CO_2+unreactive species, ➢ Carboxyl species→CO_2 ➢ Carbonyl species→CO	❖ Prediction of oxygen consumed and carbon oxides produced, ❖ Self-conserved active sites and reduction in active sites due to the formation of unreactive species, ❖ Analytical equations for the rates

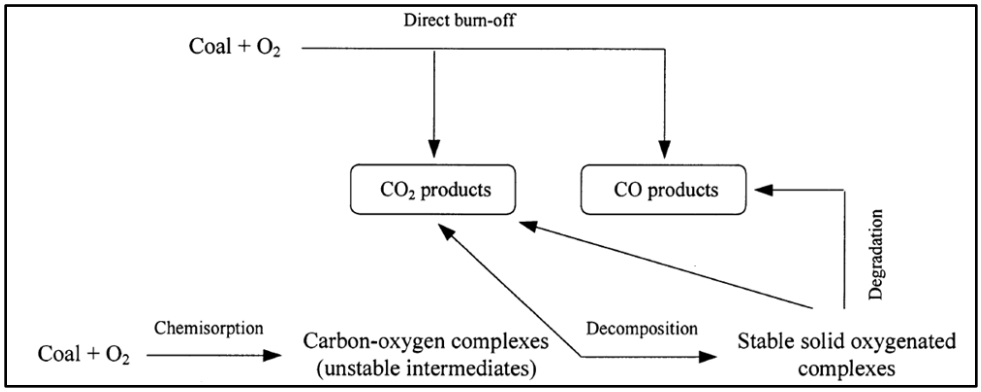

Figure 2.3 Two processes of low-temperature interaction of coal with oxygen [81]

It is noticeable, at a low temperature, the number of the active sites for oxygen adsorption usually decays exponentially, which often correlates to exhibition of the Elovich effect. At present it is, however, unlikely to describe the burn-off reaction sequence in fundamental steps due to the lack of understanding. Therefore, to a quantitative sense, many authors attempted to use the Elovich dependence (or partially) to describe the progressive decrease of the rate of sorption reaction regime with increasing uptake of active sites at a constant temperature[3, 17, 51, 79, 87, 94, 95]. The Elovich equation was often written as,

$$\frac{\mathrm{d}q}{\mathrm{d}t} = a\exp(-\alpha q) \tag{2.2}$$

Although the Elovich equation is often taken as a purely empirical term, it can be effectively applied to explain the rate of oxygen consumption with time, namely the "ageing" effect [3, 51, 96]. Whilst in reality temperature in stockpile is elevating as a result of heat accumulation and further due to the existence of burn-off reaction sequence which is highly dependent on temperature so consumption rate of oxygen is more frequently expressed in Arrhenius form with a given temperature and oxygen concentration [24, 26, 72, 97, 98], which was written,

$$r = A[C_0]^{\mathrm{n}}\exp(-E/RT) \tag{2.3}$$

Authentic Arrhenius equation has its origin in gas phase reaction regime [99, 100]. An equation of the same form as Equation 3 has also found wide application to the oxidation of coal. However usually there is no mechanistic interpretation of A and E, simply an observed temperature dependence of rate that fits an equation of this form [101]. But some other studies indicated the activation energy, *E*, may be regarded as a measure of the energy barrier to reaction, while the pre-exponential factor, *A*, correlates to the available surface area for oxidation [102]. Thus, the pre-exponential

factor depends heavily on the coal's pore structure and fine particles tend to have a larger pre-exponential factor [103]. Irrespective this dispute, it can be observed, from Equation 2.3, that coal oxidation rate is simply determined by the reaction order and two Arrhenius constants at a given temperature and partial pressure of oxygen. It is assumed that oxygen can penetrate throughout the coal without any diffusional resistance and the reaction rate between gaseous oxygen and solid coal particle is expressed as if it is a homogenous gas phase reaction [3]. To consider the diffusional restriction into the interior of coal particle, many studies introduced an effectiveness factor, which is conventionally defined as the ratio of the reaction rate under diffusional limitations to the rate which would be observed in the chemical control regime in the absence of transport or diffusional effect [85]. Detailed interpretation of the effectiveness factor can be found in the literatures [10, 57, 62, 85]. The value of the reaction order in low temperature oxidation of coal and other carbonaceous materials has been indicated to vary from 0.5 to 1 [33, 75]. More specific values of reaction order have been published are: n=1 [50, 104, 105], n=0.61 [24, 106], n=0.52 [107], and n=0.7 [52, 108]. In the case of the spontaneous combustion of coal, temperatures are extremely low and chemical kinetics play the main role on reaction rate [3]. The kinetic constants are affected by unique coal properties such as pore structure, mineral matter, volatile content, and coal rank so they varies from coal to coal. Even for a same coal the parameters can be affected by different particle sizes [103] and heating stages [4]. The value of apparent activation energy, *E*, of different coals can vary between 12 and 95 kJ/mol and more values of activation energy for low temperature coal oxidation can be found in the review work conducted by Wang *et al.* [17]. Taraba and Michalec [104] discussed the pre-exponential factor is of the greatest uncertainty giving ordinarily values differing over several orders and another study also indicated the pre-exponential factor has a typical value between 1 and 7×10^5/s [24, 72]. As a result, the Arrhenius constants for a given coal oxidation context must be determined experimentally. These experimental methods may include adiabatic testing method, heat release measurement method, and differential thermal analysis [3, 109-112].

Self-heating of coal starts with low temperature oxidation stage at which adsorption reaction sequence might manifest so the reaction rate of a coal could display a non-

Arrhenius behaviour curve. In a study of the oxidation rate of coal and coal char [96], it was shown that the oxidation rate of a coal char exhibits both an Arrhenius and Elovich kinetics from 50~100^{o}C. As can be seen in Figure 2.4(a), Jones and Newman [101] reported a non-Arrhenius behaviour of a Chinese bituminous coal in a micro-calorimeter experiment at temperatures in the range 311~338K. More recently an adiabatic testing figure of a high volatile bituminous coal from Hunter Valley coalfield of Australia indicated that an Arrhenius dependence curve above 70 ^{o}C can be found and below this temperature a straight line is impossible to be fitted at the ln(dT/dt) versus (1/T) plot, refer Figure 2.4(b) [3]. A possible explanation is adsorption reaction sequence proceeds at a high rate initially and manifests itself by driving reaction rate to a non-Arrhenius behaviour curve. With the time elapsing and temperature increasing, the adsorption reaction tails off and the direct burn-off reaction step takes a lead to the extent reaction rate starts to follow the Arrhenius-like dependence. Many numerical solutions adopted a simple Arrhenius approach to mathematically deal with consumption rate of oxygen within a stockpile [24, 26, 38, 52, 54, 57, 58, 61, 72, 73, 97, 104]. The conjunctive effects brought by the Elovich mechanism and Arrhenius dependence at low temperature coal oxidation may introduce a new dimension for numerical simulation of self-heating behaviour on a coal mass although the need of numerical assessment of Elovich parameters was called long ago [51]. Another glance at the Equation 2.3 it can be known partial pressure of oxygen also plays a role in the rate of coal oxidation at a given temperature and Arrhenius constants. It is plausible to approximate that any solid coal-oxygen complex produced during low-temperature coal oxidation would not affect the rate of oxidation if Arrhenius reaction mechanism is presumed. Gaseous products (e.g. CO, CO_2, and H_2O) produced by direct burn-off reaction and decomposition of solid complex would, however, disperse into the gas mixture and affect the concentration of oxygen although the amount of gaseous product is much less appreciable than that of consumed oxygen [84]. Early numerical works only considered the consumption of oxygen and some recent works started to incorporate effect of gaseous products with very simplified stoichiometric schemes though [24, 72, 73, 97, 104], refer Table 2.2 which summaries the main features such as transport mechanism and spatial dimension, and important parameters like physical properties and reaction kinetics of present numerical solutions to self-heating of coal mass.

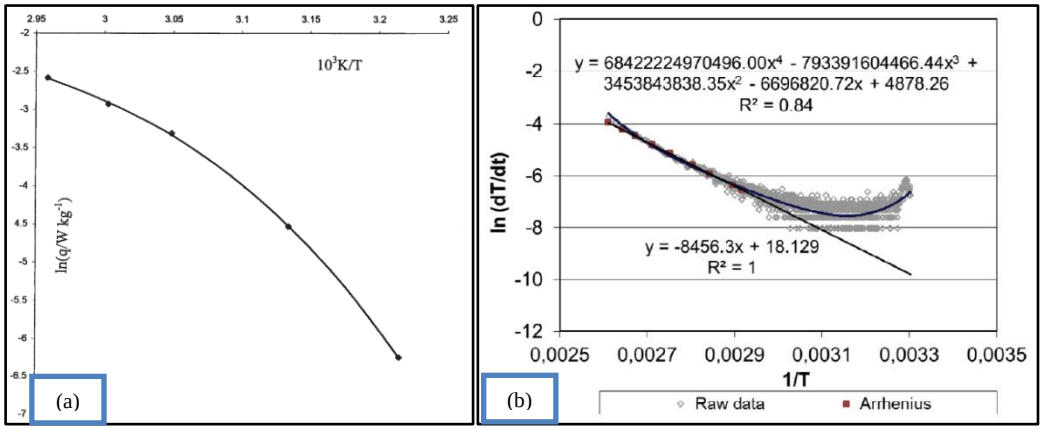

(a) Plot of ln(heat release) against 1/T for a China coal [101] (b) Plot of ln(dT/dt) against 1/T for an Australia coals [3]

Figure 2.4 Two examples of non-Arrhenius coal oxidation rates at low temperature

Table 2.2Main features and parameters of numerical solutions to self-heating of coal mass

Reference		*Main features*						*Chemical reaction parameters*					*Physical properties of coal (mass)*					
						Transport mechanism			Arrhenius constants									
		Coal type	Transient(T)/Steady(S)	Spatial dimensionality	Moisture(Y-yes/N-no)	Heat	Oxygen	Reaction order	Activation energy	Pre-exponential factor	Reaction mechanism	Heat of oxidation	Average particle diameter	Porosity	Density	Specific heat capacity	Thermal conductivity	Oxygen diffusion coefficient in gas phase
[50]		A U.S. lignite	T	1D	N	Conduction	Forced convection	1	50	-	Oxygen consumption	376 kJ/mol O_2	-	-	801	2263	0.2	-
[51]		Yallourn briquette char	T	1D	Y	Conduction & convection	Diffusion & forced convection	1	66	-	Oxygen consumption	300 kJ/mol O_2	-	-	-	-	-	-
[52]	Dry coal	-	T	1D	Y	Conduction & convection	Diffusion & forced convection	1	7	4.2×10^{-10}	Oxygen chemisorption	3 kJ/mol O_2	-	0.05, 0.2, 0.3	1500	1000	0.12	2×10^{-5}
	Moist coal							0.7	7.5	2.1×10^{-10}		3.7 kJ/mol O_2						
[54]		-	S	1D	N	Conduction	Natural convection	1	58.2	3600	Oxygen consumption	300 kJ/mol O_2	0.01	0.3	-	-	0.2	2×10^{-5}
[55]		-	S	2D	N	Conduction	Natural convection	-	-	-	-	400 kJ/mol O_2	-	-	-	-	0.16	-
[113]		-	S	2D	N	Conduction	Natural convection	1	58.2	3600	Oxygen consumption	300 kJ/mol O_2	0.01	0.3	-	-	0.2	2×10^{-5}
[59]	Forced convection model	High-volatile C bituminous coal	T	2D	N	Conduction & convection	Forced convection & diffusion	1	90	1.23×10^{9}	Oxygen consumption	300 kJ/mol O_2	0.076	0.33	1300	1004	0.114	1.5×10^{-5}
	Buoyancy-driven model			2D	N	Conduction & convection	Natural convection & diffusion	1	90	1.23×10^{9}			0.076	0.33				
	Wind-driven model			1D	N	Conduction & convection	Forced convection & diffusion	1	90, 76.6	1.23×10^{9}, 5.96×10^{7}			5.625×10^{-5}, 1.125×10^{-4}, 2.25×10^{-4}	0.33, 0.165				
[56]		-	S	3D	N	Conduction & convection	-	0	-	-	-	-	-	-	-	-	-	-
[57]		Turkish moist coals	T	1D	Y	Conduction & convection	Forced convection & diffusion	1	70	2.933×10^{6}	Oxygen adsorption	9375kJ/kg O_2	0.01, 0.02, 0.03	0.3	1100	1000	0.2	2×10^{-5}
[60]		-	S	2D	N	Conduction & convection	Natural convection & diffusion	1	58.2	3600	Oxygen consumption	300 kJ/mol O_2	0.01	0.4	-	-	0.2	2×10^{-5}

[61]	Weathered Wyoming subbituminous coal	T	2D	N	Conduction & convection	Forced & natural convection	1	57.5	8.83×10^{6}	Burn-off	-	0.023	0.096	-	-	-	-
[62]	-	T	1D	N	Conduction	Diffusion	1	57.5	8.83×10^{6}	Oxygen consumption	330 kJ/mol O_2	-	-	-	-	0.2	2×10^{-5}
[63]	-	T	1D	N	Conduction & radiation	Diffusion	1	57.5	8.83×10^{6}	Oxygen consumption	330 kJ/mol O_2	-	-	-	-	0.2	2×10^{-5}
[64]	Wyoming subbituminous coal	T	1D	Y	Conduction & convection	Natural convection & diffusion	1	57.5	8.83×10^{6}	Oxygen consumption	330 kJ/mol O_2	0.003~0.015	-	-	-	-	-
[35]	Australian bituminous coal	T	2D	Y	Conduction & convection	Forced convection & diffusion	0.7	7.5×10^{-7}	2.1×10^{-10}	Oxygen consumption	11560 kJ/kg coal	-	0.3	1260	1423	0.12	1.2×10^{-5}
[58]	Turkish brown coals	T	2D	Y	Conduction & convection	Forced convection & diffusion	1	46.81, 30.64, 21.89	1758, 1.485, 0.424	Oxygen consumption	-	-	0.3	-	-	-	-
[114]	A China coal	T	1D	N	Conduction & convection & radiation	Forced convection & diffusion	1	40	10	Oxygen consumption	-	-	0.5	-	1500	3.4	2×10^{-5}
[107]	A Spain coal	T	1D	N	Conduction & convection	Forced convection & diffusion	0.52	42	2.8×10^{-8}	Oxygen consumption	380 kJ/mol O_2	-	0.1, 0.13, 0.15, 0.17, 0.2, 0.25, 0.3	1566	1132	0.113	-
[74]	Four coals	T	2D	N	Conduction & radiation	Diffusion	1	40, 26.88, 58, 30.64	10, 6, 8.83×10^{6}, 1485	Oxygen consumption	-	-	-	-	1500	3.4	2×10^{-5}
[72]	Three U.S. coals	T	3D	N	Conduction & convection	Forced convection & diffusion	0.61	66.5, 73.6, 88.3	1.9×10^{6}, 1.1×10^{7}, 4.4×10^{8}	$Coal+O_2\rightarrow CO_2+0.1CO$	300 kJ/mol O_2	-	-	1300	1003.2	0.1998	1.5×10^{-5}
[24]	A U.S. High volatile bituminous coal	T	3D	N	Conduction & convection	Forced convection & diffusion	0.61	66.5	1.9×10^{6}	$Coal+O_2\rightarrow CO_2+0.1CO$	300 kJ/mol O_2	0.02	0.3	1240	1003.2	0.1998	-
[104]	A Czech bituminous coal	T	3D	N	Conduction & convection	Forced convection & diffusion	1	23.5 (subcritical),	1.85 (subcritical),	Oxygen consumption	250 kJ/mol O_2	-	-	-	-	-	-

								51 (supercritical)	13700 (supercritical)								
[115]	A lignite	T	2D	Y	Conduction & convection	Forced convection & diffusion	1	55	1000	Oxygen consumption	22000 kJ/kg coal	-	-	-	1500	0.12	-
[73]	-	T	2D	N	Conduction & convection	Forced convection &diffusion	0	0.75	2.1×10^{-10}	$Coal+O_2\rightarrow CO_2$	-	-	-	1200	1050	0.12	-
[26]	A China coal	T	2D	N	Conduction & convection	Forced and natural convection & diffusion	1	50	180	Oxygen consumption	400 kJ/mol O_2	-	0.1, 0.15, 0.2, 0.25, 0.3, 0.35, 0.4	-	1003.2	0.2	2×10^{-5}
[97]	A bituminous coal	T	2D	N	Conduction & convection	Forced & natural convection & diffusion	1	22 (subcritical), 50.5 (supercritical)	1.85 (subcritical), 13500 (supercritical)	$Coal+O_2\rightarrow 0.1CO_2+0.4H_2O+1.4O$-Coal (subcritical); $Coal+O_2\rightarrow 0.2CO_2+0.8H_2O+0.01CO+0.79O$-Coal (supercritical)	270 kJ/mol O_2	0.01	-	-	-	-	-
[98]	-	T	2D	N	Conduction & convection	Forced convection & diffusion	1	21.89	1	Oxygen consumption	300 kJ/mol O_2	0.04	-	1300	1003.2	0.2	2×10^{-5}

2.2 Numerical solutions to self-heating of coal mass

Although the hazard has long been acknowledged, it has also been accepted that the physical and chemical processes responsible for this problem is complicated [33]. The problem was mitigated by practical means long before the scientific accounts emerged. However, the theoretical research is in equal importance, on a quantitative basis, in assisting with the assessment and prediction of self-heating hazard and design of procedures and countermeasures to reduce this risk. Early efforts have been devoted to self-heating problem of bulky solids by thermal explosion theory, which laid firm foundation of the theoretical solution to the problem [116-119]. Afterwards a series of treatments of thermal explosion theory in solid material self-heating problem have been published [75, 120-129]. Although thermal explosion theory is able to determine criticality of a porous body with diffusion-controlled oxygen consumption [75, 122, 126, 129], it still has difficulties to directly apply this solution to self-heating problem of coal stockpile as more of the factors affecting self-heating are taken into account [33]. Additionally what raised much of the concern to coal operator is the induction period of a coal stockpile before catching a fire. The increasing demand of transient solutions poses significant challenges to the subject. Derivation of an analytical solution with less approximation to such a transient problem which might involves fluid dynamics, heat transfer, and chemical reaction kinetics would be a daunting or even impossible task so the problem is more often addressed numerically with increasing availability to high-performance computers.

To predict the self-heating behaviour of porous coal mass with progressively consumed gas species like oxygen and vapour, prior to the availability of high-performance commercial fluid dynamics simulation code, several rudimentary mathematical studies with many assumptions and simplifications though were conducted [50-64, 67, 113, 130]. Among these works, Sondreal and Ellman [50] calculated the material and energy balances for a stockpiled lignite in which heat is transferred only by conduction. Nordon [51] proposed a one-dimensional unsteady state model consisting of the differential equations for mass and energy conservation and for the reaction rate of coal oxidation. Schmal *et al.* [52] developed another one-dimensional model which included thermal impacts exhibited by

evaporation/condensation of coal moisture. Both models analysed forced convection through the packed bed by varying the air flow velocity as a system parameter. Brooks and co-workers [53, 54, 113, 130] differed from previous treatments in that natural convection was taken into account as an important mechanism for oxygen transport that is responsible for the occurrence of self-heating without the need to assume the existence of a pressure gradient over the coal bed. Young *et al.*[55] proposed a two-dimensional natural convection and conduction model in a packed bed containing a hot spot (i.e. coal stockpile, nuclear reactor) and this work reconfirmed natural convection is a feasible mechanism for oxygen transport into a coal pile where sufficient reaction may occur to sustain a hot spot. To predict the development of localized spontaneous heating within a porous coal matrix that is subjected to forced convection or in an otherwise quiescent environment in which buoyancy flow dominates, the Bureau of Mines developed three time-dependent mathematical models, which were used to calculate the temperature increase associated with chemisorption of oxygen by the coal [59].Bradshaw *et al.*[56] studied the effect of natural convection on ignition in a laterally-unbounded coal pile and stable three-dimensional flow planforms for the model were predicted. Arisoy and Akgün [57] developed a one-dimensional non-equilibrium thermal model consisting of conservation equations for oxygen, water vapour, moisture of coal, and energy for both gaseous and solid phases. Salinger and co-authors [60] critically reviewed the mathematical analysis of coupled reaction and transport in chemical reactors and analysed spontaneous heating of coal stockpiles by considering the nonlinear interactions of chemical reaction, heat transfer, and buoyancy-driven flows within and around the stockpile. Krishnaswamy and co-workers [10, 61] developed a reaction-diffusion model for low-temperature oxidation of coal and this model was incorporated in a two-dimensional model for spontaneous heating of open coal stockpiles where the influence of moisture migration can be negligible. Hull *et al.* [62, 63] developed a theoretical model for a confined space context where stockpile is sealed on all sides except the top which provides free surface and channels for oxygen diffusion. Monazam *et al.* [64] formulated a transient one-dimensional spontaneous heating model to describe the self-heating process at relatively low temperatures. Akgün and Essenhigh [58] proposed a two dimension transient model of self-heating of coal stockpile and found height and time are two primary factors in determining if a stockpile is unconditionally safe. Although the predictions of

temperature ramping profile and incubation period are very likely beyond engineering accuracy due to substantial assumptions and restrictions having been made, these fundamental models are capable of providing subsequent researchers valuable insights to the problem and offering initial guidance to assist coal operators to stack stockpile more safely.

More recently with the advance and development of more sophisticated numerical solutions, especially the availability of cutting-edge Computational Fluid Dynamics (CFD) modelling techniques and their increasing applications in coal and related industries, predictable interpretation of transient self-heating of coal mass with less restrictions and within tolerated engineering accuracy becomes possible [24, 26, 35, 36, 38, 72-74, 97, 98, 104, 115, 131]. Among these works, Moghtaderi *et al.* [35] studied the effects of wind driven flow field on self-heating behaviour of typical coal stockpiles and found wind flow plays a critical part in dynamics of flow field inside the pile and thereby affects the heating process. Krajčiová *et al.* [74] innovated a model including radiation energy balance of the coal stockpile surface and indicated solar radiation has a strong influence on the temperature ramping profile of stockpile. Yuan and Smith [72] studied effects of coal properties on self-heating problem in underground coal mine goaf areas by a CFD model. Yuan and Smith [24] further developed a three-dimensional equilibrium thermal CFD model to simulate spontaneous heating in a large-scale testing chamber with a forced ventilation system. Ejlali *et al.* [115] improved preceding models by employing a local thermal non-equilibrium approach and stated the required time to vaporize the water content and the maximum temperature is a function of porosity of porous pile, moisture content and Darcy number. Taraba and Michalec [104] numerically investigated the effects of longwall advance rate on spontaneous heating in goaf areas by a CFD model. Kim and Sohn [73] numerically validated a novel method (air blowing from bottom of stockpile and/or instalment of dual barrier) to suppress spontaneous ignition of coal stockpiles in a coal storage yard. Zhu *et al.* [26] developed a theoretical model to predict the self-ignition time and locations of coal stockpiles with relatively large diameter of coal particle. Taraba *et al.* [97] developed a CFD model to study the influences of wind on the spontaneous heating process of a coal stockpile. Yang *et al.* [38] proposed a two-dimensional model to investigate the effects of coating the bottom of coal stockpile with fine particles to control self-heating hazard. Xia *et al.*

[98] also used the CFD code to simulate the self-heating process of residual coal in longwall goaf. Zhang *et al.* [36] studied the low-temperature self-heating behaviour of multiple coal stockpiles under different prevailing wind conditions. Not only above works can eliminate more restrictions and enhance the applicability of numerical solutions to coal self-heating problems, considerable variable studies have also been conducted and many practical findings have been reported. The variable studies conducted by various investigators are summarized in Appendix A.

2.3 Theoretical basis of coal heating

2.3.1 Energy conservation

Absence of moisture

The energy description starts with Sondreal and Ellman [50] who assumed heat is only dissipated by conduction of a coal mass, which yields,

$$\rho_{\mathrm{b}} C_{\mathrm{pb}} \frac{\partial T}{\partial t} = \lambda_e \nabla^2 T + S \tag{2.4}$$

The successive terms denote the storage of internal energy which manifest itself as a transient temperature rise of bulky coal, heat diffusion and energy source which denotes liberation of reaction heat. Later, Hull *et al.* and Young *et al.* [55, 62] also used conduction as a sole heat transport mechanism when levelled stockpiles of coal are transported in a confined space like barges or rail cars, which gives,

$$(1-\varepsilon)\rho_{\mathrm{c}} C_{\mathrm{pc}} \frac{\partial T}{\partial t} = \lambda_e \frac{\partial^2 T}{\partial x^2} + (1-\varepsilon) r \Delta H \tag{2.5}$$

In Schmal's one dimensional model [52], heat dissipated by convection (the second term in equation 2.5) was included in the heat balance equation, which results,

$$(1-\varepsilon)\rho_{\mathrm{c}} C_{\mathrm{pc}} \frac{\partial T}{\partial t} + \rho_{\mathrm{g}} C_{\mathrm{pg}} u \frac{\partial T}{\partial x} = \lambda_{\mathrm{e}} \frac{\partial^2 T}{\partial x^2} + (1-\varepsilon) r \Delta H \tag{2.6}$$

Brooks *et al.* [53, 54, 113] also incorporated convective heat term in heat balance but presuming a pseudosteady state, which produces,

$$\lambda_{\mathrm{e}} \frac{\partial^2 T}{\partial x^2} - \rho_{\mathrm{g}} C_{\mathrm{pg}} u \frac{\partial T}{\partial x} + r \Delta H = 0 \tag{2.7}$$

In the forced convection model of Edwards's work [59], a non-equilibrium thermal state between gas and coal was considered and the thermal transport equation was written in cylindrical coordinates, which yields,

$$\varepsilon \rho_{\mathrm{g}} C_{\mathrm{pg}} \frac{\partial T_{\mathrm{g}}}{\partial t} + (1-\varepsilon)\rho_{\mathrm{c}} C_{\mathrm{pc}} \frac{\partial T_{\mathrm{c}}}{\partial t} + \rho_{\mathrm{g}} C_{\mathrm{pg}} U_{\check{\mathrm{r}}} \frac{\partial T_{\mathrm{g}}}{\partial x} + \rho_{\mathrm{g}} C_{\mathrm{pg}} w \frac{\partial T_{\mathrm{g}}}{\partial x} = \lambda_{\mathrm{e}} \frac{\partial^2 T}{\partial \mathrm{z}^2} + \lambda_{\mathrm{e}} \left(\frac{\partial^2 T}{\partial \check{\mathrm{r}}^2} + \frac{1}{\check{\mathrm{r}}} \frac{\partial T}{\partial \check{\mathrm{r}}} \right) + r \Delta H \tag{2.8}$$

And thermal transfer between the solid coal and the gas is governed by,

$$\rho_{\mathrm{c}} C_{\mathrm{pc}} \frac{\partial T_{\mathrm{c}}}{\partial t} = \frac{3h}{R}\left(T_{\mathrm{g}} - T_{\mathrm{c}}\right) \tag{2.9}$$

While in the wind-driven convection model, the gas and solid coal were, for a conservative estimate of induction period, assumed to be in thermal equilibrium. The energy transport equation was therefore written as,

$$\left[\varepsilon\rho_{\mathrm{g}} C_{\mathrm{pg}} + (1-\varepsilon)\rho_{\mathrm{c}} C_{\mathrm{pc}}\right]\frac{\partial T}{\partial t} + \rho_{\mathrm{g}} C_{\mathrm{pg}} u \frac{\partial T}{\partial x} = \lambda_{\mathrm{e}} \frac{\partial^2 T}{\partial x^2} + r\Delta H \tag{2.10}$$

Krishnaswamy *et al.* [61]extended the heat conservation equation to two dimensions in Cartesian coordinate system, which yields,

$$(1-\varepsilon)\rho_{\mathrm{c}} C_{\mathrm{pc}} \frac{\partial T}{\partial t} + \rho_{\mathrm{g}} C_{\mathrm{pg}} \left(u\frac{\partial T}{\partial x} + v\frac{\partial T}{\partial y}\right) = \lambda_{\mathrm{e}} \left(\frac{\partial^2 T}{\partial x^2} + \frac{\partial^2 T}{\partial y^2}\right) + r\Delta H \tag{2.11}$$

To date commercial CFD code is capable of solving 3D problem in (non-)equilibrium thermal approach. Zhu and co-workers [26] used the code established a 2D energy conservation in thermal equilibrium, the equation is written as,

$$\left[\varepsilon\rho_{\mathrm{g}} C_{\mathrm{pg}} + (1-\varepsilon)\rho_{\mathrm{c}} C_{\mathrm{pc}}\right]\frac{\partial T}{\partial t} + \rho_{\mathrm{g}} C_{\mathrm{pg}} \left(u\frac{\partial T}{\partial x} + v\frac{\partial T}{\partial y}\right) = \lambda_{\mathrm{e}} \left(\frac{\partial^2 T}{\partial x^2} + \frac{\partial^2 T}{\partial y^2}\right) + (1-\varepsilon) r\Delta H \tag{2.12}$$

Yuan and Smith [24, 72] used CFD code to develop a three-dimensional equilibrium thermal model for self-heating of coalbed in a testing chamber, which produces,

$$\left[\varepsilon\rho_g C_{pg} + (1-\varepsilon)\rho_c C_{pc}\right]\frac{\partial T}{\partial t} + \rho_g C_{pg} \left(u\frac{\partial T}{\partial x} + v\frac{\partial T}{\partial y} + w\frac{\partial T}{\partial z}\right) = \lambda_{\mathrm{e}} \left(\frac{\partial^2 T}{\partial x^2} + \frac{\partial^2 T}{\partial y^2} + \frac{\partial^2 T}{\partial z^2}\right) + r\Delta H \tag{2.13}$$

The most recently, Xia and co-workers [98] developed a non-equilibrium thermal model for self-heating of a longwall goaf, hence two separate energy equations are required,

For solid phase

$$(1-\varepsilon)\rho_{\mathrm{c}} C_{\mathrm{pc}} \frac{\partial T_{\mathrm{c}}}{\partial t} - (1-\varepsilon)\nabla(\lambda_{\mathrm{c}} \nabla T_{\mathrm{c}}) = S + hG\left(T_{\mathrm{g}} - T_{\mathrm{c}}\right) \tag{2.14}$$

For gas phase

$$\varepsilon\rho_{\mathrm{g}} C_{\mathrm{pg}} \frac{\partial T_{\mathrm{g}}}{\partial t} + \rho_{\mathrm{g}} C_{\mathrm{pg}} U_{\mathrm{g}} \nabla T_{\mathrm{g}} - \varepsilon\nabla\left(\lambda_{\mathrm{g}} \nabla T_{\mathrm{g}}\right) = -hG\left(T_{\mathrm{g}} - T_{\mathrm{c}}\right) \tag{2.15}$$

Presence of moisture

Although some fresh stockpiles are very dry due to low inherent water content of coal, they are likely to become moist with presence of rain, snow, and/or moist ambient air. In practice most coal stockpiles are moist especially some low rank coals with presence of high inherent water content and thereby heat exchanged via

transition of water phase should be incorporated in the model. In Schmal's model, additional energy conservation was proposed for a moist coal pile [52]. To adjust the model, two extra terms were incorporated in Equation (6): one for evaporation (or, with the opposite sign for condensation, first term) and another one for convective heat transfer by water vapour (second term).

$$\Delta H_m \frac{\partial(UC_{\mathrm{m}})}{\partial x} + U_{\mathrm{m}}\rho_{\mathrm{m}}C_{\mathrm{pm}}\frac{\partial T}{\partial t} + (1-\varepsilon)\rho_{\mathrm{c}}C_{\mathrm{pc}}\frac{\partial T}{\partial t} + \rho_{\mathrm{g}}C_{\mathrm{pg}}u\frac{\partial T}{\partial x} = \lambda_{\mathrm{e}}\frac{\partial^2 T}{\partial x^2} + (1-\varepsilon)r\Delta H \tag{2.16}$$

By ignoring the convective heat transfer by water vapour, Monazam *et al.* [64] proposed another equation for energy balance of a damp coal mass,

$$(1-\varepsilon)\rho_{\mathrm{c}}C_{\mathrm{pc}}\frac{\partial T}{\partial t} = \lambda_{\mathrm{e}}\frac{\partial^2 T}{\partial x^2} - \rho_{\mathrm{g}}C_{\mathrm{pg}}u\frac{\partial T}{\partial x} + r\Delta H(1-\varepsilon) + (1-\varepsilon)\Delta H_m r_m \tag{2.17}$$

Arisoy and Akgun [57] improved Schmal's model by adopting a non-equilibrium thermal model to study the effect of moisture, which gives,

For solid phase:

$$(1-\varepsilon)\rho_{\mathrm{c}}C_{\mathrm{pc}}\frac{\partial T_{\mathrm{c}}}{\partial t} = \lambda_{\mathrm{c}}\frac{\partial^2 T_{\mathrm{c}}}{\partial x^2} + (1-\varepsilon)\frac{3}{Ra}h\left(T_{\mathrm{g}} - T_{\mathrm{c}}\right) - (1-\varepsilon)\Delta H_m r_m + (1-\varepsilon)r\Delta H \tag{2.18}$$

For gas phase:

$$\varepsilon\frac{\partial}{\partial t}\left(\rho_{\mathrm{g}}C_{\mathrm{pg}} + \rho_{\mathrm{m}}C_{\mathrm{pm}}\right)T_{\mathrm{g}} + u\frac{\partial}{\partial x}\left(\rho_{\mathrm{g}}C_{\mathrm{pg}} + \rho_{\mathrm{m}}C_{\mathrm{pm}}\right)T_{\mathrm{g}} = \varepsilon\lambda_{\mathrm{g}}\frac{\partial^2 T_{\mathrm{g}}}{\partial x^2} - (1-\varepsilon)\frac{3}{Ra}h\left(T_{\mathrm{g}} - T_{\mathrm{c}}\right) \tag{2.19}$$

Later Akgun and Essenhigh [58] extended the one-dimensional non-equilibrium thermal model into two dimensions, which yields,

For solid phase:

$$(1-\varepsilon)\rho_{\mathrm{c}}C_{\mathrm{pc}}\frac{\partial T_{\mathrm{c}}}{\partial t} = \lambda_{\mathrm{c}}\left(\frac{\partial^2 T_{\mathrm{c}}}{\partial x^2} + \frac{\partial^2 T_{\mathrm{c}}}{\partial y^2}\right) + (1-\varepsilon)\frac{3}{Ra}h\left(T_{\mathrm{g}} - T_{\mathrm{c}}\right) + (1-\varepsilon)r\Delta H - (1-\varepsilon)r_{\mathrm{m}}\Delta H_{\mathrm{m}} \tag{2.20}$$

For gas phase:

$$\varepsilon\frac{\partial T_{\mathrm{g}}}{\partial t}\rho_{\mathrm{g}}C_{\mathrm{pg}} + \rho_{\mathrm{g}}C_{\mathrm{pg}}\left[\frac{\partial}{\partial x}\left(uT_{\mathrm{g}}\right) + \frac{\partial}{\partial y}\left(vT_{\mathrm{g}}\right)\right] = \lambda_{\mathrm{g}}\left(\frac{\partial^2 T_{\mathrm{g}}}{\partial x^2} + \frac{\partial^2 T_{\mathrm{g}}}{\partial y^2}\right) - (1-\varepsilon)\frac{3}{Ra}h\left(T_{\mathrm{g}} - T_{\mathrm{c}}\right) \tag{2.21}$$

2.3.2 Mass conservation

Most models assumed mass of solid coal particle remains unchanged prior to ignition and therefore mass conservation study was focused on oxygen conservation and water vapour conservation (for a moist coal stockpile). Schmal *et al.* [52]

proposed a one dimensional mass balance model for both oxygen and moisture, which yields,

For oxygen:

$$\varepsilon \frac{\partial C_{\mathrm{o}}}{\partial t} + u \frac{\partial C_{\mathrm{o}}}{\partial x} - \varepsilon D_{\mathrm{o}} \frac{\partial^2 C_{\mathrm{o}}}{\partial x^2} + (1-\varepsilon) r = 0 \tag{2.22}$$

In which the successive terms represent the local accumulation of oxygen, the convective transport of oxygen, the diffusion of oxygen, and the consumption of oxygen due to coal oxidation.

For moisture:

$$\frac{\partial C_{\mathrm{m}}}{\partial t} - \frac{\partial (U C_{\mathrm{m}})}{\partial x} = 0 \tag{2.23}$$

The successive terms represent the transient accumulation of moisture at the coal particle and the rate of evaporation (or condensation). Hull *et al.* [62] also used a one dimensional model to study the role of the diffusion of oxygen in a confined storage by eliminating volumetric convective component, which gives,

$$\varepsilon \frac{\partial C_{\mathrm{o}}}{\partial t} = \varepsilon D_{\mathrm{o}} \frac{\partial^2 C_{\mathrm{o}}}{\partial x^2} - (1-\varepsilon) r \tag{2.24}$$

Krishnaswamy *et al.* [61] developed the oxygen balance equation to two dimensions but molecular diffusion is ignored and a pseudosteady state is assumed, and these assumptions produce,

$$u \frac{\partial C_{\mathrm{o}}}{\partial x} + v \frac{\partial C_{\mathrm{o}}}{\partial y} = -r \tag{2.25}$$

Arisoy and Akgun [57] developed another one-dimensional conservation model for both oxygen and moisture, with similar form of Schmal's model,

For oxygen:

$$\varepsilon \frac{\partial \rho_{\mathrm{o}}}{\partial t} + u \frac{\partial \rho_{\mathrm{o}}}{\partial x} = \varepsilon D_{\mathrm{o}} \frac{\partial^2 \rho_{\mathrm{o}}}{\partial x^2} - (1-\varepsilon) r \tag{2.26}$$

For moisture:

$$\varepsilon \frac{\partial \rho_{\mathrm{m}}}{\partial t} + u \frac{\partial \rho_{\mathrm{m}}}{\partial x} = \varepsilon D_{\mathrm{m}} \frac{\partial^2 \rho_{\mathrm{m}}}{\partial x^2} + (1-\varepsilon) r_{\mathrm{m}} \tag{2.27}$$

Akgun and Essenhigh [58] developed a more complete mass conservation model for both oxygen and moisture in two dimensions, which produces,

For oxygen:

$$\varepsilon \frac{\partial \rho_{\mathrm{o}}}{\partial t} + \left(u \frac{\partial \rho_{\mathrm{o}}}{\partial x} + v \frac{\partial \rho_{\mathrm{o}}}{\partial y} \right) = \varepsilon D_{\mathrm{o}} \left(\frac{\partial^2 \rho_{\mathrm{o}}}{\partial x^2} + \frac{\partial^2 \rho_{\mathrm{o}}}{\partial y^2} \right) - (1-\varepsilon) r \tag{2.28}$$

For moisture:

$$\varepsilon \frac{\partial \rho_{\mathrm{m}}}{\partial t} + \left(u \frac{\partial \rho_{\mathrm{m}}}{\partial x} + v \frac{\partial \rho_{\mathrm{m}}}{\partial y} \right) = \varepsilon D_{\mathrm{m}} \left(\frac{\partial^2 \rho_{\mathrm{m}}}{\partial x^2} + \frac{\partial^2 \rho_{\mathrm{m}}}{\partial y^2} \right) - (1-\varepsilon) r_{\mathrm{m}} \tag{2.29}$$

Carras and Young [33] summarised a general form of mass balance which can be applied in both oxygen and water vapour, the general form was written as,

$$\varepsilon \frac{\partial C}{\partial t} + \varepsilon U \nabla C - D \nabla^2 C + S = 0 \tag{2.30}$$

Yuan and Smith [24, 72] developed a generic mass transfer equation in three dimensions by ignoring localized accumulation of gaseous species, which gives,

$$\rho u \frac{\partial C_\mathrm{o}}{\partial x} + \rho v \frac{\partial C_\mathrm{o}}{\partial y} + \rho w \frac{\partial C_\mathrm{o}}{\partial z} = \rho D_\mathrm{o} \frac{\partial^2 C_\mathrm{o}}{\partial x^2} + \rho D_\mathrm{o} \frac{\partial^2 C_\mathrm{o}}{\partial y^2} + \rho D_\mathrm{o} \frac{\partial^2 C_\mathrm{o}}{\partial z^2} + S \tag{2.31}$$

More recently the oxygen conservation equation proposed by Zhu *et al.* [26] and Xia *et al.* [98] has the same form as the generalised description of Equation (2.30),

$$\varepsilon \frac{\partial C}{\partial t} + \left(u \frac{\partial C}{\partial x} + v \frac{\partial C}{\partial y} \right) = D \left(\frac{\partial^2 C}{\partial x^2} + \frac{\partial^2 C}{\partial y^2} \right) - (1 - \varepsilon) r \tag{2.32}$$

$$\varepsilon \frac{\partial C_\mathrm{o}}{\partial t} + \nabla(-\varepsilon D \nabla C_\mathrm{o}) + U \nabla C_\mathrm{o} = r \tag{2.33}$$

2.3.3 Momentum balance

By making the Boussinesq approximation which essentially states that the temperature variation of the fluid properties can be ignored except for the density, and that the density dependence is only considered when it gives rise to buoyancy convection [132] and using Darcy's model to replace the shear stress tensor, Young *et al.* [55] proposed the motion equation in porous coal pile,

$$-\nabla P - \frac{\rho_\mathrm{am}\, g}{k} U + \rho_\mathrm{g} g = 0 \tag{2.34}$$

Later in buoyance-driven model of Edwards's work [59], a similar manner was used to develop the motion equation into two components, which shows,

$$\begin{cases} \dfrac{\partial P}{\partial x} = -\dfrac{\mu}{k} u \\ \dfrac{\partial P}{\partial y} = -\dfrac{\mu}{k} v + \rho_\mathrm{am}\, g \left(1 - \dfrac{T_\mathrm{am}}{T_g} \right) \end{cases} \tag{2.35}$$

The permeability *k* of coal matrix is approximated by the Blake–Kozeny equation for laminar flow in packed beds [24, 26, 59, 61, 72, 73, 115, 133], which gives,

$$k = \frac{\varepsilon^3 d^2}{150(1-\varepsilon)^2} \tag{2.36}$$

Many other works also used Darcy's law to describe flow in porous stockpile and additionally incorporates buoyancy convection as a possible mechanism of flow in porous medium as formulated by Edwards's work [35, 58, 60, 61]. The equation was generalised by Carras [33] and the universal form is written as,

$$U = \frac{k}{\varepsilon \mu} (-\nabla P + \rho g) \tag{2.37}$$

The first term in Equation 2.37 describes flow due to a pressure gradient while the second term describes the buoyancy due to gas density changes with temperature. For a very coarse coal stockpile (3~20cm), Zhu *et al.* [26] argued it is more appropriate to describe flow in Brinkman's law because of high Darcy number and Reynolds number [134], and motion of gas flow should be written as,

$$\begin{cases} \frac{\partial P}{\partial x} = \mu \frac{\partial^2 U}{\partial x^2} - \frac{\mu}{k} u \\ \frac{\partial P}{\partial y} = \mu \frac{\partial^2 U}{\partial y^2} - \frac{\mu}{k} v + \rho_{\mathrm{g}} g \left(1 - \frac{T_{\mathrm{am}}}{T_{\mathrm{g}}}\right) \end{cases} \tag{2.38}$$

Nevertheless above models yields a steady flow field, to date, commercial CFD code is capable of handling a transient flow field which can be given by [66],

$$\rho_{\mathrm{g}} \left(\frac{\partial U}{\partial t} + U \nabla U\right) = -\nabla P - \varepsilon U \frac{\mu}{k} + \mu \nabla^2 U - \rho_{\mathrm{g}} g \beta \left(T_{\mathrm{g}} - T_{\mathrm{am}}\right) \tag{2.39}$$

In which the successive terms represent the transient momentum response, advection of momentum, pressure gradient, Darcy force, Brinkman effects and buoyant force.

2.3.4 Continuity

The continuity equation also assumes the validity of the Boussinesq approximation, which gives rise to the continuity equation [33, 55, 60, 61],

$$\nabla U = 0 \tag{2.40}$$

In a quasi steady-state approximation for the gas flow, the mass flux can be defined in terms of a stream function [55, 58, 59],

$$\begin{cases} \rho_{\mathrm{g}} u = -\frac{\partial \psi}{\partial \mathrm{y}} \\ \rho_{\mathrm{g}} v = \frac{\partial \psi}{\partial \mathrm{x}} \end{cases} \tag{2.41}$$

With CFD code, Kim and Sohn [73] proposed a three dimensional transient continuity equation with absence of the Boussinesq approximation, which yield,

$$\frac{\partial \rho}{\partial t} + \frac{\partial \rho u}{\partial x} + \frac{\partial \rho v}{\partial y} + \frac{\partial \rho w}{\partial z} = 0 \tag{2.42}$$

2.4 Experimental methods

It has been revealed that oxidation of coal results in the following processes: (a) consumption oxygen and evolution of gaseous products; (b) changes in the mass and physical structure; (c) modification of the molecular structure of coal and its elemental composition; (d) self-heating of coal due to heat generated from oxidation [17]. Various experimental methods were developed to quantify these changes during coal oxidation, refer Table 2.3.

Table 2.3A summary of experimental methods employed for studying oxidation and self-heating of coal

Parameters measured	Experimental method	Description	Representative works
Oxygen consumption and gaseous products evolution	Isothermal reactor and static oxygen sorption	An oxidation medium flows through the coal bed in a sealed sample container while the temperature is holding approximately constant throughout the system. Gas analysers are used to measure the reduction in oxygen concentration. This reduction reflects the amount of oxygen absorbed and is used to rank liability of coal to spontaneous combustion. One drawback of such a test is that it is time-consuming to reach adsorption equilibrium when gas-adsorption experiment on a coal sample is conducted at low temperatures.	[7, 96, 135-137]
	Gaseous products evolution	Besides oxygen consumption, many gaseous products like carbon dioxide, carbon monoxide, methane, hydrogen, ethylene, and ethane evolve during coal oxidation. The composition and quantities of the mixed gas have a correlation with the elevated temperature. The coal oxidation reactor is often made in adiabatic or programmed controlled temperature conditions. A Gas Chromatograph (GC) is often used to determine the concentrations of various gas species of the effluent gas at regular temperature increments. The gas evolution trend that occurs in response to heating of coal can be a useful tool for early detection of a spontaneous combustion incident.	[5, 21, 138-141]
Changes in the mass and physical structure	Thermogravimetric Analysis (TGA)	TGA is a thermoanalyticmethod in which changes in mass of a coal are measured as a function of temperature elevation, or as a function of time. The thermogravimetric(TG) and differential thermogravimetric (DTG) information can be applied to develop the kinetic models of coal oxidation and combustion[17]. However due to instrumental accuracy and inherent moisture, TGA has limited application in studying coal oxidation at low temperatures.	[111, 142-147]
	Microscopic observation	Various microscopic methods such as Scanning Electron Microscopy (SEM), Atomic Force Microscopy (AFM), X-Radiation (X-Ray), Nuclear Magnetic Resonance (NMR), were used to identify the macerals and mineral matter on fresh coal surface and effects of oxidation upon the optical properties of coal and coal macerals were also examined.	[148-153]
	Pore volume distribution	Apparatus like mercury porosimeter were employed to measure pore size distributions of different coals and correlates the information to oxidation rates of these coals.	[8, 108]

Coal molecular structure and elemental composition modification	IR, FTIR, XPS,SIMS and 13^{C} NMR	Various physical and chemical analytical techniques have been applied to identify and quantify solid oxygenated complexes generated from coal oxidation. These techniques include Fourier Transform Infrared spectroscopy (FTIR), Infrared spectroscopy (IR), Secondary Ion Mass Spectrometry (SIMS), X-ray Photoelectron Spectroscopy (XPS), and 13^{C} Nuclear Magnetic Resonance (13^{C} NMR).	[6, 86, 154-165]
	ESR and EPR	A free radical is any atom or molecule that has a single unpaired electron in an outer shell. Free radical concentration increases during coal oxidation and this was deemed to be a result of breakdown of organic functional group. Techniques like Electron Spin Resonance (ESR) and electron paramagnetic resonance spectroscopy (EPR) have been used to investigate free radical involvement in the oxidation of coals.	[166-170]
Self-heating	Isothermal and adiabatic calorimeters	These instruments are usually equipped with a calorimetric vessel containing the coal sample, with the vessel surrounded by a layer of heat insulation and an external temperature control unit. In isothermal calorimeters, the vessel is maintained at a constant temperature, and the heat released by chemical reactions occurring in the sample is determined by measuring the heat dissipated to the environment. By placing the entire isothermal calorimeter in an oven it is also possible to carry out the measurement at different temperatures. In adiabatic calorimeters, the heat liberated from coal oxidation is not allowed to transfer to the ambient, and the released heat is then calculated from measuring the temperature rise within the vessel. The adiabatic conditions are often achieved using an oven, within which the sample is enclosed, and temperature of the oven is increased to match that detected by a thermometer within the sample.	[9, 135, 171-173]
	Adiabatic oven	Like adiabatic calorimeter, coal sample is placed in a reaction vessel in which heat transfer with ambient is minimised by placing the reaction vessel inside an adiabatic oven or oil bath. The oven temperature is controlled automatically to catch up with that of the sample, thus minimising heat losses. This method is used to directly measure heating rates of coal oxidation and the information can be used to determine low temperature coal oxidation kinetics.	[174-179]
	Differential Thermal Analysis (DTA)	DTA is another thermoanalytic technique in which the testing material and an inert reference material are designed to undergo same thermal cycles and meanwhile any temperature difference between them is recorded. DTA test of coal involves heating of a small amount of coal sample at a controlled increment, and continuously recording the temperature difference between the coal sample and the inert reference material. The information of temperature difference against the temperature is then used in the analysis of the heat evolution and chemical reactions occurring during coal oxidation.	[142, 144]

	Basket heating	The method was developed by Bowes and Cameron [75, 180]on basis of the Frank-Kamenetskii model for thermal explosion of piled solids. The procedure has the following steps: A basket of particular size and shape, filled with prepared coal sample, is placed in an oven in which the temperature is allowed to reach a preset level. A thermocouple inside the coal sample indicates whether combustion occurs. If the sample does not ignite, the experiment is repeated with the oven temperature preset to a higher value. The minimum ambient temperature for spontaneous combustion of coal is then determined. A series of experiments can be carried out for baskets of the same shape but different sizes, so as to determine the critical temperatures for baskets of different sizes. For practical applications, the experimental data can be used to evaluate a safe dimension of a coal stockpile and for determining the apparent chemical kinetics for coal oxidation by a means of the Frank-Kamenetskii model.	[33, 75, 112, 180]
	Crossing Point Temperature (CPT)	This method provides information about the onset of significant self-heating in a coal sample under specific conditions. The method often involves following steps: (1) crushing coal sample to a standard size; (2) subjecting the sample to a specific atmosphere before and during a test; (3) sample is placed in an oven at a predetermined initial temperature; (4) increase oven temperature at a constant and standardised rate and the sample temperature is monitored; (5) measuring the temperature at which sample temperature exceeds that of the oven, indicating ignition has taken place. The CPT can be used for ranking the propensity of coal to self-heating.	[171, 181-184]
	Differential Scanning Calorimetry (DSC)	DSC is also a thermoanalytic technique in which the difference in the amount of heat required to increase the temperature of a coal and reference material is measured as a function of temperature. Both the coal and reference are maintained at the same temperature throughout the experiment. The reference sample should have a well-defined heat capacity over the range of temperatures to be scanned. The result of a DSC experiment is a curve of heat flux versus temperature or versus time. The information can be used to assess the reaction kinetics of coal oxidation.	[111, 145, 185, 186]

2.5 Detection

There has been continual debate about the incubation period for spontaneous combustion and used the time as a buffer to control the spontaneous combustion. However, the reliance is problematic because incubation period depends on a range of factors from specific on-site conditions to properties of coal. The oxidation process occurs at ambient temperatures and a heating may not be detected until the temperature reaches two or three times the ambient temperature. It is important to realise that the time required for a heating to develop to a dangerous stage is hard to determine because it is unlikely to be certain when the heating has initiated. Only the time from when the heating is firstly detected to when miners must be withdrawn is available for effective action. Therefore early indication of an onset heating is very crucial because it allows time for exercising control measures before the situation escalates to a serious contingency.

2.5.1 Physical indicators

The observation of physical signs is an important alternative for early detection. These physical signs are: (1) smoke; (2) haze; (3) sweating; (4) smell; and (5) heat[187]. Smoke consists of ultra-fine particles (<1μm diameter) which are either incompletely combusted solid material or recondensed volatile organic matters. Smoke is, however, not an early indicator of spontaneous combustion because the coal temperature will have overtaken 300^{o}C before smoke is observed. A haze can be generated by the condensation of volatile components of coal and/or water vapour evaporated due to heatings. Hazes occur at lower temperatures than smoke but it should be noted hazes can also be produced from other sources like diesel vehicle emissions. Sweating is the condensation of water vapour which is evaporated from heating of coal mass on cooler surfaces. Sweating is an earlier indicator than smoke or haze. The presence of an unusual smell is also an indicator of spontaneous combustion of coal. The nature of the odour is derived from the volatile organic compounds liberated as the coal heats up both as distillation products and also as oxidation products. However smell is a human sense that varies from individual to individual regarding sensitivity and capture of the odour. The temperature rising due toa spontaneous heating can be detected in a few ways. Direct measurement of the increase in temperature by thermocouples or other devices is limited to contact with the hot mass of coal or the immediate hot gaseous products stream. Indirect methods

like infrared techniques are capable of detecting hot spots remotely and are widely used for detection of heatings.

2.5.2 Gas monitoring

As discussed many types of gases would be generated during coal oxidation at different temperatures. Gases including CO_2, CO, CH_4, H_2, C_2H_4, C_2H_2, and other higher hydrocarbon gases are liberated due to decomposition and pyrolysis of oxygenated hydrocarbons [25, 188]. In laboratory gas evolution tests are useful in determining the behaviour of the coal as it heats and the development of gaseous indicators for early detection. These tests may be performed in small scale or bulk scale techniques. Figure 2.5provides a general order (also known as "fire ladder") of evolution of gaseous products of coal oxidation against temperature.

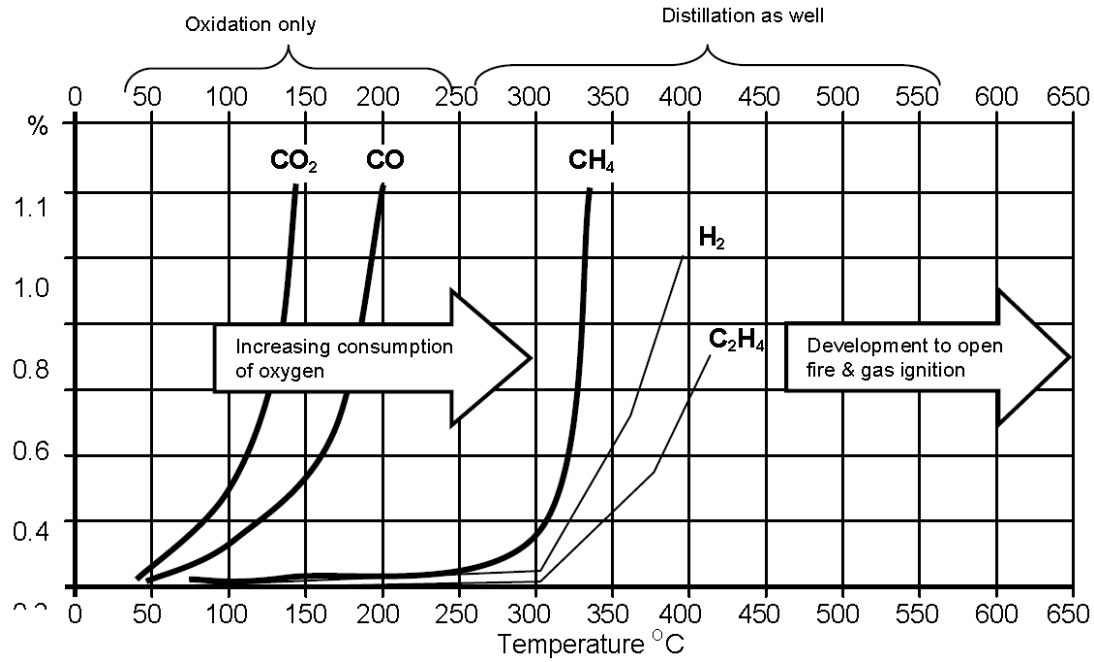

Figure 2.5 A general hierarchy of gas evolution against temperature

It can be seen the first gas liberated is carbon dioxide but besides coal oxidation the gas may also source from coal seam gas. The followed is carbon monoxide, methane, and hydrogen. The information of methane is possible to be misleading as it is also a part of coal seam gas. If temperature keeps going (generally>100^{o}C), ethane and ethylene may be generated. The two gases can be used to forecast an advanced heating. Higher hydrocarbons appear as temperature is really high and the presence of the gases indicates a serious heating is taking place and countermeasures must be exercised. As discussed different types of gases and different concentrations of a particular gas would be generated at different temperatures. This information can be

used to aid to forecast onset heating of underground coal through interpretation of gas monitoring data. Therefore monitoring of mine atmosphere especially composition of goaf gas offers a means of early prediction of mine fire and allows implementation of proper controlling actions. The widely used mine atmosphere monitoring techniques include: (1) Tube bundle system, (2) Telemetric system, (3) Gas chromatography, and (4) Portable detector.

2.5.2.1 Tube Bundle System (TBS)

A tube bundle system (TBS) is a continuous gas monitoring system for drawing gas samples through tubes running from multiple monitoring spots located in underground coal mines to surface testing analysers. The analysers are typically analysed for methane, oxygen, carbon monoxide and carbon dioxide. Results of the gas analyses are displayed and logged for further interpretation. TBS is a well-developed technology and has been used in coal mines around the world for more than 50 years [189]. The primary uses of a TBS are detecting early development of spontaneous combustion and determining atmosphere behind sealed areas. A schematic of a tube bundle system is shown Figure 2.6.

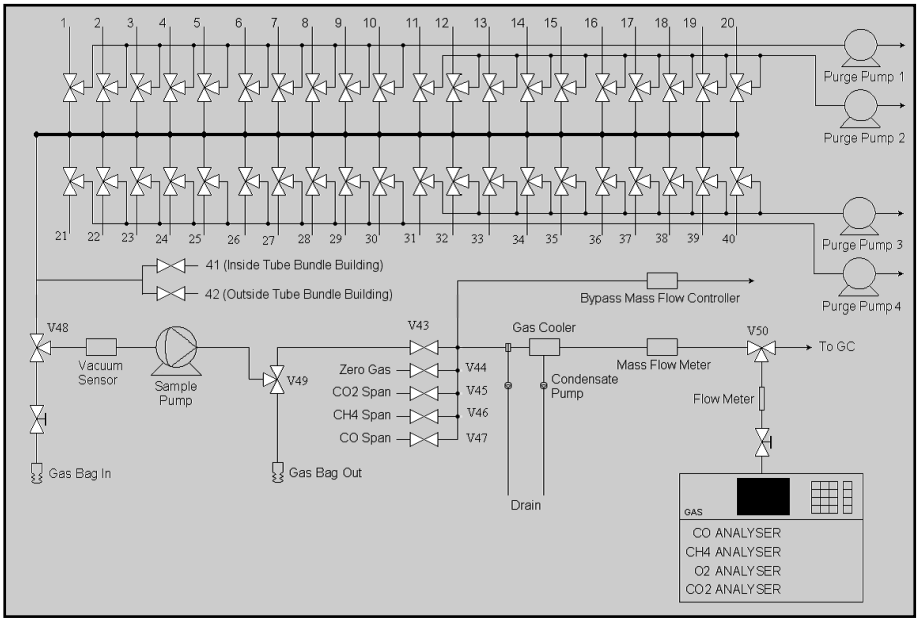

Figure 2.6 A scheme of TBS [187]

A major advantage of the tube bundle system is that it draws the sample to the surface and no additional underground trips are required to collect gas samples. This is particularly advantageous in emergency situations when working force may have been evacuated from the mine and re-entry is prohibited. The deployment of rescue teams to collect samples during spontaneous combustion events may result in the

tragic loss of life when the spontaneous combustion activity has acted as an explosion source if gas mixture falls into explosive range. Strategic placement of sampling locations can overcome the need to send crew underground to collect samples and avoid such tragic outcomes in an emergency. Another advantage is there is no need for the analysers to be intrinsically safe and to withstand underground harsh conditions. The reason is that the analysers are deployed on the surface and therefore instrumentation designed to be operated in a laboratory environment can be used.

There are also some disadvantages of TBS application. To draw the gas sample from underground a negative pressure is applied to the plastic tube via pumps, there is the possibility that the untested gas sample would be diluted if somewhere the tube is damaged or connection fittings are not properly sealed. Modern tube bundle systems incorporate the logging of vacuum pressures and the activation of alarms if pressures fall outside expected values. This assists the operator to determine if leaks develop or flow through the tube becomes restricted [187]. The lengths of tube are normally very long up to several kilometres and it can take over one hour for gas samples to reach the surface or even longer if water or dirty particle matter builds up in tube. It is very critical for mine operators to know this "time gap" particularly in emergency situations. Since the samples are often being drawn from harsh environments (humid and dusty), they are required to undergo conditioning prior to being passed to the sensitive analytical instruments. For the system to remain operational these sample conditioning components must be well maintained on a regular basis.

2.5.2.2 Telemetric System (TS)

TS is generally used where real time data is required and can therefore provide early warning for the onset of mine fire especially belt fire in roadway. The telemetric sensors include several types including catalytic combustion (for methane detection), electrochemical (for carbon monoxide and oxygen detection) and simple infra-red detectors (carbon dioxide and methane detection) [27]. The sensors make the measurement and the signal is fed back to the surface data acquisition and display system on real time. An installation of the sensors is shown in Figure 2.7. Most of these sensors (except infra-red) require the presence of oxygen to trigger a chemical reaction and thus induce change of electrical current to be measured. Therefore they are unsuitable for monitoring areas of low oxygen concentration such as sealed or

non-ventilated goafs. The sensors used for telemetry systems are often limited in their range of detection: carbon monoxide is often only capable of being measured up to 50ppm, methane up to 5% and carbon dioxide up to several percent [187]. They are generally more unstable, can be cross-sensitive with other gases and have a much lower operational life expectancy than the types of analysers that are used for TBS. Despite these limitations, the real time monitoring capability of this type of system is very important for providing early warning of spontaneous combustion for a mine site.

Figure 2.7 Telemetric detector installedin underground

2.5.2.3 Gas Chromatography (GC)

GCs are used to provide accurate analysis of components that are not routinely monitored by TS or TBS. These components, including hydrogen and hydrocarbons such as ethylene and ethane, are very possible to be critical in determining the severity of a heating incident. GC is the only technique when assessing the underground atmosphere after a fire or an explosion as neither TBS nor TS are capable of measuring the high carbon monoxide concentrations and hydrogen which contribute significantly to the presence of explosive gas mixture. The working principle of GC is shown in Figure 2.8. A gas sample is introduced into a column and is pushed through the column by an inert “carrier gas” (argon, helium, or nitrogen). The gas sample has intended interactions with the packing in the column during passing through the column. A particular gas species has a unique interaction in the column and as a result, different gas components are separated and exit the

column at different and predictable time orders. Thus this allows the measurement of individual components using a detector placed at the column outlet.

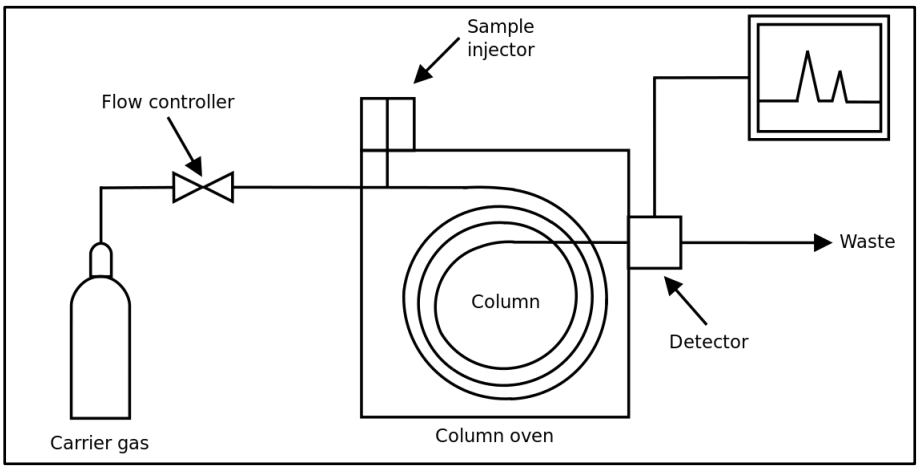

Figure 2.8 Working scheme of a GC

For GC application at coal mine site, Simtars developed a Computer Assisted Mine Gas Analysis System–CAMGAS, for use at underground mines with dedicated software. NSW Mines Rescue Service has also developed a similar system SMARTGAS. Since 1990s GCs have been installed at Australian mine sites, this technique has reduced sample analysis times and improved sensitivity. However, analysis times of the conventional GCs were too slow for the high volume sampling rates required during emergency situations. Additionally they required relatively frequent maintenance and a high level of operator expertise. The traditional systems are no longer considered to be an appropriate analytical tool for gas monitoring during a spontaneous combustion incident. The introduction of ultra-fast micro gas chromatographs into the market resulted in a wider acceptance and use of gas chromatographic systems at coal mine sites [27]. They provide analytical run times of between 1-3 minutes for the analysis of key spontaneous combustion gas components. They generally utilise a single Thermal Conductivity Detector (TCD), require less maintenance than conventional GCs and are relatively simple to operate. GC is intended for detailed determinations of small numbers of gas samples. It can be used to confirm the results and accuracy of other monitoring systems like TS and TBS. It is ideal for determining concentrations of key spontaneous combustion indicator gases.

2.5.2.4 Portable detector

The portable detector contains sensor heads similar to those installed in the telemetric detectors and an electronic digital display is also fitted. Most modern

portable monitors have data loggers or persons who are operating the monitors have to manually record the results. The device was designed to measure concentrations of gas components including carbon monoxide, methane and oxygen. There are now improved detectors which are capable of monitoring six or more gas components. The device is intended as an early warning device of dangerous conditions and an alarming is activated once pre-set gas concentrations are exceeded. The technique is ideal for a detailed investigation at a specific spot in real time. The major problems with these devices are cross sensitivity (particularly H_2S interference with other gases) and contamination [187]. The monitor can be used to pinpoint the source of an emission, to check the reading of a fixed sensor or monitoring point and to identify layering.

2.5.2.5 Monitoring location

To keep effectiveness of a monitoring system, it is paramount to install the monitoring points in right locations where key spontaneous combustion gases can be detected. If a sampling point somehow deviates the intended detecting source, the readings often lead to either an over estimate or under estimate of the severity level of a spontaneous combustion incident.

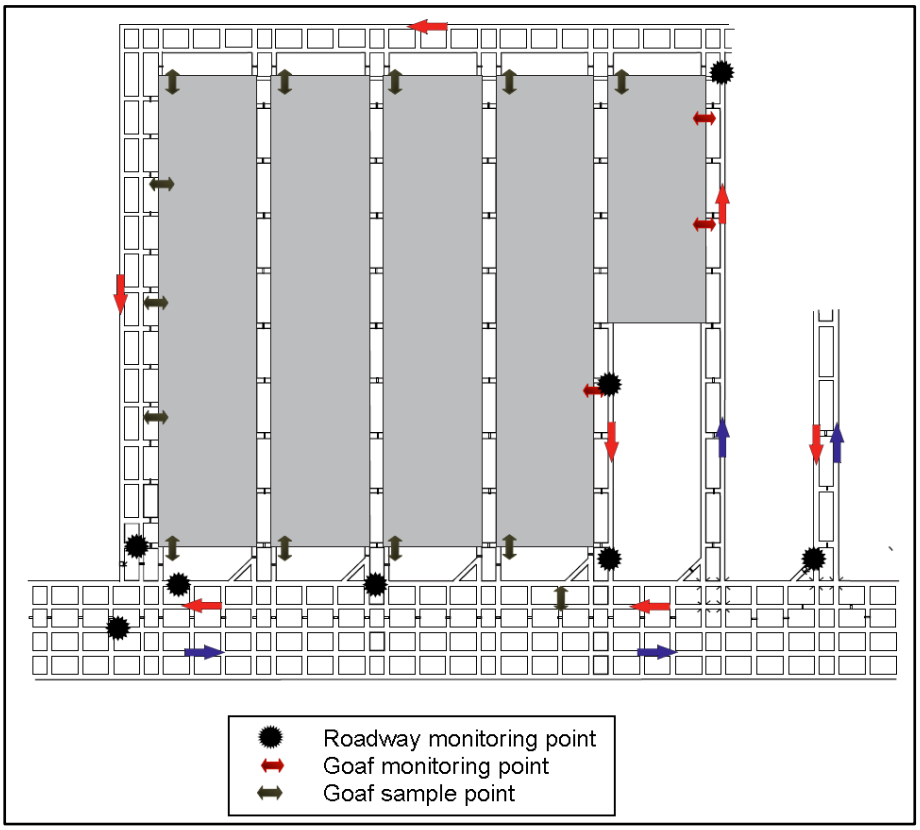

Figure 2.9 Suggested allocation of gas monitoring points for a longwall panel [27]

Generally monitoring points must be located where heatings are likely to develop and extra consideration should be given to layering of methane and warm spontaneous combustion gases may rise up in a goaf. Monitoring points should be allocated in panel returns, behind goaf seals and in the main airways of the ventilation circuit. Figure 2.9 provides a suggested plan for the distribution monitoring points for a longwall panel. It includes surrounding gateroads and goaf monitoring points for the current and adjacent longwall goafs. Location and frequency of sampling should be based upon results of atmospheric analysis, stability and an assessment of the hazard [27].

2.5.2.6 Data interpretation

Interpretation of the gas monitoring data is equally important. However there are several problems with using direct monitoring concentrations of gases to estimate the status of an on-going incident. These problems include: (1) dilution with other gas streams; (2) indicator gases come from other sources like seam gas or diesel combustion; (3) fails to indicate the intensity of a heating. To overcome these problems, indicators utilising combinations of gas concentrations and/or air velocity have been developed. These methods may include:

- Graham's ratio;
- CO/CO_2 ratio;
- CO make;
- Trickett's ratio;
- Young's ratio;
- H_2/CO ratio;
- Air free analysis.

The detailed explanations and calculations of these indices are given in many literatures [187, 190, 191]and therefore will not be provided here. The indices are also an important element in mine Trigger, Action, Response, Plans (TARPs). The three most useful indicators for TARPs are:

- Graham's ratio: the ratio steadily increases as the heating progresses and it indicates the intensity or temperature of a heating;
- CO/CO_2: the ratio also gradually increases as the heating progresses (not suitable for mines where main seam gas is CO_2);
- CO make: the value compensates for varying airflow quantity.

2.6 Control

2.6.1 Inertisation

The concept of inertisation is to exclude oxygen rich air from a fire or heating by the introduction of an oxygen-free medium which mostly refers to gas but liquid is also included. This has been the most widely used and the most principal mean of extinguishing or controlling goaf heatings for decades. Inertisation of a goaf area can be an effective immediate control if provision has been made for it to done quickly. This allows time for investigation and implementation of a long term control. If surface access is not available for inertisation and an underground supply system has not been installed, sealing the whole of the mine may be the only option. Inertisation of the whole of the mine will then extinguish the heating. Many different inert gases can be used for fire control, but the three sources (i.e. Gaseous Combustion Products (GCP), carbon dioxide, and nitrogen) are preferable considering availability, cost and other factors. The methods of inertisation could be categorised on basis of origins of the inert gases. The classification of inertisation is compiled as Figure 2.10.

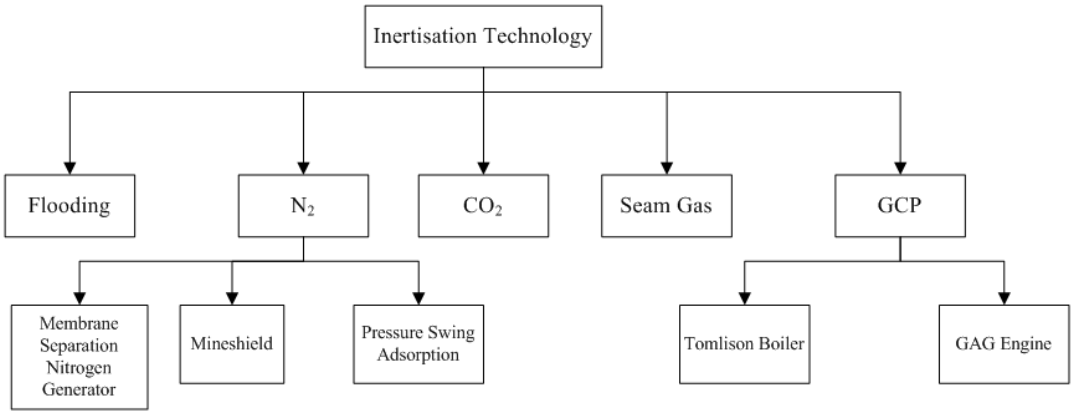

Figure 2.10 A category of inertisation technology

2.6.1.1 Flooding

Our predecessors had no access to more advanced inertisation technology and limited access to gas monitoring devices. They therefore had no choice but simply either extracted mining equipment and working force or sealed and flood mining area once fire was detected. Flooding with water is excellent at quenching fire for cooling strata purpose though. Two methods may be used: one quenches the fire by slowly submerging the heated material under water, the other utilises water and local gradients to prevent oxygen reaching the heating site. Apart from that, introduce of water can reduce gas volume in goaf to some extent and as a result reduce influence

of barometric alterations. However, extra care must be taken because goaf seal might be breached as hydrostatic pressure is growing in goaf [187].

2.6.1.2 Seam gas

Main composition of coal seam gas is methane and carbon dioxide and therefore seam gas could be a source of inert gas. However, the flaws of seam gas being used as inert gas are also obvious:

- Liberation of seam gas is very likely to be insufficient or accumulate at a slow rate as the pressure increases in sealed areas;
- As a main source of seam gas, methane is inherently combustible and explosive, and for the atmosphere to become sufficiently fuel-rich to exclude oxygen it almost invariably passes through the explosive range [187].

2.6.1.3 Membrane Separation Nitrogen Generator (MSNG)

The mechanism of producing nitrogen of a MSNG is to allow a flux of dried, compressed and filtered air flow through a polymeric hollow fibre. Different air components have different permeable velocities through the sidewall of polymeric fibre. Specifically, oxygen, carbon dioxide, and water vapour percolate through the membrane prior to nitrogen and as a result nitrogen is allowed to flow through its centre and emerge as product flowing out of its outlet. A bundle of hollow fibres are installed to form a high performance nitrogen generation module which allows expansion of existing systems for more capacity as opposed to installing a larger unit. Figure 2.11 describes how nitrogen is produced by MSNG and Figure 2.12 illustrates how the whole process is organised, respectively.

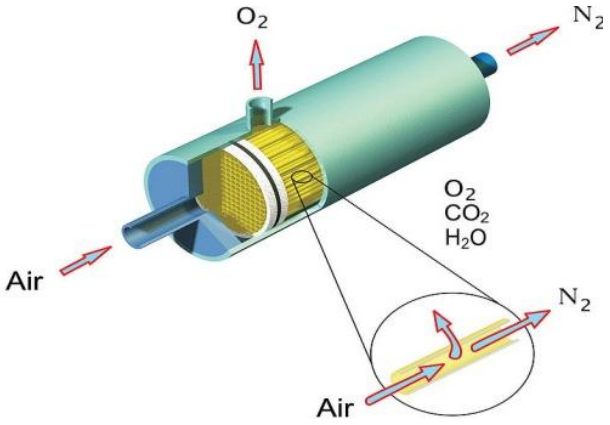

Figure 2.11 Flux distribution inside the fibre

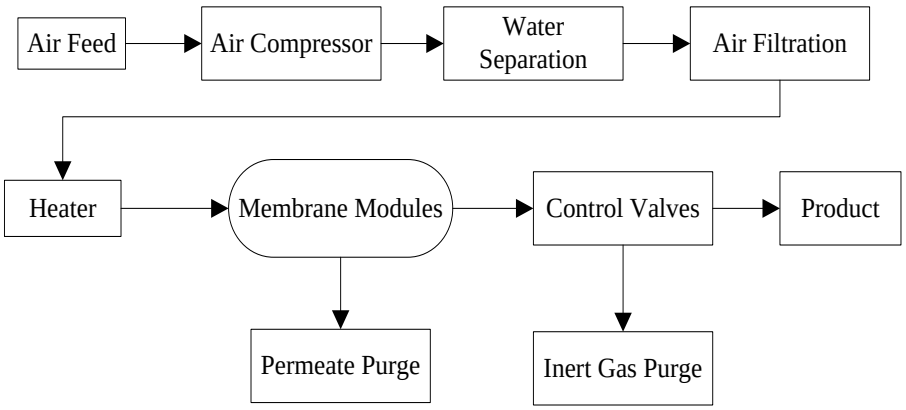

Figure 2.12 A typical working scheme of MSNG

An example of on-site MSNG unit used in Australian mining industry is the Advanced Membrane Supply Approach (AMSA) Floxal system which was owned and operated by Air Liquide. The working procedure of the AMSA Floxal system is: fresh air is filtered and compressed in a standard air-cooled single stage lubricated screw air compressor. Compressed air is cooled with a heat exchanger and dried with a refrigerated air drier. A condensate drain and two coalescing filters remove the liquid carryover entrained in the compressed air. An activated carbon filter removes hydrocarbons that may carryover past the filters. The clean dry air is then heated to ensure a uniform feed air temperature into the nitrogen membrane modules. As air passes through the membrane modules, oxygen and remaining water vapour are vented (discharged through the waste gas header) and nitrogen gas is concentrated. An oxygen analyser continuously monitors the produced nitrogen to ensure that oxygen levels are maintained at all times. Nitrogen gas is discharged from the AMSA at nine bar pressure[192]. The operation of the AMSA Floxal system is monitored and controlled by a Programmable Logic Controllor (PLC). The first record of the Floxal system used in Australia was Mining Technologies Australia (MTA) contracted with Air Liquide Australia to build, own and maintain two mobile Floxal on-site units in November 1998. The unit was initially designed to dilute both methane and oxygen at cutting head of the highwall mining system with capacity of producing 500m^3/hr inert gas. Air Liquide has then developed a bigger unit with capacity of 1934 m^3/hr to meet the specific requirements of underground mines. Figure 2.13below is a photographic view of the AMSA Floxal system.

Figure 2.13 A photographic view of the AMSA system used in Australia

2.6.1.4 Pressure Swing Adsorption (PSA) nitrogen generator

An alternative on site nitrogen generation method is called PSA process in which a bed of activated absorbent called Carbon Molecular Sieve (CMS) is applied to preferably capture O_2, CO_2, and H_2O molecule and allow N_2 molecule to pass through the CMS containing vessel. This process is operated with constant temperature, close to ambient temperature, and above atmospheric pressure. Then pressure is reduced to some degree to extract nitrogen molecule into the surge tank for further purification or application. Later the remaining pressure is removed to draw off oxygen molecule etc. to accomplish absorbent regeneration. The conceptual drawing of adsorption process is shown as Figure 2.14. The two processes could be multiply repeated to acquire purer product and continuous flow of nitrogen. It should be noted two adsorber tanks are involved concurrently to alternately accomplish pressurisation/adsorption process and depressurisation/desorption process.

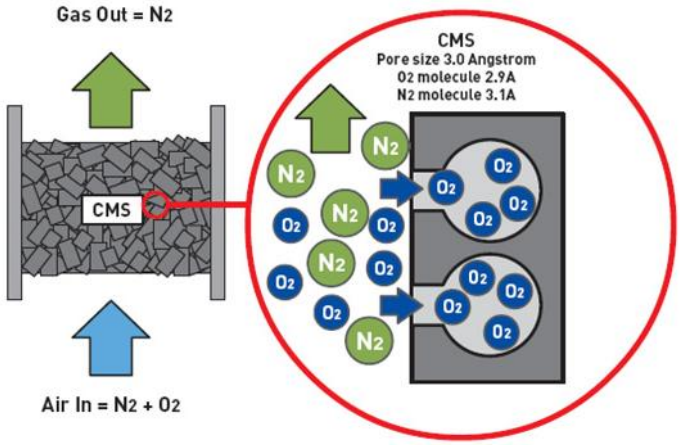

Figure 2.14 Conceptual drawing of adsorption process

PSA units are available in Australia, and at least 12 installations were operating in processing industries since 2004 [27]. Advantages of PSA nitrogen generator are:

minimal operation and maintenance is required; start-up and shut-down is controlled by a PLC; the plant operates at moderate temperatures and pressures; lower cost. However, the PSA unit is quite new to Australia mining industry. The rate of installation of modern PSA plants on a world-wide basis is increasing rapidly now. This technology may be well suited to the needs of Australian mining industry.

2.6.1.5 Mine shield

Mineshield unit operates by converting liquid nitrogen to gaseous nitrogen which is subsequently injected through a 150 mm hose and downhole into underground coal mine atmosphere. It was developed and owned by the NSW Mines Rescue Board at the Hunter Valley Rescue Station in response to the frequency of heatings in underground mines in 1980s and the Appin explosion in 1979 [193]. Figure 2.15 is a photographic view of the Mineshield inertisation unit.

Figure 2.15 Photographic view of the Mineshield unit

The main components and other requirements of Mineshield are[193]:

a) 40 tonne liquid nitrogen tanker ("mother tanker");
b) Two nitrogen cryogenic units;
c) Vaporiser trailer;
d) LPG (Liquefied Petroleum Gas)supply tanker;
e) Pump unit;
f) Site hardstand area;
g) Water supply(10,000L at start-up, plus ongoing supply)
h) A 400 kVA power supply, provided by grid or generator;
i) Communication lines and lighting;
j) Road access and turning facility for B-double tankers.

The flow rate is variable between 1 and 17 tonnes liquid nitrogen per hour. One ton nitrogen in liquid equates about 850 m^3 gaseous nitrogen, so the flow rate range is synonymously 0.24~4m^3/s gaseous nitrogen. The long term flow rate is approximately 10 tonnes per hour (approx. 2m^3/s gaseous nitrogen) and is dependent upon the road tankers continuing delivery of the liquid nitrogen. Mineshield was

firstly used for recover operation after 1986 Moura No 4 explosion. The detailof the first application of Mineshield were given by a report released by Department of Mines and Energy, Queensland State Government with respect to 1986 Moura No 4 explosion incident [194].

2.6.1.6 Tomlison Boiler (TB)

In order to overcome the Mineshield logistic and liquid nitrogen transport difficulties, some on-site inert gas generators were developed and introduced at the end of the 20^{th} century. The TB unit is one of them. The TB unit is a low flow GCP generator which produces CO_2 enriched exhaust gases from a diesel engine. A typical composition of the exhaust gases produced by the TB unit is:

a) Oxygen content—less than 2%;
b) Carbon dioxide content—12.5%~13.5%;
c) Nitrogen content—84%~85%;
d) Carbon monoxide—ppm level, but 1000ppm is expected if oxygen concentration less than 0.1% is obtained[195].

The exhaust gases were cooled from initial temperature of 1200^{o}C via a heat exchanger and air blower to a temperature of about 40^{o}C. This gas is then compressed in a water ring compressor to about 0.1 bar prior to discharging into mine goaf via a 150 mm hose and downhole. Figure 2.16 below shows a TB unit in operation. The capacity can be up to 1800 m^3/hr in full operation.

Figure 2.16 The TB unit in operation[27]

The first trial of TB application in coal mining industry were accomplished by both Cook Resource Mining (CRM) Ltd Cook colliery and South Blackwater Coal (SBC) Ltd Laleham mine in association with Statutory Management Services and a final formal ACARP report incorporating full details of this project was formed. This trial was primarily motivated by the findings and recommendations of the Moura No. 2 Inquiry after examining application of Mineshield and intended to produce fundamental and permanent modifications in the current inertisation approaches and protocols. Although the TB unit experienced a number of mechanical and electrical problems which resulted in down time of effective pumping at both sites, the inertisation results were promising and a demonstration arised was the TB unit has enormous potential for the elimination of potential explosive hazards.

2.6.1.7 GAG

GAG (Gorniczy Agregat Gasniczy) jet engine inert gas generator is another GCP generator with the highest flow rate (20~25 m^3/s) of all inert gas units used in mining industry. GAG jet engine was originally devised from a Polish military trainer aircraft engine and subsequently modified to produce inert gas by fitting with a afterburner and a diffusive cooler ensure that the engine no longer develops thrust or allows a flame to enter the atmosphere[196].Two GAG units were purchased following recommendations from the Moura No 2 explosion investigation at a cost of $1.3 million in early 1998 and handed over to the Queensland Mines Rescue Service (QMRS) for operation and maintenance. Typical gas makes and other important specifications of GAG engine are tabulated in Table 2.4. It should be noted CO make is substantially deviated from data cited from MDG 1006 TR which indicates approx. 400 ppm when turned correctly. Figure 2.17 and Figure 2.18show a photo of GAG engine sitting on truck and its schematic diagram respectively.

Table 2.4 Main operational parameters of the GAG inert gas generator[193]

Parameters	Unit	RPM	
		7200	11000
Flow	m^3/s	13.95	33.25
Fuel Consumption	litrs/min	17	32.5
Cooling Water for afterburner at 70kPa Range 60~90kPa	litrs/s	5	5
Water cooling system exhaust gas cooling at 350kPa Range 200~450kPa	litrs/s	7.5	7.5
Output gas temperature	°C	85	85
Gas make: Oxygen Carbon Dioxide Nitrogen Carbon Monoxide	 % % % ppm	 0~0.5 13~16 80~85 3	 0.5~2 13~16 80~85 3

Figure 2.17 GAG engine set up for transportation and use

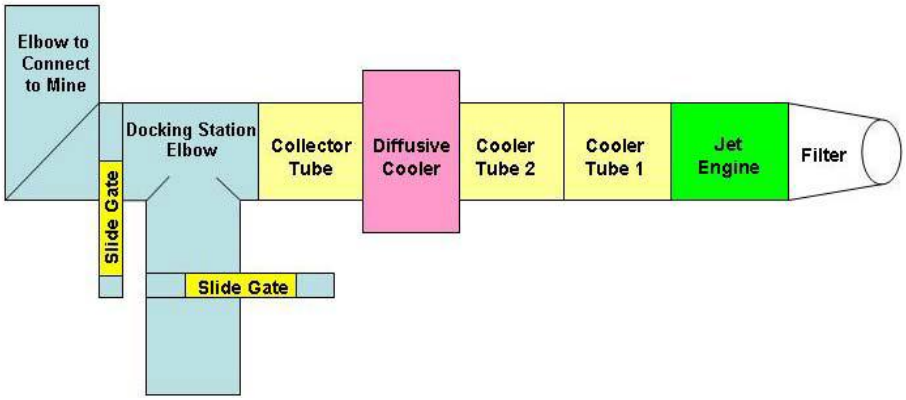

Figure 2.18 A schematic plan view of the GAG unit[197]

2.6.1.8 Carbon dioxide

Carbon dioxide is widely used in fire quenching system. It can be produced in relatively larger quantities in most countries in both solid phase (dry ice) and liquid phase. Although nitrogen and GCP are the most widely used inert gases in preventing coal mine goaf heatings, carbon dioxide has some unique features in inertising mine atmosphere. They are:

- Has an excellent cooling effect;
- Denser gas than air and can be settled in the heating area;
- Resistance to ventilation flow patterns;
- Resistance to thermal effect of the heating;
- Availability in larger volume of supply.

Extra precautions must be taken when introducing CO_2 to the underground coal mine atmosphere due to:

- It is noxious in high concentration;
- A risk of flowing to other down dip areas, like pump stations;
- It is an irritant on the skin because it forms carbonic acid in presence of water;
- Difficult to remove even with good ventilation;
- Potential to create an explosion due to substantial increase of volume in gaseous phase if solid CO_2 (dry ice) is introduced directly to fire site.

2.6.2 Complete excavation

The most direct traditional fire extinguishment method is digging out, which physically removes the burning coal and superheated materials. This method is confined to heatings that are relatively small and close to the roadway surface. Such heatings generally occur behind the lagging of mined roadways [187]. While it may result incomplete extinguishment, it is however difficult because this type of heating is often in confined and poorly ventilated areas, and thus exposes working crew to noxious gaseous products liberated from coal combustion, heated materials, and falls of roof. Though the operation may be successful, the resulting cavity must be filled with non-combustible materials and totally sealed to prevent the oxygen rich gas ingress. For these reasons such a control measure is seldom used today. It was reported excavation is a main method to fight coal fires in the Ruqigou coalfield due to lack of water and soil [25].

2.6.3 Injection of grouts, gels, foam sealants and oxidation inhibitors

Sujanti and Zhang [198] investigated the effects of inorganic matter on spontaneous combustion behaviour of a Victorian brown coal in an isothermal reactor to obtain critical ambient temperatures of the fresh coals, water-washed coals, acid-washed coals, and acid-washed coal doped with eleven chemical additives. It was found potassium chloride, montan powder, and sodium chloride were the most effective inhibitors, followed by magnesium acetate, and calcium chloride. The presence of sodium nitrate and ammonium chloride in the coal samples failed to exhibit significant influence on the spontaneous combustion. Calcium carbonate, sodium acetate, potassium acetate, and pyrite however promoted the spontaneous combustion. It was also indicated that the effectiveness of these promotion and inhibition agents was enhanced with an increase in the additive loading. Lu *et al.* [139] showed that injection of MEA-1A retardant (a water-soluble high-molecular compound) into a coal sample blocks partial surface pores and restricts access of oxygen into the coal. Following the occurrence of a self-heating event at the Longgu mine (North China), the MEA-1Asolution was injected in the goaf and two days later, less concentration of gaseous products of coal oxidation was detected and the risk of spontaneous combustion was significantly reduced. Taraba *et al.* [199] examined inhibition effects of both inorganic (chlorides, sulphates, nitrates, phosphates, and sulphites) and organic (formates, acetates, urea, and thiourea) substances by measuring heat generated from immersion of coal samples in the additive solutions. It was indicated urea has the highest inhibiting efficiency of coal oxidation at low temperatures.

Colaizzi [200] developed a technology utilising cellular grout (foam containing) to mitigate coal fires by spraying the material on the exposed surface of coal. Extinguishment can be accomplished by injecting grout directly into the heated zone. It was also indicated cellular grout injection is safer at lower cost than conventional techniques such as complete excavation. The use of large quantities of fly ash in the process is environmentally sound by providing for disposal of coal mine reject. It has been also reported grout injection is a very widely used fire control practice in China [25].Where the pressure differences associated with a heating are small and where airflow is found to be via small cracks extending throughout a large area, it may be advisable to apply a surface coating of grout to the strata. This can be done either by

hand application or by spraying. Spraying is rapid and enables large surface areas of roadway to be sealed in a relatively short time, while hand methods are good for spot filling of small areas. In moving ground, the coating has to be constantly replaced if the seal is to remain effective. Gel fire extinguishing technology has been a new fire-fighting technology developing quickly in recent years, integrating the functions of cooling, inhibition and water-consolidation and solving the problems of water-loss in the process of grouting and flooding [201]. Xue and Cui [202] classified colloids developed for the control of spontaneous combustion into three categories: gels, large-molecule colloids and compound colloids. The gels consist of a base material, an additive for fast gelatinization, and water. The large-molecule colloids are composed of large-molecule materials and water. Compound colloids are made by adding some additives in the gels or large-molecule colloids to enhance mechanical strength. Two systems have been developed for the colloid injection technique for spontaneous combustion control: an underground based system suitable for controlling small-scale spontaneous combustion and a surface-based method suitable for controlling large-scale spontaneous combustion. It has been also indicated different types of colloids should be used for different types of coal fire [201].

Ray and Singh [203] discussed high pressure and high stability foam is a new and effective method to suppress spontaneous combustion. The foam is produced by high pressure foam generator which has two independent units: pumping unit and foam generating unit. The foam is produced from a mixture of water and 5% foaming agent. This mixture is pumped into the foam generating unit and meanwhile nitrogen is introduced to the foam-generating unit at a certain pressure. At the outlet of the foaming unit a fire resistant hosepipe is attached by which the foam is transported to the place of infusion. The high pressure nitrogen foam was then applied to control an open fire in an experimental roadway and this technology proved to be effective and promising to quench open fires. Zhou *et al.* [204] developed a three-phase foam, consisting of non-combustible material (fly ash or mud), nitrogen, and water, to control coal fires. The foam was made by injecting nitrogen into slurry containing the foam agent. The foam swelled and filled goaf and covered the coal left in the goaf. The nitrogen encapsulated in the foam can remain a long time in the goaf to extinguish the mine fire. The foam contained solid materials such as fly ash or mud, which helped to keep the foam stable for a long period. As the foam cells ruptured,

the fly ash and mud, as a result of its viscosity, can cover the coal in the goaf and therefore prevented further oxidation of the coal. Following an occurrence of coal fire in China Baijigou coal mine in October 2003, massive amount of the three phase foam were made on surface ($620m^3/h$ production rate) and pumped into goaf by eleven boreholes. The fire was then effectively controlled and the face recovered production after two months.

2.6.4 Pressure balancing

Pressure balancing methods are primarily concerned with controlling (or eliminating) mine ventilation pressure differentials to reduce or arrest the flow of air to a heating. Other spontaneous combustion control techniques such as seal erection, flooding, and grout injection are generally attempted firstly. Consideration is normally given to pressure balancing only as a last resort. The available methods of balancing pressure across an area or along a length of roadway are [187]:

- Increasing pressure at the point by allowing ingress of intake air;
- Decreasing pressure at the point by direct connection to return air;
- Removing/reducing pressure differential along a road by eliminating/reducing airflow;
- Isolating an area from frictional pressure drops by the use of seals and ducting to ventilate through the area;
- Installing mechanical means to raise or lower the pressure in a confined area.

Air leakage into goaf through cracks around a seal greatly increases risk of heating in goaf. Available techniques are sealing these cracks by surface coating with grout, and erection of a pressure balancing chamber. Surface coating is relatively simple and effective when coal body around seal is integrated and limited number of cracks is induced by ground stress. However when coal rib around the stopping is ineffective, adequate sealing becomes increasingly difficult and construction of a pressure balancing chamber seal is more suitable. Heating evolution within an abandoned area is very sensitive to variations in airflow pressure in the surrounding roadways. A minor change of the pressure is likely to significantly promote the heating activity or reactivate a smoulder heating. A schematic view of the pressure balancing chamber is provided in Figure 2.19. The chamber is capable of balancing and self-compensating for ventilation changes and makes it independent of power supply failure or equipment breakdown.

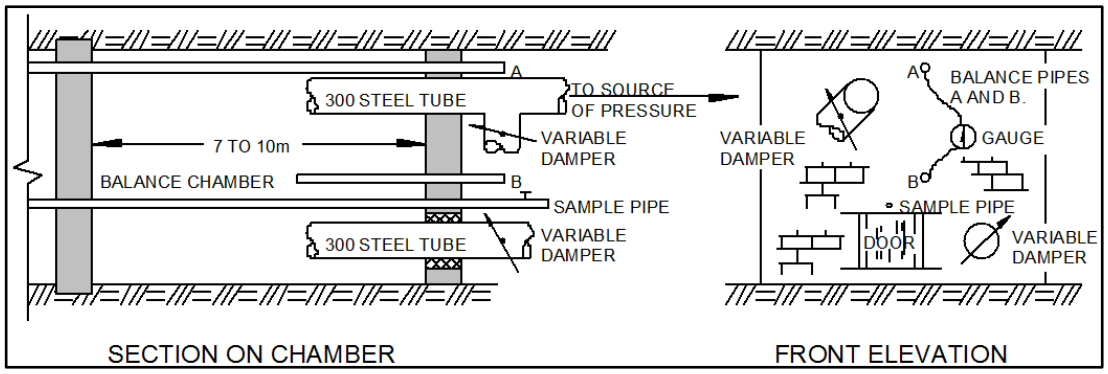

Figure 2.19 Working scheme of pressure balancing chamber [187]

2.6.5 Rapid sealing

Provision for rapid sealing of whole/parts of the mine is a necessary element of a spontaneous combustion management plan. The purpose of the operation is to isolate the heating from an oxygen supply, to produce an inert atmosphere in the sealed area, and to hinder a formation of an explosive gas mixture. If a spontaneous combustion event has been foreseen and effective countermeasures have been taken, there is the possibility of simply isolating the affected area by rapid sealing such as closing doors. If not, sealing operations may become difficult and time consuming. If there is surface access remained to the area above the heating spot, the sealing option is available by using fly ash or other roadway filler. The operation often involves introducing a large amount of inert gas into affected area from the surface by Thomlinson Boiler, Floxal unit, Mineshield or other means. If persons are withdfreshn from the mine because of a rapid development of spontaneous combustion event, sealing operations can only be conducted remotely and techniques for remote sealing include [27]:

- Injection of fly ash through boreholes;
- Injection of roadway filler materials such as “Rocsil”;
- Inflatable seals; and
- Remotely operated fire doors.

3 A CRITICAL INVESTIGATION OF SPONTANEOUS COMBUSTION IN SHENDONG COAL MINES

3.1 Introduction of Shendong coalfield

3.1.1 Location and allocation of coal mines

Shendong Coalfield is located in the northern part of Shaanxi Province, bordering Shanxi Province, Shaanxi Province and Inner Mongolia Region, refer Figure 3.1. The coalfield has a total mining area of 31,200 square kilometres and a proven reserve of 223.6 billion tonnes. It is the largest integrated coal reserve in China and accounts for a quarter of the national proven reserves. Due to good coal quality and simple geological conditions, this coalfield has been developed to China's largest energy base by 2000. Shendong Coal Branch of Shenhua Group was approved by the State Council and the entity was responsible for the construction and operation of several iconic coal mines in China.

Figure 3.1 Location of Shendong coalfield

The currently operated Shendong coal mines are only a small part of Shendong coalfield and the rest reserve is awaiting future plan. Shendong mining area is located in the northern part of Shenmu County, the western part of Fugu County, and the southern part of Ordos City. The coal mines also scattered along both sides of

Wulanmulun River that is the largest river flowing through the mining area. The mining area is about 38~90km from north to south, 35~55km from east to west, with an area of about 3481km^2. The special railways in the mining area are connected with several main railway lines through which the produced coal can be transported to Port Qinhuangdao or power plants situated in large towns adjacent to Shendong coalfield. Because the coalfield is located in semi-arid areas of remote western part of China, the mining area was originally sparsely populated. However, due to the development of coal mines in recent decades, a number of factories and communities have also been developed. A close-up map view of Shendong coal mines can be seen in Figure 3.2. The Shendong mining region consists of five exploration areas with a total area of 3481km^2. Detailed investigation and geological survey exposed total 35.4 billion tons coal reserve and more specific classification of coal reserve can be seen in Table 3.1. Since 2000 a number of coal mines have been constructed and annual productions of some of them have exceeded 20 million tons coal. Allocation of these coal mines and their production rates are shown in Appendix B.

Figure 3.2 A close-up map view of Shendong coalfield

Table 3.1 Classification of coal reserves of Shendong coal mines

Reserve classification	Billion tons	Percentage
A+B (Recoverable reserves)	10.16	28.67%
C (Designed reserves)	16.25	45.87%
D (Prospective reserves)	9.02	25.46%

3.1.2 Topographical features

Shendong mining region is located in the Maowusu desert area of the Ordos Plateau. Surface of mining area is widely covered by 20~50m thick quicksand and semi-fixed sand. Average altitude of the mining area is about 1200m, which belongs to a typical semi-arid plateau continental climate. Average annual rainfall is 194~531mm while annual evaporation ranges from 2297mm to 2838mm.There is only one major river, Wulanmulun river (also known as Kuye river), running through the mining region. Owning to the topography most of the rainfall is lost by surface runoff, which is not conducive to the infiltration of groundwater recharge and rainfall infiltration to rock and soil layer is normally less than 15%. Geological structure of the mining area is simple, strata are gently distributed, and tectonic fissures are not developed. All these geological features are not conducive to the storage of groundwater so the artesian head is high but water quantity is low. The basic characteristic of hydrogeological condition in this area is that the total amount of groundwater is relatively small but it is often enriched locally and poses a threat to coal mining operations. The northwest of the mining area is the Kubuqi desert, which is mostly composed of quicksand and sand ridge. The central area consists of a group of high plains and small lakes scatter due to undulating terrain. The southwestern part is low and flat and covered with sand ridges and sand dunes. Hills and valleys form in the northeast and topsoil of them is thin. The overall landscape is high in northeast and low in southeast. Figure 3.3 provides a few representative photographic views of landform in Shendong coal mines.

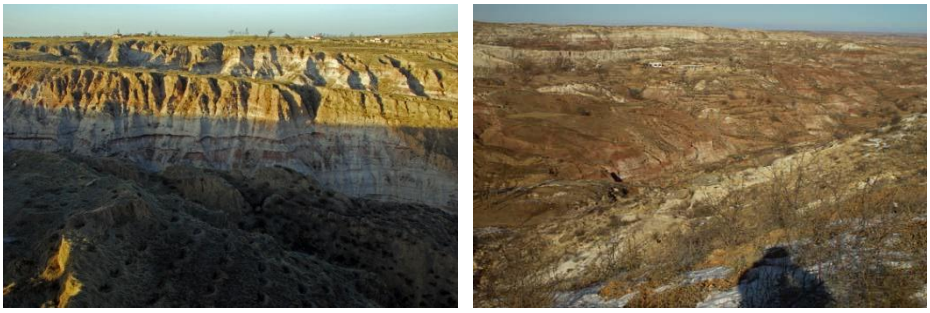

Figure 3.3 Photographic views of landscape in Shendong coalfield

3.1.3 Geological and geotechnical conditions

The central area of Shendong coalfield is situated in the northeastern part of Ordos's large coal-bearing basin. From regional geological structure perspective, the coalfield is located at the juncture of Dongsheng and Shanbei monoclinic warps. The

geological structure is simple and the whole area is mainly monoclinic structure. Faults are not developed except Daliuta coal mine in which some faults drop up to 30m.Characteristic features of regional strata are summarized in Table 3.2.

Table 3.2A simplified strata condition in Shendong coalfield

System	Series	Formation	Thickness (m)	Lithological characters
Quaternary	Holocene	Q_4	0~25	Lacustrine facies, alluvium and aeolian
	Upper pleistocene	Q_{3m} (Malan)	0~40	Light yellow sandy loess, calcareous nodules, with columnar joints.
Tertiary	Pliocene	N_2	0~100	The upper part is red, khaki-coloured clay and loose sandstone, the lower part is greyish yellow, reddish brown, green yellow glutenite, conglomerate.
Cretaceous	Klzd	J_3-K^2_{lsh} (Dongsheng)	40~230	Light grey, grey, yellow, purple red mudstone, siltstone, fine sandstone, sandy conglomerate, mudstone, sandstone intercalation, sandwich thin layer of mudstone. Cross bedding is more developed. The top layer of common coarse sandstone, with gravel, thick layer.
		J_3-K^1_{zsh} (Yijinhuoluo)	30~80	Light grey, grey, green, brown, purple mudstone, siltstone, sandy mudstone, fine sandstone and sandstone, sandstone, conglomerate, a thin layer of fine calcium sandstone band. Developed oblique bedding, lower common large cross-bedding. Unconformable contact with the underlying strata.
Jurassic	Middle	J_{2a} (Anding)	10~80	Light grey, grey-green, yellow-purple brown mudstone, sandy mudstone, medium sandstone. Calcium containing tuberculosis.
		J_{2z} (Zhiluo)	1~278	Grey, grey-green, purple-red mudstone, sandy mudstone, fine sandstone, medium sandstone, coarse sandstone. The lower part is bedded with thin coal seams and oil shale, containing one coal group. Parallel to and unconformable contact with the underlying strata.
	Lower and middle	J_{1-2y} (Yanan)	7~247	Grey sandstone, dark grey, grey-black sandy mudstone, mudstone and coal. Containing six coal groups. Parallel to and unconformable contact with the underlying strata.
	Lower	J_{1f} (Fuxian)	110	The upper part is light yellow, grey-green, purple-red mudstone, sandstone. The lower part is mostly sandstone, locally bedding with mudstone layers. The bottom is light yellow conglomerate. Parallel to and unconformable contact with the underlying strata.
Triassic	Upper	T_{3y} (Yanchang)	35~312	Yellow, grey-green, purple, grey and black lump sandstone. Grey-black, grey-green mudstone and coal line. Parallel to and unconformable contact with the underlying strata.
	Middle	T_{2er} (Ermaying)	87~367	Grey-green sandy conglomerate, conglomerate, purple mudstone, siltstone.

The main coal-bearing strata belong to the Yan'an Formation (J_{1-2y}) which was extensively developed and composed of many layers of coal, yellow-green sandstone, and mudstone. Geological investigation revealed total thirteen coal seams which are divided into five coal seam groups. Eight coal seams are minable with total thickness exceeding 30m. Main recoverable coal seams were named as 1^{-2}, 2^{-2}, 3^{-1}, 4^{-2} and 5^{-2} coal seam and most coal mines are currently operated in 1^{-2}, 2^{-2}, and 3^{-1} coal seams. Coal-bearing strata are almost flat and slightly dip to south. Coal seams are regularly distributed and geological disturbance is not developed. All these features are ideal for large-scale coal mining operations. Additionally, the coal-bearing strata can be characterized by shallow cover (mostly around 100m), thin rock bed (minimum 1.4m only), thick loose sand (10~50m thick aeolian sand above the rock bed), and water enriched in the loose layer.

3.1.4 Propensity of Shendong coals to spontaneous combustion

Physical properties and macroscopic characteristics of coals from all coal seams of Shendong coalfield are similar. Coal is dense and hard and its bulk density is about 1.3t/m^3. Microscopic examinations indicate coals from all coal seams are composed of clarain, durain, victrain, and fusain. Another feature is content of fusain is relatively high. According to the reflectivity of victrain and microscopic examination of coal, it was found most coals are mainly the first stage of low metamorphic bituminous coal and have low content of ash, sulphur, phosphorus, and other hazardous components. The coals are good thermal power coals by virtue of its relatively high calorific value. In addition some coals have good reactivity to carbon dioxide and can be used for coal gasification. Ignition temperatures of all coals are about 300^{o}C and they are quite readily to initiate a fire. To accurately grasp the knowledge of liability of different Shendong coals to spontaneous combustion, coal samples from many coal mines were sent to laboratory of China Coal Research Institute to examine their tendencies to spontaneous combustion. The results are tabulated in Table 3.3 and it can be seen most coals are very liable to spontaneous combustion [205].

Table 3.3 Testing results of propensities to spontaneous combustion of Shendong coals

Coal mine	Sampling location	Sample code	Oxygen adsorption/ml · g^{-1} *	Classification	Propensity rating
Daliuta	2^{-2} Longwall	DL-001	0.9	I	Very liable
Huojitu	1^{-2} Bin	Hj-001	0.87	I	Very liable
Huojitu	2^{-2} Cut through	Hj-002	0.83	I	Very liable
Bulianta	2^{-2} Longwall	BL-001	1.06	I	Very liable
Shangwan	2^{-2} Main heading	SW-001	1.06	I	Very liable
Shangwan	3^{-1} Maingate belt	SW-002	0.95	I	Very liable
Wulanmulun	2^{-3} Maingate	WL-001	1.08	I	Very liable
Majiata	2^{-2} Open cut	MJ-001	0.98	I	Very liable
Halagou	2^{-2} Heading	HL-001	0.84	I	Very liable
Dahaize	3^{-1} Heading	DH-001	0.92	I	Very liable
Yujialiang	5 Longwall	YJ-001	0.78	II	Liable

***The oxygen adsorption rate is an industrial standard to examine liability of coal to self-heating. Amount of oxygen adsorption is measured by following procedures: (1) placing 1g pulverized coal in an isothermal vessel and a constant temperature 30°C is maintained during the test; (2) Pure oxygen is allowed to pass the granular coal and GC is used to measure amount of oxygen consumption from effluent gas. The rating system also considers volatile and sulphur content of coal and its detailed interpretation is provided in Appendix C.**

3.1.5 Mine construction and mining plan

As stated geological conditions of Shendong coalfield are simple and not many geological disturbances were identified. Coal seams are almost flat and distribute evenly. All these features are suitable for large scale coal mining operations. Through analysis of mining system, logistic inclined shaft is a major restrain to construction of a highly productive and efficient coal mine. Considering flexibility of truck transport system, Shendong coal mines firstly used drift development method in China. By this way mine materials and equipment can be transported directly to working face and development heading by truck, which maximises capability of auxiliary transport system. The drift development method eliminates the multi-section layout and mine drift is directly connected with the mains. Longwall panels are arranged on both flanks of the mains and length and width of longwall face greatly increase. Compared to conventional coal mining layouts, Shendong mining layout is significantly simplified and production rate is therefore greatly promoted. For some large area coal mines, whole mine is still divided into several sections and each section has its own auxiliary shaft to shoulder ventilation and auxiliary transport burden. Coal is still transported through mains and an exclusive drift for coal haulage. This will not only guarantee coal productivity but also solve whole mine ventilation and auxiliary transport problems for a large area coal mine. Several

typical Shendong coal mine layouts can be seen in Appendix D, E, and F. Since 1998 Shendong coal mines have imported specially designed and cutting-edge mining equipment from the United States, Britain, Germany, and Australia. Through the upgradation of mining technology and equipment, mining procedures like coal production, heading development, auxiliary transportation, and coal haulage were greatly promoted. A series of mining technology innovations and breakthroughs including rapid heading development of long roadways, long distance conveyor transport system, mine safety technology, and efficient coal production system were achieved. All these technologies lead to more than ten million tons coal production within a single longwall operation.

3.2 Spontaneous combustion incidents

3.2.1 Statistics

From 1987 to 1998, Shendong coal mines faced less pressure of coal production and most coal mines were mainly under construction. Only a few longwall faces were being operated and most of them were up-dip mined. The goafs were mostly flooded to prevent oxidation of residual coal and therefore few spontaneous combustion incidents were reported for the time being. Afterwards with the increase of production pressure, more longwall faces were installed and put in operation. The upper coal seams of a number of coal mines were gradually extracted and a few coal mines started to mine the underlying coal seams. The two coal seams are usually closely distributed. As underlying coal seam is mined, more mining-induced cracks are developed and very likely to propagate to surface. Integrity of overlying goafs and pillars are also broken and more airflow is drawn into goafs. As stated Shendong coals are mostly very liable to spontaneous combustion and therefore it is more readily to develop a spontaneous combustion incident in overlying goafs and coal production operation in underlying coal seam are adversely impacted. After 2000 more self-heating incidents were reported and culminate to an open fire incident occurred in longwall goaf 12306 of Bulianta coal mine in 2012. From 1998 to 2012 self-heating incidents of Shendong coal mines are summarised in Figure 3.4.

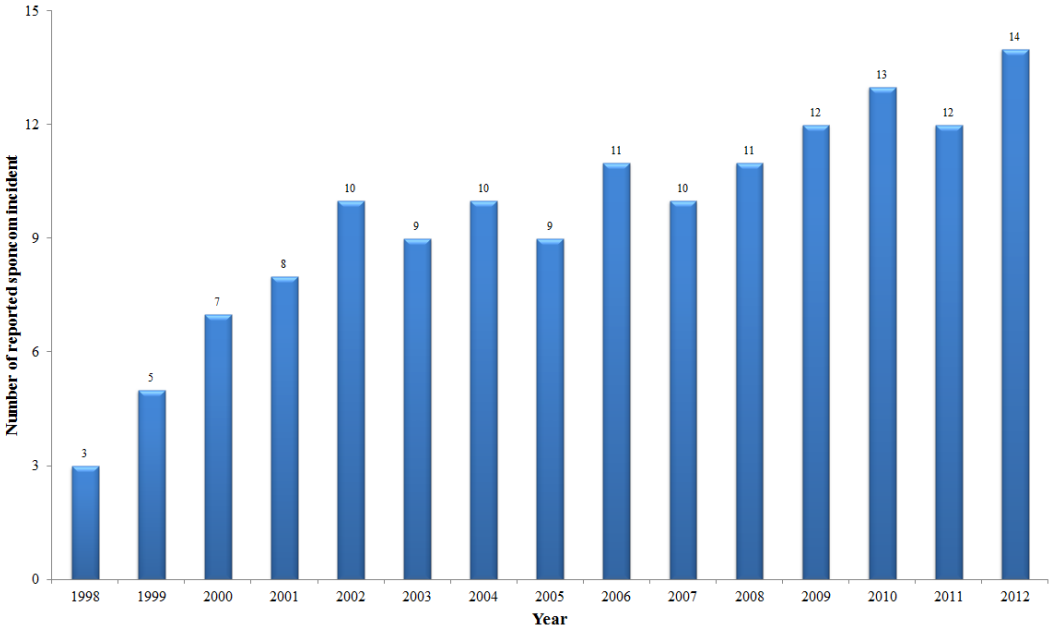

Figure 3.4 Number of reported spontaneous combustion incidents from 1998 to 2012

3.2.2 Contributor analysis

Contributors of spontaneous combustion can be broadly assessed through three main aspects: quality of coal, geological condition, and mining plan, refer Figure 3.5. To identify the characteristic problems of spontaneous combustion in Shendong coal mines, the common features of coal mining are analysed based on the factors spontaneous combustion of coal shown in Figure 3.5. The key features are:

- Most coals from Shendong coalfield are very liable to spontaneous combustion due to their high volatile content and low ignition temperature.
- When preparing a longwall panel by double-roadway driven method, one cut-through is required every 50m due to limitation of continuous miner. The cut-through greatly damages integrity and completeness of coal pillars and therefore they are more readily to be crashed in goaf with strata caving. The crashed coal pillar is a source contributing to spontaneous combustion.
- Immediate roof of longwall face is instable and very easy to cave and hence 0.3~0.5m top coal is reserved to protect the roof during longwall cutting. This part of coal is left in goaf and also contributes to self-heating.
- Coal seams of Shendong coal mines are buried under shallow cover and rock beds within the cover are normally thin. Mining-induced cracks are quite developed and likely to propagate to surface. Most mines are using exhaust

ventilation system and therefore these connected channels would draw more airflow into goaf.

- Upon preparing longwall panel, besides of necessary gateroads, additional start-off line, flood discharge roadway, and cut through are required to be developed. More number of roadways implies more complexity of ventilation in panel. Considering some seals are not quickly constructed or poorly constructed, more airflow leaks into goaf and deteriorate spontaneous combustion problem.
- Shendong longwall panels are usually several kilometer's long and longwall faces are 240~360m wide. Life expectancy of longwall panel is long enough to develop a spontaneous combustion incident.
- As stated Shendong coal mines are mining in multiple coal seams and these coal seams are closely distributed. With depletion of upper coal seam, many mines start to extract lower coal seam. To prevent spontaneous combustion problem, longwall goaf of upper coal seam is flooded upon sealing. The flooded goaf needs to be drained as second coal seam is mined. The flooded coal is exposed to air and somehow exhibits higher propensity to spontaneous combustion.
- After coal pillars are crashed, 4~6 longwall panels are connected and it is therefore more difficult to identify source of airflow leakage. Once spontaneous combustion incident occurred, it is also more unlikely to locate "hot spot" and put right control to right locations.

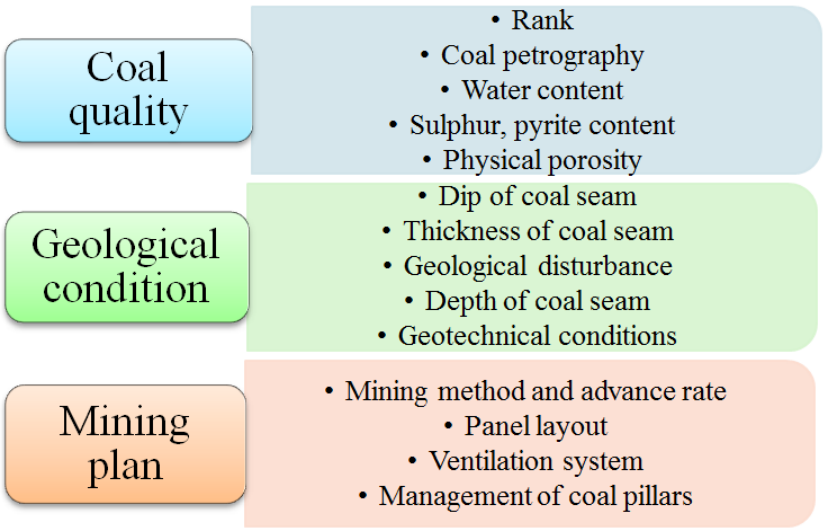

Figure 3.5 General contributors of spontaneous combustion in coal mines

Through above analysis of common features of Shendong coal mining operations, the characteristic problems of spontaneous combustion are identified and their correlations are also clarified, refer Figure 3.6. The problems will be given much more details in next section.

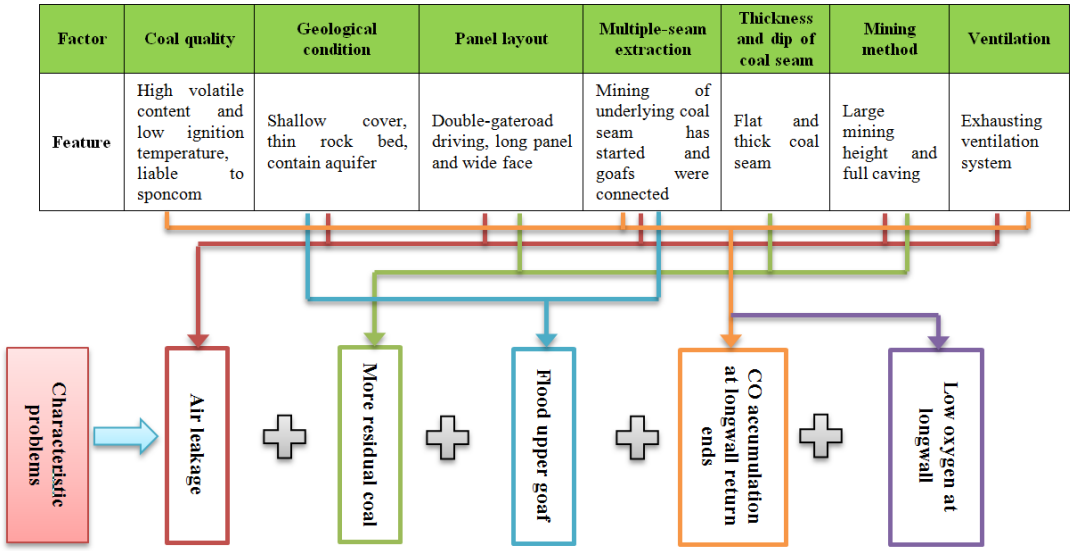

Figure 3.6 Correlation of mining features and characteristic spontaneous combustion problem

3.3 Detailed analysis of characteristic spontaneous combustion problems

3.3.1 Air leakage from surface

3.3.1.1 Generation and propagation of mining-induced cracks

According to the theory and experience of mining subsidence, mining-induced cracks are likely to be very developed if a coal seam is mined under shallow cover. The induced cracks can be categorised into two groups. One group crack named edge crack usually appears around fringe of longwall goaf and perpendiculartolongwall face. The cracks are developed by stretch of strata caving and normally have large gaps and drops. Another group of cracks in the goaf surface is the dynamic crack. The cracks locate in front of the working face and advances with the working face. They appear in the dynamic stretching zone in the front of the working face and have relatively small gaps and drops. The direction of the fracture is roughly parallel to the mining face and perpendicular to the advance direction of the face. The length of the crack is approximately the same as the mining face width of the working face and is continuously generated and closed with advance of the working face. Based

on field measurement, Hu *et al.* [206] and Wu *et al.* [207] also demonstrated that the dynamic cracks are linear and roughly parallel to longwall face. The cracks generate and close with advance of longwall face. Curve cracks are developed around longwall goaf boundary and parallel to direction of longwall advance.

Before having an understanding of how mining induced cracks develop to surface, mechanism of strata caving in a specific working site must be fully grasped. As shown in Figure 3.7, strata above longwall goaf from bottom to top usually fall into three groups with advance of longwall face. The first group including immediate roof caves with advance of longwall face. Above the caving zone is the crack zone in which strata break through and mining induced cracks fully developed rather than cave to goaf because of consolidation of the caving zone. The top zone is the bending zone where no cracks break through the strata and the strata only slightly bend and cause surface subsidence. Figure 3.7 shows a usual case of strata caving process in coal mining but it varies from site to site.

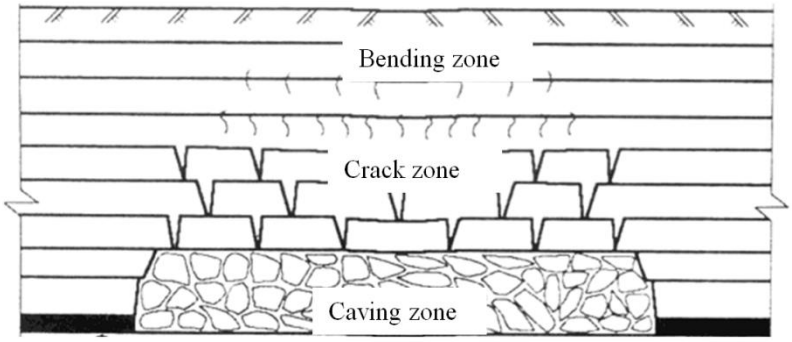

Figure 3.7 A schematic view of strata caving process in coal mining

Coal seams in Shendong mining area are mined under shallow cover which is mainly composed by a thick loose layer and a rock layer. The primary roof is the rock layer and stability of all strata and surface depends on this rock bed which is also called a key stratum. The stability of the key stratum is affected by stress redistribution and eventually breaks with progressive extraction of coal. Case of strata caving in 12403 longwall face of Daliuta coal mine is used to exemplify the general process of strata caving in Shendong coal mines. Geotechnical parameters of the strata are shown in Table 3.4 and the simplified caving process is shown in Figure 3.8.

Table 3.4 Geotechnical parameters of strata above 12403 LW face of Daliuta coal mine

Strata	Thickness (m)	Density/t m^{-3}	UCS (MPa)
Aeolian sand	8	1.6	0
Sandy gravel	6	2	1.1

Weathered layer	3	2.3	7.1
Mudstone & siltstone	6.4	2.5	47
Quartzose sandstone	8.6	2.4	45
1^{-2} coal seam	6	1.3	13.4

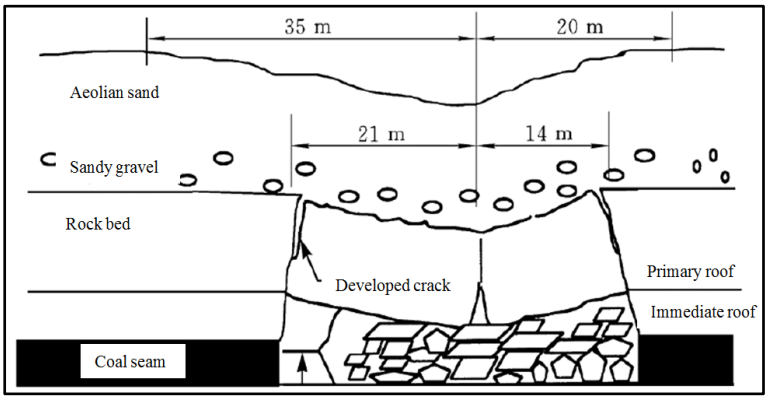

(a) Start of coal seam extraction

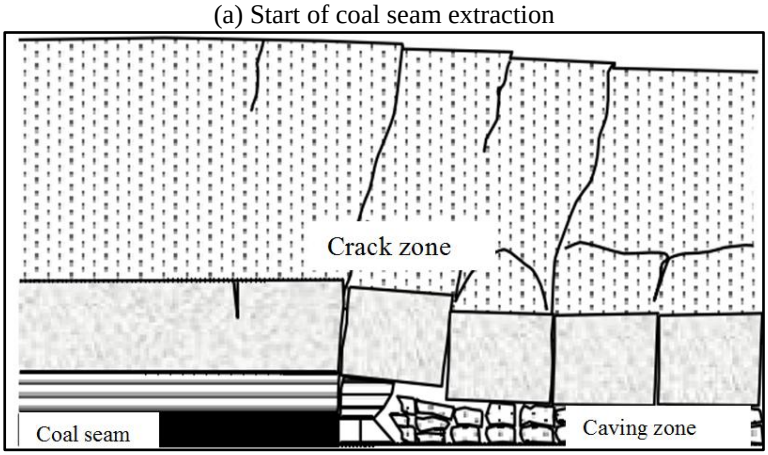

(b) Periodical weighting with longwall advance

Figure 3.8 Two sketches of strata caving of 12403 LW face of Daliuta coal mine

Three steps caving process would be gone through with advancing of longwall face. The three consecutive steps are first caving of immediate roof, first caving of primary roof, and periodic caving of primary roof. Detailed interpretation of three steps is provided in Figure 3.9.

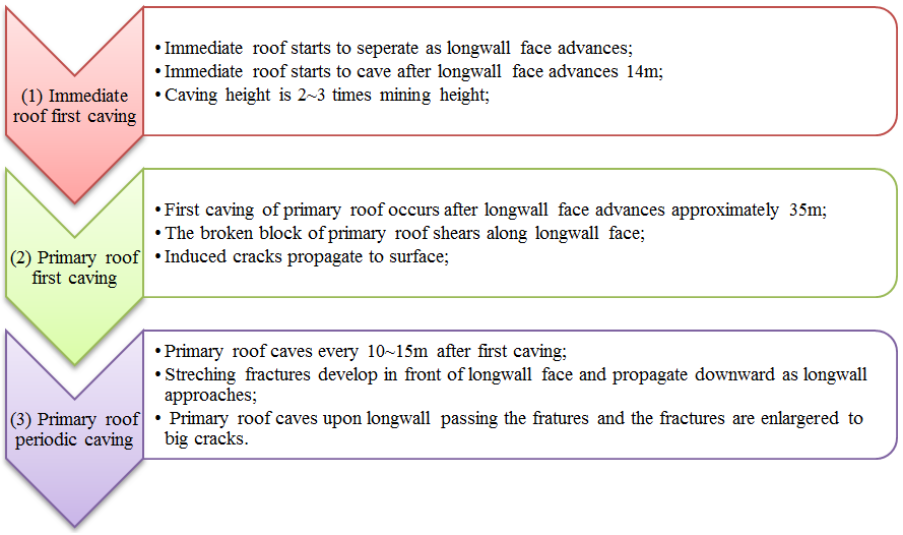

Figure 3.9 Three steps of strata caving in 12403 LW face of Daliuta coal mine

Based on the analysis, unlike conventional "three zones" of strata caving, only two zones can be identified in Shendong coal mines. The two zones are:

- ❖ Caving zone: Primary roof firstly and periodically caves and caving height is 2~3 times mining height;
- ❖ Crack zone: Length of crack exceeds thickness of primary roof and cracks propagate to surface.

Due to the relatively shallow cover and high mining height in Shendong coal mines, mining induced cracks penetrate through strata and propagate to surface and therefore the cracks have great potential of air leakage into goaf. With the continuous extraction of coal seam, cracks parallel to the working face periodically emerge and close because of periodic collapse of primary roof and consolidation of caved rock in goaf. Based on field measurement, the spacing of the dynamic cracks is about 14m in Bulianta coal mine and 10~14m in Shigetai coal mine. Meanwhile cracks around goaf edges develop parallel to the mining boundary. In contrast to dynamic cracks, the location of edge cracks is usually 50m behind longwall face. In the process of mining, new edge cracks firstly appear 90~100m to centre line of longwall face and expand forward and outward as longwall advances. Ultimately edge cracks fully develop and are difficult to be closed. Surface loose layer is mainly composed of sandy soil and its permeability is good. In addition climate of Shendong area is dry so surface cracks would not be closed for a long period and function as air leakage channel, refer Figure 3.10.

Figure 3.10 Two photographic views of mining induced cracks in Daliuta mine

After completion of longwall panel, edge cracks are distributed as a shape of "O" ring around longwall goaf. The cracks in the start-off line and the finishing line are symmetrical as shown in Figure 3.11. Based on results of numerical and physical simulation, Fan *et al.* [208] found the dynamic cracks would be closed as longwall face advances and they are likely to be closed more shortly if longwall face advances faster. However edge cracks especially those locating at start-off line are hard to be closed and therefore pose a great risk of air leakage and water ingress. Conventionally edge cracks develop outside of longwall goaf boundary but in Shendong coal mines, edge cracks form inside of longwall goaf due to its large extraction height and longwall advance rate. Edge cracks relatively concentrate and their angles are mostly perpendicular to coal seam. All these features potentially reduce resistance of airflow through these channels and hence deteriorate the situation.

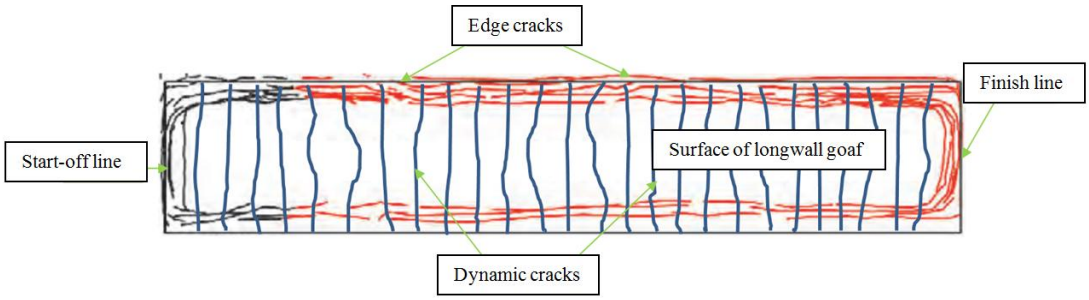

Figure 3.11 A sketch of mining-induced cracks on surface of longwall goaf

Above analysis of mechanism of generation and propagation of mining induced cracks is discussed on basis of case scenario of single coal seam extraction. In Shendong coal mines multiple coal seams are being extracted and coal seams are closely distributed. As the second coal seam is mined, primary roof periodically caves again and new caving zone and crack zone are created. More cracks are

generated and develop to surface. Old cracks and new cracks connect and further enhance air leakage into longwall goaf. Field measurement indicates air leakage velocity of underlying coal seam is higher than upper coal seam, which justify the discussion.

3.3.1.2 Air leakage measurement

Field measurement of surface air leakage is mainly conducted by using tracer gas sulfur hexafluoride (SF_6). SF_6 gas is non-toxic and odourless and its natural content in atmosphere is extremely low. The gas is also chemically stable, easy to be detected and strongly diffusive and is therefore usually used as tracer gas. The procedures of air leakage measurement are as following:

1) Based on mine ventilation map identify possible airflow leakage paths, sources of air leakage, and destinations of airflow leakage path;
2) Release SF_6 gas at sources of air leakage and use gas bags to collect gas sample at possible destinations of airflow leakage path on a reasonable interval basis;
3) Send gas bags to laboratory and use GC to test concentration of SF_6 gas;
4) Based on testing results determine air leakage paths and leakage velocity on each path.

Figure 3.12 provides two photographic views of air leakage measurement on site. Measured air leakage velocity of several typical Shendong longwalls is summarised in Table 3.5. Quantity of air leakage of whole mines and longwalls is shown in Table **3.6** and Table **3.7** respectively.

Figure 3.12 On site measurement of air leakage in Shigetai coal mine

Table 3.5 Measured air leakage velocity of typical Shendong longwalls

Coal mine	Longwall	Air leakage velocity m/min
Bulianta	31302	3.1~8.7
	31301	2.0~8.0
	22305(before pressure balance)	17.1~55.4
	22305(after pressure balance)	7.9~19.9
Daliuta	20401	3.5~28.0
Shigetai	12401	3.4~9.4
	22402	3.3~10.2

Table 3.6 Total quantity of air leakage of Shendong coal mines

Coal mine	Total intake m^3/min	Total return m^3/min	Leakage percentage %	Ventilation mode
Bulianta	25657	26799	4.5	Exhaust
Shangwan	24700	27007	9.3	Exhaust
Daliuta	25334	25589	1	Exhaust
Huojitu	22172	21005	5.6	Force
Shigetai	21798	22654	3.9	Exhaust
Wulanmulun	11379	11637	2.3	Exhaust

Table 3.7 Total quantity of air leakage of Shendong longwalls

Coal mine	Longwall	Intake m^3/min	Return m^3/min	Leakage m^3/min	Ventilation mode
Bulianta	22307	2065	2127	62	U+Force
	12412	1712	1776	64	U+Exhaust
	12521	1845	1877	32	U+Exhaust
Buertai	42105	1633	1472	161	Y+Exhaust
	22107	1288	1070	218	Y+Exhaust
	22203	1039	1177	138	Y+Exhaust
Daliuta	52302	2335	2347	12	U+Exhaust
	52306	2352	2361	9	U+Exhaust
Huojitu	12314	1437	1428	9	U+Force
	$12^{Upper}314$	1244	1244	0	U+Force
	22305	1313	915	398	U+Force
Shangwan	12302	1950	2013	63	U+Exhaust
	22101	1852	1901	49	U+Exhaust
	$12^{Upper}308$	1896	1925	29	U+Exhaust
Shigetai	$22^{Upper}206$	505	550	45	U+Exhaust
	$22^{Upper}301$	710	746	36	U+Exhaust
	31203	1556	1530	26	U+Exhaust

It should be noted that the air leakage velocity mentioned in Table 3.5 is the ratio of the linear distance between the releasing point and measuring point and the real

measured time. The actual airflow leakage path in the fractured rock mass is a meandering path rather than a linear path and the actual airflow leakage velocity is probably much larger than the values given in Table 3.5. Measurements in Shigetai coal mine also indicate the air leakage in intake gateroad close to longwall face is relatively serious and leakage in middle of longwall face and return side is relatively small. As a result more sealing practices should be put in two gateroads of longwall panel especially on the intake side. While in longwall 22305 of Bulianta coal mine, the field measurement results show air leakage in both gateroads is serious (slight more leakage was detected on return side) and relatively small in middle of longwall face. Measurements in all main coal mines also suggest surface cracks sealing control measures should be exercised in cracks within 200m to longwall face especially those edge cracks because dynamic cracks can be closed spontaneously but edge cracks develop all the time. In addition air leakage velocity mainly relates to two factors: pressure differential between surface and longwall face and size of crack. The velocity increases with size of the crack and pressure differential. Size of crack closely correlates to quality of topsoil. If more water is contained in top sandy soil, cracks are more likely to be smaller and so is the air leakage. Pressure differential is affected by barometric pressure and quantity of air leakage is larger with a larger variation of barometric pressure.

3.3.2 Residual coal in longwall goaf

3.3.2.1 Source of residual coal

(1) Top coal and floor coal

To align coal cutting, AFC, and chocks during longwall mining and meanwhile due to fragility of floor and immediate roof, 0.3~0.5m top coal or floor coal requires to be remained. This coal is left in goaf and crashed by roof caving and therefore pose a great risk of spontaneous combustion.

(2) Top coal above two gateroads

The main operating coal seams in Shendong coal mines are 6~7m thick. Two gateroads (about 4m high) are usually developed along coal seam floor and as a result, 2~3m top coal above gateroads is left in goaf and self-heating incidents could occur under favourable conditions.

(3) Transitional coal at two ends of longwall face

In order to improve the recovery rate of coal resources, more and more coal mining operations tend to develop a large height longwall face (>6m).As a result3m gap is incurred between mining height and gateroad height. A transitional zone (about 30m) is required to cut two ends of longwall face to maintain integrity of gateroads, refer Figure 3.13. This coal is the third source of residual coal.

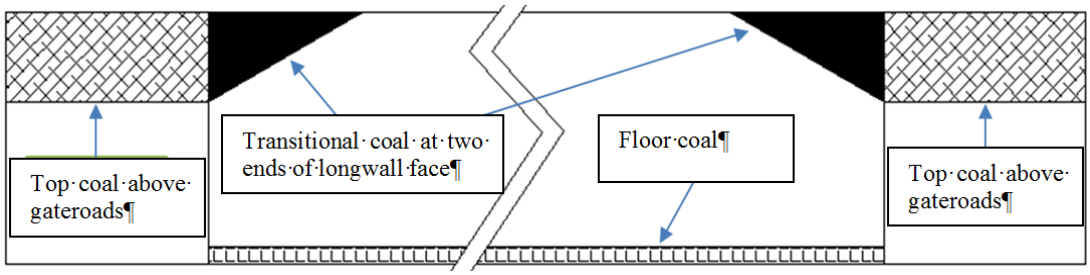

Figure 3.13 Source of residual coal on longwall face

(4) Panel chain pillars

As stated double gateroads are usually developed in longwall panel and 30m wide coal pillar is remained between two gateroads. One cut-through is driven every 40~50m and integrity of the coal pillar is greatly damaged and coal pillar is very possible to be crashed in longwall goaf.

3.3.2.2 Calculation of residual coal

Two scenarios are considered to calculate the amount of residual coal in each longwall panel of Shendong coal mines. One case is large height mining face (6~7m) and another one is a medium height longwall face (3~4m). The detailed parameters are shown as following:

(a) Large height longwall face

Assume longwall face is 250m wide, length of longwall panel is 4000m, average thickness of coal seam is 7m, extraction height is 6.5m (0.5m top or floor coal is kept), width of gateroad is 6m, height of gateroad is 4.5m, width of chain pillar is 30m, and density of coal is 1.3t/m^3.

(b) Medium height longwall face

Assume longwall face is 250m wide, length of longwall panel is 4000m, average thickness of coal seam is 4m, extraction height is 3.5m (0.5m top or floor coal is reserved), width of gateroad is 5m, height of gateroad is 3.5m, width of chain pillar is 30m, and density of coal is 1.3t/m^3.

Quantity of residual coal of the two scenarios is shown in Table 3.8. It can be seen approximately 20% coal is left in goaf. Please note if coal pillars in start-off line and finishing line of longwall panel is taken into account, the percentage of residual coal must increase.

Table 3.8Estimation of amount of residual coal of two mining scenarios

Scenario	Total coal/t	Top coal above gateroads/t	Top/floor coal/t	Transitional coal/t	Coal pillar/t	Total residual coal/t	Percentage /%
a	8176000	78000	500000	195000	739200	1512200	18.5
b	4672000	24000	500000	0	422400	946400	20.3

3.3.3 Flooding longwall goafs of upper coal seam

3.3.3.1 Hydrological geology

Shendong coal mining area is located in the eastern edge of Maowusu desert area of the Ordos Plateau. This area belongs to eroded wind-type landform and surface ditch is developed. Aeolian sand is widely distributed in this area and loess cover and bedrock is casually exposed. The overall landform is higher in the northwest while lower in the southeast. The range of altitude is +1000~1300m and average altitude is about 1200m. Drops of landform are normally less than 200m. Continental arid climate dominates Shendong coalfield. The climate is characterized by the following features: cold and arid in winter, hot and rainy in summer, windy and dry in spring, cool and humid in autumn; temperature differential is large in one day; short frost-free period; concentratedrainfall; and strong evaporation. Main rivers in the mining area are Mulanwulun river, Kuye river, and Beiniu river and they are all branches of Yellow River. Wulanmulun River originates in Dongsheng County near Inner Mongolia region andflows through Shendong mining area from the northwest to the southeast. The river runs through the middle of the mine and meets with Beiniu river at Fangzita County and the two rivers are renamed as Kuye river. Kuye river flows through the Shenmu County and heads into the Yellow River at Shamaotou area. Main river branches flowing through mining area are as following: creek Gongniegai, creek Kaokaolai, creek Liugen, creek Huhewusu, creek Bulian, creek Hala, creek Muhe, creek Huojitu, creek Mingaitu, creek Zhugai, creek Miao, creek Kaokaowusu, creek Majiata, creek Huangyangcheng, and creek Yongxing. Water of above creeks is mainly supplied by rainfall and water flow is therefore very unstable. Amount of the water flow peaks in summer and is very small even dry in winter. In March and

April of each year, snow and ice melt and water flow greatly increases while in May and June the climate becomes dry and water flow is very small.

Water resources are very scarce in Shendong mining area and surface water runoff is small. Groundwater is mainly derived from permeationof surface rainfall while the annual rainfall is only 108~819mmand 60-70% rainfall concentrates in July to September. Most rainfall forms surface runoff and less than 15% is infiltrated to ground soil and rock. Due to conditions of mining strata and topography, ground water is enriched and stored locally. A number of large scale and permeable aquifers are evolved and scattered in mining strata of Shendong coal mines. According to the characteristics of coal seam formation and distribution of aquifer, the hydrogeological conditions of Shendong mining area can be summarised as two basic types[209]:

(1) One is shallow Quaternary unconsolidated porous aquifers above coal seam of the Lower Jurassic Yanan Formation and the aquifers are mainly distributed in the southern coal mines including Daliuta and Huojitu coal mines.

(2) Another one is the deep-buried Cretaceous aquifer above Lower Jurassic Yanan Formation and the Zhiluo Formation and these aquifers cover the western and northern part of the mining area.

3.3.3.2 Impacts of flooding upper longwall goaf to spontaneous combustion

Coal and water resources coexist in a geological body and formation and movement would follow their own rules without destruction of coal mining. Coal mining damages the natural balance of movement of groundwater and a “funnel” shaped strata are formed due to coal seam extraction. Within its radius of influence, ground water tends to flow into lower longwall goaf and therefore water level decreases and aquifers become thinner and permeable. As stated Shendong coal mines are being operated under shallow cover. The first minable coal seam is 1^{-2} or 2^{-2} coal seam and they are normally 40~70m beneath surface. Range of thickness of the two coal seams is 3~8m. Large extraction height (6~7m) longwall face is used to maximise coal recovery rate. Massive coal extraction under shallow cover leads to generation of large cracks and these cracks are very likely to propagate to aquifers above coal seam or even to mine surface. Therefore water in aquifers quickly flows into goaf through these mining induced channels and even causes water inrush incidents.

Several coal mines embark on mining second coal seam due to depletion of coal resource of first coal seam. After the first coal seam is mined, the thickness of the aquifer of the Quaternary loose layer and its water level has been changed and the natural state of ground water flow has been damaged, which leads to flooding of longwall goaf of first coal seam. Considering the second coal seam lies closely to the first coal seam (20~50m), water of upper coal seam goaf must be drained before mining the second coal seam. Upon water drainage of longwall goaf, as shown inFigure 3.14, airflow starts to migrate to the goaf through mining induced cracks. Residual coal is exposed to oxygen rich air and spontaneous combustion incident is likely to outbreak under favourable conditions.Under the influence of lower coal seam extraction and further caving of overlying strata, residual coal and coal pillars of upper goaf is further crashed and connection with lower goaf would be formed and therefore poses higher risks of spontaneous combustion.

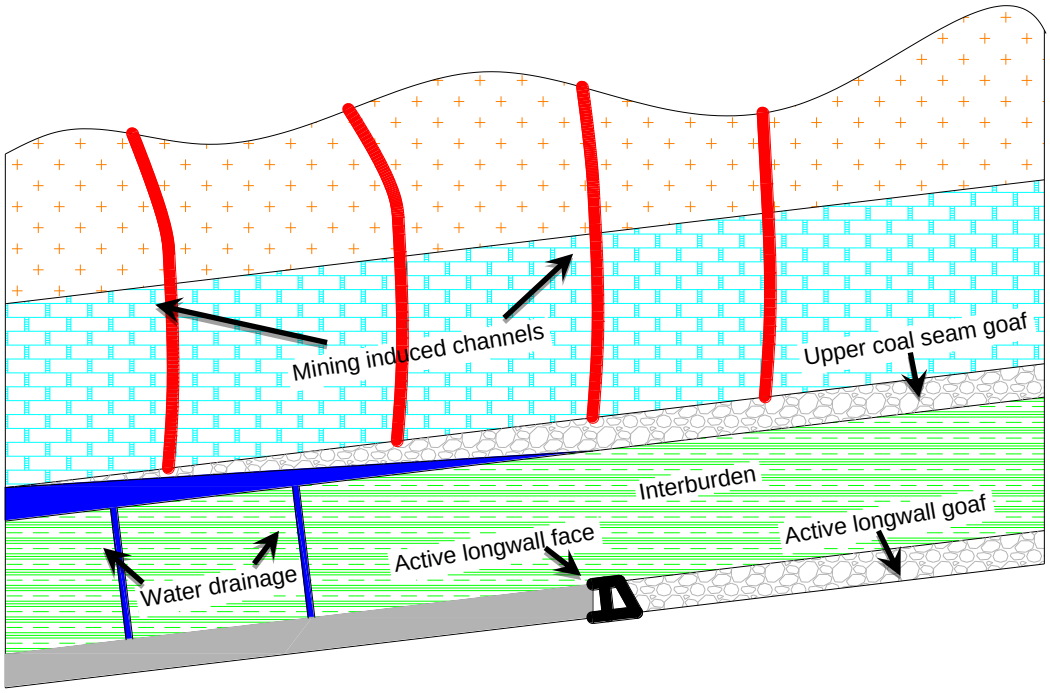

Figure 3.14 Effects of goaf water drainage to spontaneous combustion

Spontaneous combustion incident occurred in 22305 longwall of Bulianta coal mine in 2012 is used to demonstrate the effects of water drainage on spontaneous combustion. LW22305 located section three of Bulianta coal mine and adjacent LW22304 goaf is northwest to LW22305. Above LW22305 is LW12306 goaf locating upper coal seam. Average thickness of 2^{-2} coal seam is 7m and designed mining height is 6.8m and roof is allowed to fully cave in goaf. Interburden of the

two coal seams is 40m thick. 1^{-2} coal seam has been totally extracted several years ago and mining induced cracks have fully developed and reached surface. Goafs in 1^{-2} coal seam were flooded because of water ingress from surface rainfall and above aquifers. All longwall faces cut coal up-dip and hence most of water stay near start-off line of 12306 goaf. To keep coal mining safely of LW22305, flood in 12306 goaf especially in start-off line area must be drained before mining LW22305. Upon completing water drainage of LW12306, residual coal in the goaf was exposed to oxygen again and serious oxidation of coal took place. On May 6th of 2012 high concentration of CO (11915ppm) was detected in water drainage borehole. On May 7th high and rising concentrations of CO, C_2H_6, and C_2H_4 were continuously monitored. Extremely concentrated CO (35208ppm) was detected from gas sampling hole of 12306 longwall goaf on May 12th. High concentration of CO (20912ppm) and blue smoke were also detected from gas sampling hole of 22305 goaf. 1600ppm and 500ppm CO were then detected at longwall face return corner and tailgate, respectively. It was clear serious coal oxidation and even open flame incident occurred in 12306 goaf and air leakage between two goafs existed. Shortly LW22305 was sealed after advancing 117m since commencement.

3.3.3.3 Oxidation characteristics of flooded coal

(a) Interaction of coal with water

Coal, unlike other combustible material, exerts much more complex processes interacted with moisture. It has been reported water is present in coal particles as many forms and a generalised classification is bulk, capillary, multilayer, and monolayer water [210-212]. Bulk water dwells at the external surface of coal particles or in the inter-particle voids and water condensed in a coal pore structure is usually denoted as capillary water. Multilayer water, occurring in thin layers next to the walls of coal pores (a few molecular diameters in depth), is weakly bonded to hydrogen atoms in coal aliphatic or aromatic structure, while monolayer water is strongly hydrogen bonded to oxygen-containing functional groups at the pore surface [210]. More classifications of water in coal can be derived in a review work conducted by Yu and co-workers [213]. The fact that water exists in many forms implies the complex nature of coal-water interactions. Besides the mentioned physical interaction of coal with water, moisture can also be a crucial part in chemical oxidation. These effects are generalised and tabulated in Table 3.9.

Moisture plays an important part in determining the nature, rate and extent of self-heating in the stockpiled coal. The overall effect of moisture on self-heating of coal stockpile can be divided into two major aspects, namely (i) the effect of moisture transfer (evaporation, condensation, diffusion and convection) on the overall heat balance; (ii) the effect of moisture (at equilibrium or during drying or wetting) on the rate of coal oxidation [178]. It is widely reported water in a coal may chemically and physically promote or inhibit coal oxidation and self-heating behaviour of coal.

Table 3.9 Generalised effects of moisture in coal oxidation and self-heating

Literatures	Promotion of coal oxidation and self-heating
[214, 215]	Heat gain in adsorption of water
-	Heat gain from vapour condensation
[4, 17, 216, 217]	Drying can free more active surface
[216]	Water is a critical element in oxidation of pyritic sulphur
[17, 210]	Facilitate the formation of unstable intermediates at the early stage of coal oxidation
[169]	Tightly bound moisture generates radical sites
Literatures	Inhibition of coal oxidation and self-heating
[17, 210, 216]	Water can occupy active sites in coal surface and block pores
[218]	Vapour pressure in pores blocks access for oxygen
-	Heat loss from evaporation
[75]	Water can increase effective thermal conductivity of coal mass and thereby facilitate heat dissipation
[219, 220]	Drying might cause collapse of some pore structures

The interactions between water vapour and coal can either exothermic or endothermic, mostly depending on whether water condenses or evaporates. The equilibrium moisture content of coal is determined by the difference between the humidity level of the surrounding air and the inherent moisture content [33]. It is thus necessary to consider both of them simultaneously to study the effects of the moisture on the coal self-heating process. For example, dry air flowing over moist coal stockpile will adsorb the moisture and leads in temperature decrease due to evaporation; while moist air flowing over dry coal pile will condense the water vapour to coal surface and results in temperature rise because of heat gain from condensation and wetting. As inherent water plays a contradictory role in impacting

consumption rate of oxygen, theoretically a critical moisture range for a specific coal exists below or above which oxygen consumption rate is likely to be reduced. The implication of the critical water content is that if water content is higher than this critical value, extra water forms multilayer at the surface of coal pores increasing diffusion resistance for oxygen into interior of coal; whilst below this value, only a portion of the active sites have access to the monolayer water molecules and this slows down the chemisorption reactions [17, 210]. It has been suspected that the value of critical water content equals to the amount of water being adsorbed in monolayer. Table 3.10summaries some of the critical water contents for different coals.

Table 3.10 Reported critical water contents for different coals

Literatures	Coal type	Critical moisture content/%
[217]	A New Zealand subbituminous coal	8.1
[216]	Brown coals	5~10
	Two lignites	6~7
	A sub-bituminous coal	~6
[50]	A U.S. lignite	~20
[221]	Brown coals	5~8
	Subbituminous coals	1.5~2
	Bituminous coals to anthracites	0.5~0.7
[178]	A New Zealand sub-bituminous coal	8.3
[210]	A Australia bituminous coal	<0.8

(b) Self-heating characteristics and gaseous products of oxidation of flooded coal

In Shendong coal mines residual coal of upper coal seam is likely immersed into water for months or even years. Coal swells by adsorbing water and organic and inorganic compounds which adhere to surface of coal will gradually dissolve. Afterwards water slowly migrates to pore structure of coal and cleans and enlarges pores of coal. As a result pore volume and specific surface area of the coal are increased compared with that of fresh coal before immersion, especially for 2-10nm diameter pores[49].Figure 3.15 and Figure 3.16 compares difference of surface pore structure of Bulianta 2^{-2} coal before and after water immersion [48]. Pore structure is widely distributed at surface of Bulianta coal and a great number of organic and inorganic compounds are contained in the pores. Long time water immersion will dissolve these compounds and create more micro-pores and enlarger diameters of

macro-pores. Pore structure of Bulianta coal is more developed after long period of water erosion.

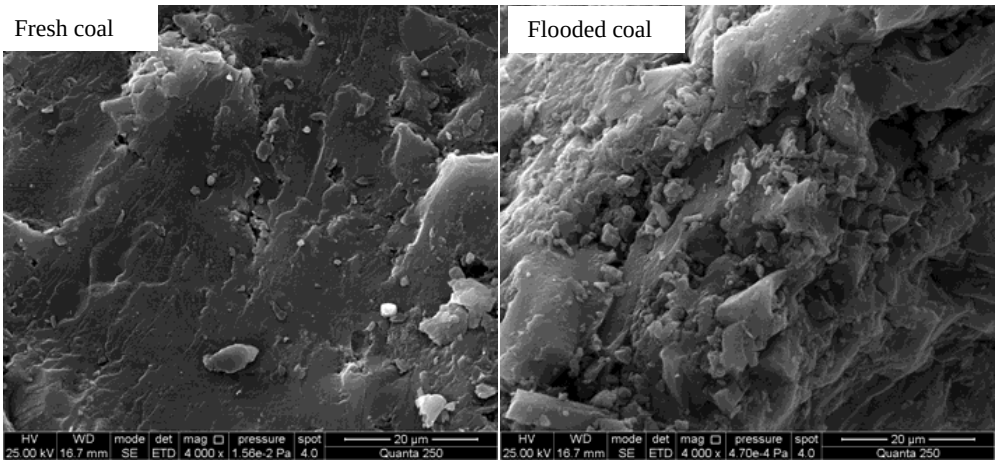

Figure 3.15 SEM micrographs of fresh and flooded Bulianta 2^{-2} coal at 4000 times magnification [48]

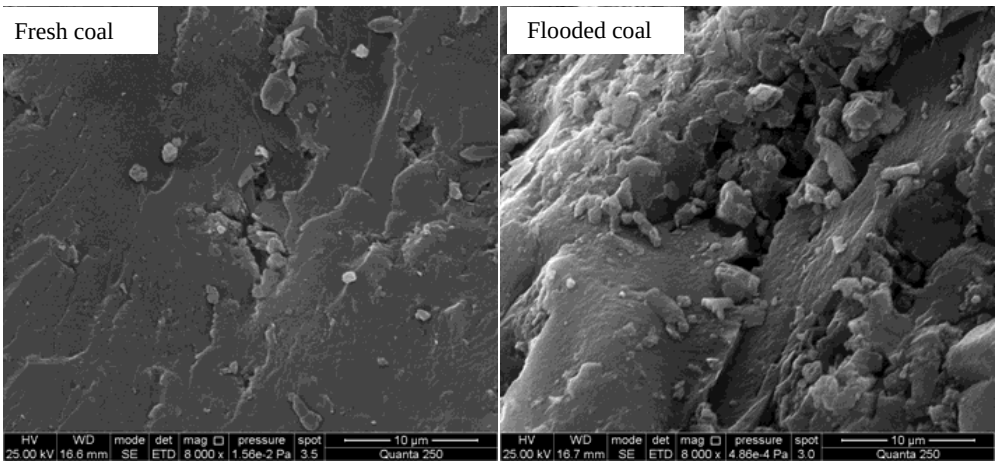

Figure 3.16 SEM micrographs of fresh and flooded Bulianta 2^{-2} coal at 8000 times magnification [48]

Deng *et al.*[46] measured exothermicity and oxygen consumption rate of oxidation of a flooded Shendong coal, refer Figure 3.17 and Figure 3.18. It is obvious that the two parameters increase with temperature. It can be also observed the two parameters of flooded coal are slightly higher than fresh coal before 60^{o}C and lower between 60~130^{o}C and higher again for temperature passing 130^{o}C. Before 60^{o}C rates of coal oxidation and moisture evaporation are quite low. Water is a necessary medium and reactant in initial coal oxidation and heat generated by "wetting" further enhances initial oxidation of flooded coal. With rising of temperature, oxidation and water evaporation rate increases and heat generated by coal oxidation is greatly consumed by water evaporation. It is the primary reason of exothermicity and

oxidation rate of moist coal is less than dry coal between 60~130°C. When temperature passes 130°C, water in flooded coal is almost totally evaporated and more free surface of coal pore is exposed. Therefore oxidation rate of flooded coal becomes higher again at higher temperatures.

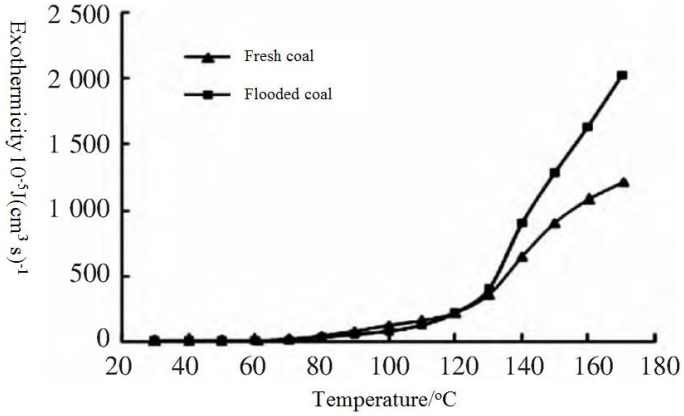

Figure 3.17 Exothermicity of oxidation of fresh coal and flooded coal [46]

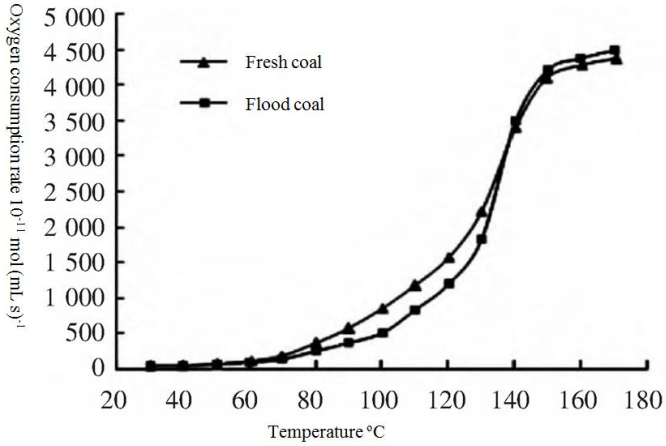

Figure 3.18 Oxygen consumption rate of oxidation of fresh coal and flooded coal [46]

Wen *et al.* [47] conducted a study to test spontaneous combustion index gases of a flooded Shendong coal, refer Figure 3.19, Figure 3.20, Figure 3.21, and Figure 3.22. The trend of CO and CO_2 generation can be seen in Figure 3.19 and Figure 3.20 respectively. Figure 3.21 and Figure 3.22 show trend of produced C_2H_4 and C_2H_6 of coal oxidation. It can be observed the amount of produced CO and CO_2 of fresh coal is higher than flooded coal before 130°C while inversely for the trend for temperature higher than 130°C. The reason is water dwells and blocks pore structure of coal at low temperature and thus the number of free active sites for oxidation of

fresh coal is larger than that of moist coal. With more free surface of coal is exposed at high temperature, oxidation rate of wet coal is however higher than fresh coal.

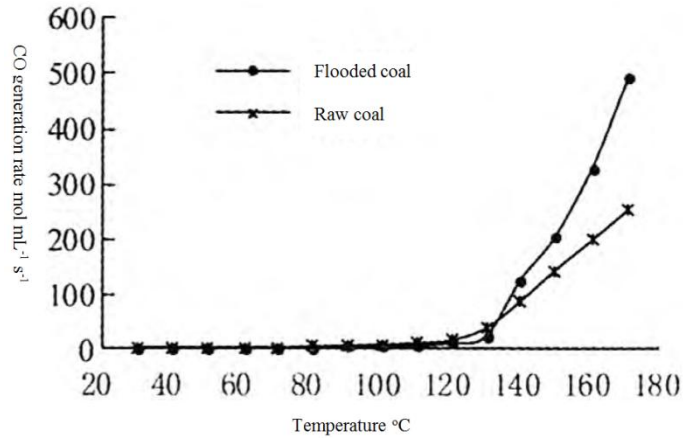

Figure 3.19 Trend of CO generation of oxidation of fresh and flooded coal [47]

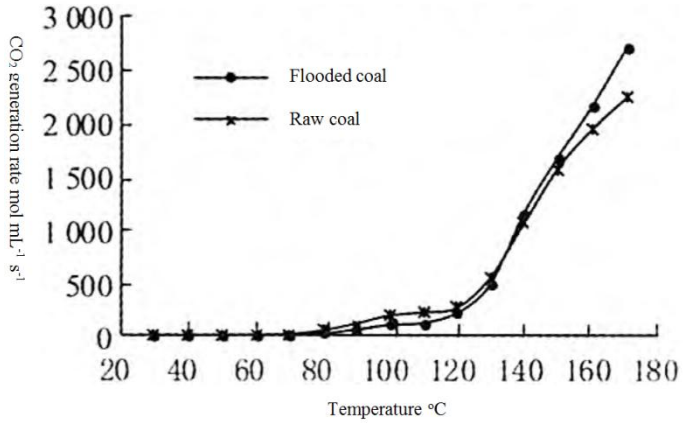

Figure 3.20 Trend of CO_2 generation of oxidation of fresh and flooded coal [47]

C_2H_4 and C_2H_6 are two important index gases of spontaneous combustion and would only be produced when coal is heated at an advanced stage. It can be seen in Figure 3.21 C_2H_6 produced by fresh coal is detected at 110^{o}C while the temperature for detection of the gas of flooded coal decreases to 90^{o}C. A similar trend is found for C_2H_4. The reason is believed long time immersion of water destructs pore structure of coal and more free surface is exposed at high temperature.

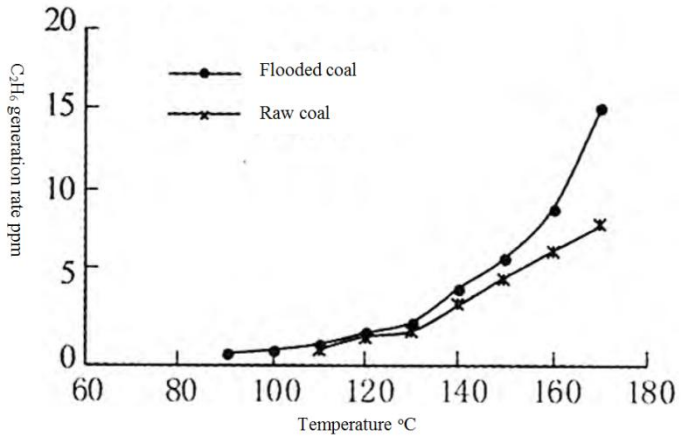

Figure 3.21 Trend of C_2H_6 generation of oxidation of fresh and flooded coal [47]

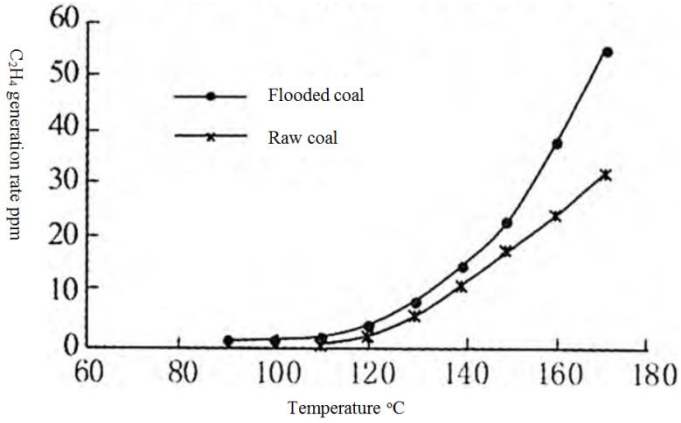

Figure 3.22 Trend of C_2H_4 generation of oxidation of fresh and flooded coal [47]

3.3.3.4 Identification of spontaneous combustion risky location in upper goaf

Airflow migrates into goaf through mining induced channels as water is drained from upper seam goaf. Considering centre area of goaf is normally consolidated by strata caving but some areas are unconsolidated. These unconsolidated or semi-consolidated areas include two gateroads, start-off line, and finish line. These areas would stay unconsolidated for many years and above these areas edge cracks are quite developed and would not be closed spontaneously. Therefore continuous airflow is leaked into these areas where oxygen content is high enough to draw a fire. As discussed for large height mining face, top coal above gateroads and transitional coal are left in goaf. Coal pillars adjacent to start-off line and finish line tend to be crashed for a long time. Due to presence of oxygen rich gas in these areas, spontaneous combustion risk is greatly enhanced.After water is drained, at interface of original water and residual coal, one side is moist coal and another side is dry coal. With influence of moisture, self-heating process of the mixed coal at interface is

considerably promoted. The detailed mechanism of self-heating of mixed coal is not fully obtained though. Upon water drainage the spontaneous combustion risky locations in upper goaf are: two gateroads, start-off and finish line, and interface of moist coal and dry coal. The identification of these risky areas helps put right control in place.

3.3.4 Low oxygen gas present in longwall face

Longwalls in Shendong coal mines are advancing fast and longwall goafs are usually interconnected due to developed mining induced fissures. Goaf gas ingress is more concentred and irregular and poses a great threat to working crew in longwall face. Since 2008 incidents of presence of rich nitrogen gas (oxygen content<15%) in longwall face have occurred on a daily basis in many longwalls such as LW12612 of Daliuta coal mine, LW22032 of Bulianta coal mine, and LW45207 of Yujialiang coal mine.

3.3.4.1 Source of nitrogen

(a) Nitrogen contained in coal seam

Nitrogen is major composition of air and amount of nitrogen contained in coal seam is normally low. Nitrogen presented in coal seam comes from following sources:

(1) Ingress from outcrop

If original coal seam gas is mainly composed of CH_4,CH_4 tends to move upward because heavier N_2 is brought from outcrop of coal seam and stays in deep coal seam.

(2) Water inrush

More or less nitrogen is dissolved into surface water and nitrogen is transported into coal seam by water infiltration.

(3) Coalification

A large amount of CH_4 and NH_3 is produced during coalification and degassing of coal. If red bed exists adjacent to coal seam, Fe_2O_3 in the red bed reacts with NH_3 and releases N_2. Produced N_2 may migrate into coal seam or above strata.

Gas content of Shendong coal seams is summarised in Table 3.11. It shows main composition of coal seam gas in Shendong coalfield is nitrogen but sources of the nitrogen are not fully understood though.

Table 3.11 Gas contents of Shendong coal seams

Coal seam	Gas content (m^3/t)	Composition			
		CH_4 (%)	CO_2 (%)	N_2 (%)	CO (%)
Daliuta 2^{-2}	0.088	0.00	11.8	88.2	0.00
Liuta 2^{-2}	0.104	0.00	3.3	96.7	0.00
Yujialiang 4^{-2}	0.117	0.00	16.1	83.8	0.00
Shigetai 3^{-1}	0.112	0.00	2.1	97.9	0.00
Yujialiang 5^{-2}	0.136	0.00	9.8	90.1	0.00
Bulianta 1^{-2}	0.094	0.00	2.9	97.1	0.00

(b) Oxidation of residual coal

According to Table 3.3, most coals from Shendong coal mines are very liable to spontaneous combustion and their abilities to absorb oxygen are very strong. Also as discussed considerable amount of coal is left in goaf and consumes oxygen and as a result of it, high concentration nitrogen gas is left in goaf and tends to flow into longwall face.

3.3.4.2 Migration of nitrogen

(a) Adjacent goaf

In Shendong coal mines extraction of coal causes break and movement of overlying strata and caving zone and crack zone are formed. In the crack zone, separated fractures and vertical fractures are quite developed. Rocks in the caving zone are irregularly collapsed and distributed irregularly. The loose coefficient is relatively large, which provides a channel for nitrogen migration. Reserved coal pillars are crashed as roof caving and longwall goafs become interconnected so gas in one goaf can flow into adjacent goaf. It was found low oxygen incidents at longwall face are likely to be caused by gas migration from adjacent goaf because the incident rarely occurs at first longwall of a section and at initial mining of a longwall.

Gas monitoring data in LW12612 of Daliuta coal mine reveals concentration of nitrogen in goaf is roughly 80% and concentration of oxygen at return corner of longwall face is higher than 18% at start of the longwall face [222]. LW12611 is an old goaf adjacent to LW12612 goaf and the two goafs become connected through cut-throughs and developed cracks. As longwall face advances a few hundreds'

meters, gas from adjacent goaf (LW12611) starts to move to active goaf and causes goaf gas ingress incident in LW12612, refer Figure 3.23 which provides a schematic view of goaf has migration and air leakage between active goaf and adjacent sealed goaf. It indicates low oxygen incident at longwall face is unlikely to be caused by gas ingress from only active goaf.

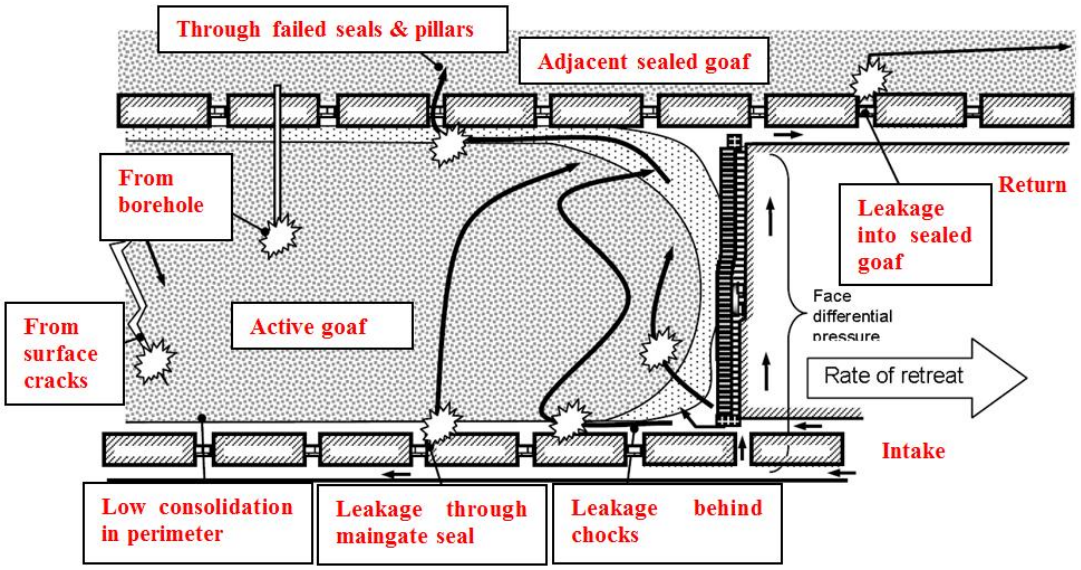

Figure 3.23 Gas migration and leakage between active goaf and sealed goaf

(b) Barometric pressure

Local metrological data shows that in the Shendong mining area, the highest barometric pressure is distributed in winter months including December, January and February. Then climate is turning warm and atmospheric pressure gradually reduces in summer. With fall and winter approaching, barometric pressure starts to rise again as shown in Figure 3.24. Figure 3.25 shows variation of daily barometric pressure in Bulianta coal mine of four different days. It can be clearly seen the maximum value of atmospheric pressure emerges between 5:00 and 10:00 in morning and the lowest pressure is between 14:00~20:00. The difference of the two values is approximately 0.7kPa.The annual variation of atmospheric pressure has certain but less than obvious influence on goaf gas migration. The main cause of abnormal nitrogen gas dispersion is frequent changes of atmospheric pressure in one day.

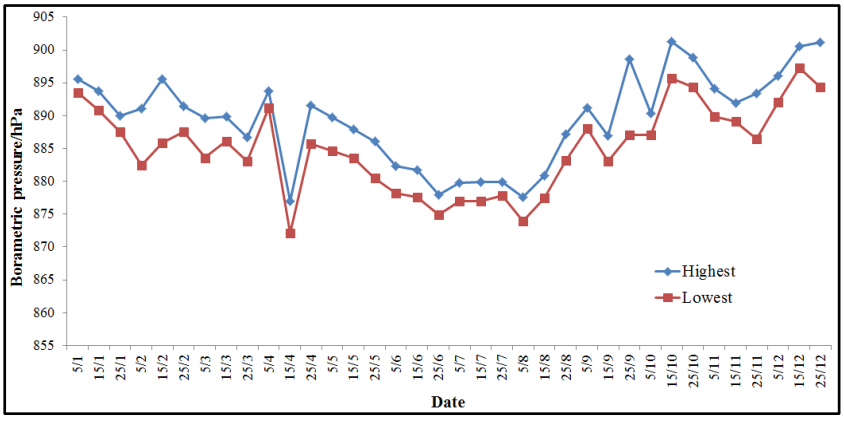

Figure 3.24 Variation of annual barometric pressure in Bulianta coal mine

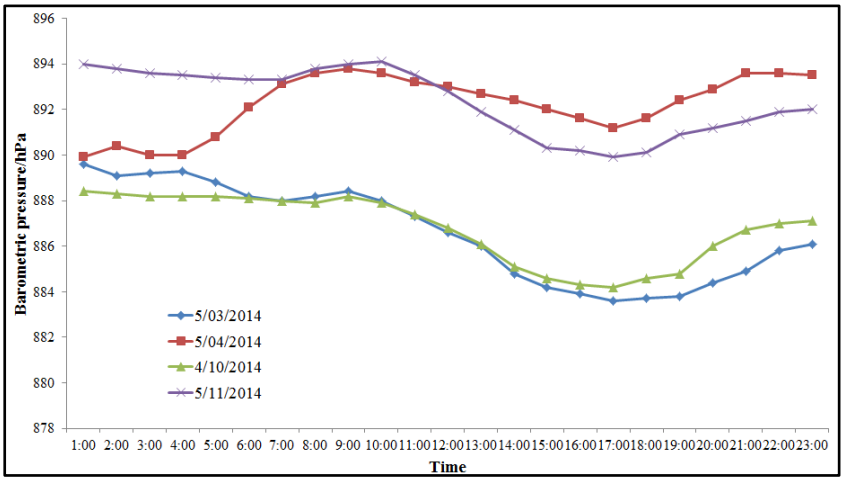

Figure 3.25 Variation of daily barometric pressure in Bulianta coal mine

Longwall goaf can be regarded as semi-sealed area and filled with high concentrations of nitrogen gas mixture. If the absolute pressure of gas in goaf changes, the volume of gas mixture must expand or shrink, which results a phenomena called “breathing of goaf”. When goaf gas is leaking out, locations such as return corner of longwall face and gas drainage borehole are more vulnerable due to relatively low pressure. As mentioned above, absolute static pressure of airflow at any underground point changes synchronously with the change of atmospheric pressure. Thus the change of barometric pressure will inevitably cause the abnormal transport of goaf gas. The larger of the pressure difference and volume of goaf, the more volume of goaf gas is leaked. In winter and spring, daily variation of temperature is noticeable and as a result of it, the change of barometric pressure is large enough to cause abnormal movement of goaf gas and variation of oxygen concentration in longwall face. According to the measured data, the oxygen concentration in the return upper corner of longwall face is consistent with the

change of atmospheric pressure. Amount of goaf gas ingress is relatively large between 16:00~22:00, which lags behind atmospheric pressure about 2 hours, refer Figure 3.26.

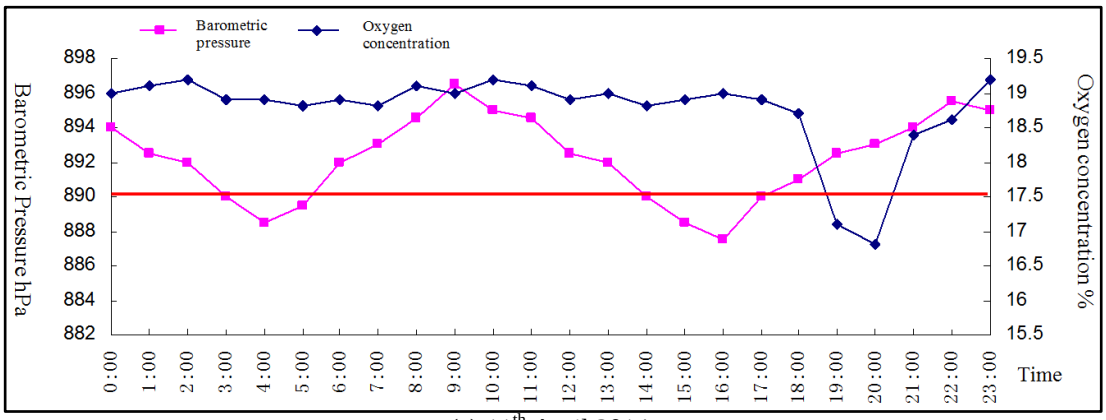

(a) 11th April 2014

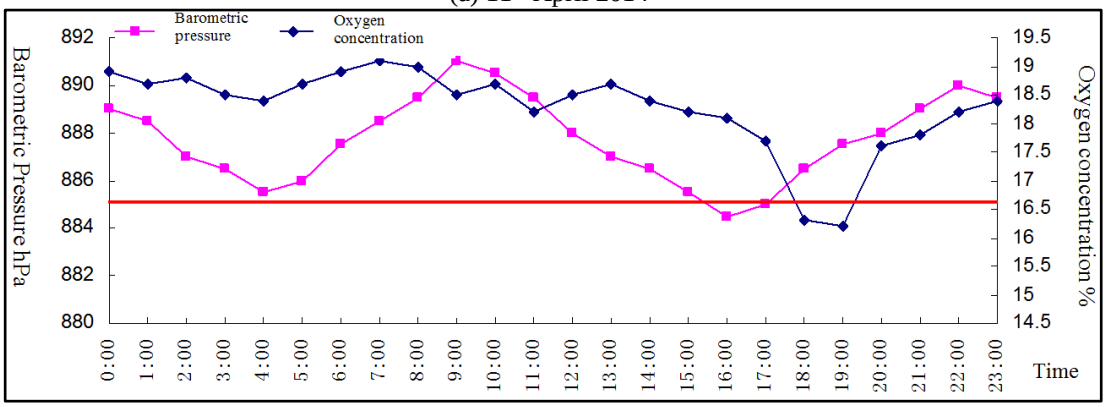

(b) 10th June 2014

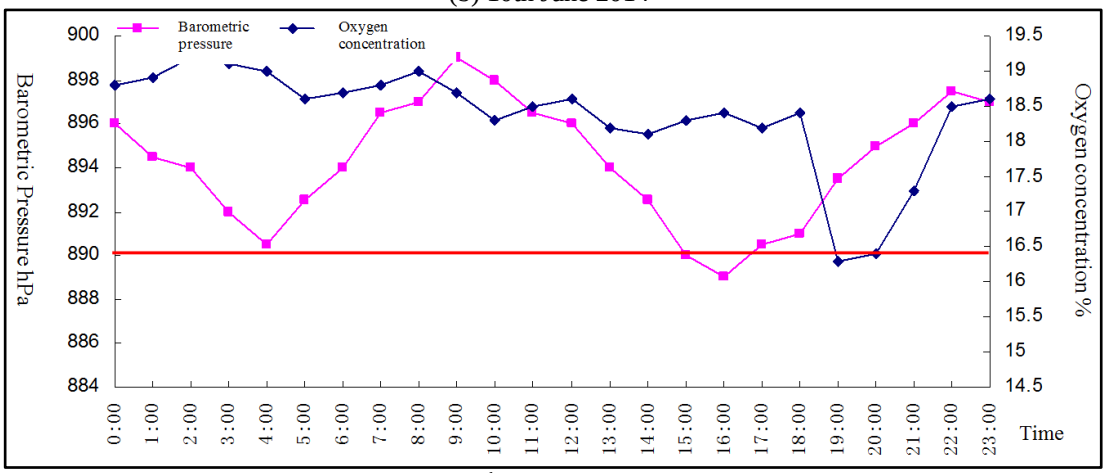

(c) 15th November 2014

Figure 3.26 Relation of barometric pressure with oxygen concentration at return corner of LW22307 of Bulianta coal mine

3.3.5 CO accumulation at return corner of longwall face

It is widely known CO is a gaseous product of coal oxidation and its production rate increases with temperature. CO is widely used to detect early self-heating of coal as

amount of produced CO is appreciable and the gas is easy to be detected even a little amount of CO is liberated. Since 2000 CO has been detected at return corner of return corner of longwall face of more than 80% Shendong coal mines. Some of the situations have exceeded acceptable level of safe production. Although high concentration CO was detected in longwall face, high temperature in residual coal and other spontaneous combustion index gases were not detected. However in some other cases concentrated CO may reflect a spontaneous heating incident of coal. Therefore source of CO and its migration must be fully understood for spontaneous combustion control in Shendong coal mines.

3.3.5.1 Oxidation of residual coal

It is widely believed the temperature at which CO is liberated varies from coal to coal. Some coal may produce CO with low-temperature oxidation and the production rate significantly grows with temperature. High level CO (30~90ppm) persists at return corner of longwall face of most Shendong coal mines but meanwhile other spontaneous combustion indicating gases like C_2H_4 are not detected. Hence this high level of CO does not necessarily originate from spontaneous combustion of residual coal. Highly concentrated CO is not only liberated at high temperature but also at ambient temperature, refer Table 3.12. Therefore under normal circumstances, noticeable amount of CO can be produced at low temperature.

Table 3.12 CO generation rates of Shendong coals at low temperature [223]

Coal sample	Critical temperature/ ^{o}C	Critical concentration/ppm	CO production rate /mL min^{-1} m^{-3}
Shangwan 1^{-2}	60	8.9	5.1
Bulianta 2^{-2}	70	7.8	4.5
Wanli 3^{-1}	60	4.9	2.8
Liuta 1^{-2}	60	8.1	4.6
Yujialiang 5^{-2}	60	6.7	3.9

3.3.5.2 CO in coal seam gas

As can be seen from Table 3.11, amount of CO contained in coal seam is very low. Considering the effect of large quantity of ventilation at longwall face, the CO situated in coal seam is unlikely to cause persistence of high level CO in return corner of longwall face.

3.3.5.3 CO from coal cutting at longwall face

As an organic macromolecule material, massive fractures are induced and molecular structure of coal is likely to be destructed by cutting coal at longwall face. As a result

of it, a large of number of free radicals is released and oxygen reacts with these free radicals to produce CO [224]. During process of coal cutting, huge energy is released as picks of shear are breaking coal and the maximum instantaneous temperature can reach more than 600^{o}C. With influence of high temperature, the number of aromatic benzene nucleus of coal increases and side chains and functionalgroups (hydroxyl-OH, methyl-CH_3, carboxyl-COOH, and ether-C-) of coal gradually decompose, accompanying by the emergence of new substances including CO[225]. A series of field measurements were conducted at longwalls of different coal seams in Shendong and it was found 10~20ppm more CO would be present at return corner of longwall face and the temperature of coal face increases 10~20^{o}C after coal cutting [225].

3.3.5.4 CO from effluent gas of diesel truck

Diesel trucks are used in Shendong coal mines to transport working crew and material due to its flexibility. However, underground trucks are fuelled with diesel and it was reported content of CO contained in effluent gas of truck is normally less than 1000ppm [226]. The produced CO pollutes underground airflow and has adverse effects on early detection of spontaneous combustion incident. To quantify the effect of effluent gas on level of CO present at return corner of longwall face, field measurements were undertaken at several Shendong longwalls (LW12406 and LW22304 of Bulianta coal mine, LW22403 of Halagou coal mine, and LW31301 of Wanli coal mine) and it was found 10~20ppm more CO was detected at intake airflow of longwall panel during frequent operation of underground trucks [227].

3.4 Summary

Shendong coal mines are an important energy reserve base in China. Spontaneous combustion is a serious hazard in Shendong coal mines due to its unique mining conditions. From geological conditions, geotechnical conditions, coal quality, and mining and ventilation method perspectives, common features of Shendong coal mines are identified and simplified as following:

- Most coals are very liable to oxidation and self-heating;
- Multiple seam extraction under shallow cover;
- Large mining height is used;
- Mining induced cracks are developed and propagate to surface;
- Upper longwall goafs are flooded;
- Coal pillars are crashed with strata caving and goafs are connected.

These common features however may cause common problems of spontaneous combustion as following:

- Serious air leakage from surface;
- Massive coal is left in goaf;
- Flooded coal exhibits higher propensity of spontaneous combustion;
- Nitrogen rich goaf gas ingress into longwall face;
- CO accumulation at return corner of longwall face.

These problems are not isolated and one problem may have great impacts to another one. Their relations can be analysed through three contributors (combustible material, oxygen, and heat) of a fire triangle. If one of the three elements is missing, fire is not able to be started or an on-going fire would be quenched. Figure 3.27 shows relations of spontaneous combustion problems in Shendong coal mines. Due to limitation of mining technology, coal seam thickness and geotechnical conditions of coal seam strata, massive tons of coal is left in goaf especially for the following locations: two gateroads, start-off line and finish line. Most Shendong coals have strong ability of oxygen adsorption and are quite subject to spontaneous heating. The coals are combustible than other coals.

Shendong coal seams are operated under shallow cover and the cover is featured with thick loose layer, thin rock bed, and rich in water. Shendong coal mines also extract multiple coal seams and large mining height is used in some mines. The intensive coal mining causes fully development of mining induced cracks and these cracks propagate to surface especially the edge cracks are hard to be closed. Exhaust ventilation system is widely used in Shendong coal mines and the negative pressure draws a significant quantity of airflow leaked into goaf. The airflow sustains self-heating of residual coal in goaf. As the mining induced channels are also likely to cut through above aquifers, longwall goaf is flooded gradually. The water in upper goaf requires to be drained upon mining underlying coal seam. During flood drainage airflow is leaked into goaf through mining induced fissures, which results self-heating of flooded coal and even spontaneous combustion incident. Shendong coals are capable of being oxidised at low temperature, which consumes a large amount of oxygen and produces noticeable amount of CO. Due to connection of longwall goafs, goaf hazardous gas including high level of nitrogen and CO is very possible to

migrate into longwall face and pose a great threat to mining crew. It is very important to identify the spontaneous combustion characteristic problems and clarify their relations. The analysis has practical significance and helps put right spontaneous combustion controls in right place.

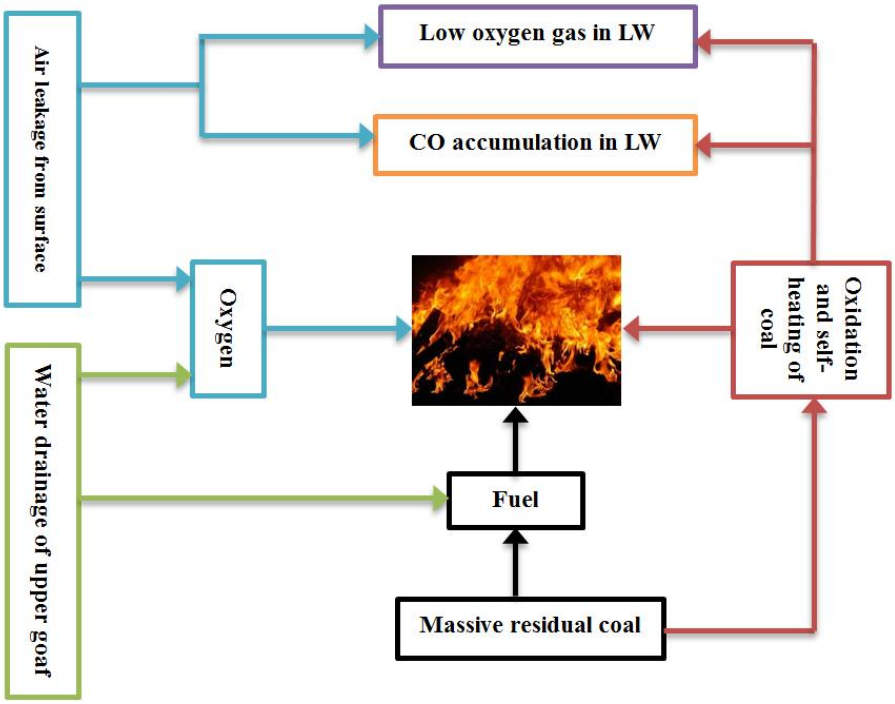

Figure 3.27 Relations of spontaneous combustion problems in Shendong coal mines

4 LABORATORY TESTS OF SHENDONG COALS

4.1 Chapter introduction

The coal seams in newly developed Shendong coal mines are generally thick and the risk of spontaneous combustion significantly increases during longwall mining due to the large quantities of broken coal left behind the chocks and its exposure to high oxygen levels in the goaf [228]. Due to depletion of the overlying coal seam, many coal mines in Shendong coalfield have been starting to extract the second seam or mined multi-seam simultaneously. As discussed in Chapter Three, residual coal in longwall goaf of upper coal seam was usually flooded or oxidisedprior to mining of longwall face of the underlying coal seam. It has been reported residual coal in upper goaf exhibit a different liability to spontaneous combustion and it is therefore required to investigate the difference and to gain a better understanding.

The ignition temperature of coal is a straightforward index to assess liability of coal to spontaneous combustion [229, 230].Such knowledge can be used to assess the severity and the incubation period of an onset heating. The ignition temperatures of Shendong coal samples can be tested following an industrial standard testing method. Briefly the method follows the following steps: a coal sample is mixed with oxidising agent (sodium nitrite) in a certain proportion; discharge the coal sample to an oven which is heated with a certain rate; the temperature at which the coal sample bursts into a fire is recorded as the ignition temperature.

A range of gaseous products would be generated during coal oxidation. These gases including CO_2, CO, CH_4, C_2H_4, C_3H_8, and other higher hydrocarbon gases are attributed to decomposition and pyrolysis of oxygenated hydrocarbons [25, 188]. Different types of gases and different concentrations of a particular gas would be generated at different temperatures (i.e. fire ladder). This knowledge can be used to determine severity and to forecast an onset heating in a longwall goaf through interpretation of gas monitoring data. In laboratory gas evolution tests are useful in determining the behaviour of the coal as it is heated and the development of gaseous indicators for early detection. The information is also used to reflect the difference of

gaseous products liberated during oxidation of different coals or a same coal treated with different circumstances. Therefore the gas evolution test is another important tests conducted in this study.

Spontaneous combustion of coal is an extremely complicated process and is influenced many factors. This process starts with low temperature coal oxidation in which heat generation is very slow. If the generated heat is less than the heat loss via conduction and radiation to the surrounding environment and convection to the ventilation flow, self-heating of coal is unlikely to sustain. If not so, extra heat is absorbed by the coal and results in rising of coal temperature, which in turn causes further increase of the rate of coal oxidation, producing more heat till outbreak of spontaneous combustion. Adiabatic heating of coal refers to a situation in which heat loss especially during low temperature coal oxidation is minimised. The adiabatic environment is accomplished by placing a reaction vessel inside an adiabatic oven or oil bath. The oven temperature is controlled automatically to equal that of the sample, thus minimising heat losses. The adiabatic testing method is more likely to provide a truly intrinsic property of coal to spontaneous combustion and a full temperature rising history. The rate of adiabatic heating is an important factor to evaluate propensity of coal to spontaneous combustion. Many studies regarding adiabatic heating of coal have been conducted [174, 175, 177, 231] and thus the adiabatic testing method is used in this study.

Before extraction of second coal seam, residual coal of overlying goaf may have undergone a pre-heating history in an oxygen deficiency atmosphere. The pre-heated coal may exhibit a different self-heating features comparing with freshly exposed coal. Among the indexes to assess propensity of self-heating of coal, low-temperature oxidation kinetics are the most fundamental and critical ones. However, studies regarding low temperature kinetic analysis of coals with pre-heating history are scarce. Many techniques were developed to determine coal oxidation kinetics, such as adiabatic oven testing method [3, 231], heat release measurement method [112, 232], and thermal analysis method [111, 186, 233-235]. Thermal analysis method is the most widely used and mature method to determine coal oxidation kinetics for both low temperature and high temperature with standardised equipment.

The thermal analysis method includes Thermogravimetric Analysis (TGA), Differential Thermal Analysis (DTA), and Differential Scanning Calorimetry (DSC). Among them DSC can not only determine chemical reaction kinetics of experimental samples but also be able to assess exothermicity of tested samples and therefore DSC is employed in this study.

4.2 Proximate and ultimate tests

4.2.1 Collection of coal samples

Four coal samples were collected from two Shendong coal mines. The coals were all freshly exposed coal at longwall face. More details of the coal samples are given in Table 4.1. The coal samples were then stored in air tight seal bags and sent to the laboratory in Shenyang branch of China Coal Research Institute. Each of the coal samples was slightly peeled and broken to two groups with a sharp end hammer. One group (group A) coal samples was further crashed to smaller size (less than $1cm^3$) and stored in a bucket full of water to mimic conditions of flooded coal. Another group (group B) coal was immediately arranged for other tests or sealed and stored in a refrigerator.

Table 4.1 Details of collected coal samples

No.	Sample name	Coal mine	Coal seam	Location	Weight/kg
1	BLT1-2	Bulianta	1^{-2}	LW12519	16.3
2	BLT2-2	Bulianta	2^{-2}	LW22307	18.6
3	SGT2-2	Shigetai	2^{-2}	LW22206	15.7
4	SGT3-1	Shigetai	3^{-1}	LW31202	17.1

4.2.2 Proximate analysis

Proximate tests of coal samples were conducted in SDLA618 coal proximate analyser manufactured by Hunan Sundy Science and Technology Development Co.,Ltd..It is an automatic apparatus for coal proximate testing. Detailed steps of the test are shown in Table 4.2. Figure 4.1is a photographic view of test in process in which coal sample crucibles are being sent to oven. Proximate tests of each coal sample were conducted three times and the average was determined as the final result. Proximate analysis of the four coal samples was tabulated, refer Table 4.3.

Table 4.2 Testing procedures of proximate analysis

No.	Steps	Detailed description
1	Coal sample preparation	Coal samples of group B were crashed in particle size 0.125~0.15mm;
2	Crucible preparation	Clean and dry water, ash, and volatile matter testing crucibles and sampling scoops;
3	Equipment calibration	Start the analyser and computer, run calibration of the analyser especially balance external and internal scales;
4	Test mode setting	Select the right testing mode based on the type of coal;
5	Discharge coal samples	A certain amount of coal samples (50~70mg for water&ash content test, 90~120mg for volatile matter test) were weighted with the external scale and were discharged to the right crucibles;
6	Position crucibles	Follow instructions of testing mode and position the crucibles to the right circular slots;
7	Initiate test	Check the flowrate of the incoming air and initiate the test;
8	Retrieve crucibles	At end of the test, retrieve crucibles and dump the remaining material into a bin;
9	Log results	Store the results in computer;
10	Ending test	Cool down the analyser and power off the analyser and the computer

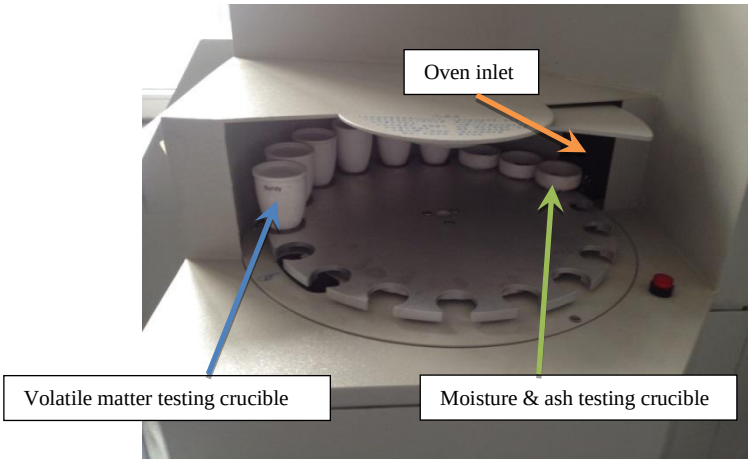

Figure 4.1 Proximate test of Shendong coal samples in process

Table 4.3 Proximate analysis of the four Shendong coals

Coal sample	Day air basis				
	Moisture (%)	Ash (%)	Volatile matter (%)	Fixed carbon (%)	Calorific value (MJ/kg)
BLT1-2	7.80	3.37	27.35	61.20	32.08
BLT2-2	7.38	4.72	29.11	58.37	31.64
SGT2-2	10.47	3.83	26.84	58.50	30.91
SGT3-1	10.50	4.14	27.74	57.13	30.77

4.2.3 Ultimate analysis

Ultimate analysis of Shendong coals were accomplished with 5E-CHN2000 ultimate analyser made by Changsha Kaiyuan Instruments Co., Ltd.. Procedures of the test is summarised in Table 4.4. Ultimate analysis of the four coal samples is given in Table **4.5**.

Table 4.4 Testing procedures of ultimate analysis

No.	Steps	Detailed description
1	Coal sample preparation	Coal samples of group B were crashed in particle size 0.125~0.15mm;
2	Equipment preparation	Power on computer and stalise the equipment, check leakage of oxygen and helium;
3	Equipment calibration	Run an analysis of a blank sample to calibrate the system;
4	Set analysis method	Select analysis method based on coal rank;
5	Discharge coal sample	Discharge coal sample 120mg to foil cup and place the cup to testing crucible;
6	Initiate test	Start test by sending order from computer;
7	Save result	Save testing results to computer;
8	Completing test	Power off and cool down the equipment and computer.

Table 4.5 Ultimate analysis of the four Shendong coals

Coal sample	Dry ash free				
	C	H	N	S	O (by diff.)
BLT1-2	80.04	4.12	1.21	0.21	14.42
BLT2-2	78.56	4.26	1.06	0.32	15.80
SGT2-2	79.02	4.22	1.13	0.26	15.37
SGT3-1	78.54	4.19	1.24	0.38	15.65

4.3 Ignition temperature test

4.3.1 Testing apparatus

Figure 4.2 is a schematic view of the testing apparatus which consists of two major units: temperature controller and heating element. The apparatus is made by HebiYingtai Instruments Co., Ltd. and the type of the apparatus is YTRD-6. Figure 4.3 shows the heating elements of the apparatus.

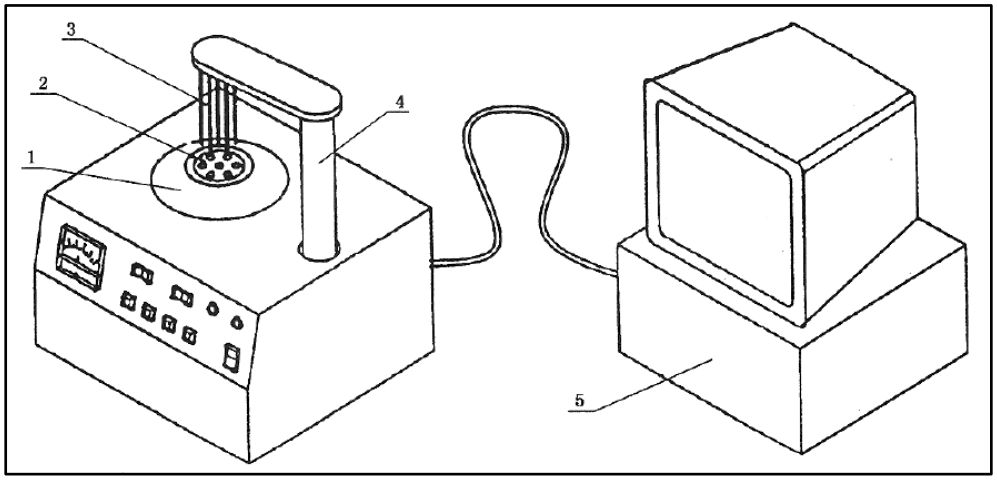

1-Heating oven；2-Copper heater；3-Thermocouple；4-Lifting rod；5-Temperature controller

Figure 4.2 A schematic view of coal ignition temperature testing apparatus

Figure 4.3 YTRD-6 coal ignition temperature testing apparatus

4.3.2 Testing procedures

Detailed testing procedures are provided in Table 4.6.

Table 4.6 Testing procedures of ignition temperature determination

No.	Steps		Detailed description
1	Coal sample preparation	Fresh coal	Fresh coal was crashed to coal particles less than 0.2mm and then place the coal particles in a vacuum dryer in which 55~60^{o}C temperature and 53kPa pressure were maintained, retrieve the coal particles for further use after two hours;
		Oxidised coal	Place 0.5~1g fresh coal particles (<0.2mm) in a flask, use a dropper to drip hydrogen peroxide solution into coal sample (0.5 mL/g coal), mix them well with a glass rod, cover the flask with a lid and place in darkness for 24 hours, remove the lid and expose the oxidised coal sample to sunlight or incandescent light for 2 hours, then place the oxidised coal particles in a vacuum dryer in which 55~60^{o}C temperature and 53kPa pressure were maintained, retrieve the coal particles for further use after two hours;
		Flooded coal	Withdraw the flooded coal after coal of group A was immersed into water for six months, place the flooded coal in the vacuum dryer for 2 hours, then crash the coal to particles less than 0.2mm (the water content of flooded coal samples were also tested, refer Table 4.7);
2	Reactant preparation		Place a certain amount of sodium nitrite in a flask, put the flask in the vacuum dryer (105~110^{o}C) for one hour, then cool down and retrieve the sodium nitrite for further use;
3	Grind coal sample and reactant		Put coal sample (0.1±0.01g) and dry sodium nitrite (0.075±0.001g) in an agate mortar, gently grind for 1~2 min, make the coal sample blended well with sodium nitrite, refer Figure 4.4;
4	Discharge coal sample		Discharge the mixed sample to a testing tube and place the tube into a slot of the copper heater, insert a thermocouple in the sample
5	Initiate test		Switch on the computer and temperature controller, define and initiate the test, the oven is heating up 5^{o}C/min;
6	End test		Power off the heater when the sample is ignited, cool down the heater and testing tube, remove the tube and clean;
7	Log results		Save result and power off computer.

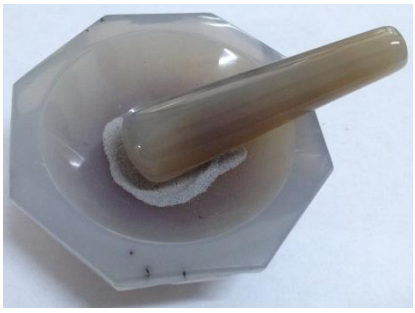

Figure 4.4 Grind coal sample together with sodium nitrite

Table 4.7 Comparison of water content with and without immersion in water

Coal sample	Original water content/%	Water content of flooded coal/%
BLT1-2	7.80	15.23
BLT2-2	7.38	14.55
SGT2-2	10.47	17.61
SGT3-1	10.50	17.19

4.3.3 Testing results

The testing results are given in Figure 4.5. As can be seen, ignition temperatures of the four fresh coal samples were all below 300^{o}C, in which the highest ignition temperature is 297^{o}C of SGT3-1 coal sample. It has been shown ignition temperatures of most China coals are higher than 320^{o}C and for an anthracite, a demonstrated coal which is not liable to spontaneous combustion, the ignition temperature is usually higher than 350^{o}C [49, 222]. If low temperature oxidation of coal is not considered, Shendong coals are more readily to develop to an open fire on the basis of the ignition temperature. Therefore more precautions might be required to be taken upon storing and transporting Shendong coals.

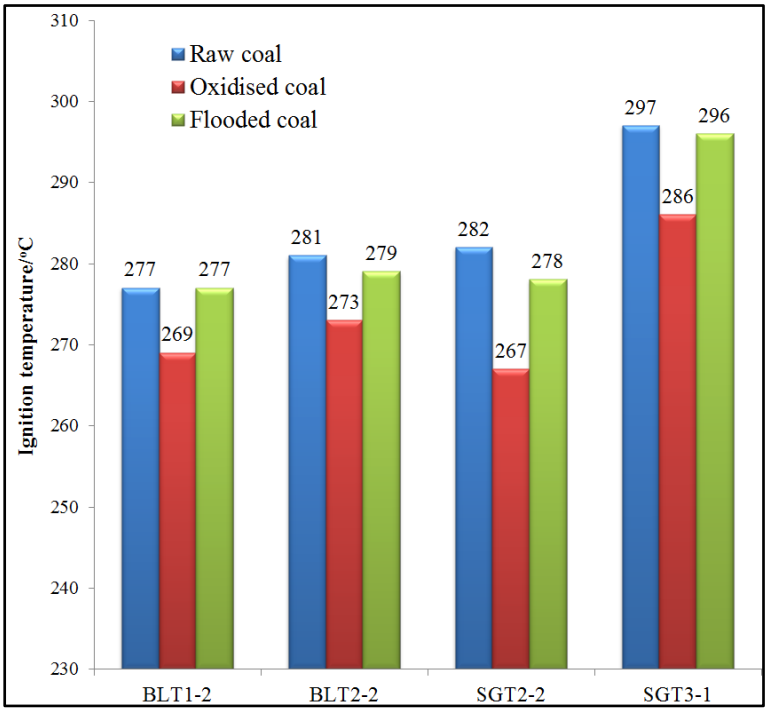

Figure 4.5 Ignition temperatures of Shendong coal samples

It can be also seen ignition temperatures of the oxidised coal samples are 8~15^{o}C lower than fresh coal samples. The variation of ignition temperature mainly reflects the difference in volatile matter of the coal samples. Therefore content or composition of volatile matter of coal sample changes after oxidation and so the energy required for volatile matter to burst. It is widely accepted the low temperature oxidation of coal might be greatly hampered if the coal has a pre-oxidation history. However the propensity of oxidised Shendong coals to spontaneous combustion should not be underestimated because the oxidised coal is easier to be ignited at a high temperature. Another finding is that ignition temperatures of the flooded coal samples remain almost unchanged or slightly drop compared to fresh coal samples. Thus it might be concluded no significant variations of volatile matter occur and slight more energy is required to evaporate the excessive moisture content for the flooded coal samples.

4.4 Gas evolution test

4.4.1 Testing apparatus

A schematic view of the gas evolution testing system is given inFigure 4.6. The overall layout of the system can be seen in Figure 4.7. The whole system is mainly composed of several units: gas supply bottles, reaction vessel and heating elements,

gas analysis unit, and data taker. Two gas bottles are used: one is nitrogen bottle which is used to terminate test and to dry coal sample if necessary and another one is compressed air bottle which is used to sustain coal oxidation. The reaction vessel is made of aluminium and coiled gas tube is fitted on the vessel to sufficiently pre-heat incoming gas. The heating elements are made of graphite resistor and the insulation material is asbestosfibre, refer Figure 4.8. The sample holder is essentially a steel disk with micro-pores which allows passing of gas. Temperature of the heater is controlled by the temperature controller which has the accuracy up to $0.5^{o}C$ per minute. Composition of effluent gas is determined by a GC and the results are logged and stored by the data taker.

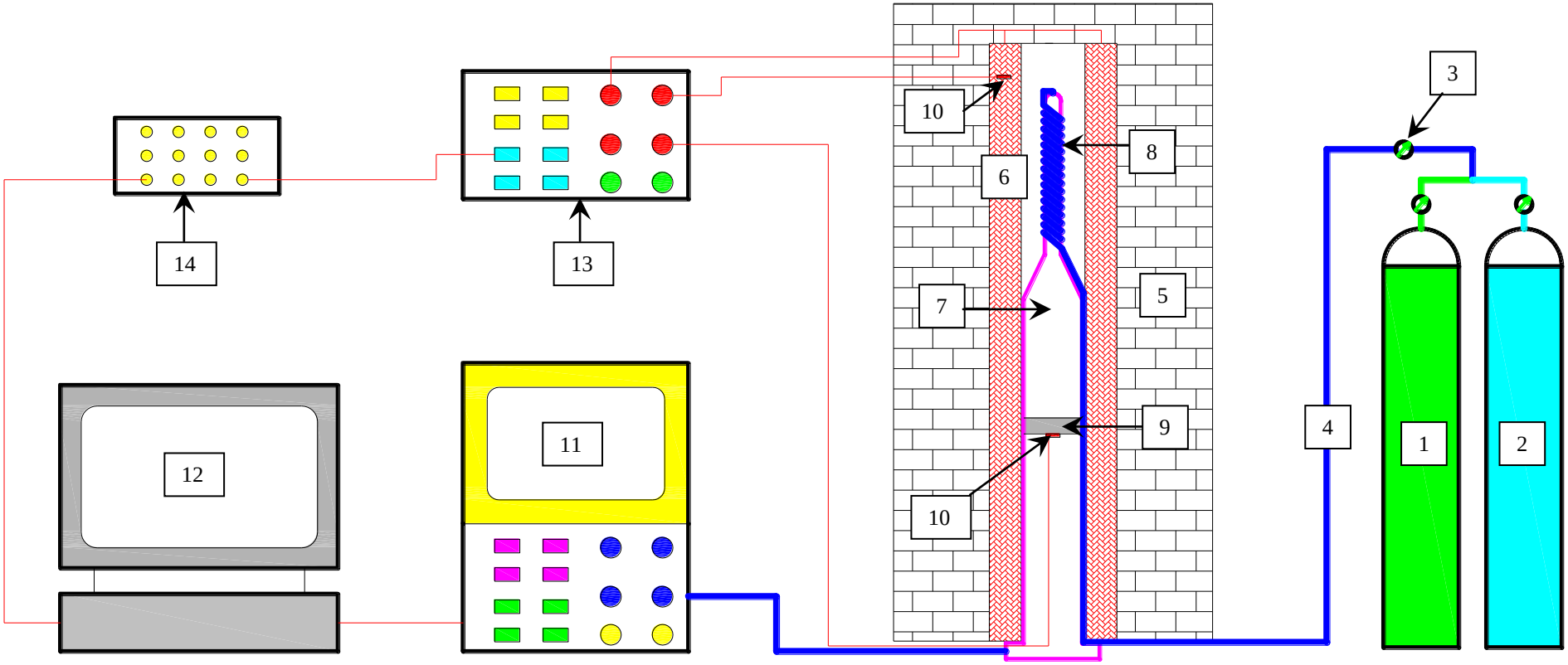

1-Nitrogen; 2-Compressed air; 3-Gasflow control valve; 4-Gas tube; 5-Insulation material; 6-Heating elements; 7-Reaction vessel; 8-Coiled tube; 9-Coal sample holder; 10-Thermocouple; 11-GC; 12-Computer; 13-Temperature controller; 14-Data logger

Figure 4.6Gas evolution testing apparatus

Figure 4.7 Overall layout of the gas evolution testing system

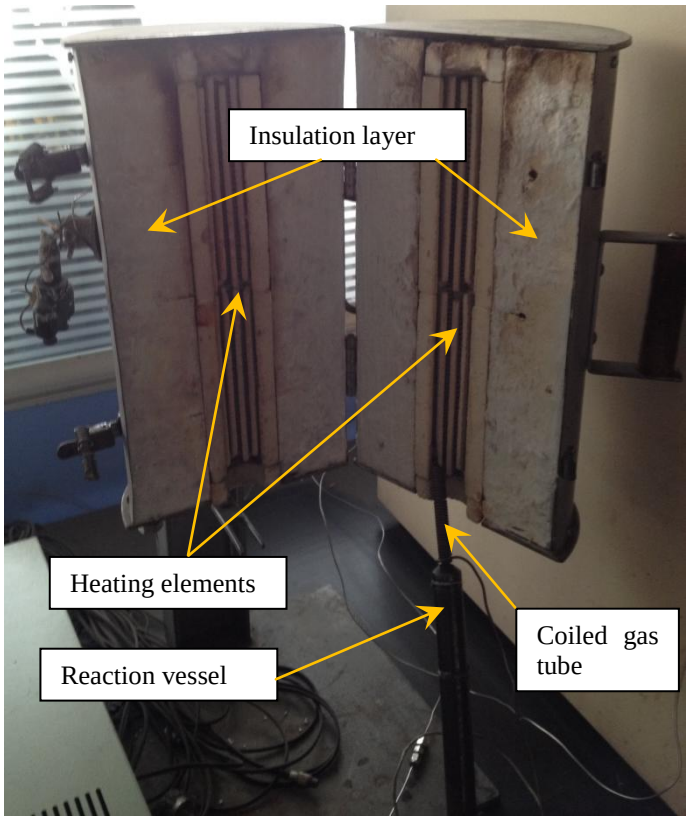

Figure 4.8 Reaction vessel and heating elements

4.4.2 Testing procedures

Testing procedures of the gas evolution test are given in

Table 4.8.

Table 4.8 Testing procedures of gas evolution test

No.	Steps		Detailed description
1	Coal sample preparation	Fresh coal	Fresh coal was crashed to coal particles between 105~125μm and stored in a sealed bag for further use;
2		Oxidised coal	Place crushed fresh coal particles (105~125μm) to a baking oven (refer Figure 4.9) filled with air, set oven temperature as 60^{o}C to mimic low temperature coal oxidation, retrieve coal sample after 24 hours;
3		Flooded coal	Withdraw the flooded coal after coal of group A was immersed into water for six months, place the flooded coal in the vacuum dryer for 2 hours, then crash the coal to particles 105~125μm;
4	Equipment calibration		Check gas leakage and calibrate GC;
5	Discharge coal sample		Place 1g coal sample to sample holder inside reaction vessel;
6	Stabilise system		Power on all the units, set temperature as 30^{o}C and pass through nitrogen for one hour;
7	Initiate test		Shut off nitrogen supply and pass through compressed air (100ml/min), set temperature tamping rate (1.5^{o}C/min before 80^{o}C and 1^{o}C/min after 80^{o}C);
8	Log data		Effluent is analysed every 12min, gas sampling bags may be used to facilitate the test at high temperatures;
9	End test		Shut off air supply and pass through nitrogen after coal temperature reaches 210^{o}C, cool down the reaction vessel and clean.

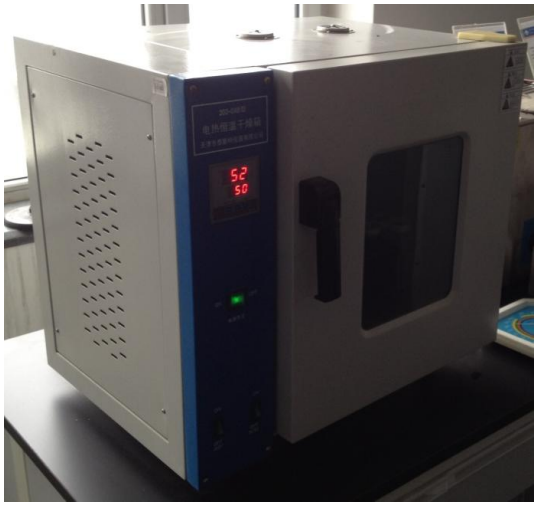

Figure 4.9 Coal baking oven

4.4.3 Testing results

The trends of gaseous products of Shendong coal oxidation are given in Figure 4.10 (CO), Figure 4.11 (CO_2), Figure 4.12 (CH_4), and Figure 4.13 (C_2H_4). As can be seen from Figure 4.10, CO was produced starting from low temperature coal oxidation and its concentration increased rapidly with temperature especially for temperature higher than 130^{o}C. It is also noticeable less CO was produced for all oxidised coal samples than that of fresh coal samples and flooded coal samples. A reasonable explanation is a part of active sites of coal has been consumed of oxidised coal sample and capability of oxygen consumption coal was hampered when the coal was re-oxidised. However, when it comes to spontaneous combustion incident prediction, same amount of detected CO might imply more serious development of spontaneous combustion of oxidised coals than fresh and flooded coals. A closer examination of the trend indicates more CO was liberated of fresh coal samples than that of flooded coal samples at low temperature. However, with coal temperature passing a critical value, the trend is reversed and the critical temperature ranged between 130^{o}C and 170^{o}C. A possible reason is: (1) at low temperature, excessive water blocked pores of coal or covered active sites attached to surface of coal and therefore oxygen consumption rate and CO production rate of wet coal samples were slightly slower than that of fresh coals; (2) at high temperature, with more water being evaporated, more active sites were exposed and water content dropped to some point where reaction rate between coal and oxygen was much facilitated and hence more CO was likely to be liberated for flooded coal samples [17]. The critical temperature range is also reasonable as it has been implied physically bonded water is mostly evaporated

before 150^{o}C [84]. The inversion of concentration of liberated CO between oxidation of fresh coals and flooded coals has also been reported in other studies[46, 47]. Trend of CO_2 production of Shendong coal samples is given in Figure 4.11 and it is found behaviour of CO_2 resembled that of CO apart that the amount of produced $CO_2$was much larger than that of CO. It is also consistent with previous findings which have suggested CO_2 is the major carbon-containing oxidation product and the molar ratio of CO_2 to CO production ranges from 2 to 5 with temperature from 56 to 140^{o}C [7, 81].

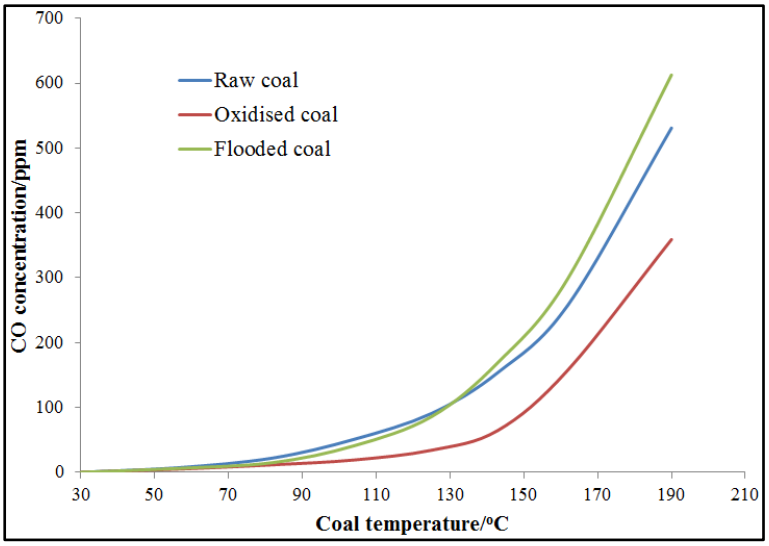

(a) BLT1-2 coal sample

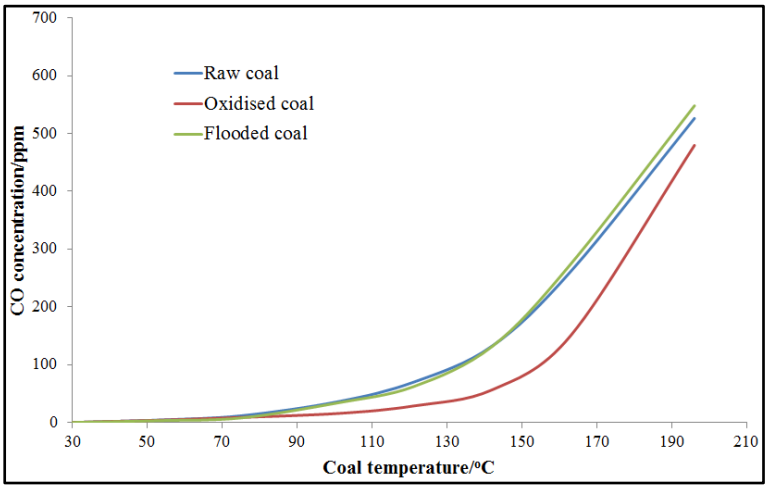

(b) BLT2-2 coal sample

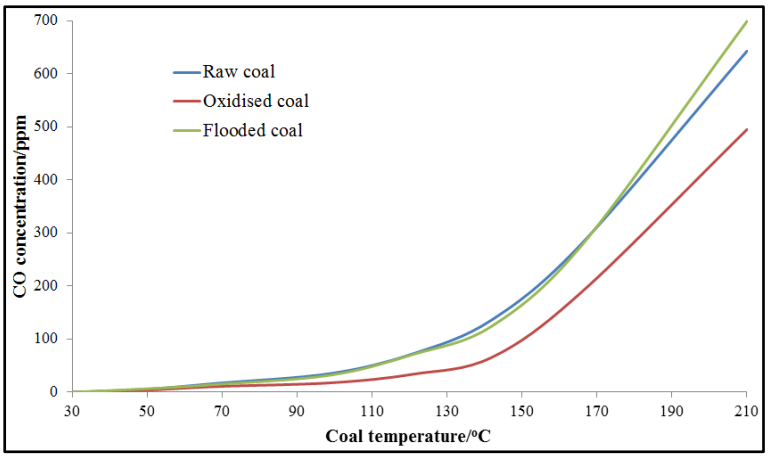

(c) SGT2-2 coal sample

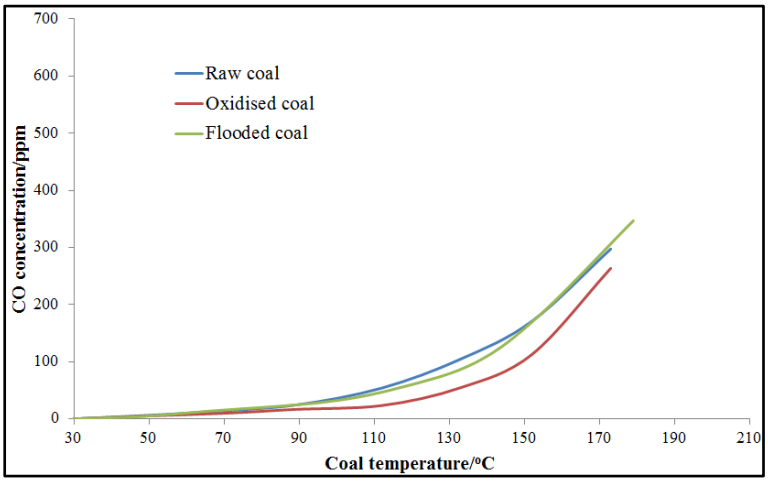

(d) SGT3-1 coal sample

Figure 4.10 CO evolutionsof the Shendong coals

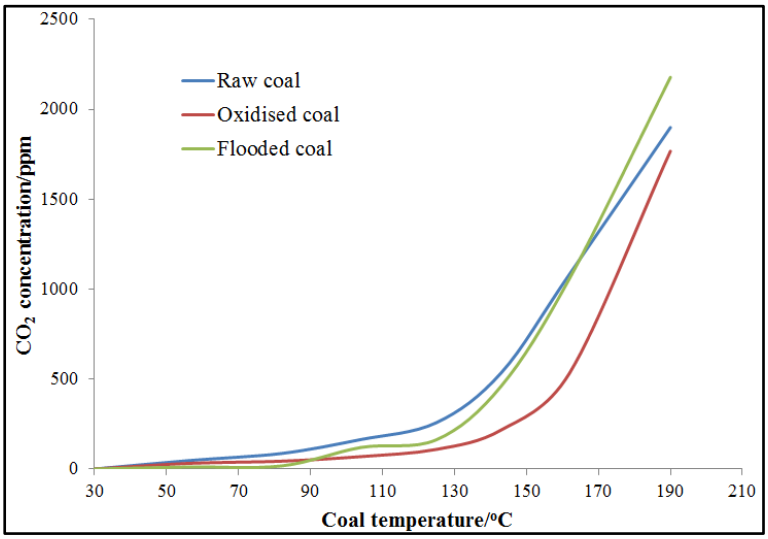

(a) BLT1-2 coal sample

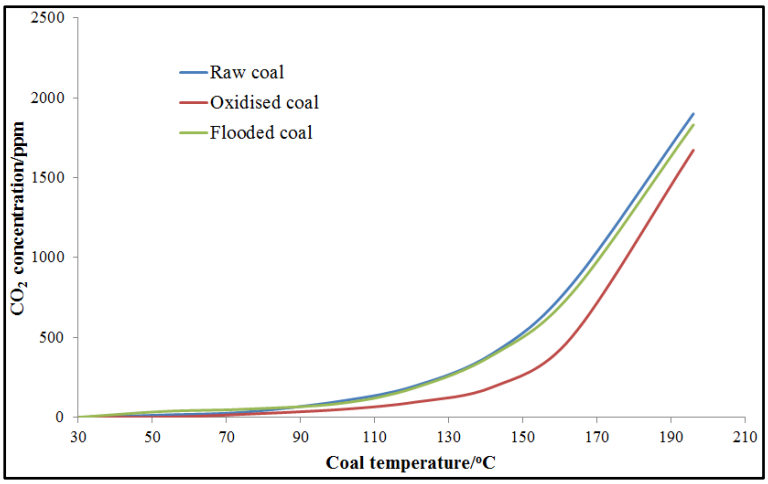

(b) BLT2-2 coal sample

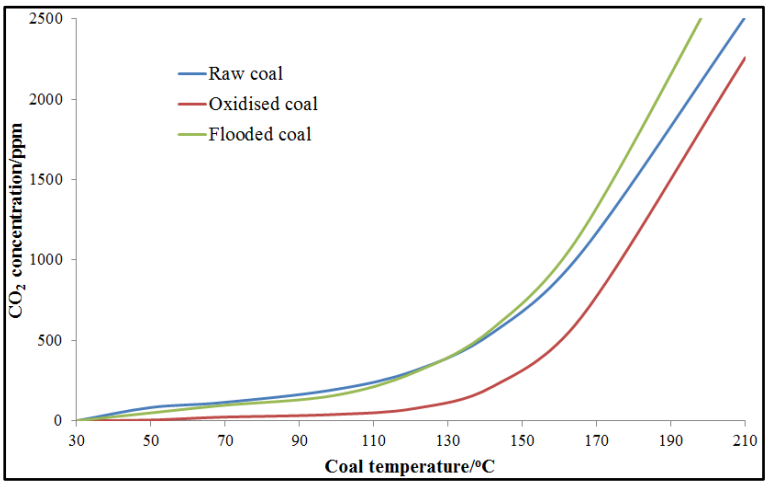

(c) SGT2-2 coal sample

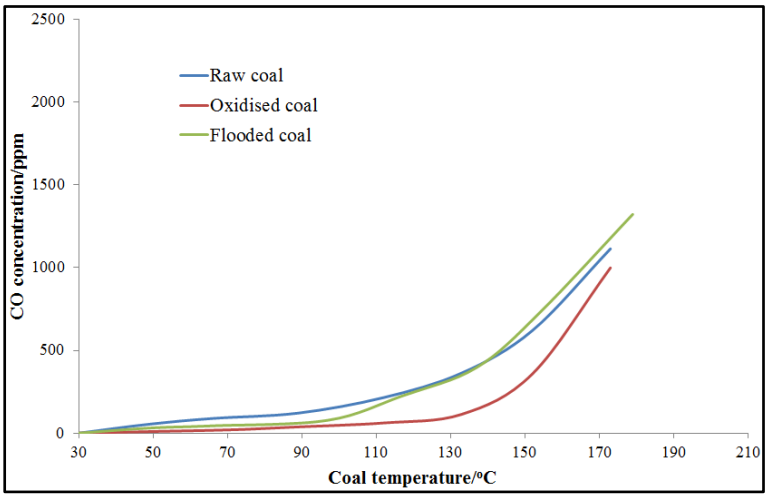

(d) SGT3-1 coal sample

Figure 4.11 CO_2 evolutions of the Shendong coals

Trend of produced C_xH_y (CH_4 and C_2H_4) gases are shown in Figure 4.12 and Figure 4.13. It is obvious production rates of C_xH_y gases of oxidised coal samples were lower than that of fresh and flooded coal samples especially at high temperatures.

Pre-oxidation history not only affects production rates of carbon-containing gaseous products but also C_xH_y gases. Another noticeable trend is significantly increasing amount of $CH_4$and $C_2H_4$was not generated before coal temperature reaches 130~150^oC. It was reported humic acids, alkali-soluable and stable solid compounds including hydroxyl (phenolic –OH), carbonyl (–CO) and carboxyl (–COOH) groups, are slowly accumulated at coal surfaces and would not be decomposed until coal temperature rises to 150^oC. Generation of gaseous C_xH_y mainly attributes to the degradation of these stable solid complexes with moisture as a reaction agent[17, 93]. Therefore it might be a possible reason that C_xH_y gases were rapidly produced for coal temperature higher than 150^oC in this test. From Figure 4.12 , it can be also found initially amount of produced CH_4 of fresh coal samples was larger than that of flooded coal samples. However, amount of produced CH_4 of flooded coal samples surpassed that of fresh coal samples after a critical temperature. Similar to the explanation of production trends of CO and CO_2, many active sites and pores were covered with water layer at low temperature and as a result, initial content of liberated $CH_4$was relatively smaller for a moist coal. With increasing evaporation of moisture at a higher temperature (130~150^oC), more active sites were exposed to oxygen and more $CH_4$was produced considering water might be an important part of decomposition of the stable compounds which were previously generated by low temperature coal oxidation. Unlike production trend of CH_4, produced C_2H_4 of flooded coal samples was more than that of fresh coal samples from very beginning. The temperature of detectable concentration of $C_2H_4$was around 130^oC at which the physically-bonded moisture of flooded coal is almost evaporated and it is a possible reason that produced C_2H_4 of flooded coal samples was more than that of fresh coal samples during the entire test.

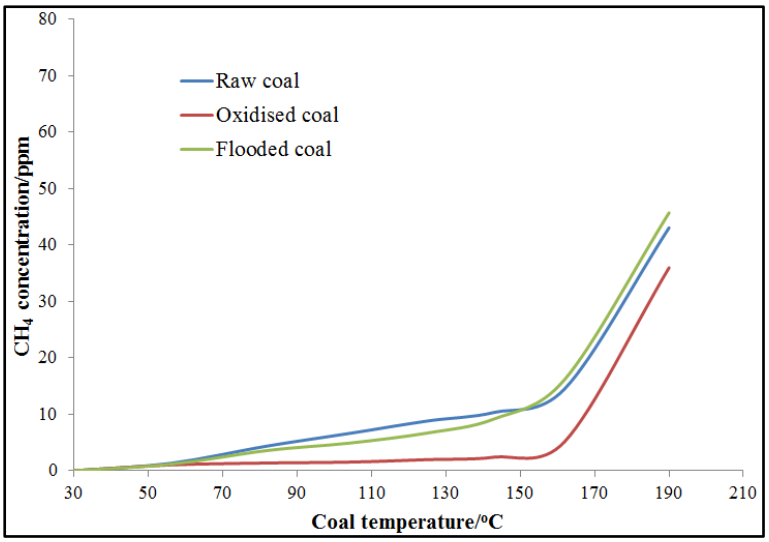

(a) BLT1-2 coal sample

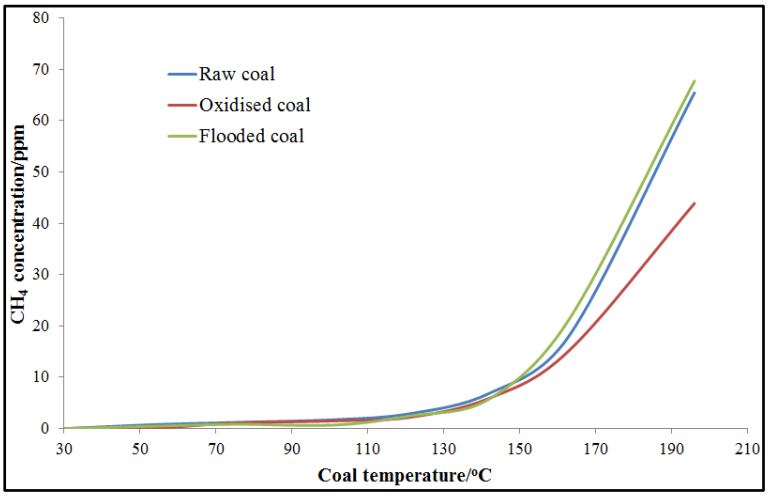

(b) BLT2-2 coal sample

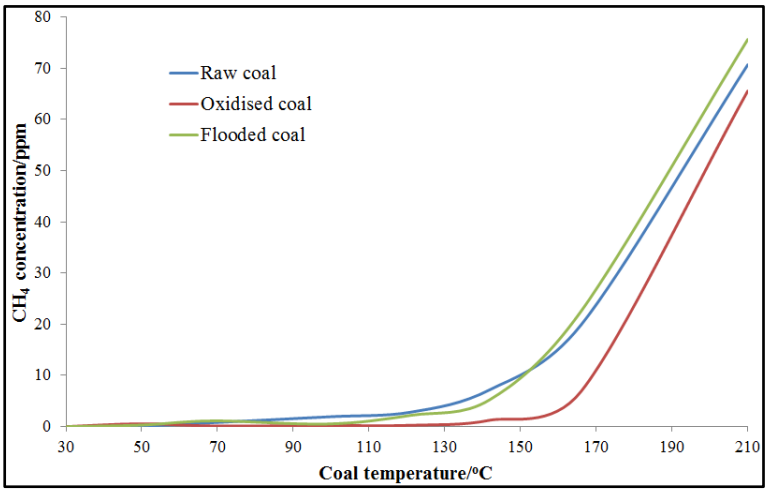

(c) SGT2-2 coal sample

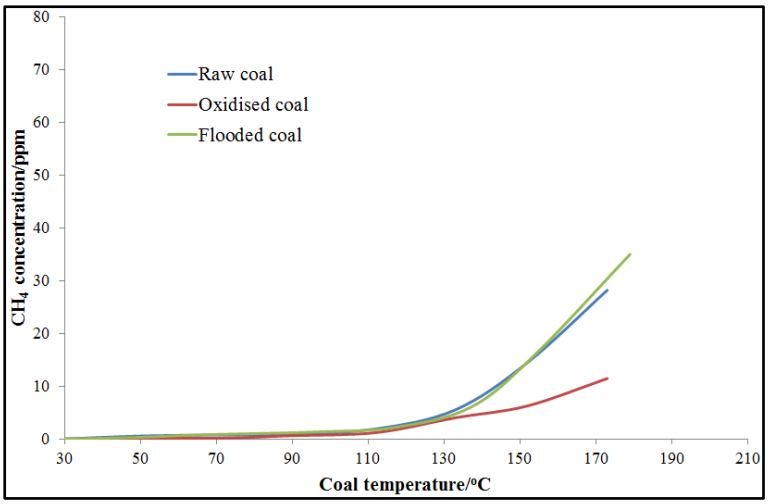

(d) SGT3-1 coal sample

Figure 4.12 CH_4 evolutions of the Shendong coals

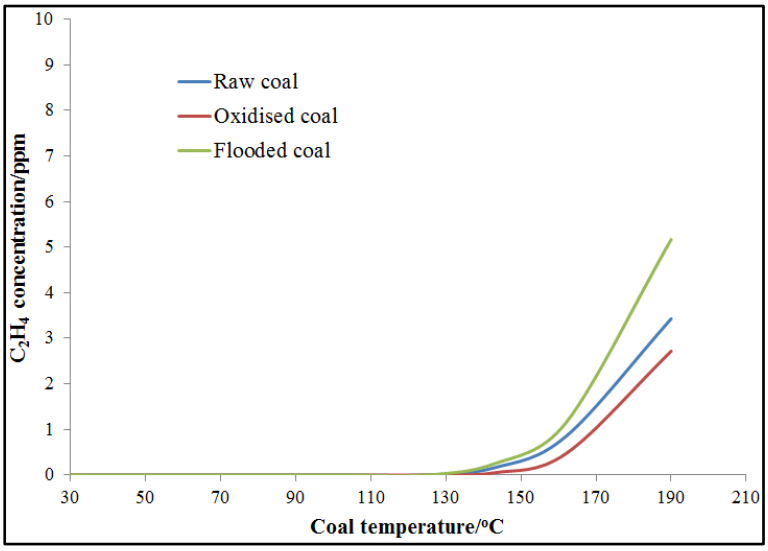

(a) BLT1-2 coal sample

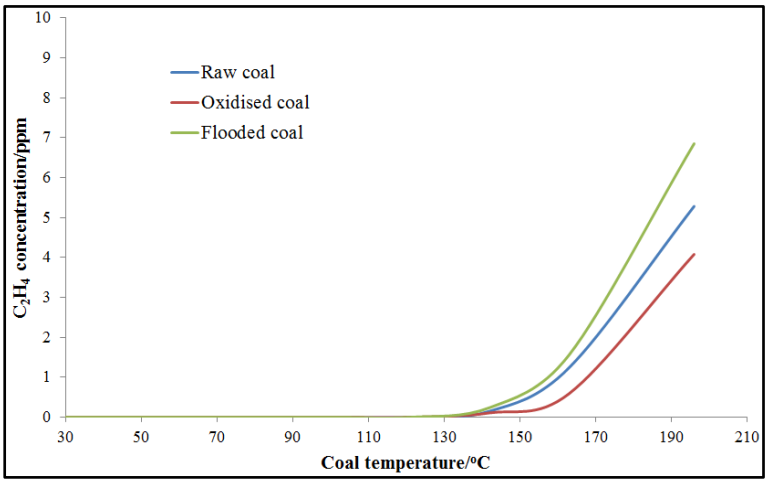

(b) BLT2-2 coal sample

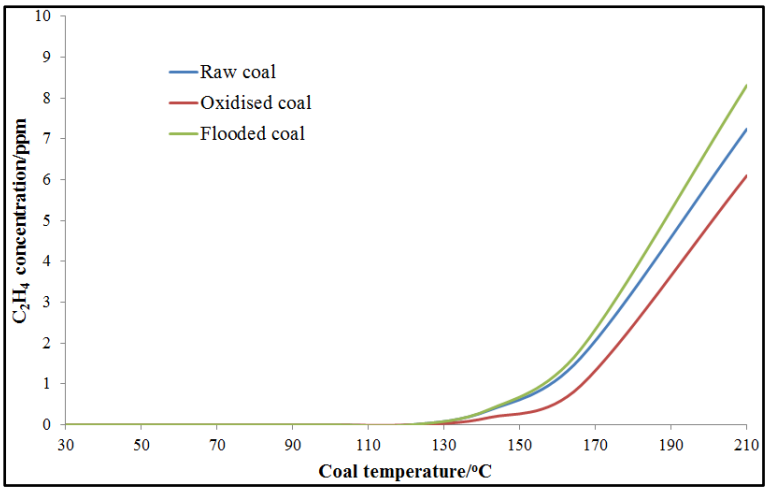

(c) SGT2-2 coal sample

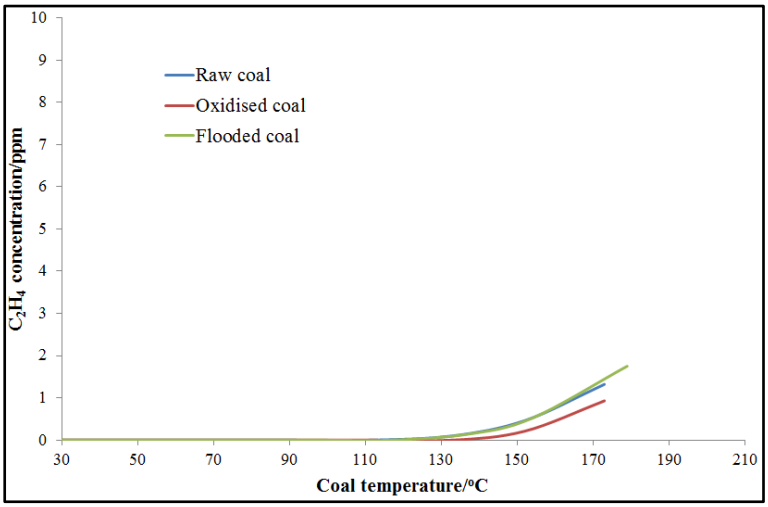

(d) SGT3-1 coal sample

Figure 4.13 C_2H_4 evolutions of the Shendong coals

4.5 Adiabatic heating test

4.5.1 Testing apparatus

A new adiabatic oxidation rig has been designed, assembled and commissioned at the University of Wollongong to determine low temperature heating behaviour of Shendong coals. Overall scheme of the testing apparatus is show in Figure 4.14. The photographic view is given in Figure 4.15. The testing rig is mainly composed of several following units.

(a) Gas supply system

Two gas bottles are used. One is oxygen and another one is nitrogen. Oxygen is used to sustain coal oxidation and nitrogen is used to dry and pre-heat the coal samples. Nitrogen can be also used to terminate the test once temperature of coal hits the upper limit (100^{o}C in this test). Before gas flows into reaction vessel, the gas is

required to pass 15m long coiled copper tube fitted in an oil bath to obtain the same temperature with coal. Along the gas tube line, associated regulators, flowmeters, and solenoid valves are installed to control the gas flow.

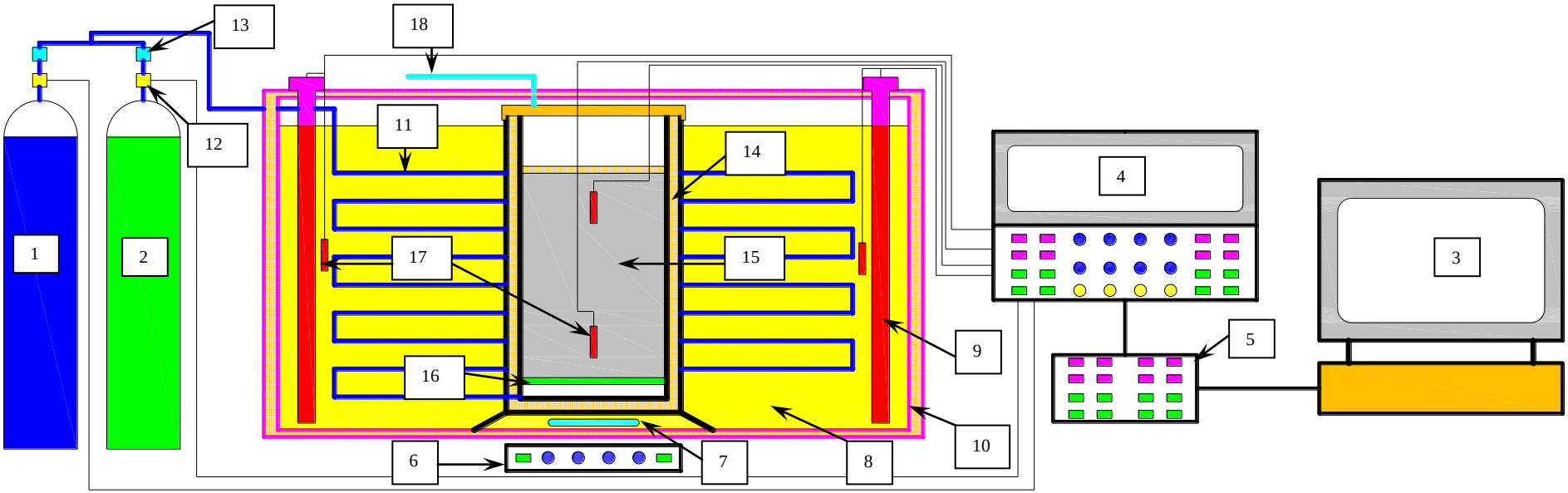

1-Nitrogen; 2-Oxygen; 3-Computer; 4-Temperature controller; 5-Data taker; 6-Magnetic stirrer; 7-Stir bar; 8-Oil bath; 9-Heater; 10-Insulation material; 11-Coiled gas tube; 12-Flowmeter; 13-Solenoid valve; 14-Reaction vessel; 15-Coal sample; 16-Porous disk; 17-Thermocouple; 18-Effluent gas

Figure 4.14 A brief scheme of the adiabatic coal spontaneous combustion testing rig

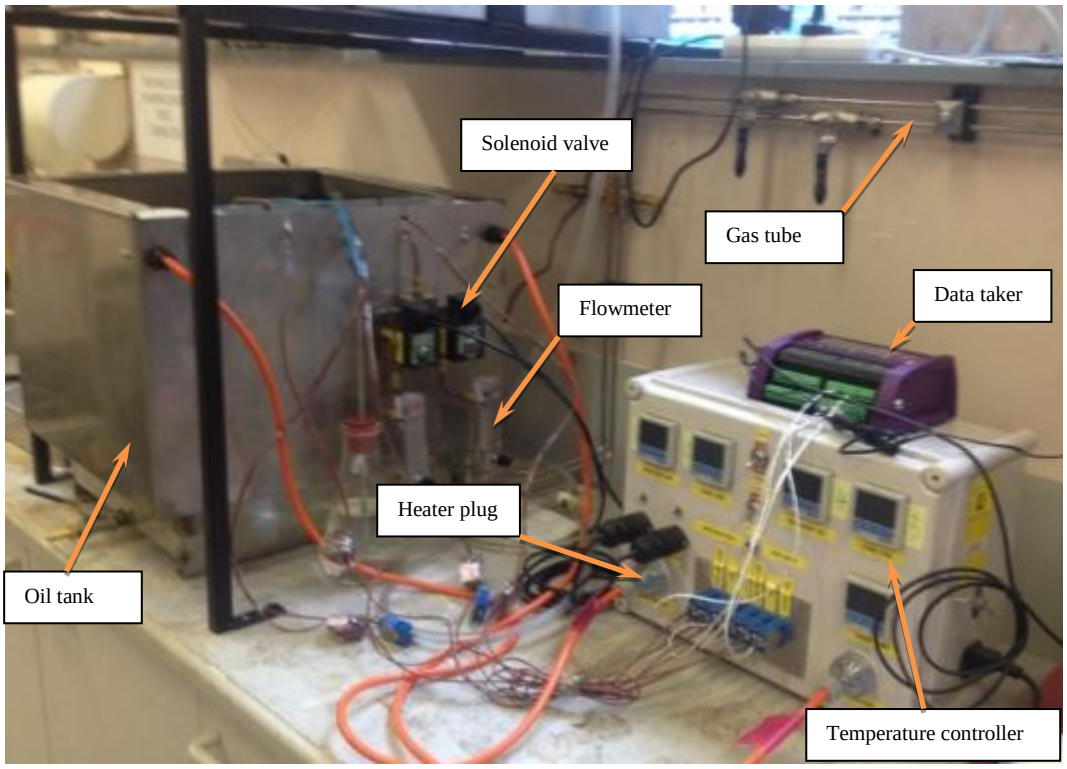

Figure 4.15 A photographic view of the adiabatic testing apparatus

(b) Temperature control system

The essence of adiabatic test is to minimise loss of heat generated from coal oxidation. By doing this intrinsic propensity of coal to self-heating can be truly assessed. In the test heat loss is minimised by equilibrating temperature of coal sample and temperature of oil bath where the coal reaction vessel is placed. The oil tank is double skinned and kaowool is used to stuff the gap for insulation. Heating is provided by four immersion heaters (2kW) held in four corners of the oil tank, refer Figure 4.16 and Figure 4.17. Several thermocouples are fitted into oil and coal sample. As long as any temperature difference between a sensor in oil and a sensor in coal sample is detected by the temperature controller, the heaters will start to operate till the differential temperature is balanced.

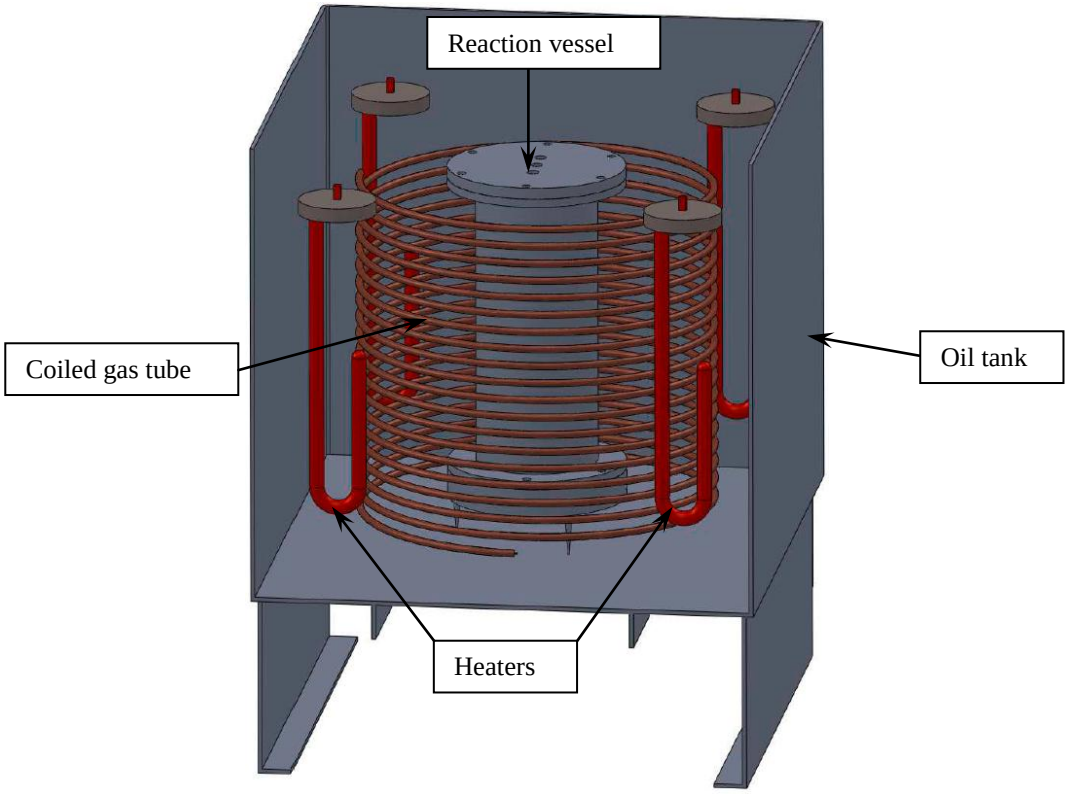

Figure 4.16 A perspective drawing of the oil tank

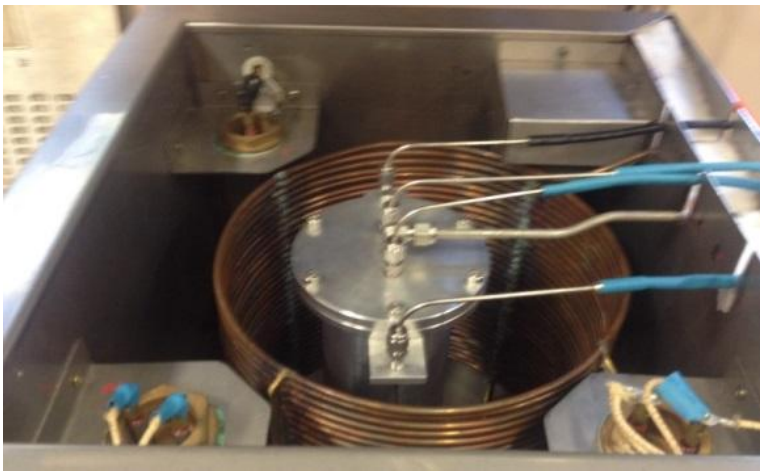

Figure 4.17An interior view of the oil tank

(c) Reaction vessel

The reaction vessel consists of mainly two units: one is the outer vessel made of aluminium and another part is an inner vessel which can be easily assembled for unloading and recharge of the coal sample, refer Figure 4.18. The bottom of the inner vessel is made of a porous disk through which gas can pass. The top of the outer vessel is fitted with a "O" ring to minimise gas leakage. A lid can be screwed to cover the outer vessel and a few holes are drilled through the lid to install thermocouples and effluent gas tube, refer Figure 4.17.

(a) Top view (b) Inner view

Figure 4.18 Reaction vessel of the adiabatic testing rig

(d) Other units

DT80 data taker is used to record temperatures of all the thermocouples. The logging interval is adjustable and the data is fed back to a specially designed program in computer. To ensure efficient temperature distribution in the oil bath, a large stirring bar powered by a large duty magnetic stirrer is placed underneath the reaction vessel. To avoid pressure building-up inside reaction vessel, a pressure relief valve (10kPa) is installed in the pipeline. To avoid coal powder blocking the gas outlet, a layer of asbestos is placed on top of coal sample.

4.5.2 Testing procedures

Testing procedures of the adiabatic self-heating testing rig is given in Table 4.9.

Table 4.9 Testing procedures of adiabatic self-heating test

No.	Testing steps		Detailed description
1	Coal sample preparation	Fresh coal	Fresh coal was crashed to coal particles less than 212μm and stored in an airtight bag for further use;
2		Oxidised coal	Place crushed fresh coal particles (-212μm) to a baking oven filled with air, set oven temperature as 60^{o}C to mimic low temperature coal oxidation, retrieve coal sample after 24 hours;
3		Flooded coal (BLT1-2 and BLT2-2)	Withdraw the flooded coal after coal of group A was immersed into water for six months, place the flooded coal in the vacuum dryer for two hours, then crash the coal to particles less than 212μm;
4	Loading coal sample		Weigh 200g coal sample and load it in the inner vessel, screw back the lid of the reaction vessel and effluent gas tube;

5	Dry coal sample	Power on temperature controller and flick to pre-heating mode in which temperature was set at 40^{o}C and solenoid valve for nitrogen is open, adjust the nitrogen flow rate to 50ml/min and maintain it for more than 24 hours;
6	Initiate test	Power on computer and data taker, flick mode of controller to differential mode in which supply of nitrogen is shut off and solenoid valve for oxygen is open, and temperature of oil starts to follow coal temperature, adjust oxygen flow rate as 100ml/min and start to log data;
7	Stop heating	Once coal temperature reaches 100^{o}C, controller shut off power of heaters and supply of oxygen and pass through nitrogen to stop coal oxidation, export data from DT80 to computer;
8	End test	Shut off supply of nitrogen when the oil bath and coal sample cool down, unload coal sample and clean, ready for next run.

4.5.3 Testing results

The testing results are given from Figure 4.19 to Figure 4.22. It can be clearly seen self-heating rates of oxidised Shendong coals greatly reduce compared to fresh coals. It equally indicates the low temperature oxidation rates of fresh Shendong coal samples are much higher than that of oxidised coals. From Figure 4.19 and Figure 4.20, it can be also found that self-heating rates of BLT coal samples slightly increase after long time immersion in water. A possible reason is the long-time immersion in water was likely to dissolve substances in coal pore structure and therefore pores in coal are enlarged or more pores are exposed as indicated in Figure 3.15 and Figure 3.16. The rate of temperature rise gives a relative measure of the oxidation rate of the coal. It is widely reported that thermal runaway of self-heating of coal occurs and temperature of coal increase rapidly beyond some critical temperatures. The critical temperature ranges from 60~100^{o}C. The average self-heating rate from 40^{o}C to 70^{o}C (R_{70}) was used as an index to evaluate liability of coal to spontaneous combustion. The latest released Intrinsic Spontaneous Combustion Propensity (ISCP) classification on the basis of R_{70} self-heating rate values is given in Table 4.10. R70 values and ISCP classifications of Shendong coal samples are given in

Table **4.11**. It shows all fresh coal samples exhibited high risk of spontaneous combustion and they still showed medium to high risk of spontaneous combustion even after they have a pre-oxidation history. The flooded coal samples present higher risk of spontaneous combustion and almost escalate to classification of "very high" in

Table **4.11**.

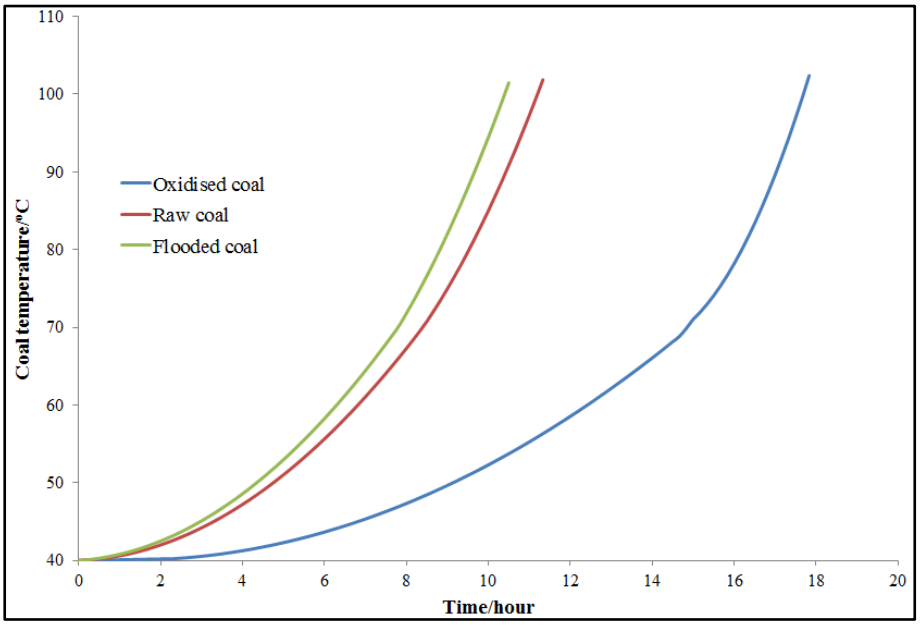

Figure 4.19 Adiabatic heating curve of BLT1-2 coal sample

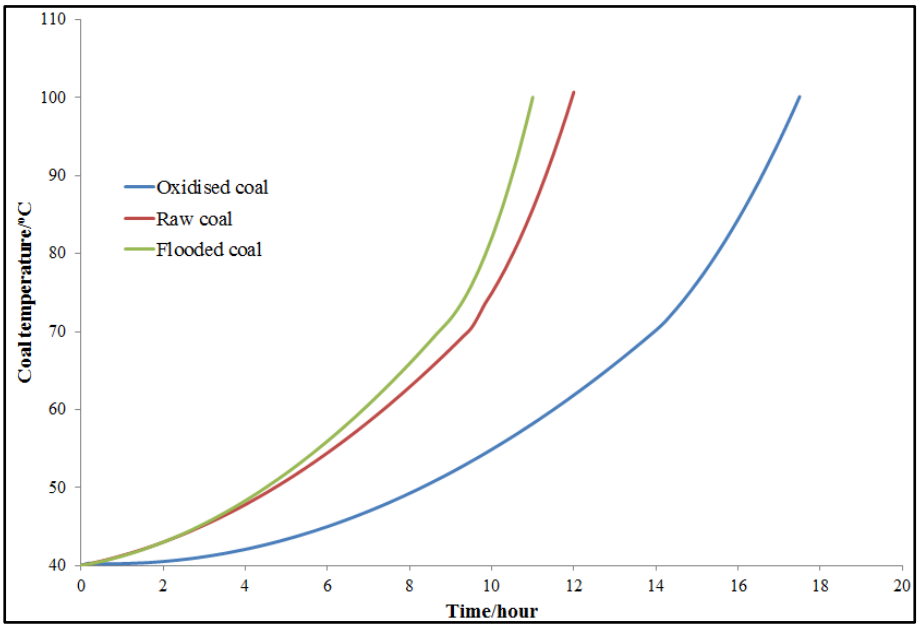

Figure 4.20 Adiabatic heating curve of BLT2-2 coal sample

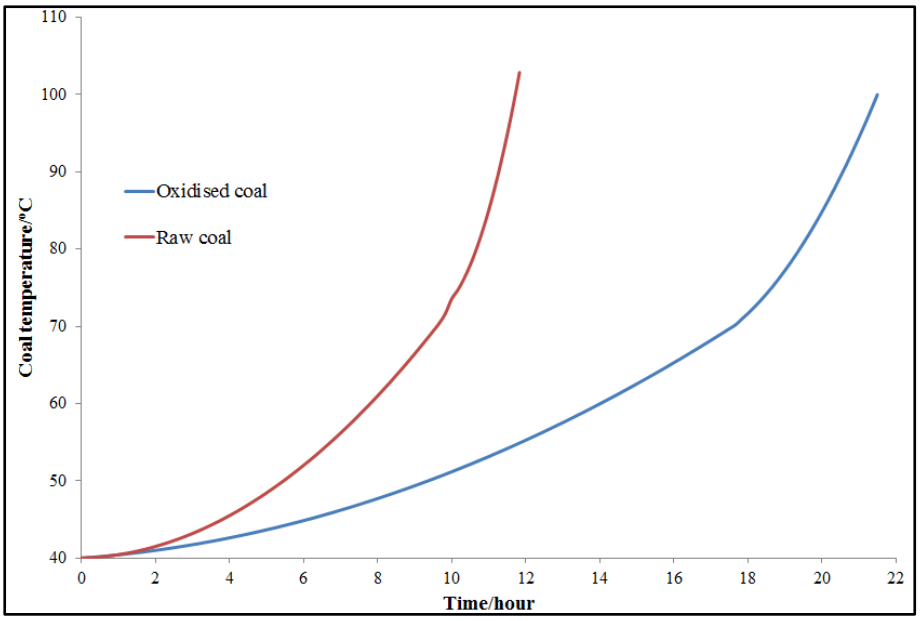

Figure 4.21 Adiabatic heating curve of SGT2-2 coal sample

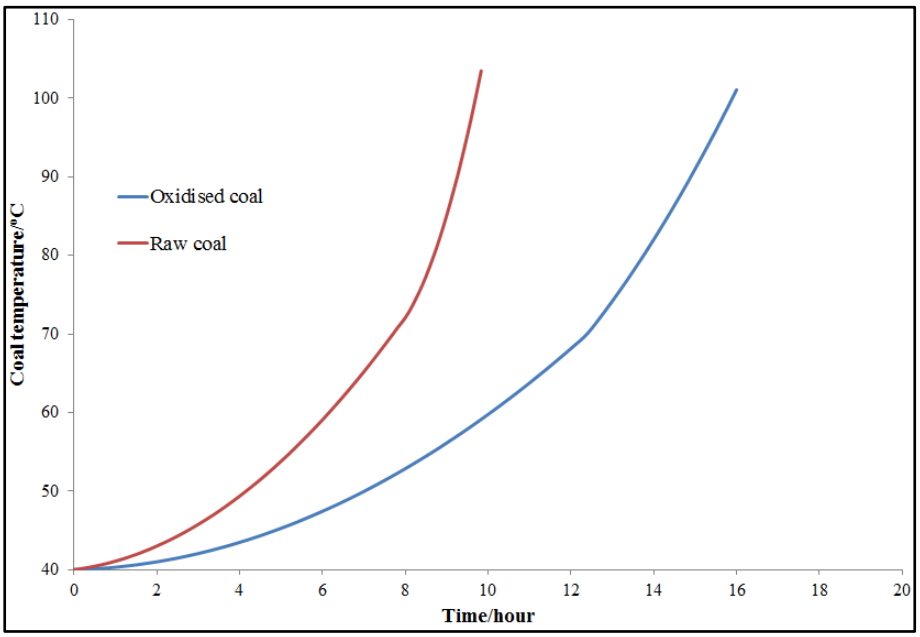

Figure 4.22 Adiabatic heating curve of SGT3-1 coal sample

Table 4.10 ISCP classification based on R_{70} values

ISCP Class	R_{70} values	Propensity rating
Class 1	R<0.5	Low
Class 2	0.5<=R<1	Low-medium
Class 3	1<=R<2	Medium
Class 4	2<=R<4	High
Class 5	4<=R<8	Very high
Class 6	8<=R<16	Extremely high
Class 7	R=>16	Exceptionally high

Table 4.11 ISCP classifications and R_{70} values of the Shendong coal samples

Coal sample	Test	Time to 70°C (hr)	R_{70} value	Propensity rating
Bu 1-2	Fresh coal	8.4	3.57	High
	Oxidised coal	15	2	High
	Flooded coal	7.8	3.85	High
Bu 2-2	Fresh coal	9.4	3.19	High
	Oxidised coal	14	2.14	High
	Flooded coal	8.7	3.45	High
Shi 2-2	Fresh coal	9.6	3.13	High
	Oxidised coal	17.6	1.71	Medium
Shi 3-1	Fresh coal	7.7	3.89	High
	Oxidised coal	12.4	2.42	High

4.6 DSC test

4.6.1 Testing apparatus and procedures

DSC experiments are carried out by using METTLER TOLEDO DSC822^e (Figure 4.23) with internal cooling system incorporated with thermal analysis program to control experimental runs. The instrument is also equipped with an external liquid nitrogen cooling system. Weight, temperature and sensitivity calibrations of the instrument are performed prior to any actual test.

Figure 4.23 Apparatus of DSC testing

SGT2-2 and SGT3-1 coal samples were used in the test. The coal samples were carefully crushed and sieved to particle size between 125μm and 150μm. A part of coal sample was discharged to the baking oven filled with nitrogen and maintain temperature at 40°C for six hours to dry most moisture of the coal sample. The dry coal sample was assigned a name as “fresh”. The rest coal sample was divided into six groups and one group was discharged into the baking oven filled with nitrogen.

The temperature of the oven was set at 50^{o}C and maintained for at least twelve hours. The preheated coal sample was given a name “50”. To mimic different pre-heating histories, similarly coal samples with preheated temperatures 80^{o}C, 110^{o}C, 140^{o}C, 170^{o}C, and 200^{o}C were prepared and the coal samples were labelled as “80”, “110”, “140”, “170”, and “200”, respectively.The coal sample (~5 mg) was placed in an aluminium sample crucible (Figure 4.24) covered by a lid with a pinhole. The cruciblewas then placed in the DSC head together with a reference crucible.The sample was firstly heated in pure $N_2$to 110^{o}C, held for 20 min to further drive off the moisture and followedby cooling down to 20^{o}C. Purge gas was then switched to air (a mixture of pure O_2 and N_2 with 20%of O_2) with a flow rate of 60 mL/min and the sample was heatedfrom 20^{o}C to 250^{o}C at a heating rate of 2^{o}C/min. The testing data from 30^{o}C to 250^{o}C was only given to skip the endothermic stage and to eliminate the irregularity of the initial data.

Figure 4.24 Used crucibles in the DSC test

4.6.2 Testing results

4.6.2.1 Exothermicity

Figure 4.25 and Figure 4.26show the heat flow of the two groups of coal sample at elevated temperatures in the DSC apparatus. As can be seen from Figure 4.25, heat flow curve of fresh SGT2-2 coal resembled that of the same coal with 200^{o}C pre-heating history. For a complete run, less heat was liberated for SGT2-2 coal samples which underwent 50^{o}C and 80^{o}C preheating history although they might generate more heat than fresh coal sample. It was noticeable more heat was produced for SGT2-2 coal samples which had 110^{o}C, 140^{o}C, and 170^{o}C pre-heating history than fresh coal sample. As can be seen from Figure 4.26, fresh SGT3-1 coal sample and coal sample which was preheated at 50^{o}C had similar curves of heat flow during the

test. Slightly less amount of heat was generated for coal sample which had 80°C preheating history. For SGT3-1 coal samples which were preheated at higher temperatures (i.e. 110°C, 140°C, and 170°C), less heat was generated initially while much more heat was released at a later stage than fresh coals. While for SGT3-1 coal sample with pre-heating history of the highest temperature, the potential of heat release was significantly reduced.

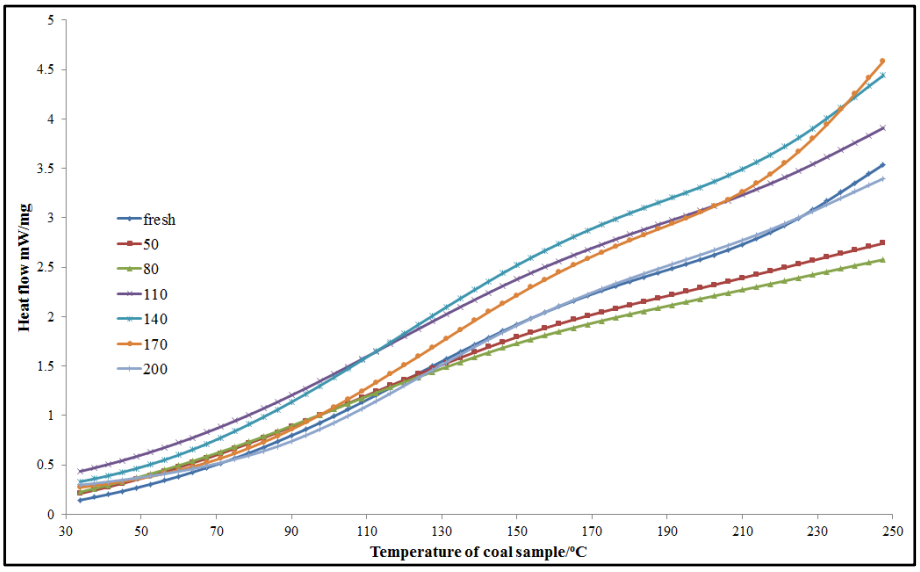

Figure 4.25 Heat flows of different SGT2-2 samples against temperature

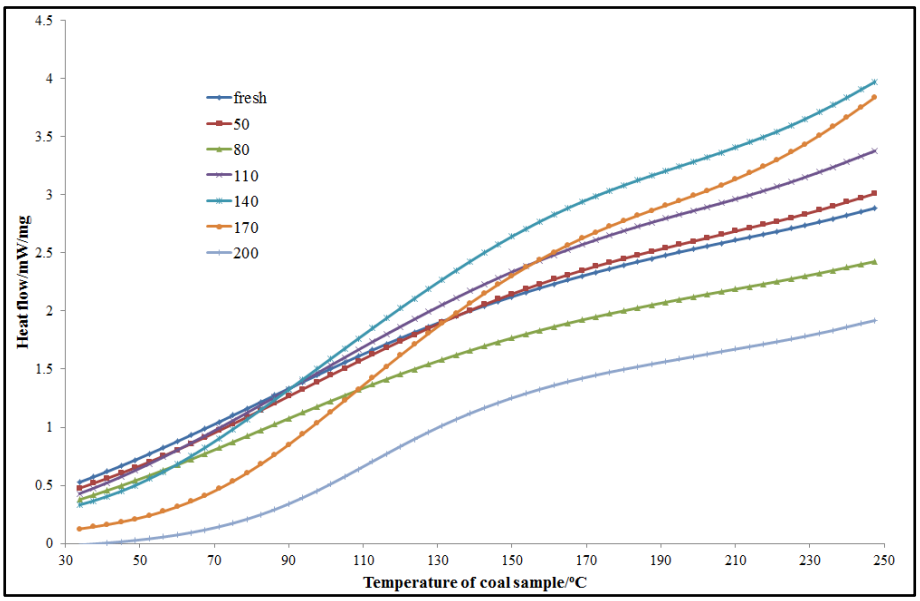

Figure 4.26 Heat flows of different SGT3-1 samples against temperature

Figure 4.27 and Figure 4.28illustrate total heat generated per unit mass of the two groups of coal sample during the test. As can be seen from Figure 4.27, fresh SGT2-2 coal sample was able to liberate 4.35J/mg heat and the exothermicity slightly decreased for coal samples that were preheated at 50°C and 80°C. However, total

heat released during the test considerably increased for coal samples which were baked at 110°C and 140°C. With further higher temperatures pre-heating history, the exothermicity started to reduce again and as a result, heat of 200°C coal sample was about 4.36J/mg which was almost the same to the fresh coal sample. A similar trend was found for SGT3-1 coal. Exothermicity of SGT3-1 coal underwent initial reduction with 50°C and 80°C pre-heating history, then a sharp growth with 110°C and 140°C pre-heating history, and another decrease for coal samples with 170°C and 200°C pre-heating history. It can be also observed, unlike SGT2-2 coal, the ability of heat generation for 200°C SGT3-1 coal reduced sharply compared with fresh SGT coal. The discrepancy may attribute to the difference of property of two coals. Further explanation however needs to be investigated.

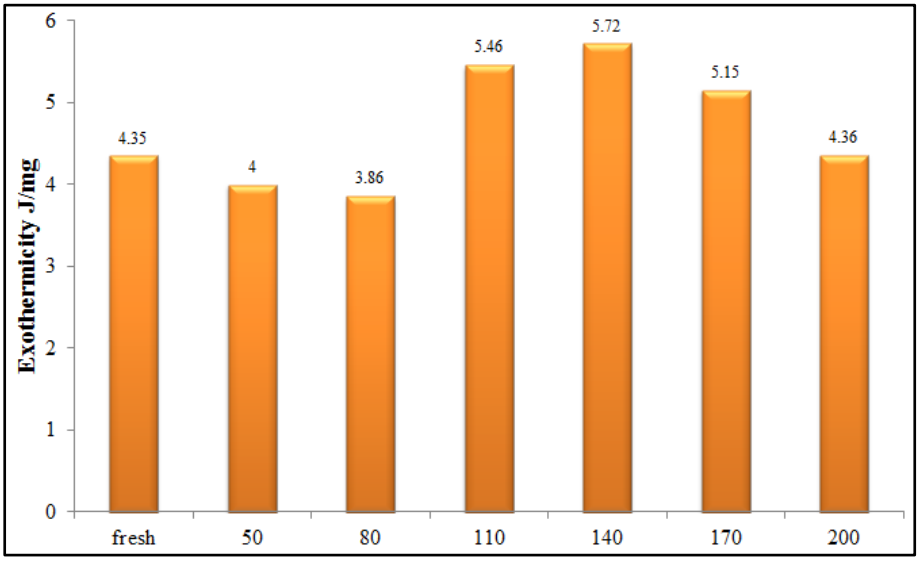

Figure 4.27 Total generated heat of different samples of the SGT2-2 coal

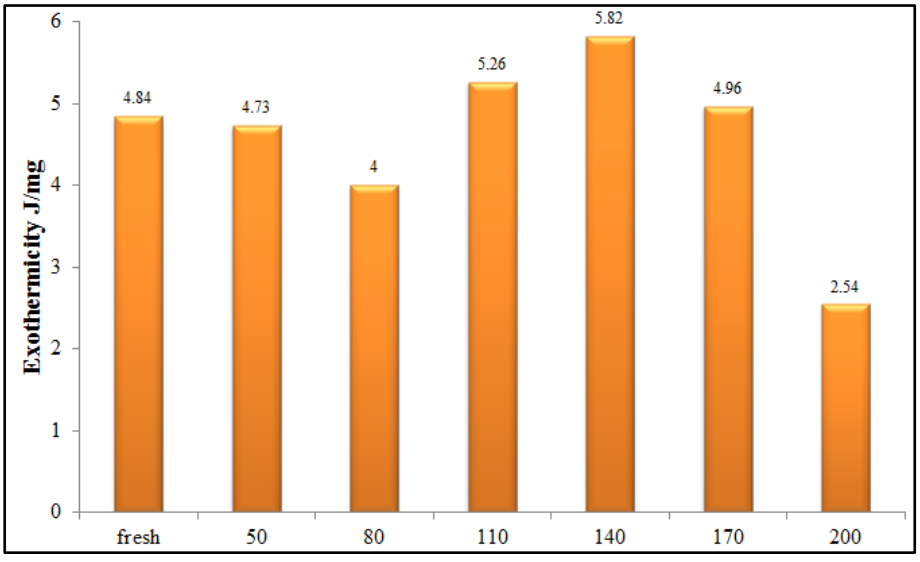

Figure 4.28 Total generated heat of different samples of the SGT3-1 coal

4.6.2.2 Kinetic parameters analysis

The Borchardt and Daniels (B/D) kinetics approach was employed to determine the kinetic parameters in this study [236-238]. The B/D method assumes that the reaction follows n^{th} order kinetics and follows the general rate equation:

$$d\alpha/dt = k(T)[1-\alpha]^n \quad (4.1)$$

Where $d\alpha/dt$ = reaction rate (s^{-1});

α (conversion rate) = $(M_o - M)/M_o$, M is the mass of reactant at time t(g), M_o is the initial mass of reactant (g);

$k(T)$ = specific rate constant at temperature T(s^{-1});

n = reaction order.

The B/D approach assumes Arrhenius dependence for kinetic reaction:

$$k(T) = Ae^{-E_a/RT} \quad (4.2)$$

Where E_a = Activation energy (J/mol);

A = Pre-exponential factor (s^{-1});

R = Gas constant, 8.314 (J/mol K)

Take Equation (4.2) into Equation (4.1):

$$d\alpha/dt = Ae^{-E_a/RT}[1-\alpha]^n \quad (4.3)$$

Substitute expression of conversion rate into Equation (4.3):

$$-dM/M_o dt = Ae^{-E_a/RT}(M/M_o)^n \quad (4.4)$$

For low temperature coal oxidation, the consumption of coal might be negligible and the mass can therefore be deemed unchanged. Rearrange Equation (4.4):

$$-dM/M_o dt = Ae^{-E_a/RT} \quad (4.5)$$

In Equation (4.5) any real time consumption on mass of coal correlates to heat release and Equation (4.6) therefore can be obtained by converting mass to heat appearance:

$$\frac{dH/dt}{\Delta H M_o} = Ae^{-E_a/RT} \quad (4.6)$$

Take natural logarithm to Equation (4.6):

$$\ln\left(\frac{dH/dt}{\Delta H M_o}\right) = -\frac{E_a}{R}\frac{1}{T} + \ln A \quad (4.7)$$

By plotting the curve of $\ln\left(\frac{dH/dt}{\Delta H M_o}\right)$ versus inverse temperature($\frac{1}{T}$), the activation energy (E_a) and frequency factor(A) can be easily calculated by interpreting the slope and interception of the linear trending lines.

The two plots of SGT2-2 coal and SGT3-1 coal can be seen inFigure 4.29 and Figure 4.30, respectively. A clear break of linear correlation can be identified for each of the plot. The critical temperatures were 143^{o}C and 127^{o}C for SGT2-2 coal and SGT3-1 coal, respectively. The break can also be found in another study [111]. The data beyond the critical temperature is called supercritical in which the high temperature kinetics are impossible to be determined due to lack of data or because the applicability of B/D method is questionable as mass of coal would starts to noticeably change at high temperatures. The data below the critical point is named subcritical and it is used to determine low temperature coal oxidation kinetics by B/D method.

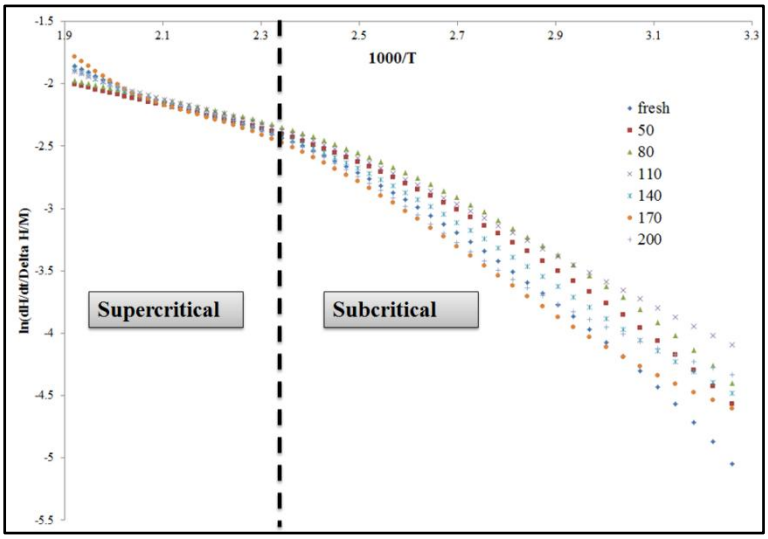

Figure 4.29 Plot of$\ln\left(\frac{dH/dt}{\Delta HM_o}\right)$against $\frac{1000}{T}$ of different samples of SGT2-2 coal

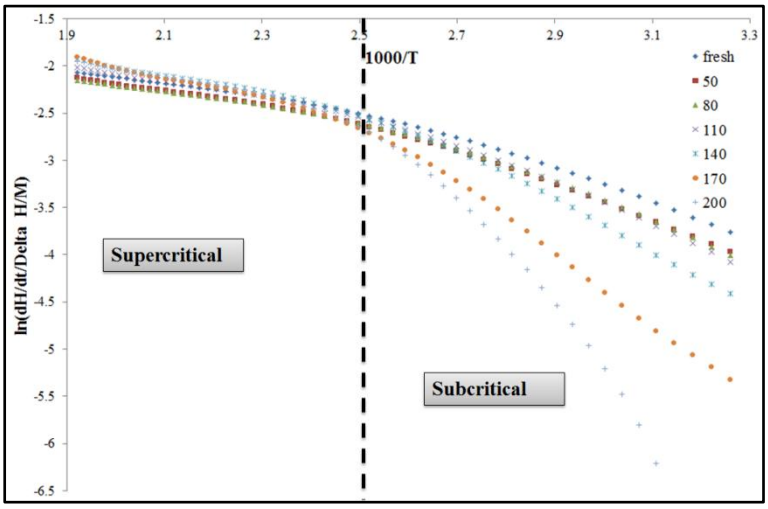

Figure 4.30 Plot of $\ln\left(\frac{dH/dt}{\Delta HM_o}\right)$ against $\frac{1000}{T}$ of different samples of SGT3-1 coal

The low temperature oxidation kinetics (i.e. activation energy and pre-exponential factor) of the two coals are listed inTable 4.12 and Table 4.13, respectively. Figure 4.31 and Figure 4.32show plot of rate constant against temperature of the two coals. From Table 4.13 it can be observed both the activation energy and pre-exponential factor of SGT2-2 coal sample decreased firstly and reached the lowest value for coal sample with 110^{o}C pre-heating history. After that the magnitude of two parameters started to increase for 140 and 170 coal samples while further reduction occurred for 200 coal sample. As can be seen from Figure 4.31, for temperatures during DSC test below 80^{o}C, SGT2-2 coal samples with pre-heating histories were more reactive than the fresh coal sample. More specifically, the order of reactivity of coal samples below 80^{o}C was 110>80>50>140>200>170. For temperature between 80^{o}C and 140^{o}C, reactivity of fresh coal sample increased the most rapidly due to the highest activation energy and inversely for the 110 coal sample due to its lowest activation energy. The reactivity of fresh coal sample surpassed 140, 170, and 200 coal sample from 80^{o}C to 140^{o}C and it was expected to exceed 50, 80, and 110 coal samples during higher temperature oxidation. It appears slight pre-heating (up to 110^{o}C) can increase reactivity of coal during low temperature coal oxidation and over pre-heated coals are likely to, more or less, lose reactivity of coal oxidation.

Table 4.12 Subcritical oxidation kinetic parameters of SGT2-2 coal samples

SGT2-2	Subcritical kinetics	
	Activation energy (kJ/mol)	Pre-exponential factor (s^{-1})
fresh	23.4	75.9
50	19.5	25.4
80	18.4	20.1
110	16.1	9.4
140	19.5	23.9
170	20.7	29.9
200	18.4	15.6

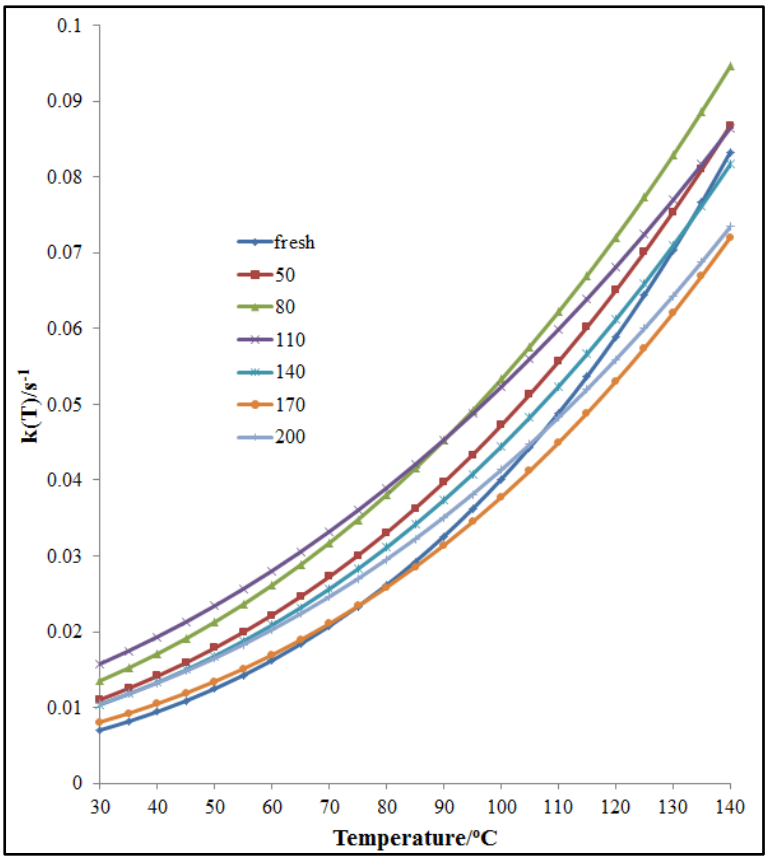

Figure 4.31 Plot of k(T) against T of SGT2-2 coals with different pre-heating histories

From Table 4.13 it is noticeable that both the kinetic parameters of SGT3-1 coal samples increased with higher temperature pre-heating history. From Figure 4.32 it can be seen, unlike SGT2-2 coal, all pre-heated SGT3-1 coal samples became less reactive than the fresh coal. It also appears more reactivity would decrease for coal samples with higher pre-heated temperature. For coal samples with higher values of activation energy (e.g. 140, 170, and 200 coal sample), the reactivity may exceed other coal samples as can be seen the final trend of the rate constant curve. It has also been reported coal oxidation may become more temperature sensitive for coals with higher activation energy [37, 103].

Table 4.13 Subcritical oxidation kinetic parameters of SGT3-1 coal samples

SGT3-1	Subcritical kinetics	
	Activation energy (kJ/mol)	Pre-exponential factor (s^{-1})
fresh	14.1	6.0
50	15.1	7.4
80	15.6	8.9
110	17.0	14.3
140	21.5	58.6
170	31.0	900.4
200	48.6	226386.7

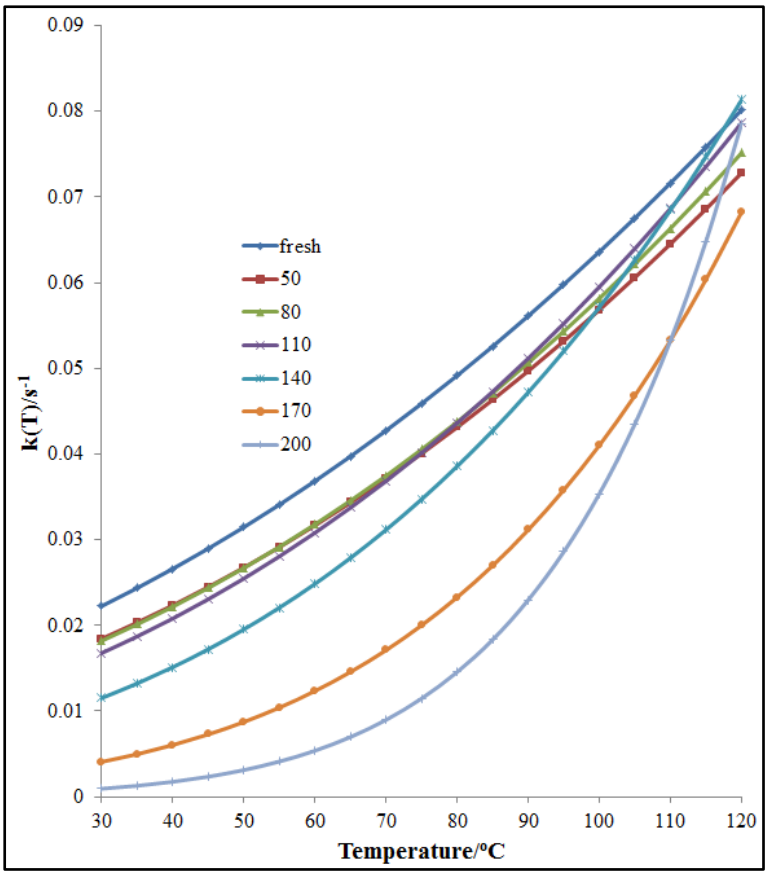

Figure 4.32 Plot of k(T) against T of SGT3-1 coals with different pre-heating histories

4.7 Summary

Main findings of laboratory tests of the Shendong coals are listed:

- Ignition temperatures of Shendong coal samples were relatively low and all below 300°C with the highest ignition temperature 297°C of SGT3-1 coal sample. Ignition temperatures of Shendong oxidised coal samples were 8~15°C lower than fresh coal samples. The propensity of oxidised Shendong coals to spontaneous combustion should not be underestimated because the oxidised coal is easier to develop to an open flame at high temperature stage. Ignition temperatures of Shendong flooded coal samples remained almost unchanged or slightly decreased compared to untreated coal samples.
- CO was produced starting from low temperature coal oxidation and its concentration increased rapidly with temperature especially for temperature higher than 130°C. Less CO was produced for all oxidised Shendong coal samples than that of fresh coal samples and flooded coal samples. More CO was liberated of fresh coal samples than that of flooded coal samples at low temperature while with coal temperature passing a critical value between

130°C and 170°C, the trend was reversed. Behaviour of CO_2 resembled that of CO apart that the amount of produced $CO_2$was much larger than that of CO. Production rates of C_xH_y gases of oxidised coal samples were lower than that of fresh and flooded coal samples especially at high temperatures. Significantly increasing amount of CH_4 and $C_2H_4$was not generated before coal temperature reaches 130~150°C. Initial amount of produced CH_4 of fresh coal samples was larger than that of flooded coal samples. However, amount of produced CH_4 of flooded coal samples surpassed that of fresh coal samples after a critical temperature. Unlike production trend of CH_4, produced C_2H_4 of flooded coal samples was more than that of fresh coal samples across the whole tests.

- Adiabatic testing results indicate all fresh coal samples exhibited high risk of spontaneous combustion and the oxidised coals still showed medium to high risk to spontaneous heating. The flooded coal samples presented a higher risk and increased to level of "very high" according to the latest ISCP classification on the basis of R_{70} self-heating rate values.
- Slight pre-heating of SGT2-2 coal would decrease exothermicity while over-heating was possible to produce more heat. Further reduction in heat liberation occurred if SGT2-2 coal was pre-heated at higher temperature (200°C). A similar trend of heat flow was found for SGT3-1 coal except that the reduction in generated heat for 200 coal sample was much more noticeable than that of SGT2-2 coal. Both the activation energy and pre-exponential factor of SGT2-2 coal decreased firstly and reached the lowest value for coal sample with 110°C pre-heating history. Then the two parameters started to increase for 140 and 170 coal samples while further reduction occurred for 200 coal sample. For testing temperature below 80°C, SGT2-2 coal samples with pre-heating histories became more reactive than the fresh coal sample. For testing temperature between 80°C and 140°C, reactivity of fresh coal sample increased the most rapidly due to the highest activation energy and inversely for the 110 coal sample due to its lowest activation energy. Both the kinetic parameters of SGT3-1 coal samples increased with higher temperature pre-heating history. All pre-heated SGT3-1 coal samples became less reactive than fresh coal. For coal samples with

higher values of activation energy (e.g. 140, 170, and 200 coal sample), the reactivity may exceed other coal samples at higher temperatures.

5 CFD MODELLING OF HEATING EVOLUTION AND INERTISATION IN A SHENDONG GOAF

5.1 Chapter introduction

CFD is commonly accepted as a broad topic embracing the numerical solution controlled by a group of governing equations which describe the motion of fluid flow, continuity and any additional conservation equations, such as energy or species concentrations[239]. Today CFD has become a powerful tool in almost every branch of fluid dynamics and engineering. CFD modelling has been used as a tool of research and design in the mining industry in many areas to assist in understanding the mechanism of fluid or gas flow in order to improve efficiency, safety and health issues[240]. Applications in mining industry include mine ventilation airflow [241-247], mine gas flow and control [248-253], mine fire and spread of smoke [254-259], inertisation [260-262], dust control [263-266], and other applications [267-270].

Due to inaccessibility of coal mine goaf, monitoring and observation of evolution of heating in such a sealed area is difficult to be performed. Therefore CFD is a potential tool in simulating spontaneous heating in goaf with sufficient validation via field monitoring data. More recently with the advance and development of more sophisticated numerical solutions, especially the availability of cutting-edge CFD modelling techniques and their increasing applications in coal mining and related industries, predictable interpretation of transient self-heating of coal mass within tolerated engineering accuracy becomes possible. Yuan and Smith [72] studied effects of coal properties on the potential for spontaneous heating in underground coal mine goafs by a CFD model. Yuan and Smith [24] further developed a three-dimensional equilibrium thermal CFD model to simulate spontaneous heating in a large-scale testing chamber with a forced ventilation system. Taraba and Michalec [104] numerically investigated the effects of longwall advance rate on spontaneous heating in goaf areas by a CFD model. Even though not many similar studies can be found, CFD technique has been sufficiently demonstrated to be a viable tool in investigating heating behaviour in longwall goaf. Hence CFD modelling is decided to be employed in studying heating evolution and associated inertisation plan in a

Shendong goaf (LW22307 goaf of Bulianta colliery). It has also been widely accepted air leakage is an important factor promoting development of heatings in sealed areas but yet, few studies regarding effects of air leakage can be found. Therefore influence of air leakage is also investigated in the study.

5.2 A brief information of LW22307 Bulianta colliery

Bulianta colliery, situated 13km south to Ordos city of Inner Mongolia Autonomous Region of northern China, is being operated in Shendong coalfield which is featured with flat and thick coal seam under shallow overburden. Mining area of the colliery is approximately 34km2 and the total proven reserve exceeds 506 million tons of coal. Due to recent upgrade of mining technology and equipment, extraction height of LW working face has increased to about 7m and annual production of the coal mine has exceeds 15 million tons of coal. LW22307 is located in 2-2 coal seam of mining section three. The depth of cover ranges from 110m to 230m with average 176m. Average thickness of the coal seam is 7.25m and the designed extraction height of LW22307 is 6.8m. The coal seam is very flat with slight dipping 1~3o. The length of LW22307 working face is 302m and range of LW22307 panel is 4954m. The roof is allowed fully caved in the goaf. The quality of coal and geotechnical conditions of the roof and floor is given in Table 5.1.

The layout and ventilation arrangement of LW22307 is shown in Figure 5.1. Maingate of LW22307 (6.0m wide and 4.5m high) was driven in coal seam and was used to transport coal and to supply part of the fresh airflow. Tailgate of LW22307 (5.4m wide and 4.5m high) was also driven in coal seam and served for airflow return. Tailgate of LW22308 (5.4m wide and 4.5m high) was also driven in coal seam and was used to supply another part of fresh air to LW22307 working face. Exhausting U shape ventilation mode was used to ventilate LW22307 and the airflow path was: drift →2-2 coal seam main→ section three main → maingate of LW22307 and tailgate of LW22308 → LW22307 → tailgate of LW22307 →maingate of LW22306 → section three return main →2-2 coal seam return main→1055 return main →$2^{\#}$return incline → south fan → surface. Totally approximately 2494m^3/h airflow was supplied to LW22307 and it was measured about 2577m^3/h airflow returned to tailgate due to leakage.

Table 5.1 Quality of coal and strata geotechnical conditions

Coal quality	Calorific value	Moisture	Ash	Fixed carbon	Volatile matter
	MJ/kg	Mad(%)	Ad(%)	FCad(%)	Vdaf(%)
	31.64	7.38	4.72	58.37	29.11
Geotechnical conditions	Strata	Lithology	Thickness(m)	Features	
	Primary roof	Sandstone	23.55～36.83 Average: 28.19	Grey with localised thin layer of mudstone.	
	Immediate roof	Mudstone	1.57-3.09 Average:3.33	Grey, rough fracture, block structure, including plant fossils.	
	Immediate floor	Mudstone	0～0.98 Average:0.47	Grey, less dense, smooth fracture, with white mica debris.	
Other factors	Seam gas	Seam gas content is 0.096m^3/t, 97% nitrogen, 3% CO_2			
	Combustibility	Very liable to spontaneous combustion, shortest incubation period is 18 days			
	Geothermal conditions	No abnormity is detected			
	Other	Floor heave occasional occurs in tailgate due to weak mudstone during longwall extraction, this affects longwall advance			

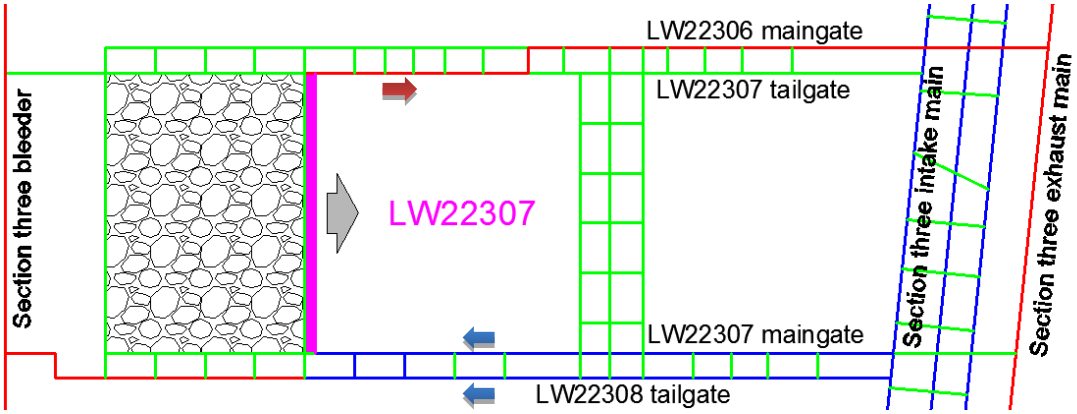

Figure 5.1 Layout and ventilation mode of LW22307

5.3 Geometric model and mesh generation

The geometries of the two domains and mesh of the model is generated via ANSYS 16.1 workbench design modeler and mesh tool, respectively. To utilize non-equilibrium thermal model in porous zone, mesh must be created in a high standard. When activate this model, a fake solid zone which overlaps the porous fluid zone is created, and this solid zone only thermally interacts with the fluid. The simplified

model is divided into four partitions: longwall face with associated gateroads, caving rock zone, residual coal zone, and seals around goaf, refer Figure 5.2. The used profiles of gateroads and seals were same to coal mine site. Length of longwall face is 302m and strike of the goaf of the base model is 1000m. Height of goaf is 30m because total thickness of the primary roof and immediate roof is about 30m. Length of the two gateroads is 150m and crossing sectional profiles of them follow the actual on-site dimension. It is assumed approximately 0.5m thick coal is left in goaf and is distributed evenly in goaf. The generated mesh is shown in Figure 5.3. Due to regular geometry of the model, structural mesh was used to avoid excessive number of elements. Mesh settings of all partitions are given in Table 5.2.

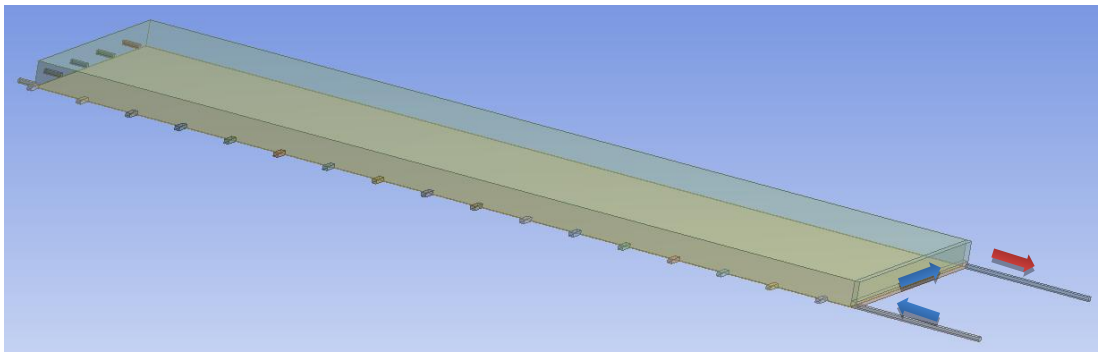

Figure 5.2 Three dimensional model of LW22307 panel in design modeler

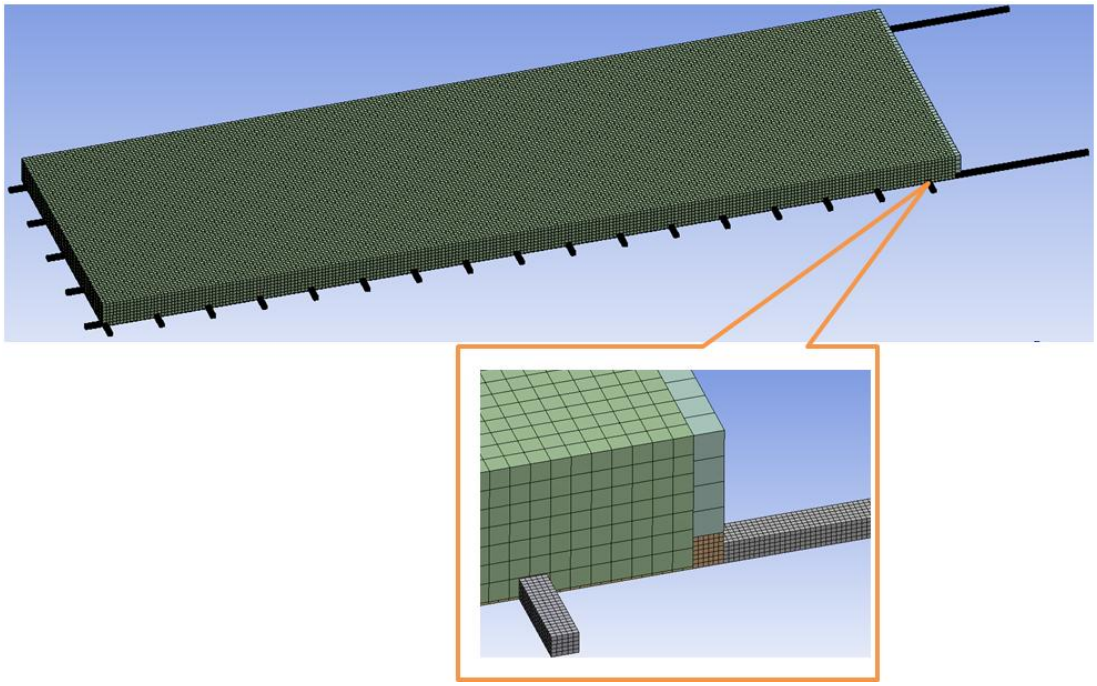

Figure 5.3 Generated mesh with a close-up view

Table 5.2 Mesh setting of the model

No.	Partition	Geometric profile			Element size/m
		Length/m (y)	Width/m (x)	Thickness or height/m (z)	
1	LW22307 maingate	150	6	4.5	1
2	LW22307 face	302	6	6.8	1
3	LW22307 tailgate	150	5.4	4.5	1
4	Goaf	1000	302	30	4
5	Residual coal layer	1000	302	0.5	2
6	Seal	20	5.4	4.5	1

5.4 Theoretical model

5.4.1 Low-temperature coal oxidation kinetics

To define coal-oxygen reaction rate with elevated temperature to a mathematical sense, a simple finite rate Arrhenius reaction mechanism is often used [24, 26, 72, 97, 98, 104], which is given,

$$r = A[C_o]^n \exp(-E_a/RT) \tag{5.1}$$

It is assumed that oxygen can penetrate throughout the coal without diffusional limitation and the reaction mechanism between gas and solid phases is deemed as a homogenous gas phase reaction [3]. This model approximates first order of coal oxidation. The Arrhenius kinetic parameters were derived from DSC test. The apparent activation energy is 23.4kJ/mol and the pre-exponential factor is 75.9s^{-1}. Yuan and Smith [24, 72]generalised that consuming one mole of oxygen by coal would generate one mole carbon dioxide and roughly 0.1 mole carbon monoxide at the early stage of coal oxidation, which yields a very simplified stoichiometric scheme of low-temperature coal oxidation:

$$\text{Coal} + O_2 \rightarrow CO_2 + 0.1CO + \text{Heat} \tag{5.2}$$

This model also employs this coal oxidation reaction scheme at low temperature range. Kaji *et al*. [9] measured the rates of heat liberation and oxygen consumption due to coal oxidation at low temperature range using coals ranging from subbituminous to anthracite and 300~379kJ heat evolved per mole of oxygen at steady state was reported. Many works [24, 54, 59, 60, 98] used 300 kJ/mol oxygen as coal oxidation reaction heat so this model also uses such a value as reaction heat.

5.4.2 Energy conservation

The heat generated by coal oxidation is modeled as a source term and written as a User Defined Function (UDF). To be more realistic to describe heat interaction inside coal mass, heat transfer between coal particles should be treated in a non-equilibrium approach. The temperature differential between the solid coal particle and gas stream is important in the thermal behaviour and it is thus necessary to represent the energy stored in each individual phase as well as the exchange of thermal energy between them, which gives energy conservation for solid coal pellet:

$$(1-\varepsilon)\rho_{\mathrm{c}}C_{\mathrm{pc}}\frac{\partial T_{\mathrm{c}}}{\partial t} = (1-\varepsilon)\lambda_{\mathrm{c}}\nabla^2 T_{\mathrm{c}} + \frac{6(1-\varepsilon)}{d\varepsilon}h\left(T_{\mathrm{g}} - T_{\mathrm{c}}\right) + r\Delta H \tag{5.3}$$

In which the successive terms represent internal energy growth of coal particle, heat diffusion in solid coal, heat convection interacted with gas stream, and heat generated by coal oxidation which is a source term. Energy balance for the gas stream is written as:

$$\varepsilon\frac{\partial}{\partial t}\left(T_{\mathrm{g}}\rho_{\mathrm{g}}C_{\mathrm{pg}}\right) + \nabla\left[\vec{v}\left(T_{\mathrm{g}}\rho_{\mathrm{g}}C_{\mathrm{pg}} + P\right)\right] = \varepsilon\lambda_{\mathrm{g}}\nabla^2 T_{\mathrm{g}} - \frac{6(1-\varepsilon)}{d\varepsilon}h\left(T_{\mathrm{g}} - T_{\mathrm{c}}\right) \tag{5.4}$$

In which the successive terms represent transient energy rise of gas stream, heat convection of gas stream, heat diffusion in gas stream, and heat convection interacted with solid coal.

5.4.3 Species conservation

Nitrogen is neither consumed nor produced during whole process of self-heating so species conservation is mainly focused on oxygen, carbon dioxide, and carbon monoxide in gas stream according to the assumed reaction scheme, which give rise to the species conservation:

$$\begin{cases} \text{For oxygen: } \varepsilon\frac{\partial(\rho C_{\mathrm{o}})}{\partial t} + \varepsilon\nabla(\rho\vec{v}C_{\mathrm{o}}) - \nabla\left(\rho D_{\mathrm{o}}\nabla C_{\mathrm{o}} + D_{\mathrm{T,o}}\frac{\nabla T}{T}\right) + r = 0 \\ \text{For carbon dioxide: } \varepsilon\frac{\partial(\rho C_{\mathrm{i}})}{\partial t} + \varepsilon\nabla(\rho\vec{v}C_{\mathrm{i}}) - \nabla\left(\rho D_{\mathrm{i}}\nabla C_{\mathrm{i}} + D_{\mathrm{T,i}}\frac{\nabla T}{T}\right) - r = 0 \\ \text{For carbon monoxide: } \varepsilon\frac{\partial(\rho C_{\mathrm{j}})}{\partial t} + \varepsilon\nabla\left(\rho\vec{v}C_{\mathrm{j}}\right) - \nabla\left(\rho D_{\mathrm{j}}\nabla C_{\mathrm{j}} + D_{\mathrm{T,j}}\frac{\nabla T}{T}\right) - 0.1r = 0 \end{cases} \tag{5.5}$$

In which the successive terms represent the local accumulation of species, the convective transport of species, the diffusion term of species caused by variation of species concentration and temperature, and the fraction consumed or produced by coal oxidation.

5.4.4 Momentum balance in porous medium

Navier-Stokes equation is normally used to describe momentum balance for compressible flow as density of fluid varies with temperature and elapsing of time in this case. Reform Navier-Stokes equation by adding viscous term to solve flow momentum balance in porous stockpile, which produces:

$$\frac{\partial}{\partial t}\left(\rho_{\mathrm{g}}\vec{v}\right)+\nabla\left(\rho_{\mathrm{g}}\vec{v}\vec{v}\right)=-\nabla P+\nabla(\vec{\tau})+\vec{F}-\varepsilon\frac{\mu}{k}\vec{v} \tag{5.6}$$

The permeability *k* of coal matrix is approximated by the Carmen–Kozeny equation for laminar flow in packed beds [133]:

$$k=\frac{\varepsilon^3 d^2}{150(1-\varepsilon)^2} \tag{5.7}$$

5.4.5 Continuity in porous medium

Mass change of bulk coal due to coal oxidation at low temperature is ignored. This model also assumes isotropic porous medium and therefore for single phase flow in isotropic porous medium, the continuity equation can be written as:

$$\frac{\partial\rho}{\partial t}+\nabla(\rho\vec{v})=0 \tag{5.8}$$

5.5 Modelling setting and boundary conditions

The model consists of two types of domains: (i) goaf and coal layer are treated as porous domain and,(ii) the remaining domains including maingate, tailgate and longwall face is considered as the free flow field. As discussed, permeability of goaf and coal layer is determined by the Carmen–Kozeny equation. It has been studied that porosity value varies from 0.17 to 0.41 in goaf and around the perimeter of the gob and immediately behind the face shields, the porosity was the largest, while near the centre of the gob, the value was the smallest [72].It is assumed average diameter of residual coal and rock is 0.1m and 0.4m respectively. A combination of a number of hyperbolic and polynomial functions was used to establish the profile of permeability distribution in goaf and residual coal. It is also assumed the profile has no difference along z direction.

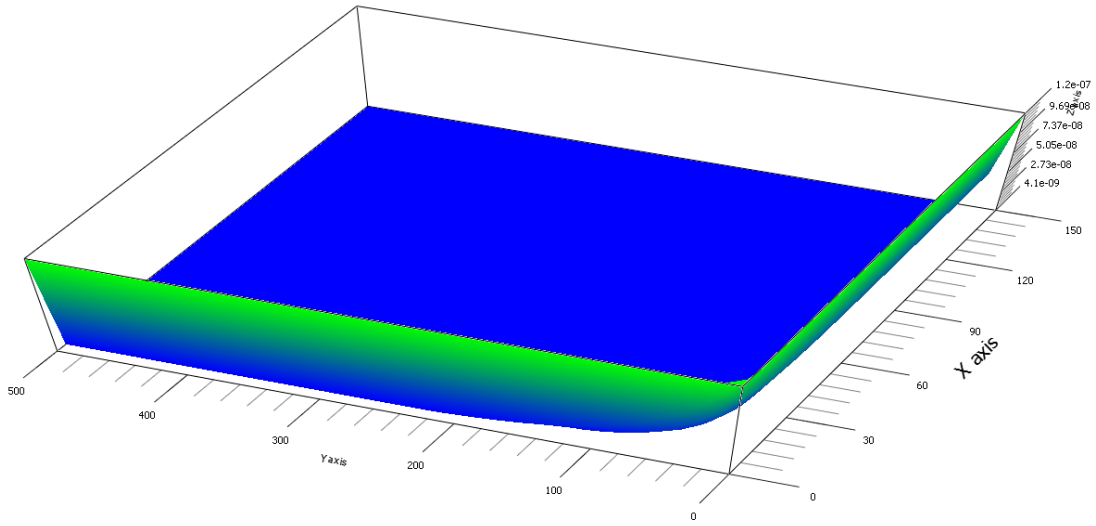

Figure 5.4 Permeability profile of residual coal in a quarter goaf

Figure 5.4 gives permeability profile of residual coal of a quarter of goaf (0<x<150m, 0<y<500m). It can be seen the permeability of coal layer ranges from 4.1e-9 to 1.2e-7$m^2$and permeability immediately behind face and around perimeter is larger than that in centre of goaf.

Airflow stream is considered to be fully turbulent in free flow field including gateroads and longwall face and thus is solved by Fluent RNG k-ε model. To suppress turbulent viscosity in porous coal mass, laminar zone option is enabled. Many works [24, 26, 53, 54, 56-58, 61, 73, 115] have also suggested natural convection is also a possible mechanism of oxygen transport so full buoyancy effect is also activated in this model. Like previous works conducted by Yuan and Smith [24, 72], two-step simulation approach is used: (i) a simulation is conducted firstly without turning on generation and consumption of species and heat source to obtain a steady flow in the goaf and residual coal; (ii) the transient simulations with generation and consumption of species and heat source are conducted using the steady flow field as the initial conditions. Important parameters are shown in Table 5.3. Boundary and initial conditions employed in the model is shown in Table 5.4.

Table 5.3 Important input parameters in this model

Parameters	Value	Unit
Specific heat capacity of coal	1200	J kg^{-1} K^{-1}
Specific heat capacity of rock	900	J kg^{-1} K^{-1}
Apparent activation energy	23.4	kJ mol^{-1}
Heat of coal oxidation	300	kJ mol^{-1} O_2
Apparent order of reaction	1	
Arrhenius pre-exponential factor	75.9	s^{-1}
Gravitational acceleration	9.8	m s^{-2}
Diameter of residual coal	10	cm
Diameter of caved rock	40	cm
Heat transfer coefficient	3	W m^{-2} K^{-1}
Density of coal	1300	kg m^{-3}
Density of rock	2650	kg m^{-3}
Thermal conductivity of coal	0.2	W m^{-1} K^{-1}
Thermal conductivity of rock	2.8	W m^{-1} K^{-1}
Time step	300	s

Table 5.4 Initial and boundary conditions employed in this model

Condition		Gas flow	O_2 transport	CO_2 transport	CO transport	Temperature
Initial conditions		V=1.54 (m/s)	C_o=0	C_i=0	C_j=0	300K
Boundary conditions	Inlet in maingate	Velocity inlet	C_o=0.23 (mass fraction)	C_i=0	C_j=0	300K
	Wall	No flux	No flux	No flux	No flux	Adiabatic
	Interface	Convection flux	Diffusion and convection flux	Diffusion and convection flux	Diffusion and convection flux	Conduction and convection
	Outlet in tailgate	Outflow	-	-	-	-

5.6 Base model result and validation

5.6.1 Steady results

As LW22307 of Bulianta colliery was planned to advance more than 4000m, permeability of goaf is relatively stable after advancing a certain distance and a1000m long model is selected as the base model. Before running the model in a transient way with activation of reaction heat, a steady flow field is solved at the first place. Figure 5.5 and Figure 5.6 display the velocity contour and velocity vector projected in a plane across the residual coal layer. It can be seen high velocity airflow (>0.004m/s) is able to travel into coal mass 30~100m and the fresh air can penetrate deeper at intake side than that at return side. It is also indicated in deep goaf, more airflow is present around perimeter of goaf rather than centre of goaf due

to high porosity and permeability on goaf fringe. Figure 5.7 shows oxygen concentration contour of the base model. It can be seen high concentration oxygen can migrate into goaf approximately 400m behind face at maingate side and only about 100m at tailgate side. Figure 5.8 and Figure 5.9 shows CO concentration contour and dispersion pattern at initial temperature, respectively. Most CO is generated at intake side due to presence of high oxygen gas mixture and more occurrences of coal oxidation. It can be also observed liberated CO is unable to travel around the entire goaf perimeter and starts to divert to return side at middle of the goaf.

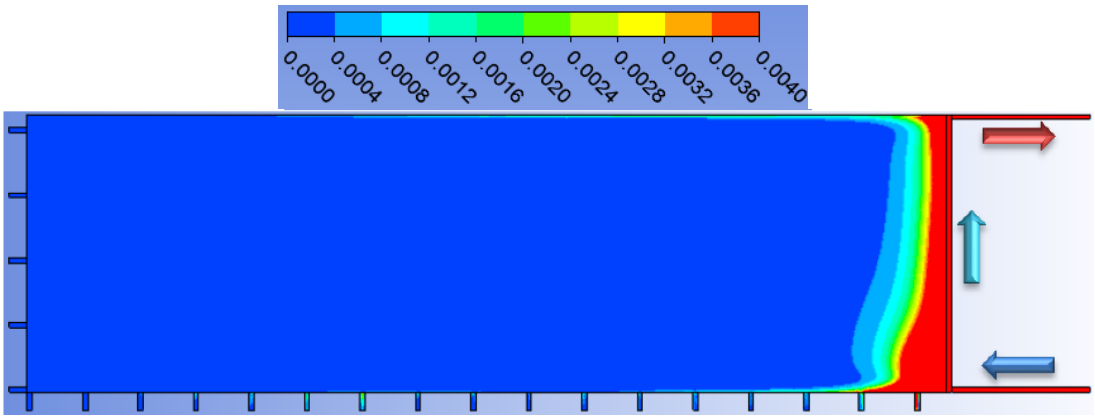

Figure 5.5 Velocity (m/s) contour of the base model

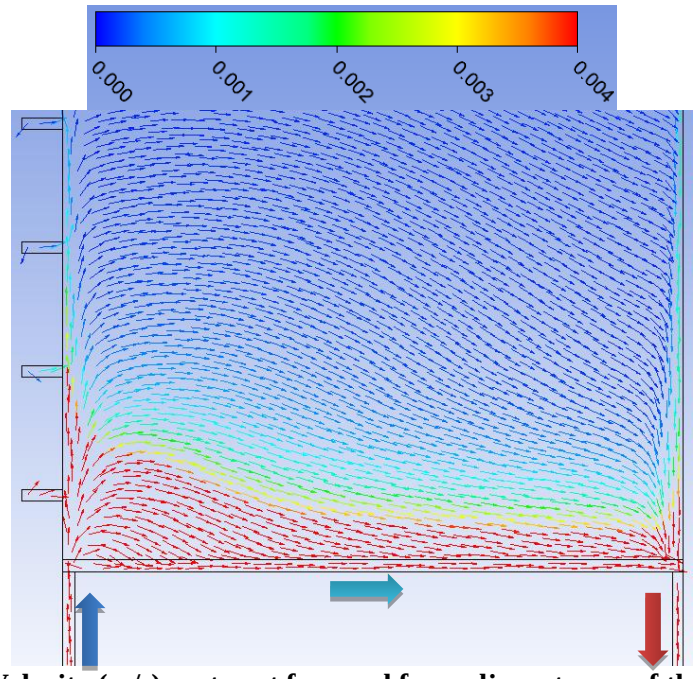

Figure 5.6 Velocity (m/s) vector at face and face adjacent area of the base model

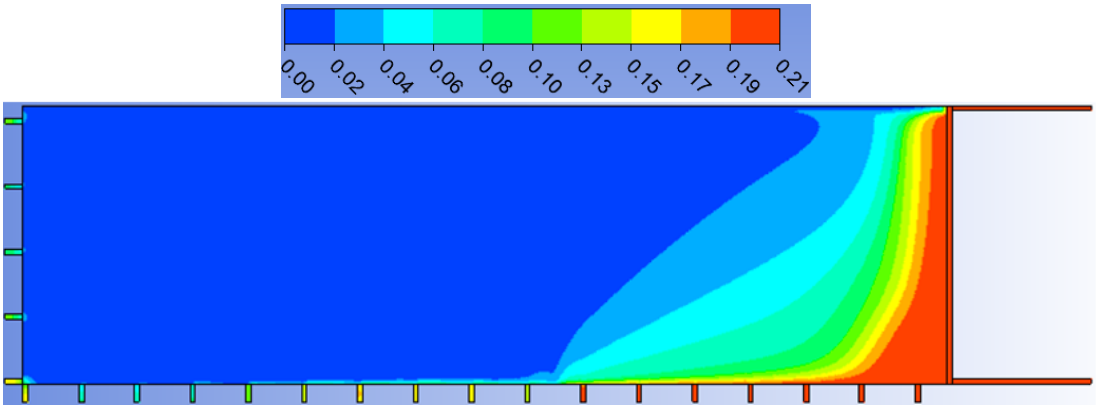

Figure 5.7 Oxygen (%) contour of the base model

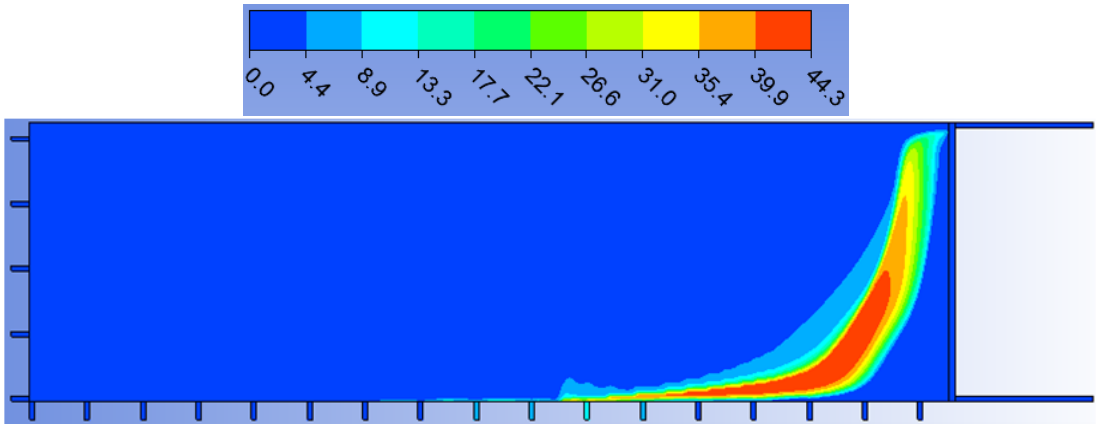

Figure 5.8 CO (ppm) contour of the base model

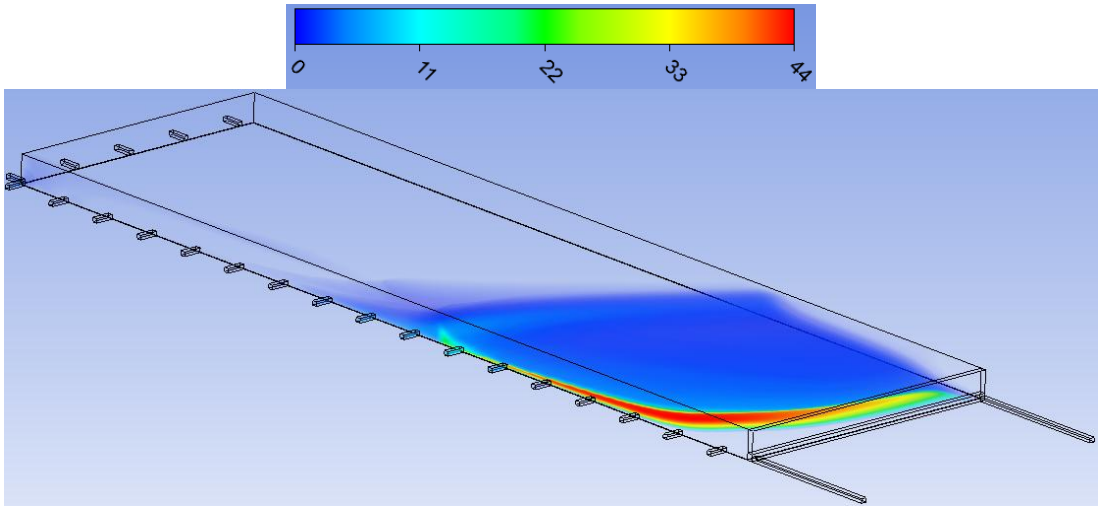

Figure 5.9 CO (ppm) volume rendering of the base model at 300K temperature

5.6.2 Transient results

After the steady flow solution is solved, reaction heat is activated to acquire the evolution of heating. Figure 5.10 shows heating development in layer of residual

coal with time. Heating is not developed immediate behind face due to strong heat dissipation of high velocity airflow stream. Heating is also not developed in deep goaf due to presence of low level oxygen. Heating is most likely to develop in an intermediate zone where airflow stream is able to supply enough oxygen to sustain continuous oxidation reaction and meanwhile, heat dissipated by convection is less effective than heat generated by oxidation. Figure 5.11 shows CO evolution trend at different days and it can be seen main reaction zone overlaps high temperature zone. Figure 5.12 provides the trends of maximum temperature rising and CO make at different days. It can be observed initially temperature increased very slowly while after a critical temperature (around 350K at day 26), the maximum temperature shot up and is likely to reach ignition temperature in few days. According to the simulating result, incubation period is roughly 29 days. Similar trend can be found for CO make. A "textbook" classification of levels of CO make is given in Table 5.5.

Table 5.5 Classification of CO make level [27]

Level	Threshold value (liter/min)	Indication
Level one	10	Require investigation
Level two	20	Considerable danger exists
Level three	30	Extreme danger exists

According to the classification system, on day 16 the level one is triggered at temperature 320K. Therefore if monitored temperature from any spot exceeds 20K above ambient temperature, investigation must be put in place. On day 27 the second level is activated and maximum temperature reached higher than 380K, which indicates an advanced heating incident is taking place and mitigation measures must be exercised. On day 29 level three is triggered and the maximum temperature is close to ignition temperature. Under such emergency circumstance, quick reaction plans like mine evacuation and seal of longwall panel should be considered. The strike of the heating zone is about 300m and advance rate of the longwall face is 15.7m per day. Approximately only 20 days are required to fully leave the heating zone in suffocation zone of goaf. Hence with normal advance rate of longwall face and without air leakage from other sources, serious heating in Shendong goaf is unlikely to occur.

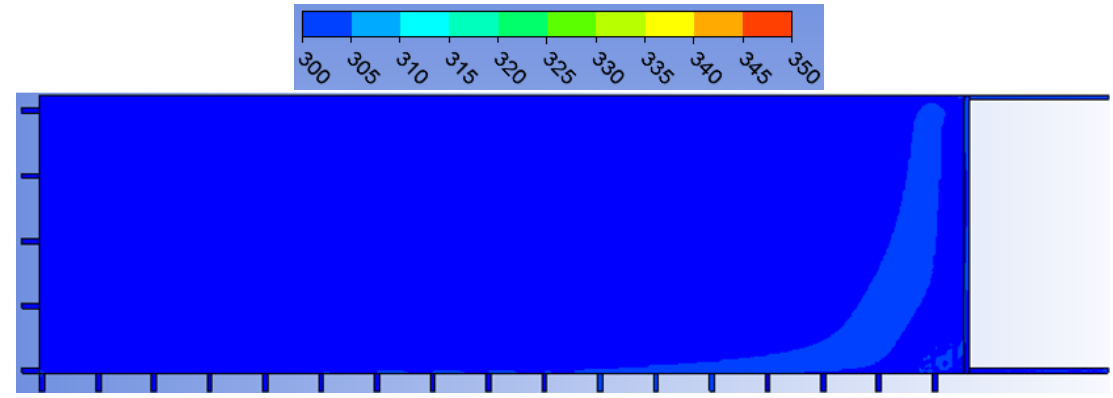

(a) Day 5

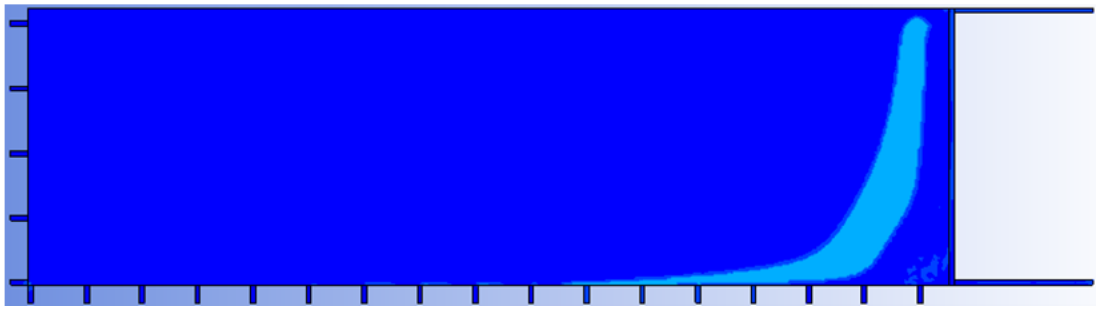

(b) Day 10

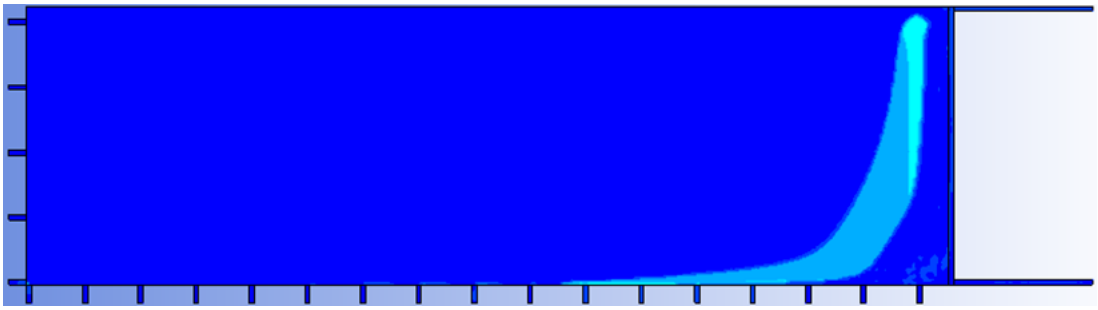

(c) Day 15

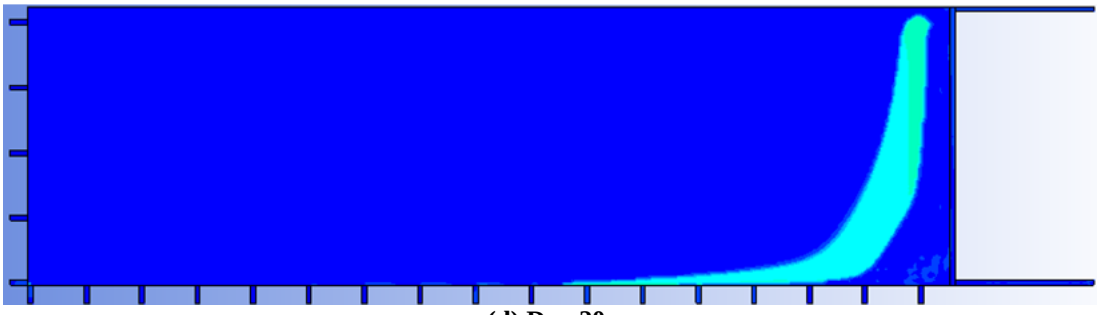

(d) Day 20

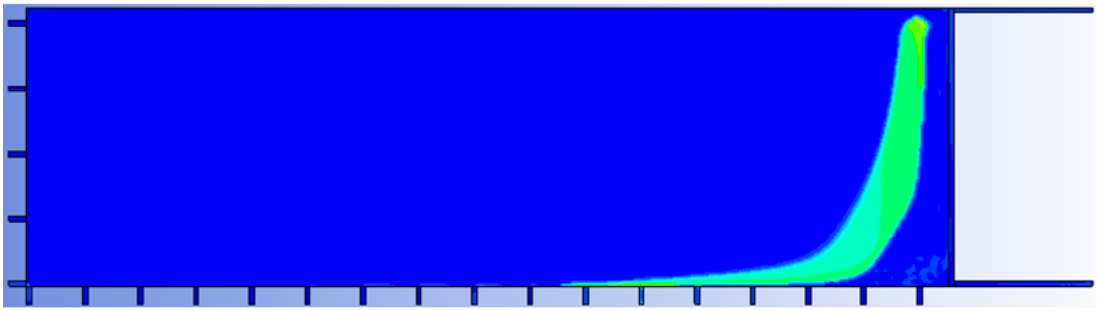

(e) Day 25

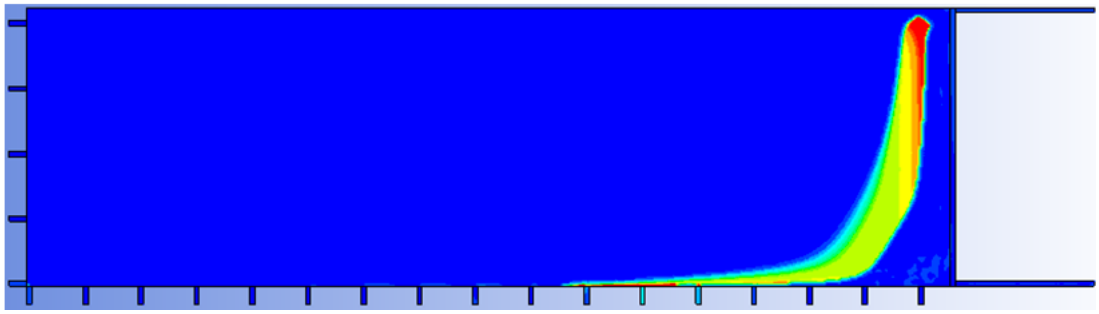

(f) Day 30

Figure 5.10 Temperature (K) contour against time of the base model

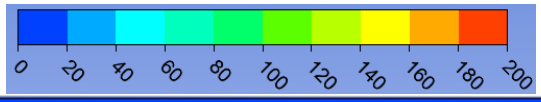

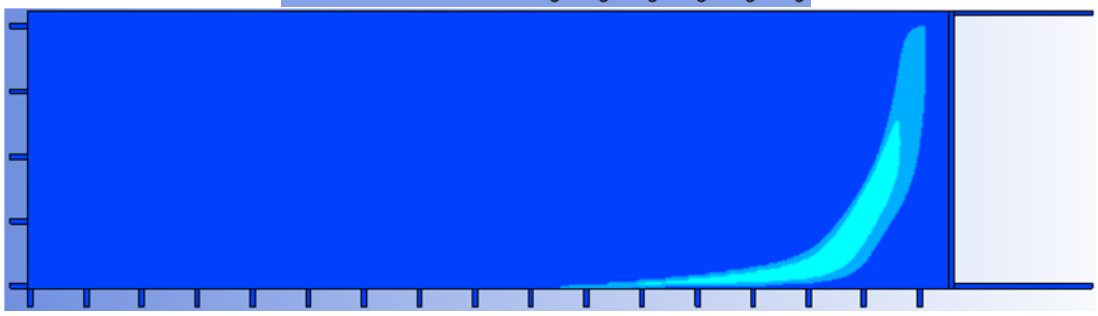

(a) Day 5

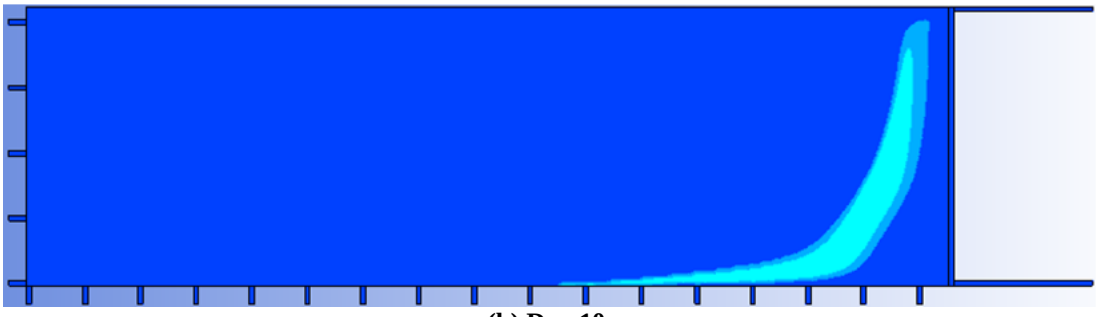

(b) Day 10

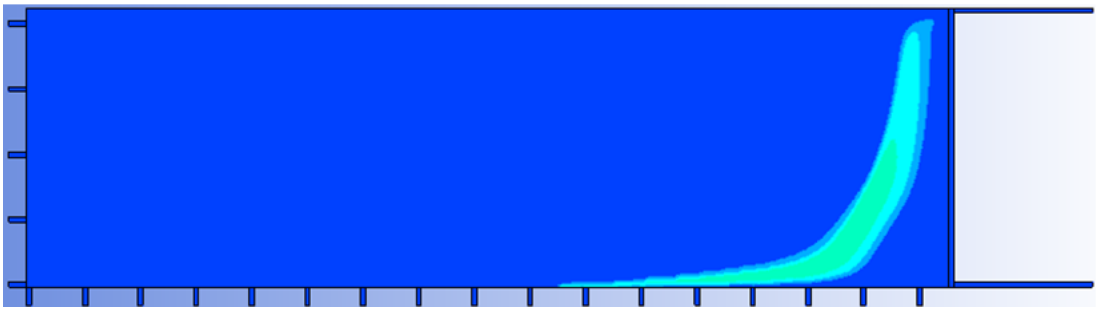

(c) Day 15

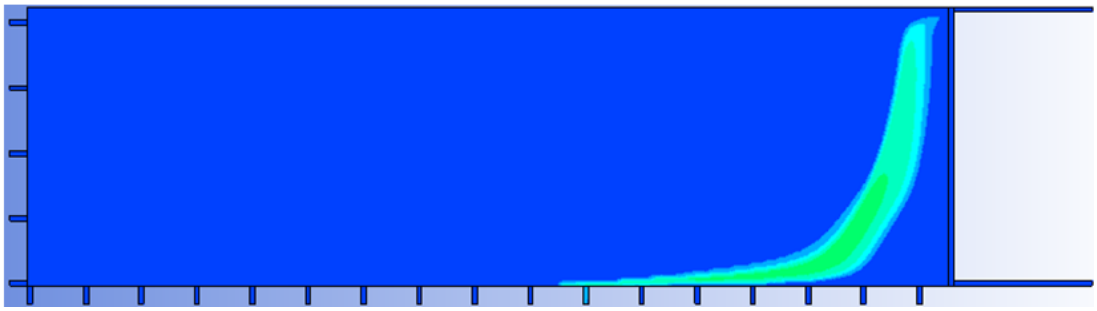

(d) Day 20

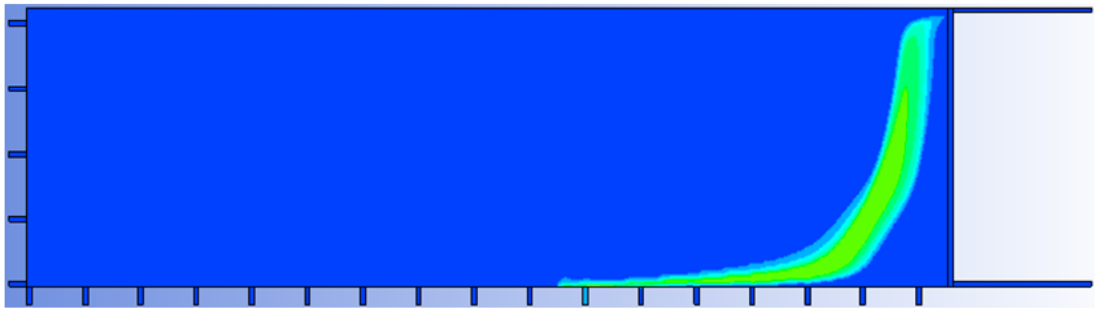

(e) Day 25

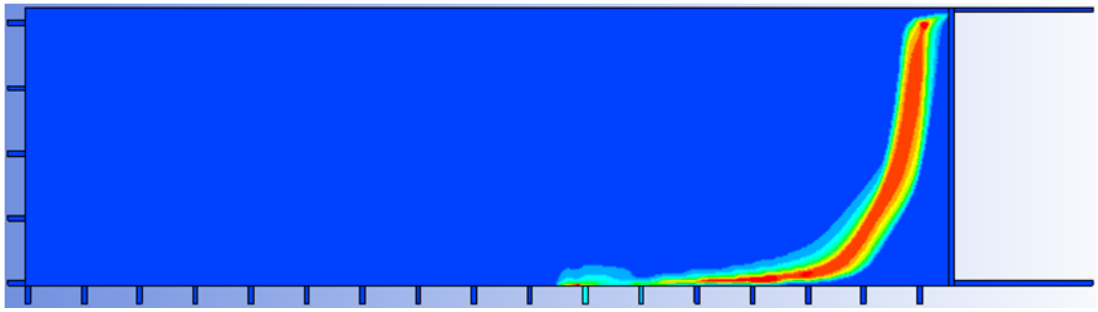

(f) Day 30

Figure 5.11 CO (ppm) evolution against time of the base model

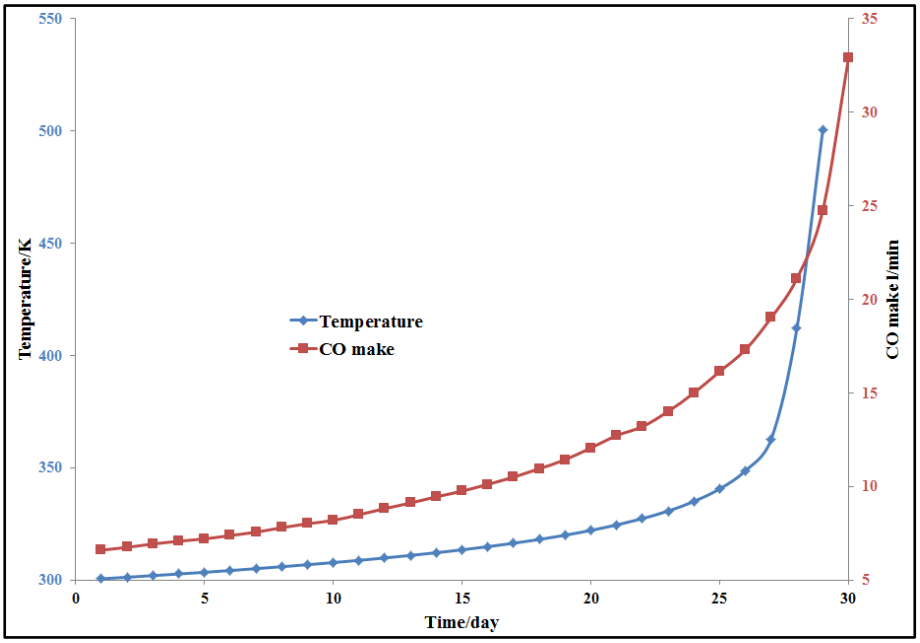

Figure 5.12 Trend of maximum temperature and CO make of the base model

5.6.3 Model validation

Validation and calibration of the base model, as an integrated procedure of the CFD numerical modelling, is carried out using the field gas monitoring data. Figure 5.13 and Figure 5.14 show comparison of real monitoring and simulated oxygen level from maingate side and tailgate side, respectively. A good agreement can be observed between the modelled result and field gas monitoring data at intake side. It can be also seen oxygen level is able to reduce to a safe level in terms of sustaining heating of coal 350m behind face. However, at return side, site monitored oxygen concentration is slightly higher than simulated data. The differential levels may attribute to airflow leakage into goaf. Figure 5.15 and Figure 5.16 show comparison of real monitoring and simulated CO level from maingate side and tailgate side, respectively. Similar to variation of oxygen level, a good agreement can be observed at intake side while monitored CO at return side is much higher than simulated values. The big gap is possibly due to gas leakage from goaf LW22306 in which the gas mixture may consist of high level of CO. An internal report shows incubation period of Shendong coals ranges from 18 to 33 days on basis of experimental results. The simulation result of base model has indicated a period of 29 days is required to develop to an ignition incident. The period falls into the range of the experimental results. Therefore the model is considered to be viable in simulating both steady flow field and transient temperature field.

Figure 5.13 Oxygen level validation at intake side

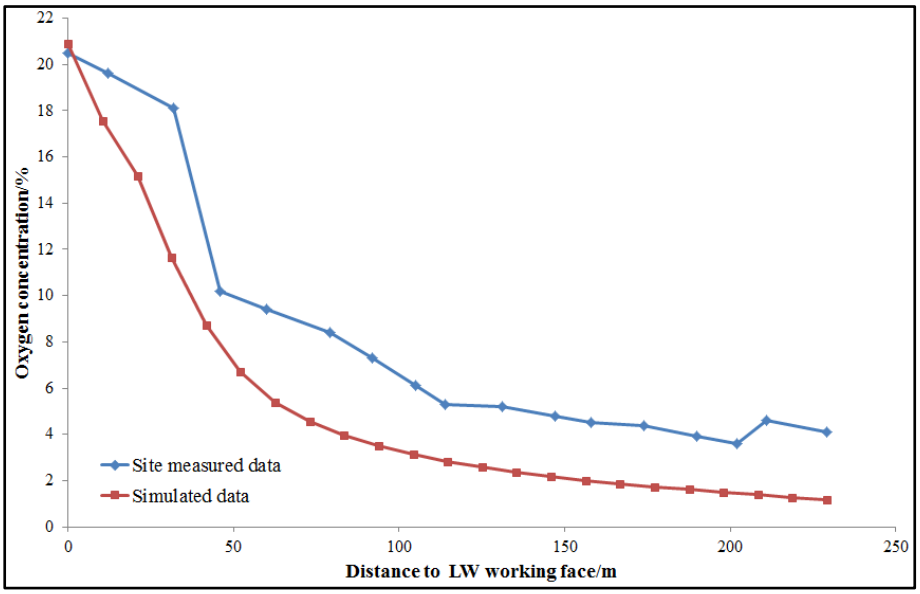

Figure 5.14 Oxygen level validation at return side

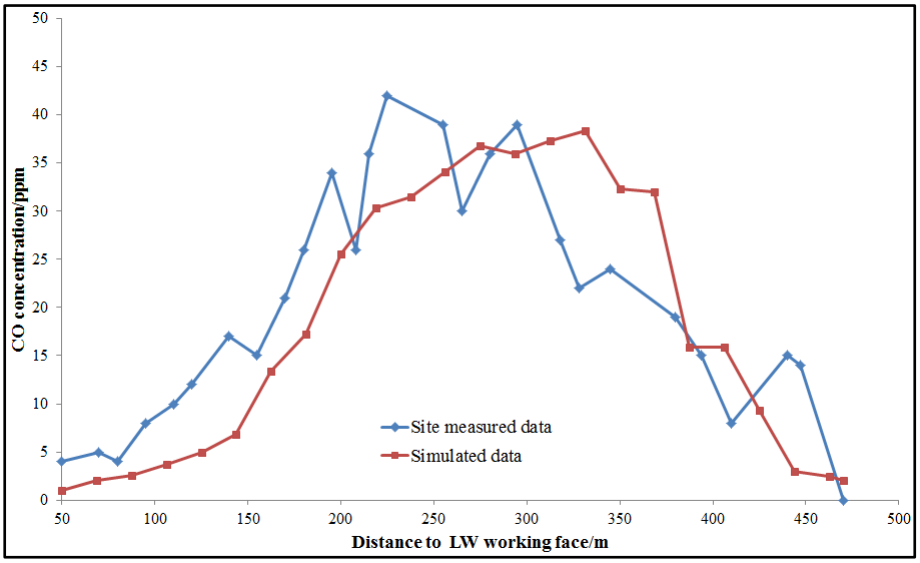

Figure 5.15 CO level validation at intake side

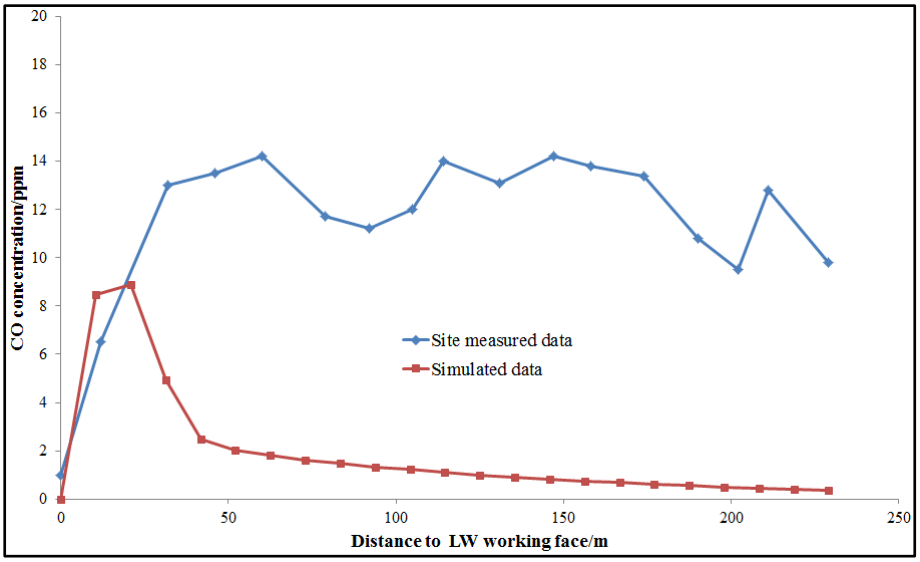

Figure 5.16 CO level validation at return side

5.7 500m Model

5.7.1 Model results

The base model results have indicated high velocity and oxygen rich gas stream is unlikely to travel around entire perimeter of a 1000m goaf. Under normal advance rate and periodic caving process, heating behind longwall face is hard to develop even without a proactive inertisation plan. However there is a possibility high velocity airflow travels around goaf fringe and high oxygen gas may present in start-up area at initial mining stage when dimension of goaf is relatively smaller. To investigate such a possible scenario, a model with range of 500m is developed. Figure 5.17 provides the velocity distribution in coal layer of the 500m model. It can

be seen high velocity gas stream is able to travel to deep goaf. Figure 5.18 illustrates oxygen distribution in coal layer of the 500m model and it can be observed high oxygen level gas is present at start-up area and thus poses a potential heating hazard. Figure 5.19 and Figure 5.20 give temperature field and CO evolution after different periods, respectively. Besides heating and CO generation behind longwall face, even more serious heating and higher volume CO can be developed in start-up area. Unlike heating behind longwall face, heating in start-up area would not be eliminated with advance of longwall face. Therefore an inertisation plan is required to suppress heating developed in start-up area.

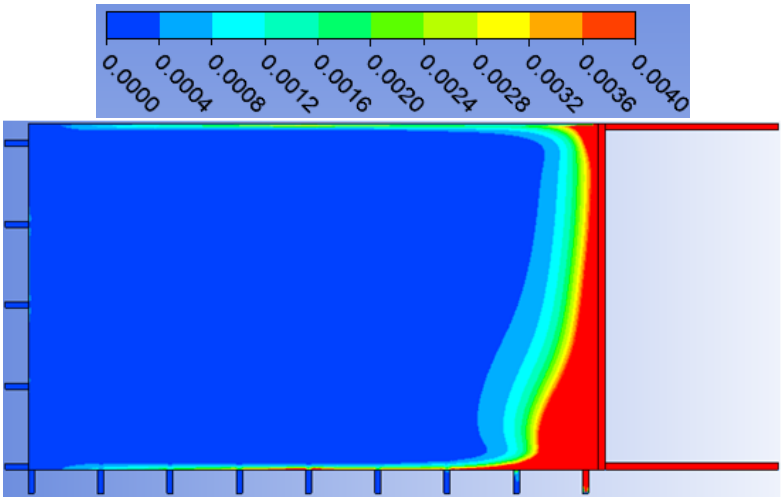

Figure 5.17 Velocity (m/s) contour of 500m model

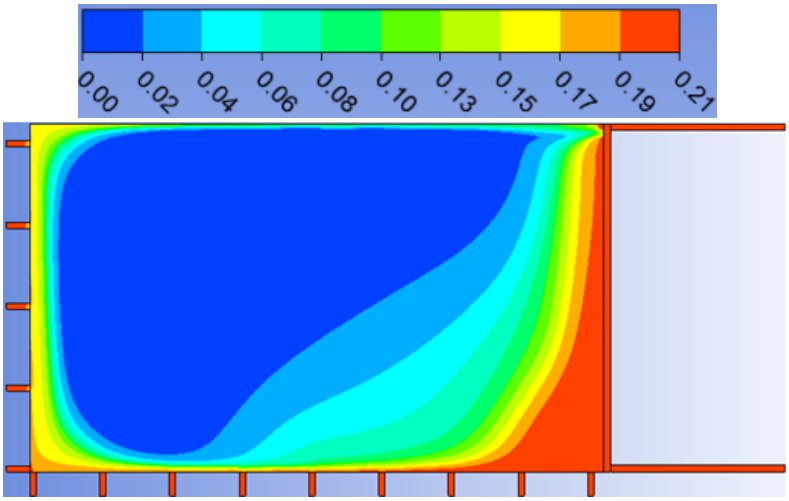

Figure 5.18 Oxygen (%) contour of the 500m model

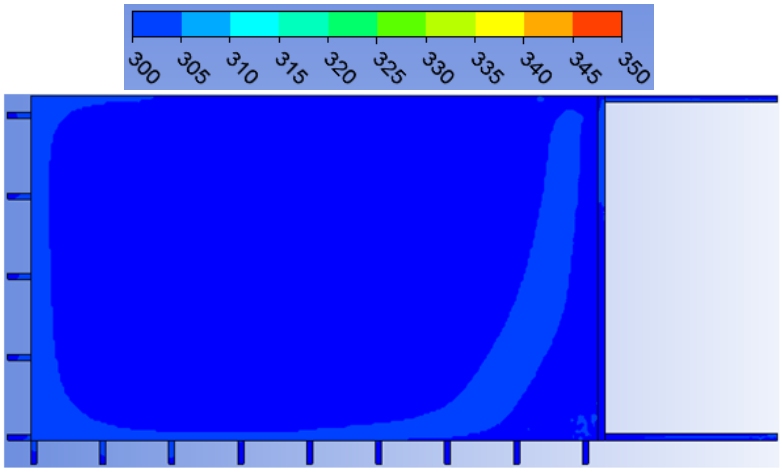

(a) Day 5

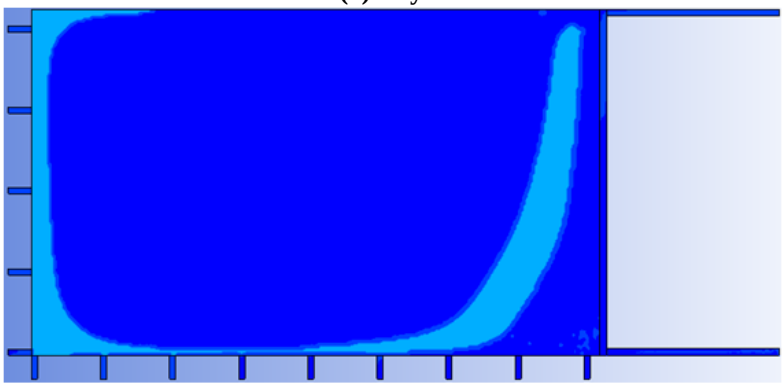

(b) Day 10

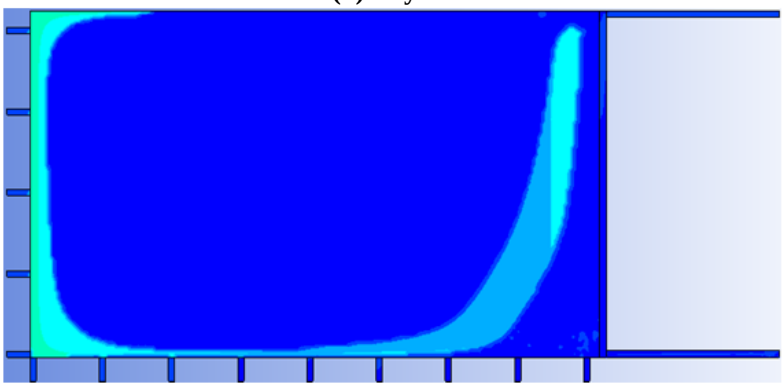

(c) Day 15

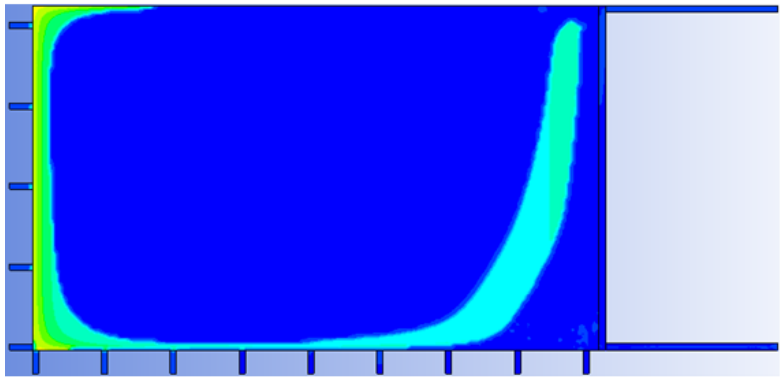

(d) Day 20

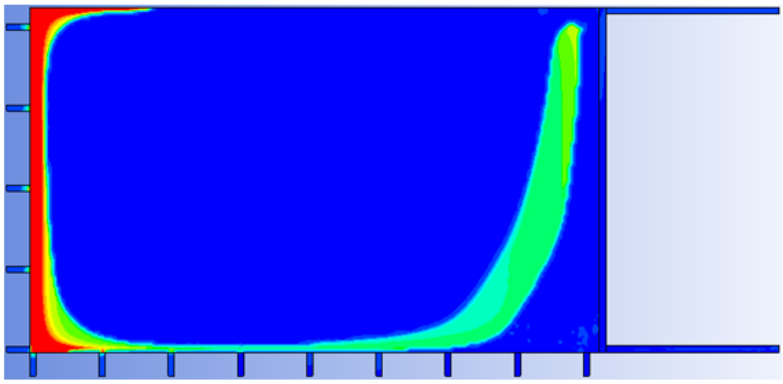

(e) Day 25

Figure 5.19 Temperature (K) contour against time of 500m model

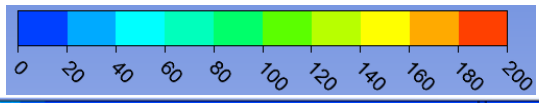

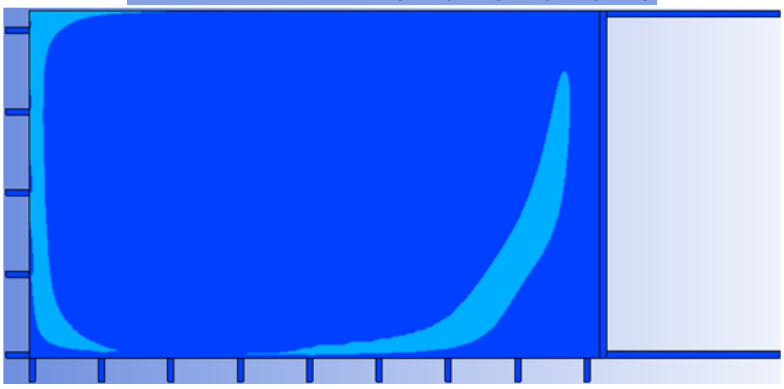

(a) Day 5

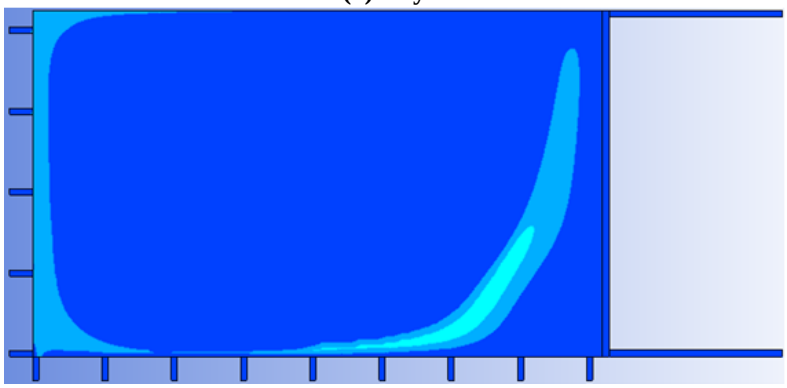

(b) Day 10

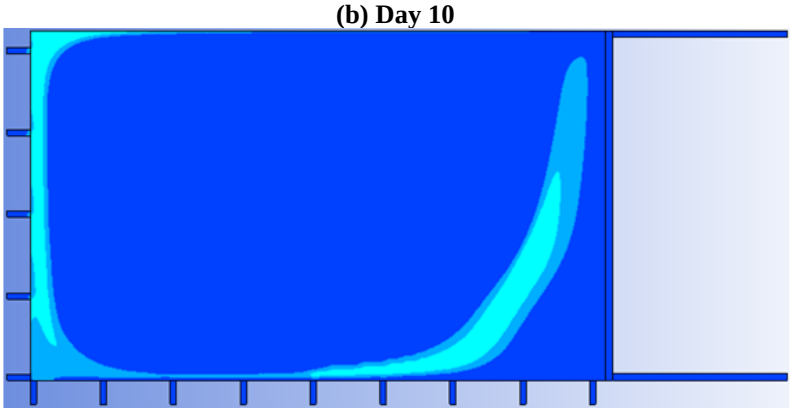

(c) Day 15

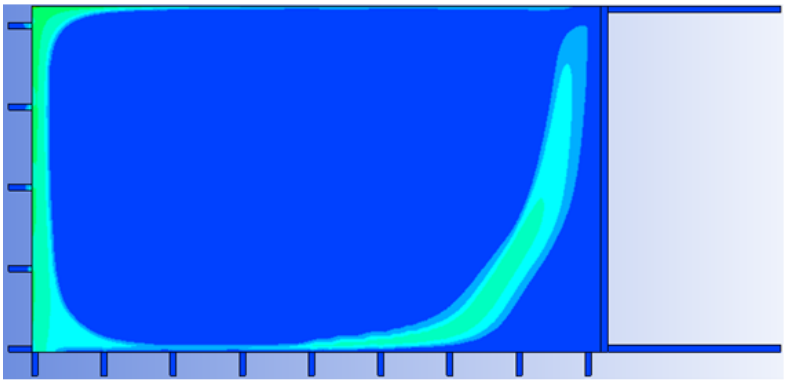

(d) Day 20

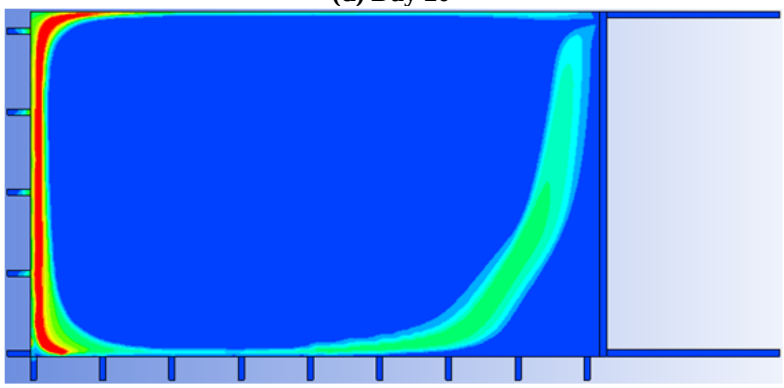

(e) Day 25

Figure 5.20 CO (ppm) evolution against time of the 500m model

Figure 5.21 provides the maximum temperature rising and CO make profile with time. It takes roughly 25 days for spontaneous heating to develop to an open fire. According to the referred triggering levels of CO make, first level is reached on day 8 when the maximum temperature is around 308K. Second level is triggered on day 22 when the maximum temperature has increased to more than 350K. Level three is triggered on day 25 when the combustion is very likely to be taking place. A variety of models with different lengths 700m, 750m, and 800m are also conducted and it is found high oxygen level gas is unable to migrate to start-up area as long as length of goaf is larger than 750m. The details of these models are omitted here. It takes approximately 47 days for longwall to advance 750m and such a period is sufficient for an advanced heating to be developed at start-up line zone. Therefore a proactive plan is needed at initial mining stage before longwall advances 750m.

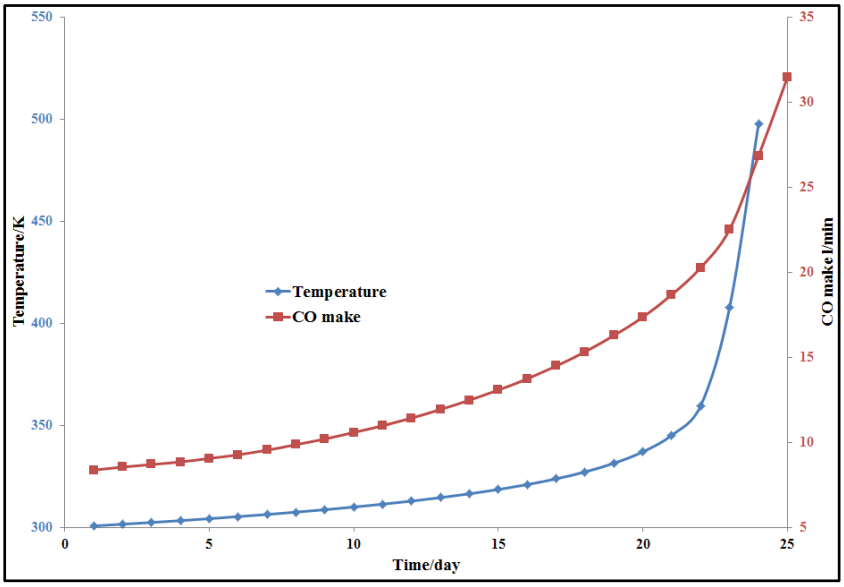

Figure 5.21 Trend of maximum temperature and CO make of 500m model

5.7.2 Proactive inertisation plan

Two Membrane Separation Nitrogen Generators (MSNG) are equipped in Bulianta colliery. The maximum capacity of each nitrogen generator is 488m^3/h (0.136m^3/s). The MSNG can be transported and operated in harsh underground environment. Figure 5.22 illustrates inertisation effects of full capacity nitrogen injection (488m^3/h) behind different seals. It is found full capacity nitrogen injection from seal C, D, E, F, or G is able to exclude oxygen rich gas from start-up area. It is postulated lower volume of nitrogen injection may also fulfil the duty and therefore inertisation effects of nitrogen injection with half capacity (244m^3/h) is simulated. Figure 5.23 shows inertisation effects with half capacity injection quantity behind seal C, D, E, F, and G. It is shown the half quantity nitrogen injection is still able to have good effects of inertisation but low oxygen concentration gas can leak into start-up area for nitrogen injection behind seal G. Figure 5.24 shows inertisation effects with quarter capacity nitrogen injection (122m^3/h) behind seal D, E, and F. It can be found such low quantity of nitrogen injection fails to fully exclude high oxygen gas from start-up area. Therefore the best proactive inertisation plan is nitrogen injection behind seal D, E, or F with at least 244m^3/h flow rate. During the inertisation operation other seals must be erected in good quality to avoid nitrogen escape from these seals.

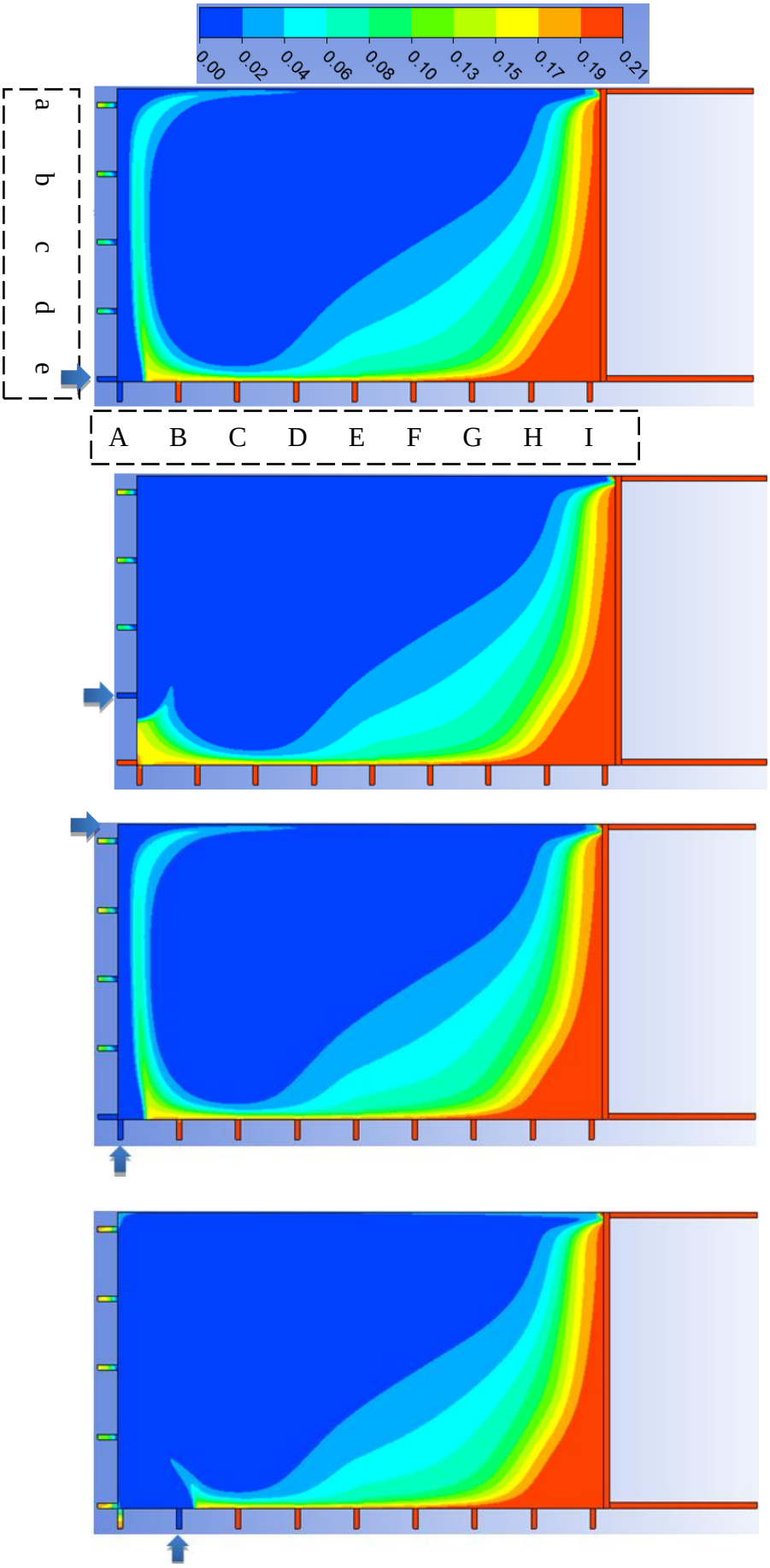
0.00
0.02
0.04
0.06
0.08
0.10
0.13
0.15
0.17
0.19
0.21
a
b
c
d
e
A B C D E F G H I

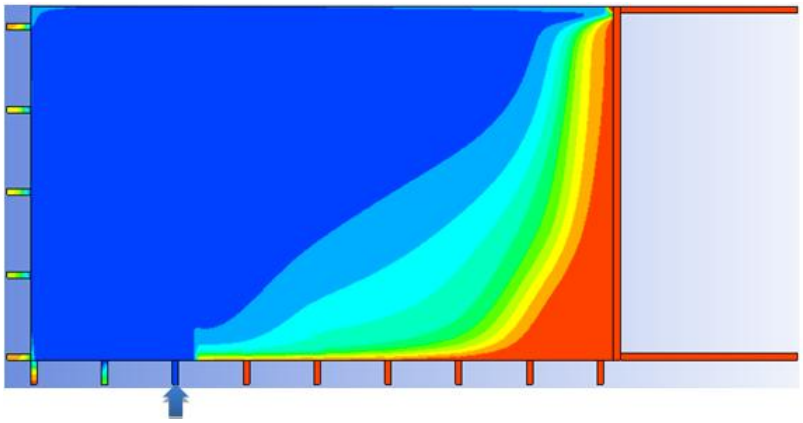

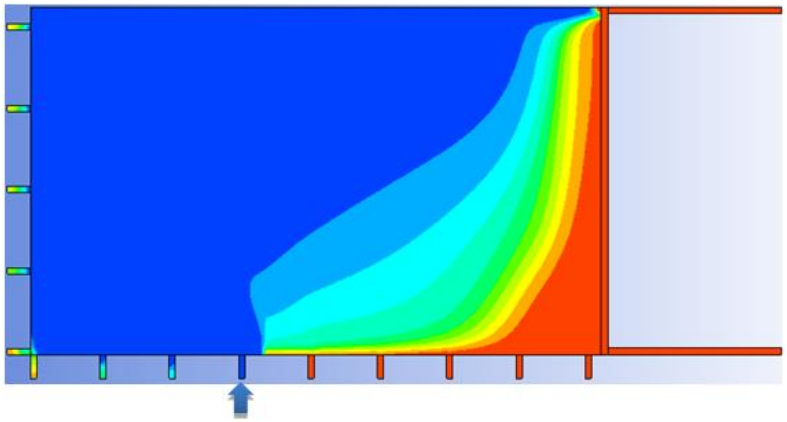

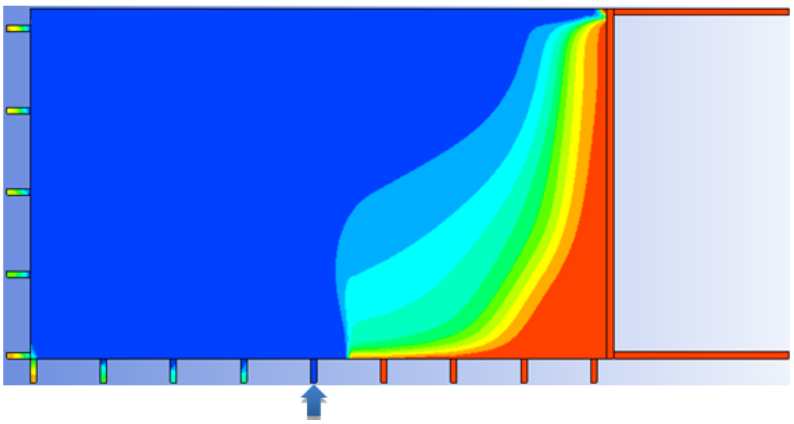

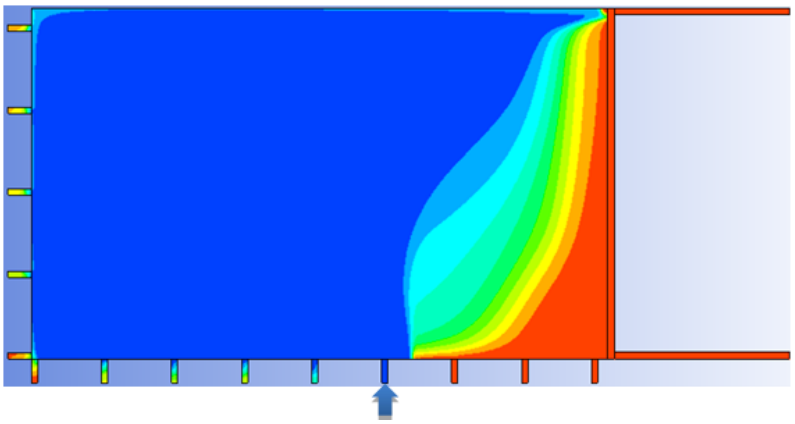

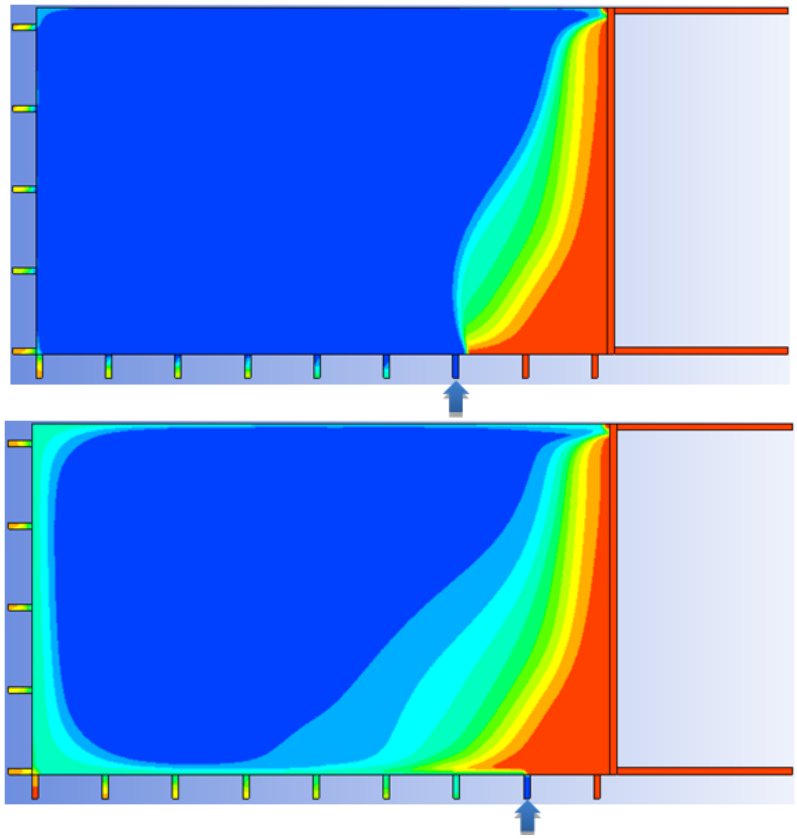

Figure 5.22 Oxygen level in coal layer with full capacity nitrogen injection at various locations

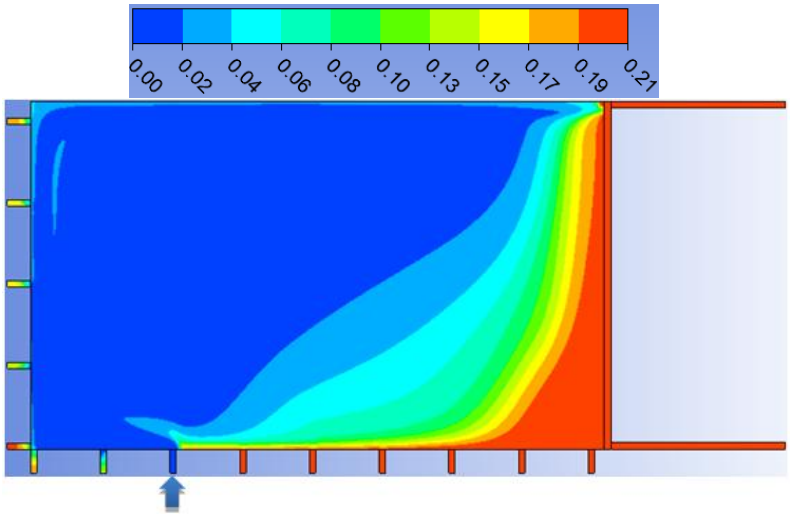

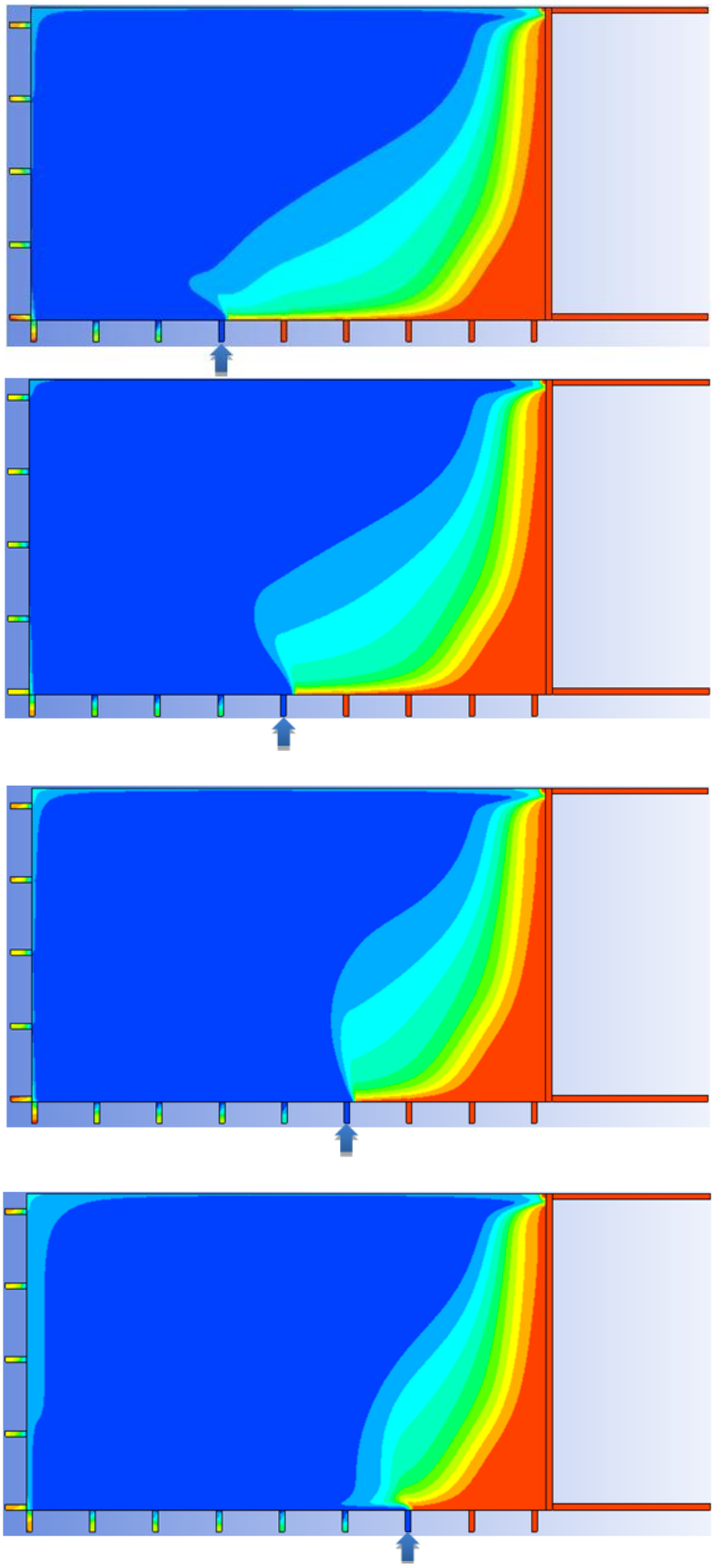

Figure 5.23 Oxygen level in coal layer with half capacity nitrogen injection at various locations

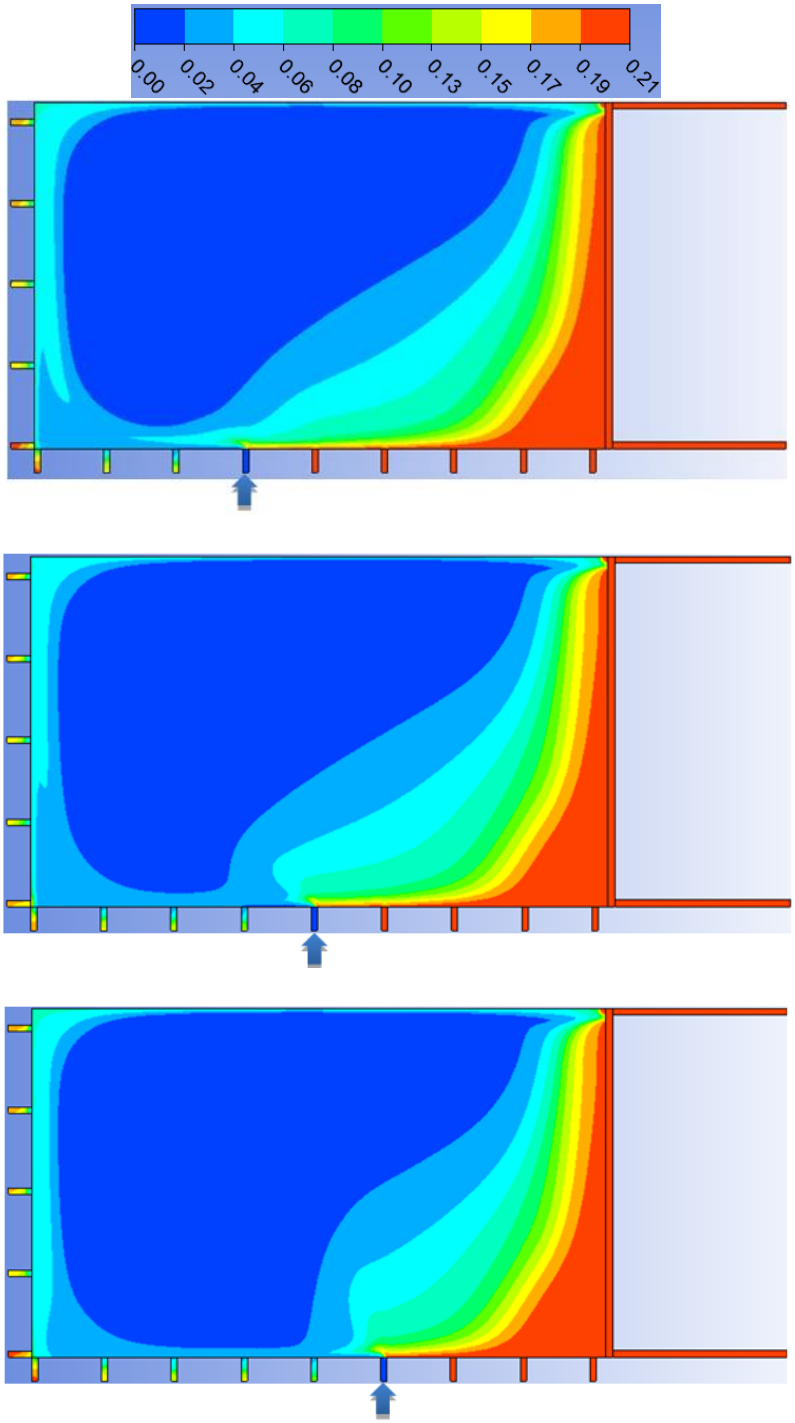

Figure 5.24 Oxygen level in coal layer with quarter capacity nitrogen injection at various locations

5.7.3 Reactive inertisation plan

5.7.3.1 Nitrogen injection behind one seal

There is one possibility that initially proactive inertisation practice is not performed, a heating is developed in start-up area after a period of mining. To suppress the on-going heating development, a reactive inertisation plan is required. To investigate

such a scenario, it is assumed the heating is detected on day 15 and inertisation behind one seal with full capacity nitrogen injection (488m^3/h) immediately commences. From the proactive inertisation plan (Figure 5.22), it is known nitrogen injection behind seal C, D or E has the best inertisation effect. It is also considered it may take longer for nitrogen injection behind seal D and E to disperse to the location where heating is most likely to be developed. Therefore seal C is likely to be the best location for single nitrogen injection spot. Figure 5.25illustrates oxygen level in coal mass after different periods of nitrogen injection behind seal C. It can be observed it needs about nine days for nitrogen to fully disperse to heating area. Figure 5.26 compares temperature fields without and with inertisation on day 20, 25, and 30. It can be seen the heating can be well suppressed in start-up area with the proposed reactive inertisation plan. Figure 5.27 provides a detailed view of cooling effects of inertisation for an extended period. It is assumed temperature of generated nitrogen is 300K. It can be seen the temperature is brought down very slowly though due to very low velocity of nitrogen flow.

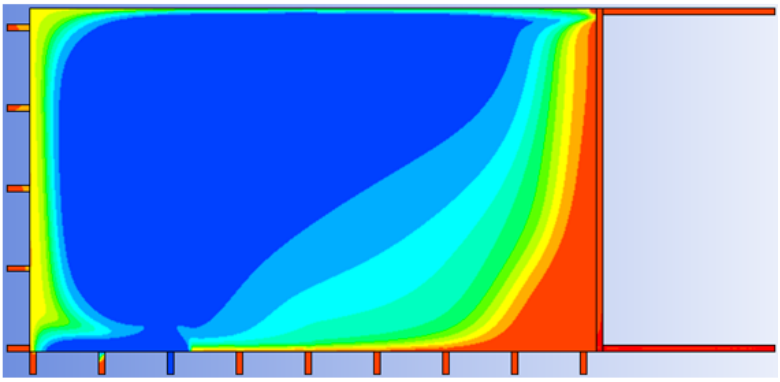

Day 16

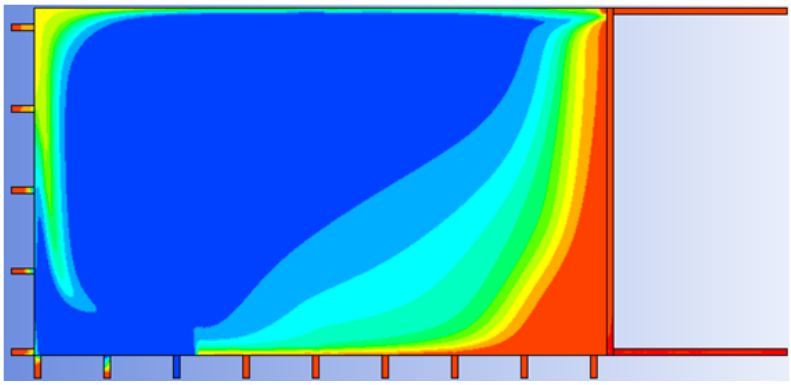

Day 18

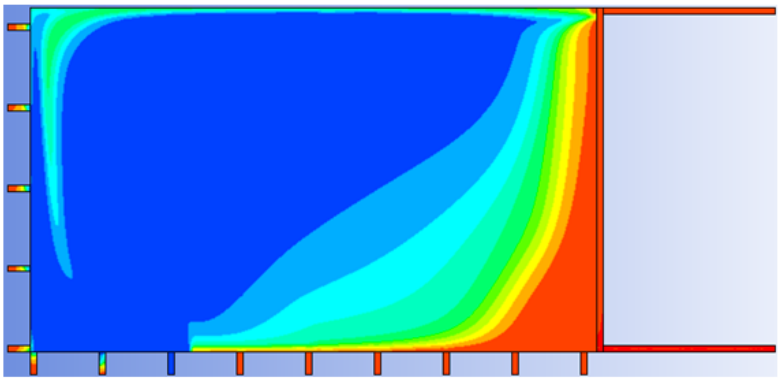

Day 20

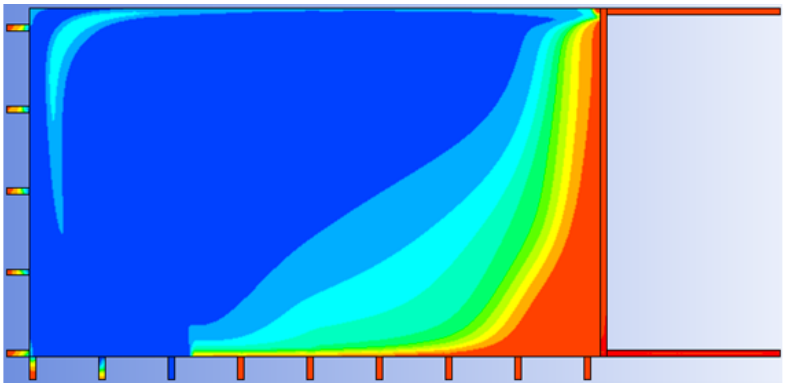

Day 22

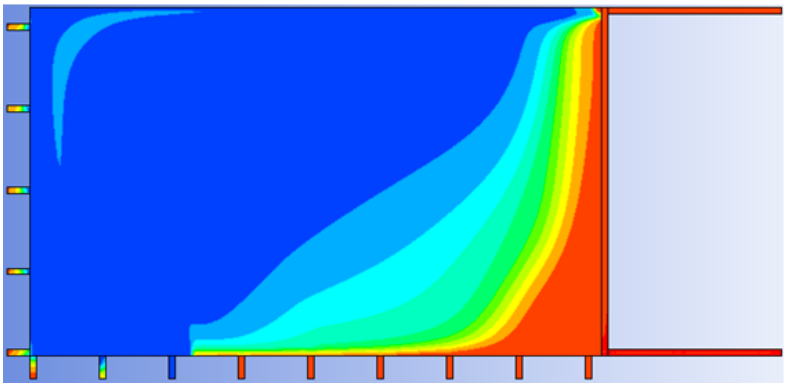

Day 24

Figure 5.25 Oxygen level in coal layer with nitrogen injection behind seal Cafter different periods

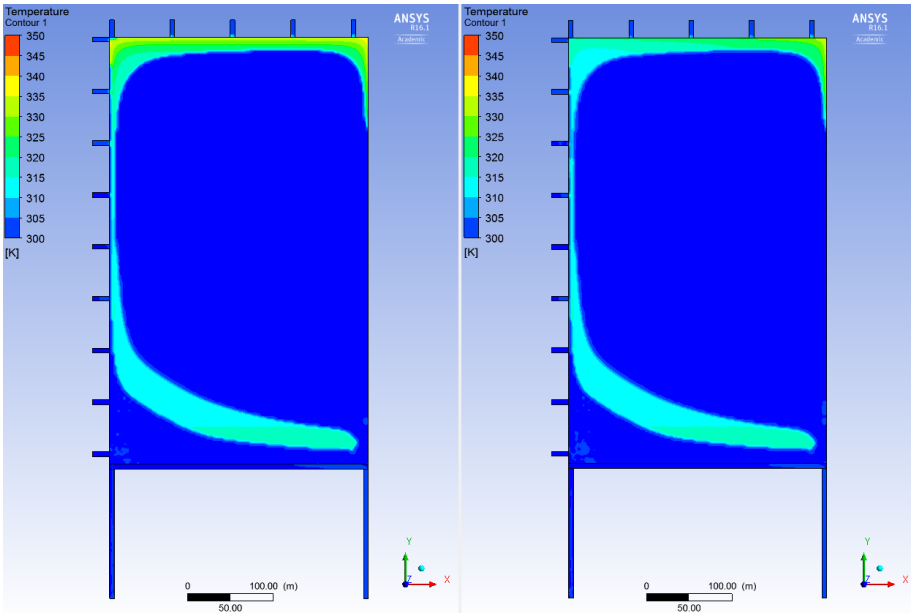
Temperature
Contour 1
350
345
340
335
330
325
320
315
310
305
300
[K]
ANSYS
R16.1
Academic
0
100.00 (m)
50.00
Y
Z
X

Day 20

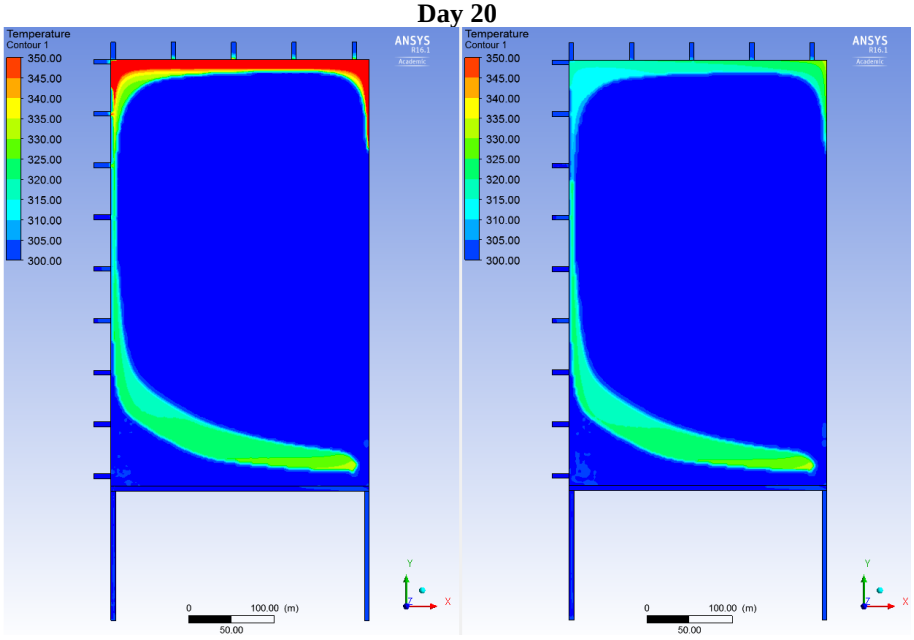
Temperature
Contour 1
350.00
345.00
340.00
335.00
330.00
325.00
320.00
315.00
310.00
305.00
300.00
ANSYS
R16.1
Academic
0
100.00 (m)
50.00
Y
Z
X

Day 25

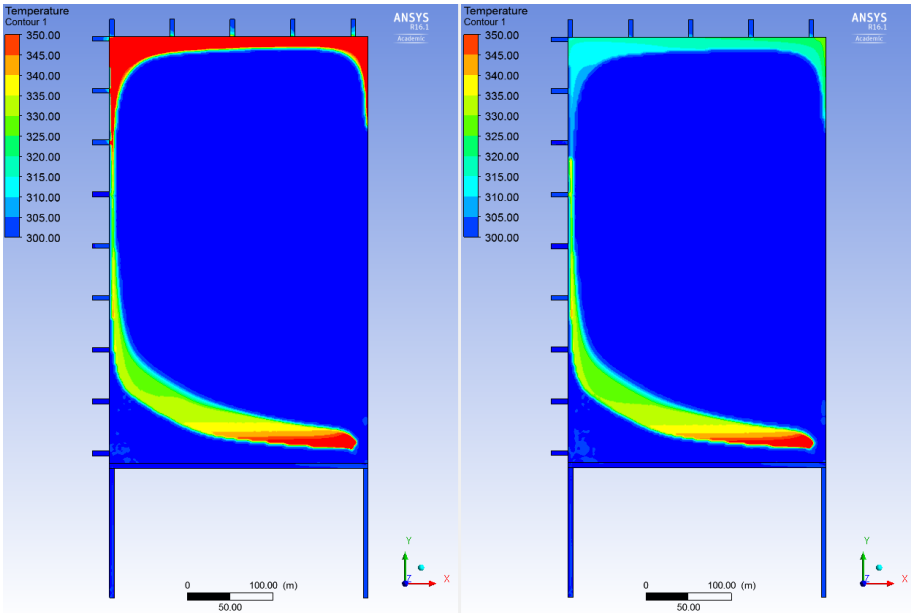

Day 30

Figure 5.26 Comparison of heating evolution without and with nitrogen injection behind seal C

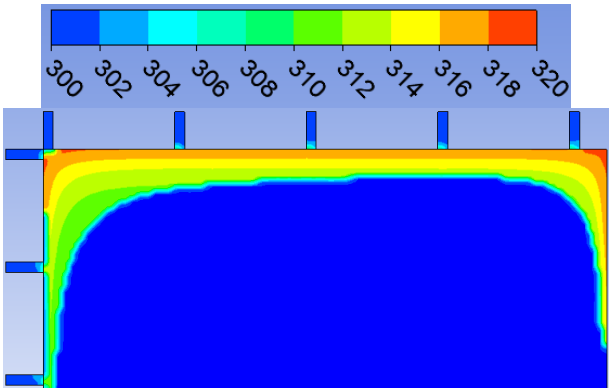

Day 15

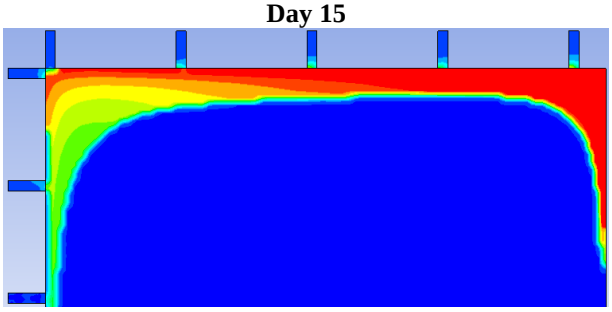

Day 20

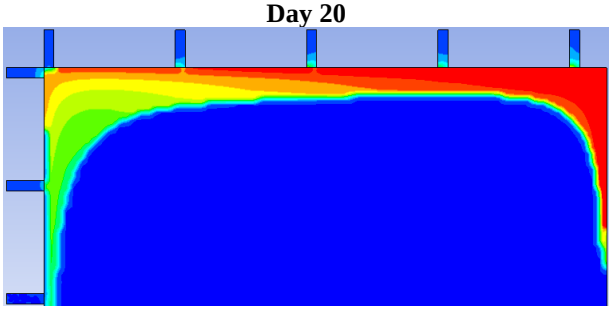

Day 25

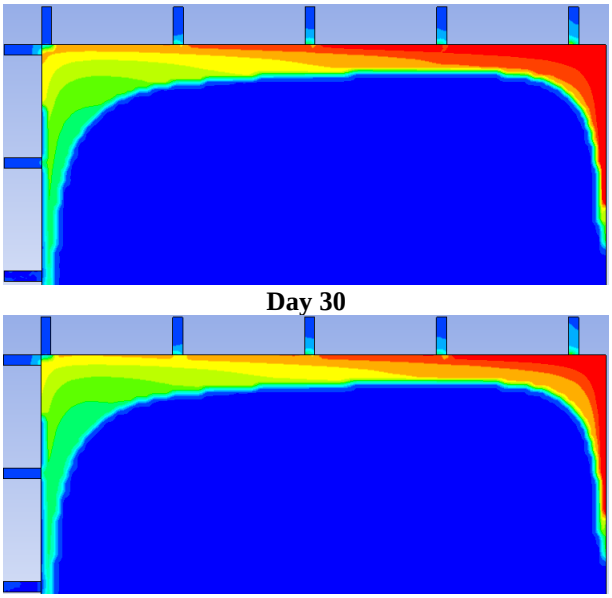

Day 30

Day 35

Figure 5.27 Cooling effect of nitrogen injection behind seal C after an exteded period

5.7.3.2 Nitrogen injection behind two seals

It has been investigated reactive inertisation operation behind one seal is effective but very slowly. To suppress the heating more effectively, the two nitrogen generators are mobilised and nitrogen is injected behind two seals. Nitrogen injection behind seal C is maintained to dilute incoming oxygen rich gas mixture and another nitrogen injection behind seal c is commenced to directly suppress heating. Figure 5.28 illustrates oxygen level in coal mass after different periods of nitrogen injection behind seals C and c. It can be observed it needs only five days for nitrogen to fully disperse to heating area. Figure 5.29 compares temperature fields without and with inertisation on day 20, 25, and 30. It is obvious that the heating can be well suppressed in start-up area with inertisation behind the two seals. Figure 5.30provides a detailed view of cooling effects of inertisation behind two seals for an extended period. It can be seen the temperature is brought down more effectively than nitrogen injection from merely one seal.

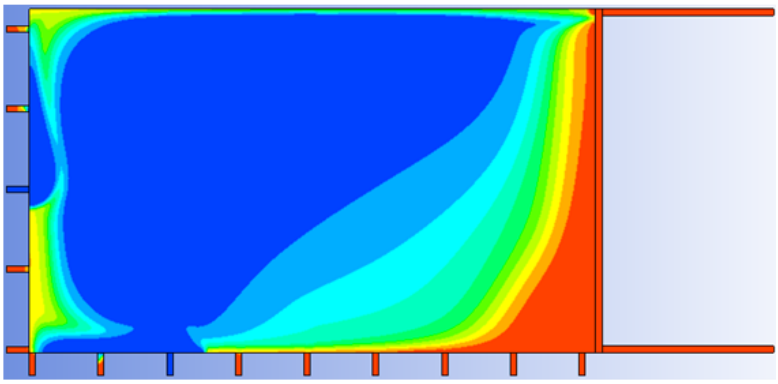

Day 16

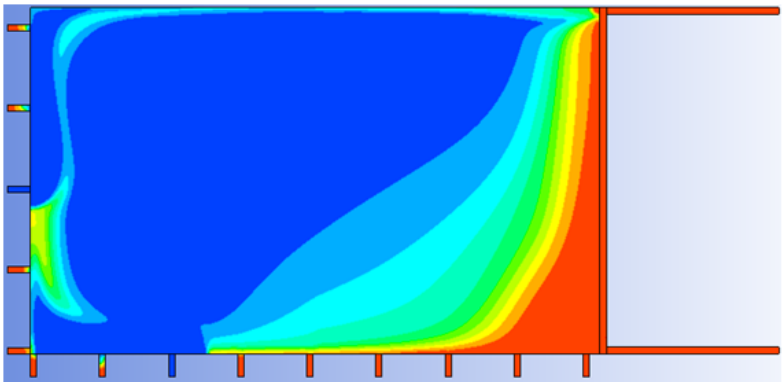

Day 17

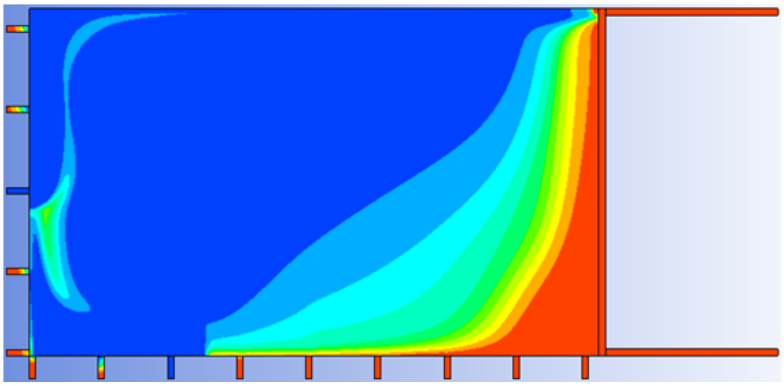

Day 18

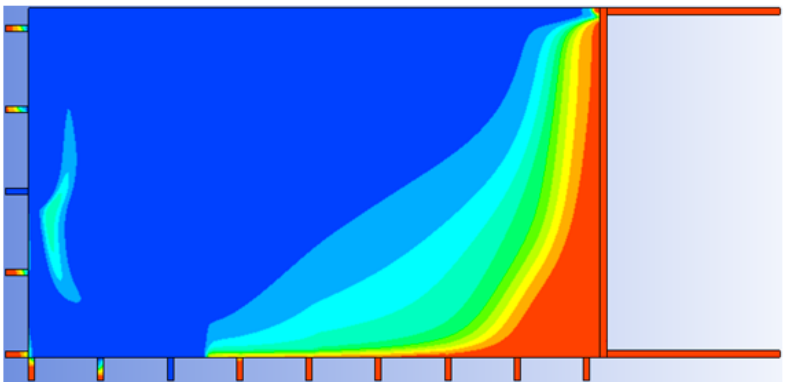

Day 19

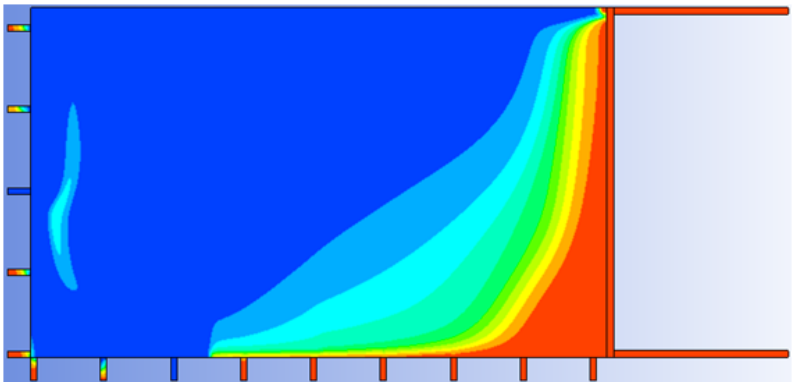

Day 20

Figure 5.28 Oxygen level in coal layer with nitrogen injection behind seals Cand c after different periods

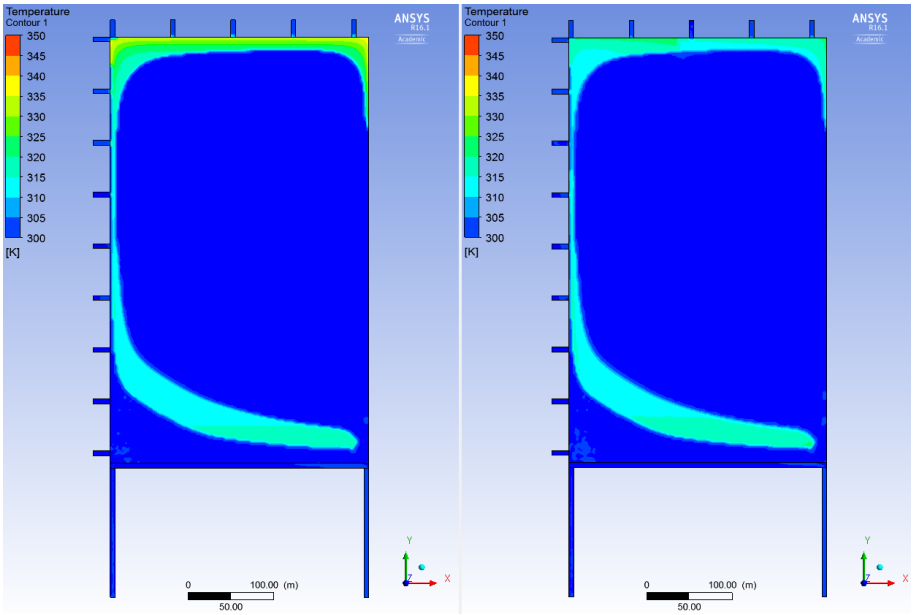

Day 20

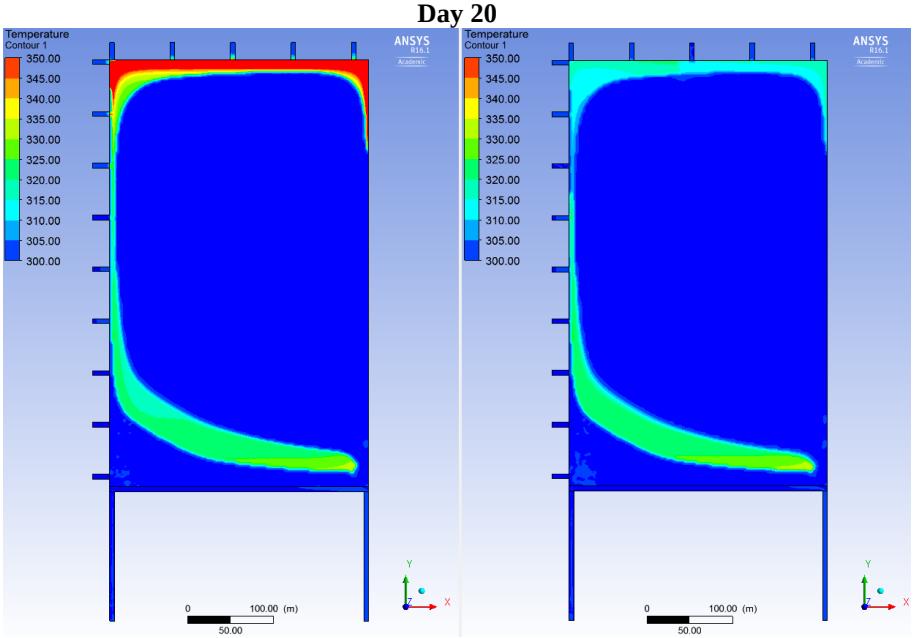

Day 25

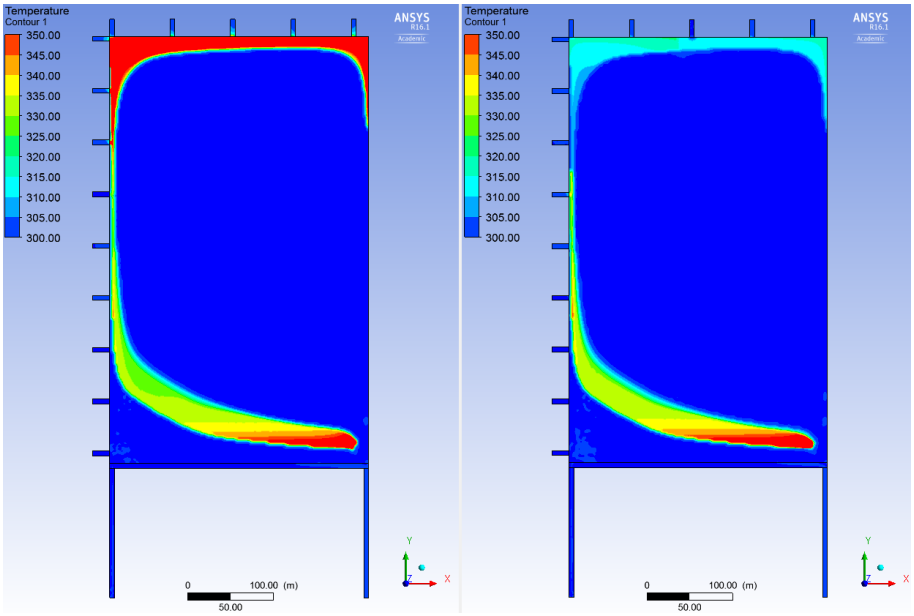

Day 30

Figure 5.29 Comparison of heating evolution without and with nitrogen injection behind seals C and c

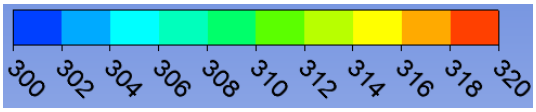

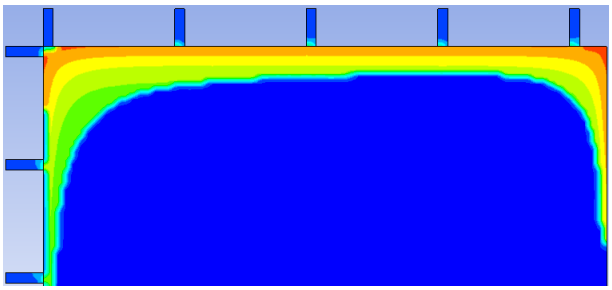

Day 15

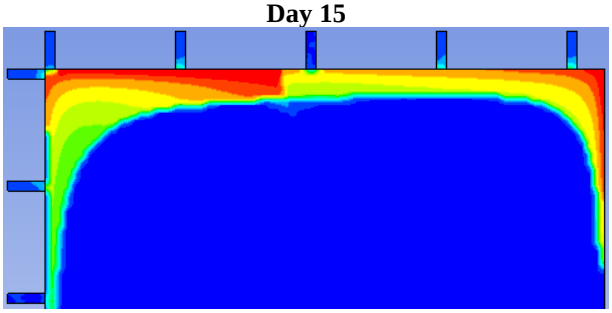

Day 20

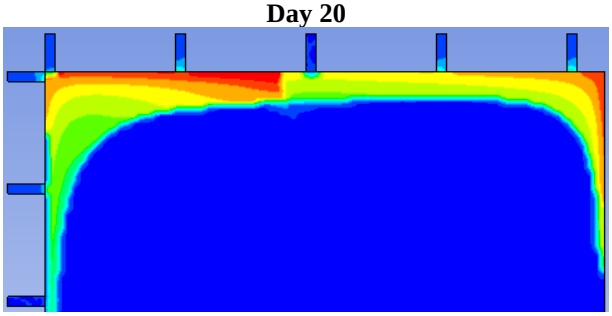

Day 25

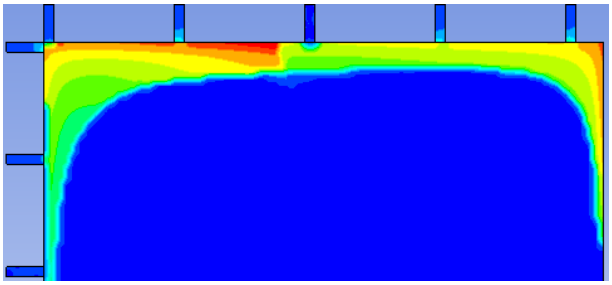

Day 30

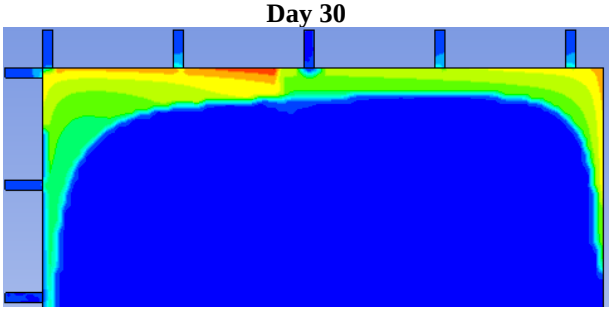

Day 35

Figure 5.30 Cooling effect of nitrogen injection behind seals C and c after an extended period

5.8 1000m model with air leakage from mining induced cracks

In Chapter three it has been discussed in many details that air leakage into goaf is a major contributor to heating occurrence in goaf. Besides regular air leakage from normal ventilation behind longwall face, some other abnormal sources of air leakage are illustrated in Figure 5.31. The abnormal air leakage may come from three sources: (1) adjacent goaf; (2) poorly constructed seals; and (3) mining induced cracks. Gas leakage from adjacent goaf is mainly composed of high nitrogen level gas mixture and therefore such leakage is unlikely to promote heating development but may cause presence of low oxygen gas in longwall face and high CO concentration at return corner. The second source of air leakage is from seals around goaf but the quantity of such leakage can be very small if seals are constructed in good quality. Utilisation of pressure balancing chamber or positive pressure nitrogen chamber can also minimise or even eliminate air leakage across seals. It has been also investigated fresh air is likely to flow into goaf through mining induced cracks because the cracks develop to surface due to large extraction height and shallow cover. The cracks fall into groups: (1) dynamic cracks periodically develop and are closed with advance of longwall face; (2) edge cracks develop around goaf perimeter and are not able to be closed. Therefore fresh air is mostly leaked from edge cracks. Total air leakage can be calculated by difference of airflow quantity between intake and return. It is monitored 63m^3/min (2495m^3/min at intake and 2558m^3/min at return)is leaked into

goaf when LW22307 advance about 1000m. It is assumed air is all leaked from edge cracks. To mimic such a situation, a narrow slot (1m wide) is made on top of goaf and such quantity of fresh air is allowed to travel through the slot.

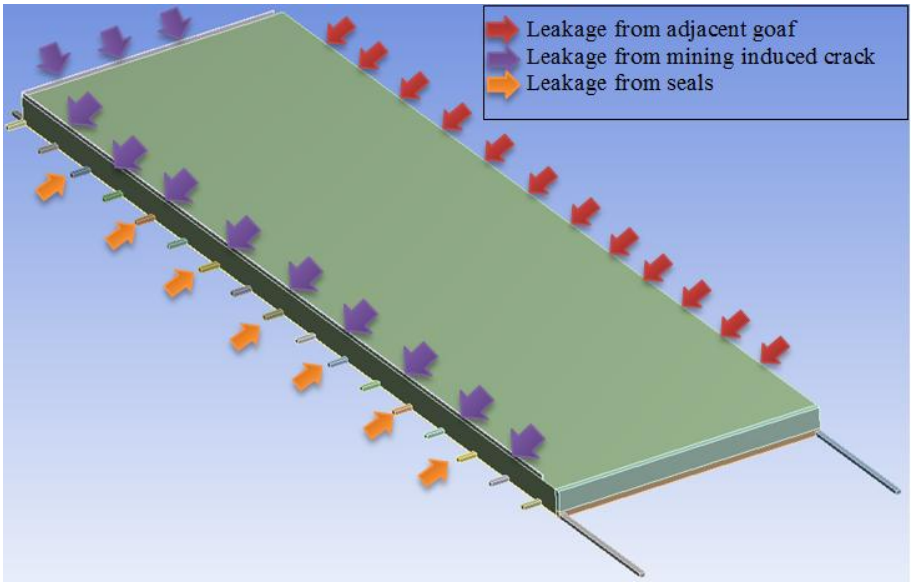

Figure 5.31 A shematic view of abnormal sources of air leakage into goaf

5.8.1 Model results

Figure 5.32 and Figure 5.33 show velocity distribution and oxygen level contour of the 1000m model with leakage from edge cracks, respectively. Due to leakage of fresh airflow, oxygen rich gas mixture is able to be present in start-up area. It is therefore postulated heating may develop in such a zone. Figure 5.34 and Figure 5.35providetransient temperature field and CO evolution after different periods, respectively. It can be seen heating is developed in start-up area as expected and the heating evolves even quickly than heating behind longwall face. High level of CO is also liberated in a less confined zone than that of heating.

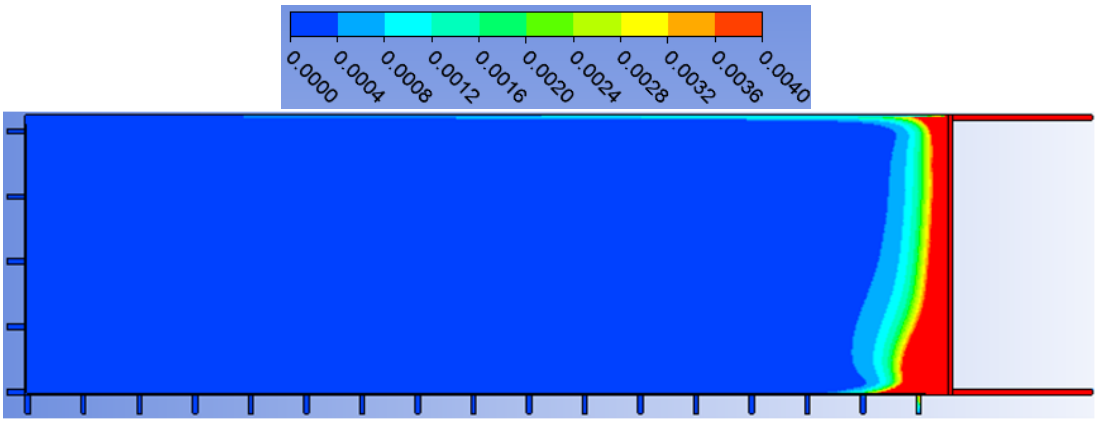

Figure 5.32 Velocity (m/s) contour of 1000m model with leakage from edge cracks

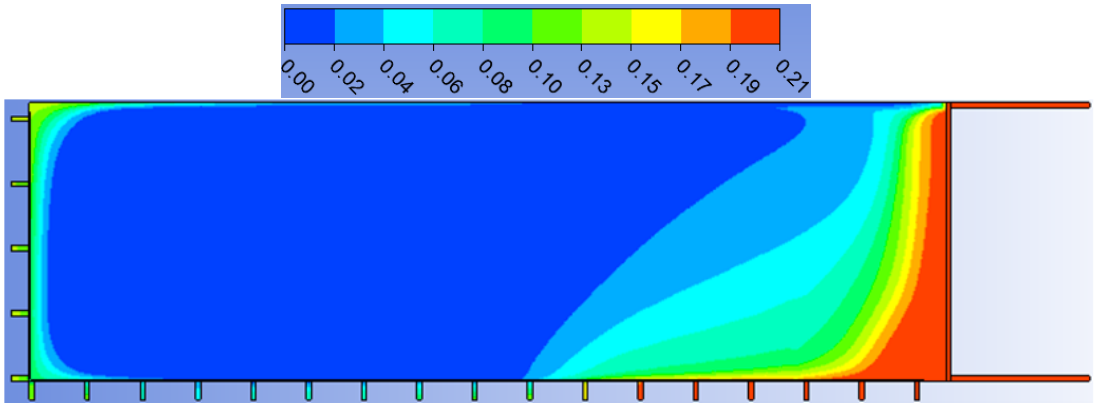

Figure 5.33 Oxygen (%) contour of 1000m model with leakage from edge cracks

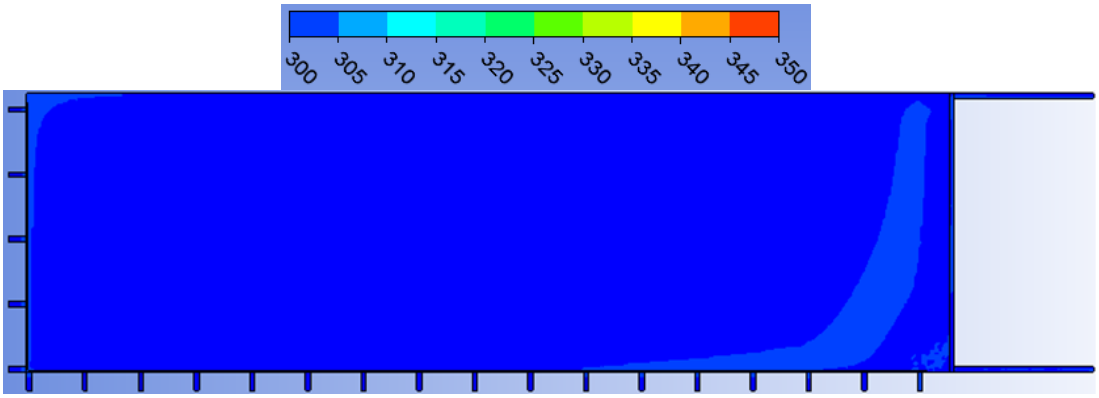

(a) Day 5

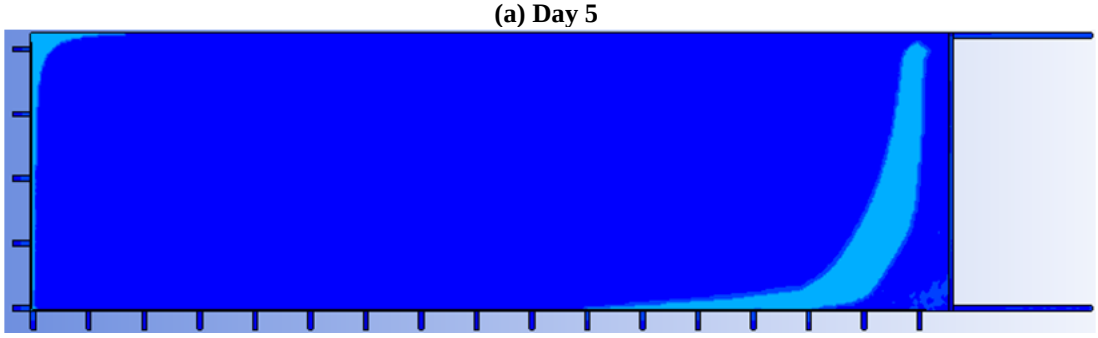

(b) Day 10

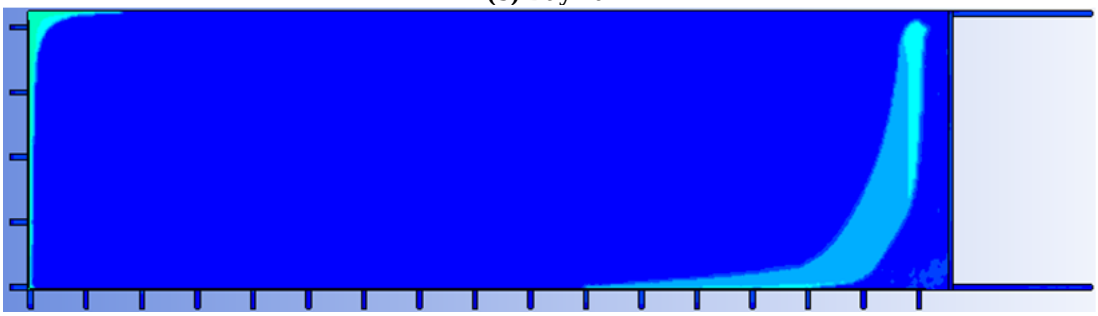

(c) Day 15

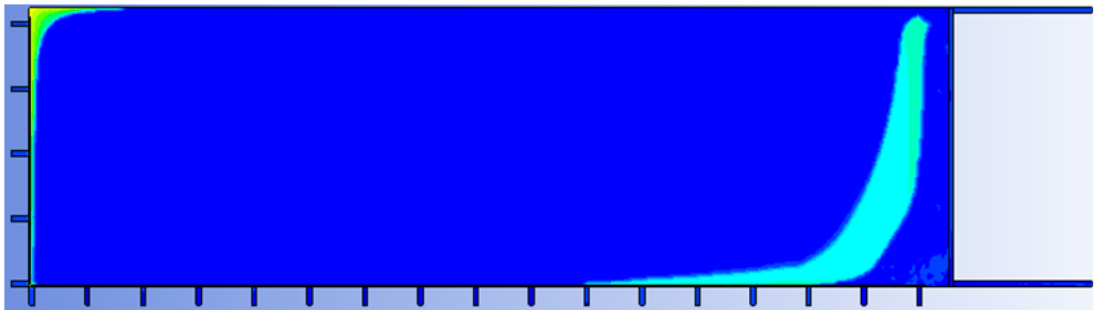

(d) Day 20

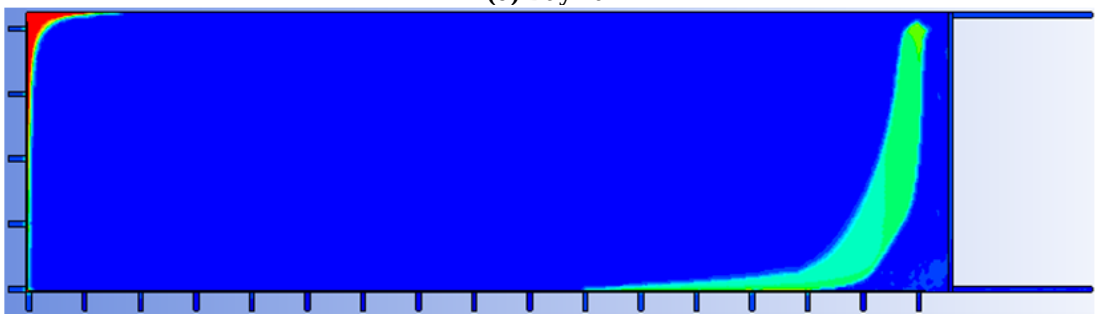

(e) Day 25

Figure 5.34 Temperature (K) contour against time of 1000m model with leakage from edge cracks

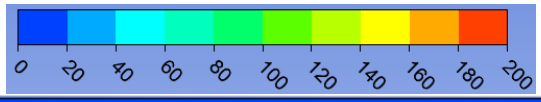

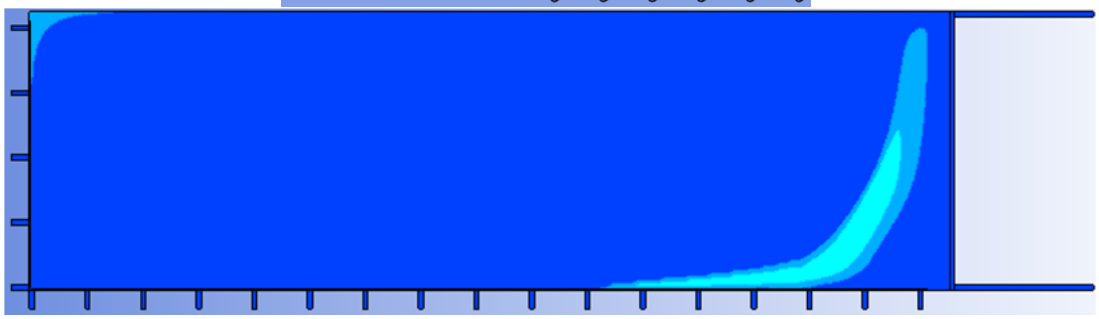

(a) Day 5

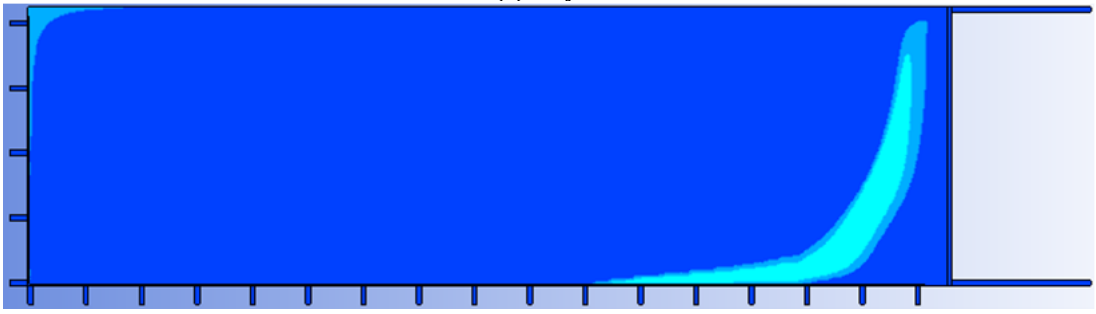

(b) Day 10

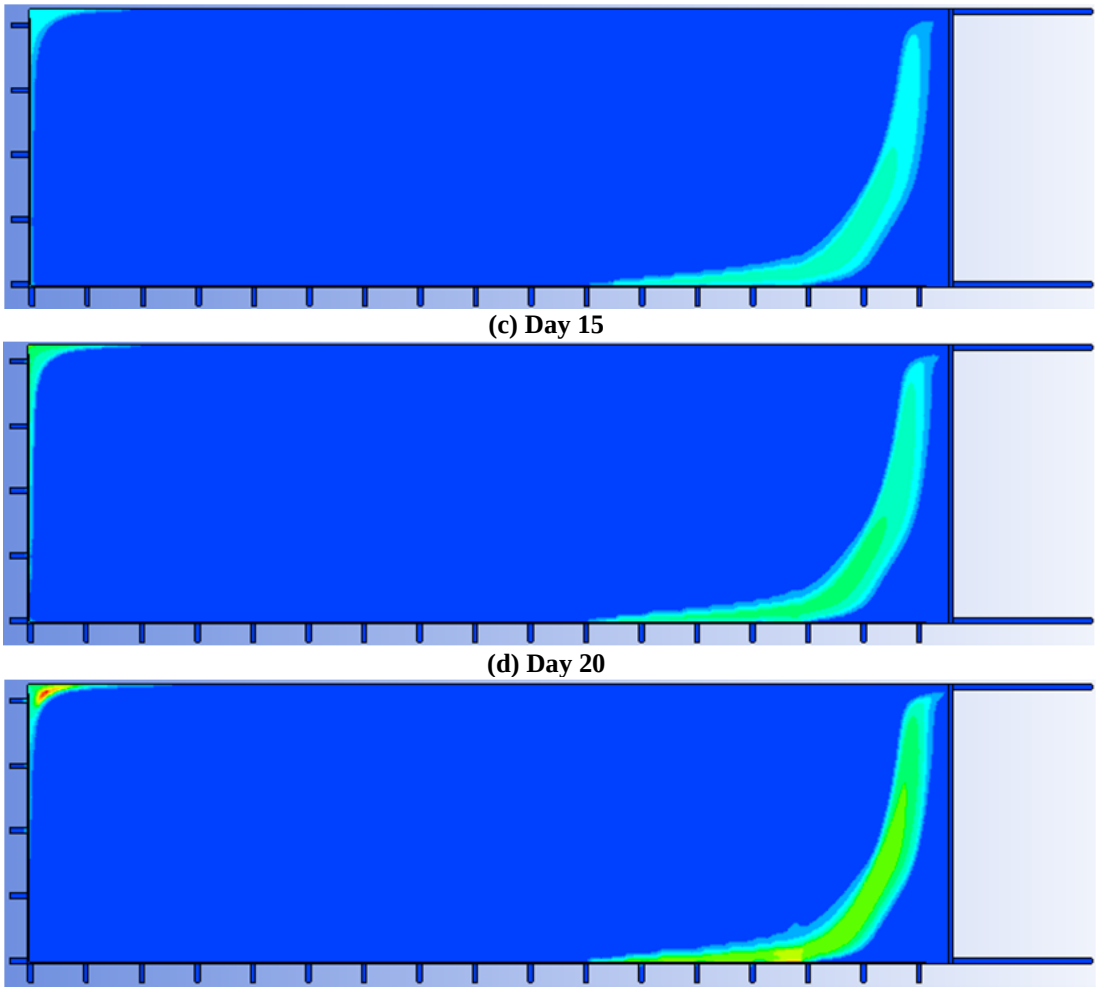

(c) Day 15

(d) Day 20

(e) Day 25

Figure 5.35 CO (ppm) evolution against time of the 1000m model with leakage from edge cracks

Figure 5.36 shows profile of the maximum temperature and CO make with time of the 1000m model with air leakage from edge cracks. The incubation is about 25 days and trend of CO make is inconsistent with that of temperature rising within high temperature range. The CO make shows no rapid increase while the maximum temperature shot up beyond 20 days. In this model, CO make is not able to correctly indicate the severity of the heating probably because high level CO is generated at a very confined zone. The classification of CO make level should be adjusted under such a circumstance. As heating is developed in start-up area and the heating is unlikely to be suffocated with advance of longwall face, a proactive inertisation plan is required with air leakage from edge cracks.

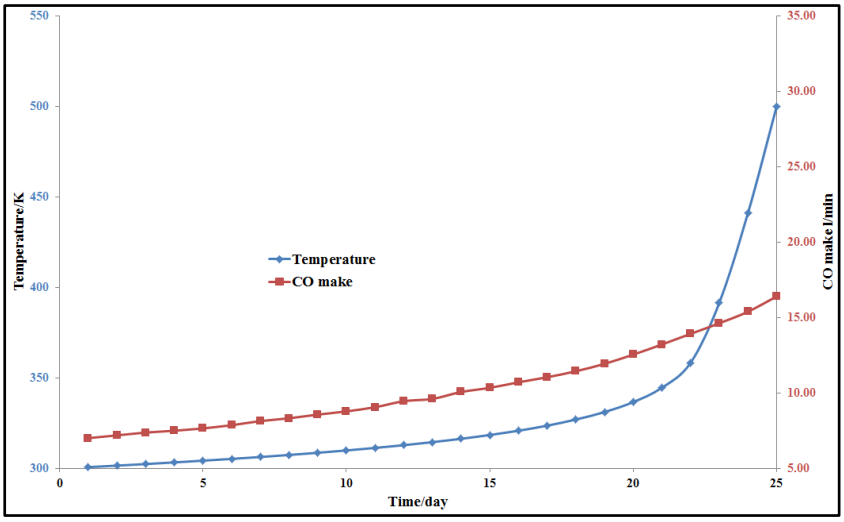

Figure 5.36 Trend of maximum temperature and CO make of 1000m model with leakage from edge cracks

5.8.2 Proactive inertisation plan

Figure 5.37illustrates inertisation effects of one nitrogen generator running in full capacity (488m^3/h) and nitrogen injection behind different seals. It is found nitrogen injection behind seal a, b, c, or d is able to exclude oxygen rich gas from start-up area. Figure 5.38shows inertisation effects with half capacity (244m^3/h) injection quantity behind seal a, b, c, and d. It can be found the half quantity nitrogen injection is still able to have good inertisation effects. Figure 5.39shows inertisation effects with quarter capacity (122m^3/h) injection quantity behind the four seals. It can be seen such low quantity nitrogen injection behind seal a, b, or c is still able to prevent heating evolution in start-up area. Therefore a proactive inertisation plan for air leakage from edge cracks is nitrogen injection behind seal a, b, or c with at least 122m^3/h flow rate. During the inertisation operation other seals must be erected in good quality to avoid undesirable nitrogen dispersion from these seals.

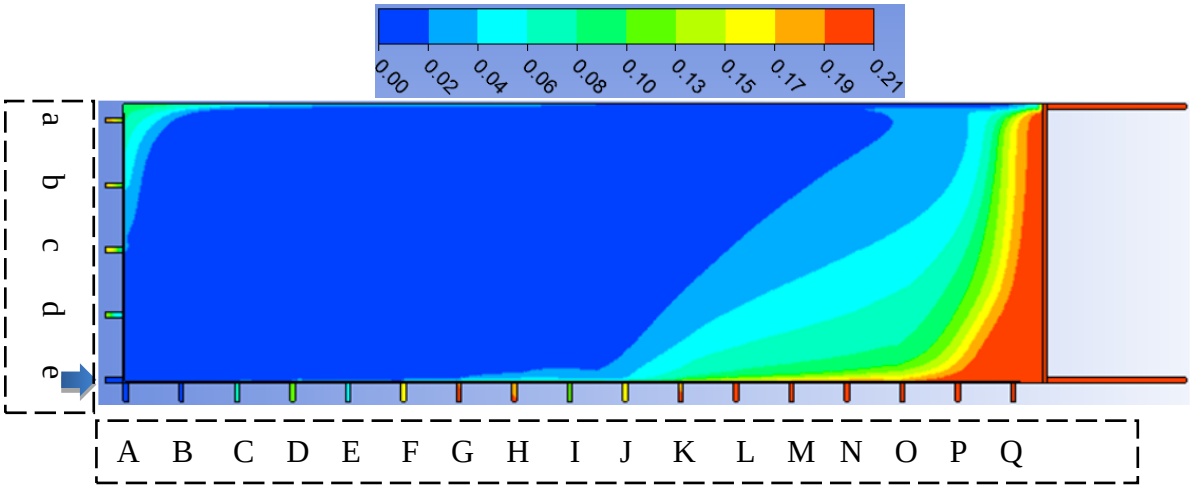

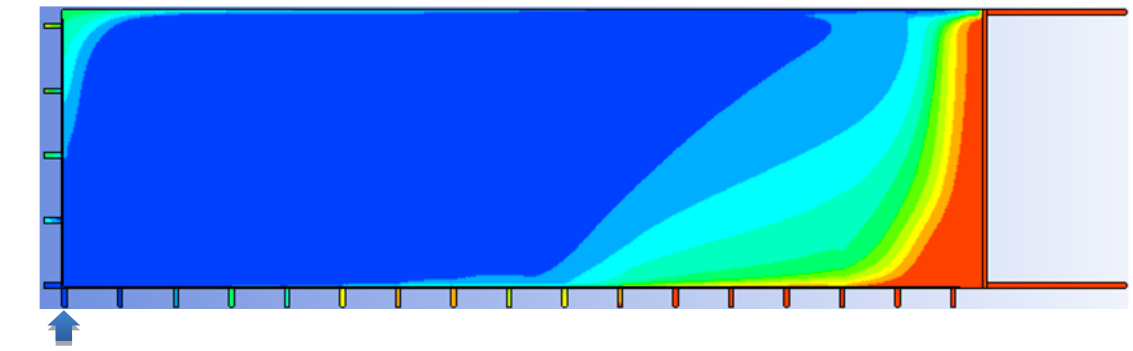

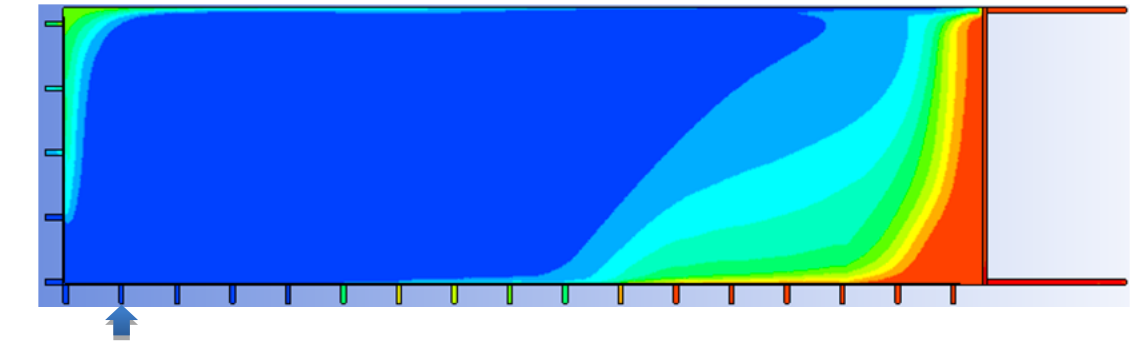

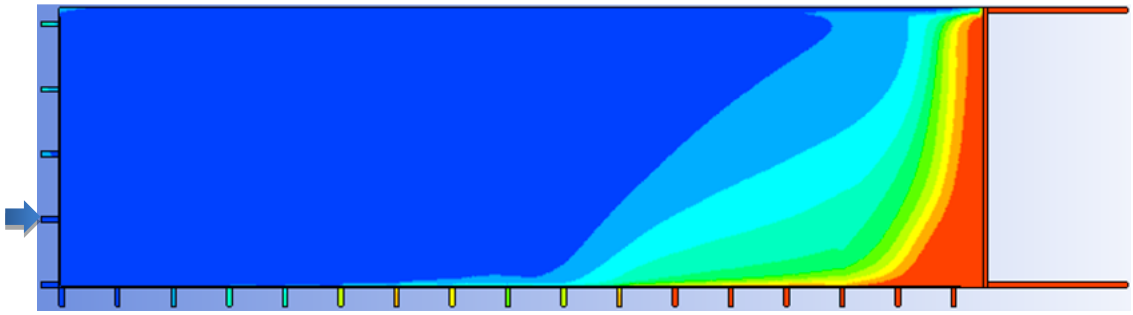

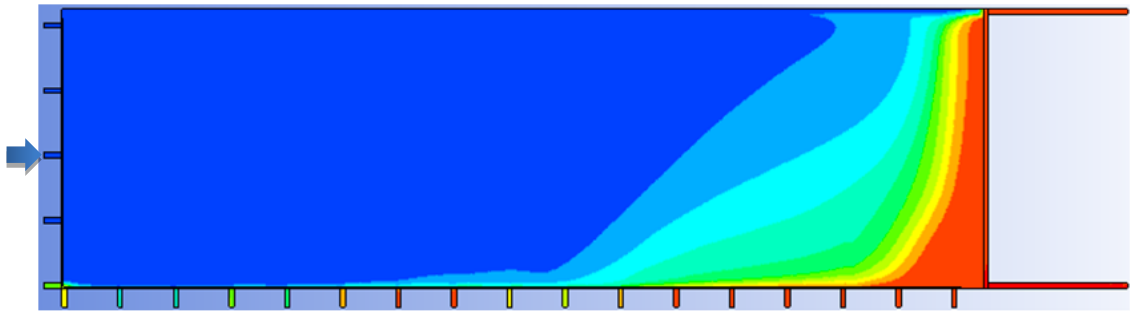

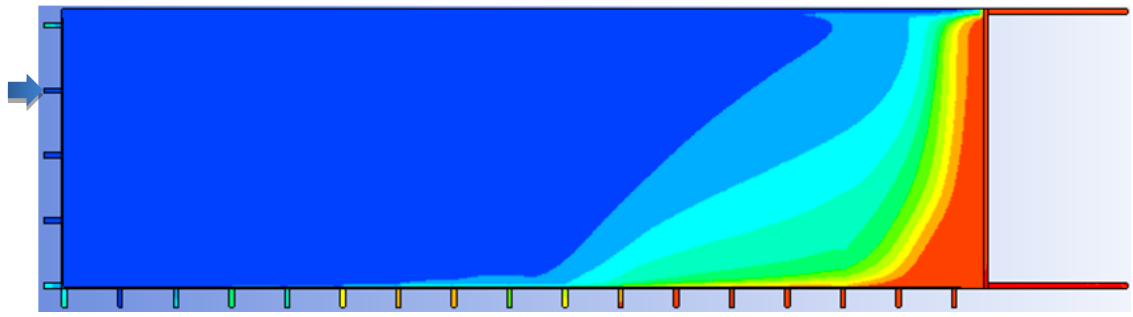

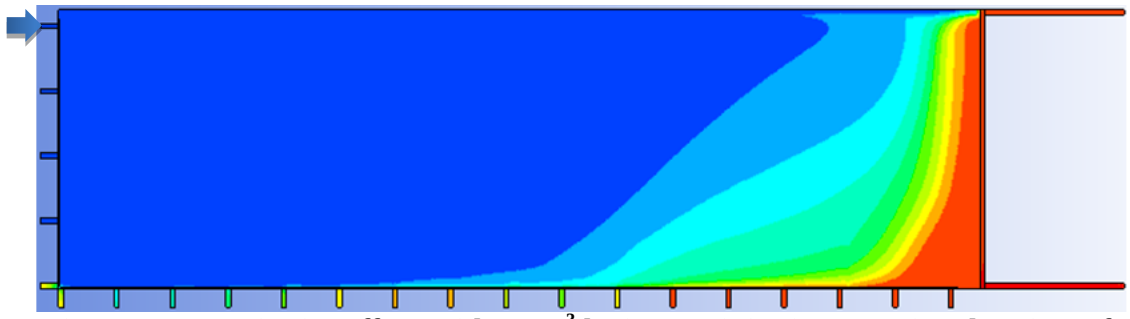

Figure 5.37 Inertisation effects with 488m^3/h nitrogen injection at various locations of 1000m model with air leakage from edge cracks

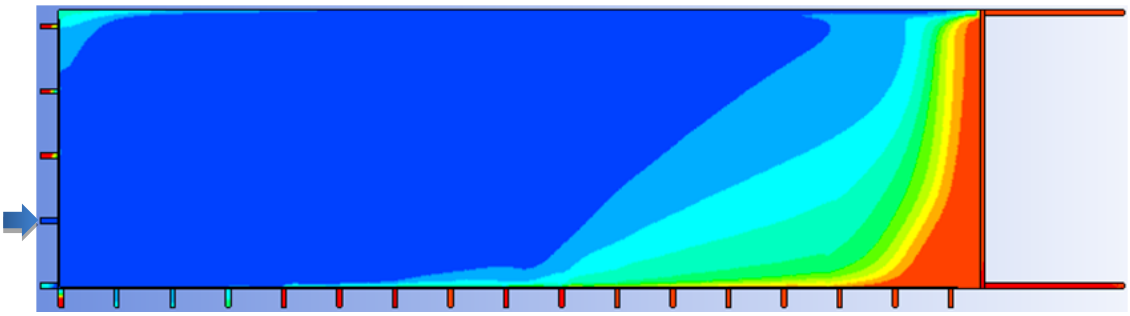

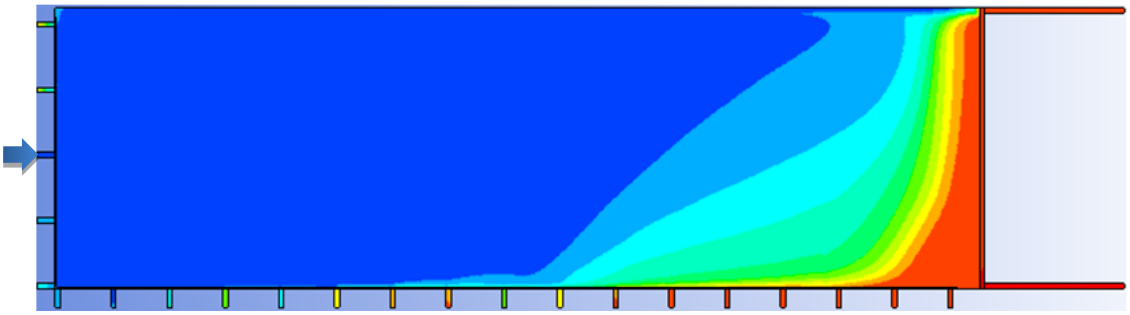

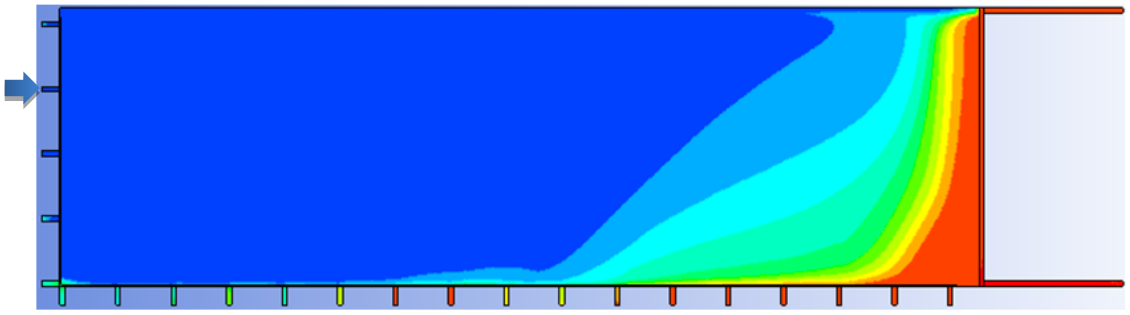

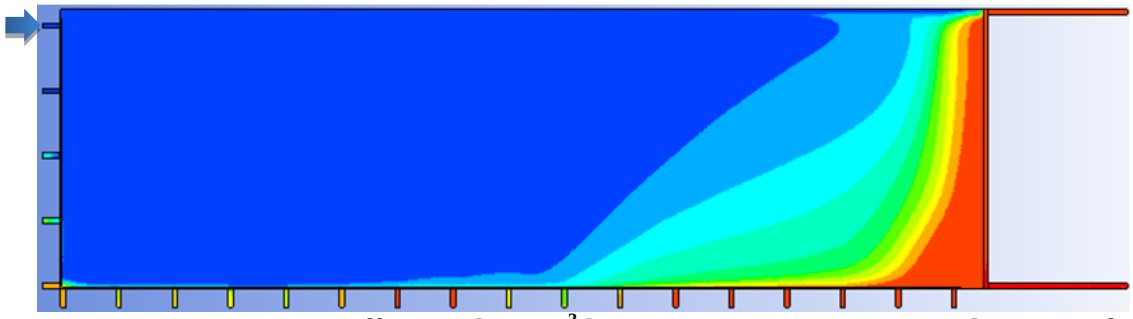

Figure 5.38 Inertisation effects with 244m^3/h nitrogen injection at various locations of 1000m model with air leakage from edge cracks

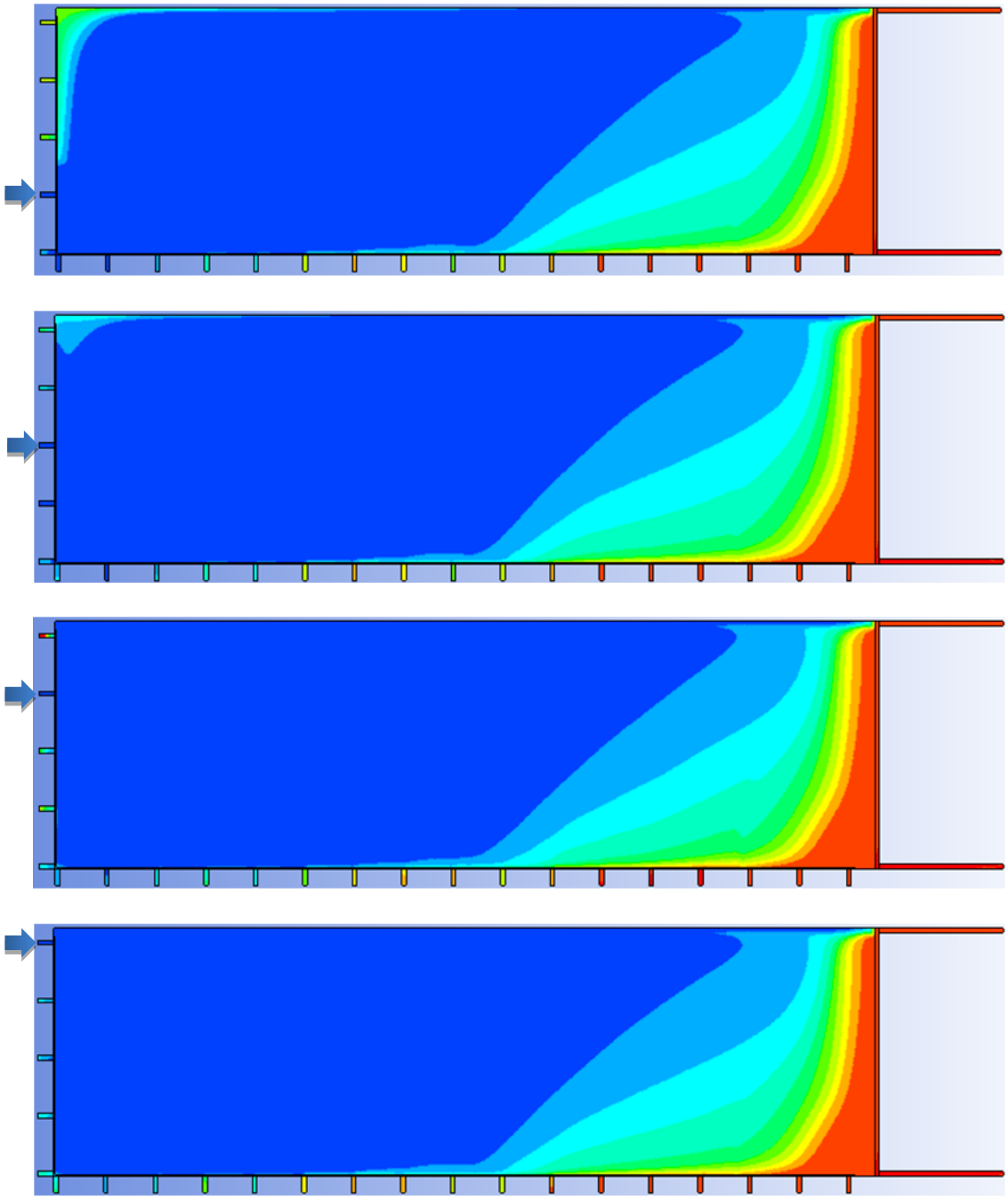

Figure 5.39 Inertisation effects with 122m^3/h nitrogen injection at various locations of 1000m model with air leakage from edge cracks

5.8.3 Reactive inertisation plan

5.8.3.1 Nitrogen injection behind one seal

Similar to scenario assumed for 500m model, on day 15 the heating is detected and nitrogen injection behind c is immediately started. Figure 5.40 illustrates dilution of oxygen with nitrogen injection behind seal c after different periods. It takes roughly 10 days to completely exclude high oxygen gas from start-up area. Figure 5.41 provides the heating development with the proposed reactive inertisation plan. It can be seen most of the heating can be suppressed but it fails to bring down the temperature at localised area. Hence higher volume of nitrogen injection or nitrogen injection behind two seals is required.

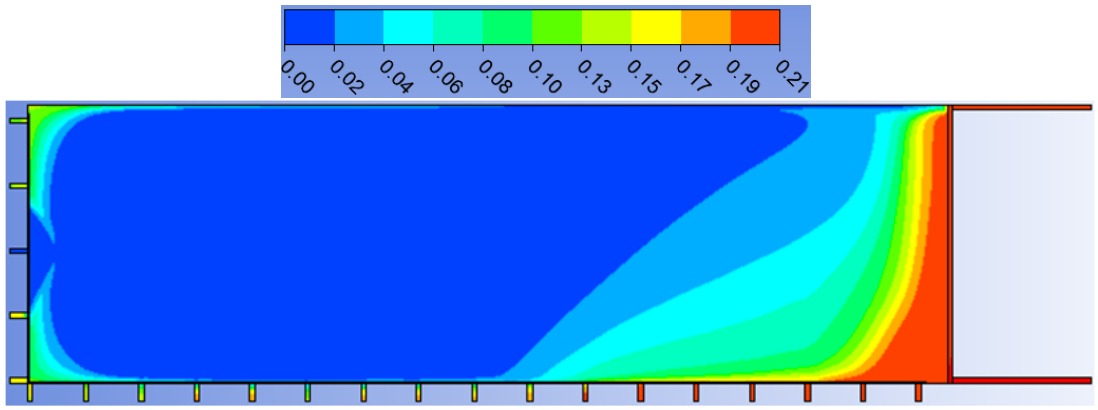

Day 16

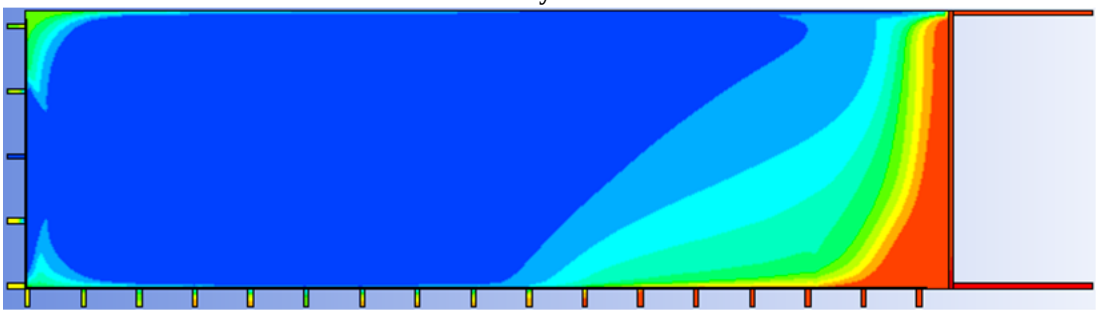

Day 18

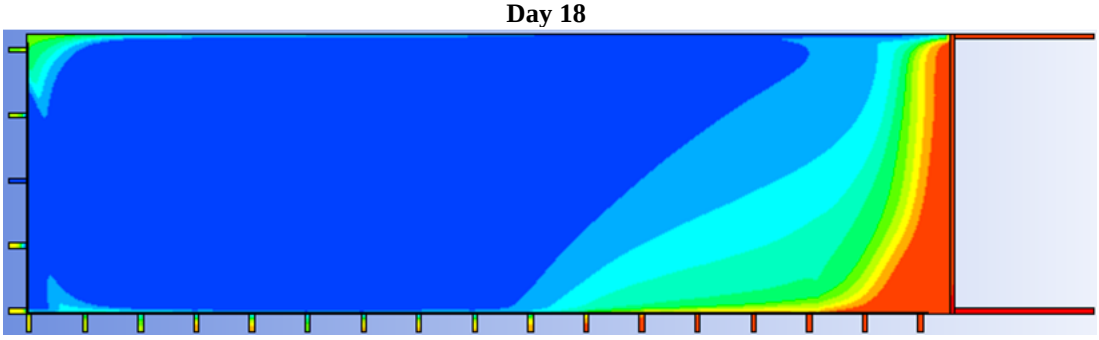

Day 20

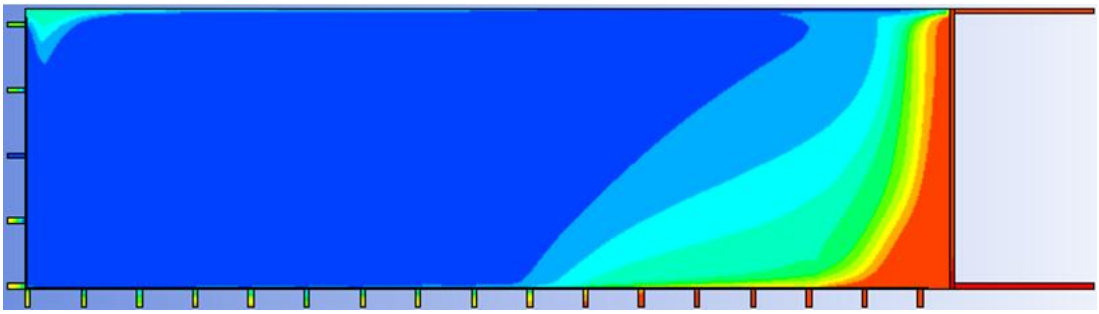

Day 25

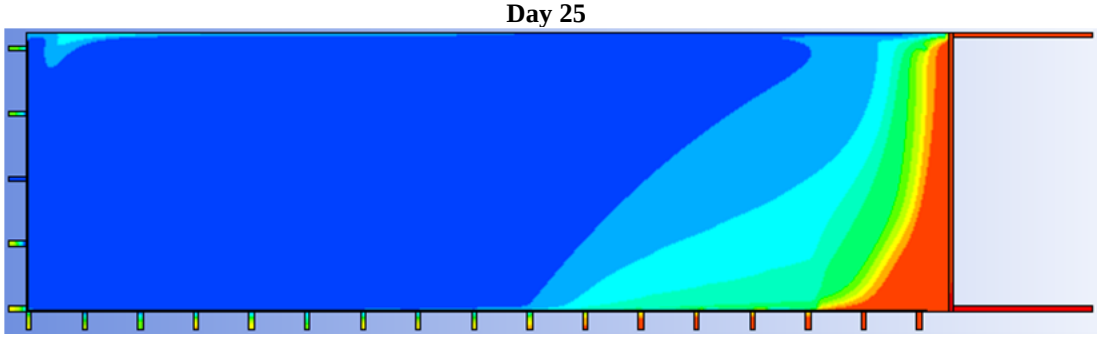

Day 30

Figure 5.40 Oxygen level in coal layer with nitrogen injection behind seal cafter different periods

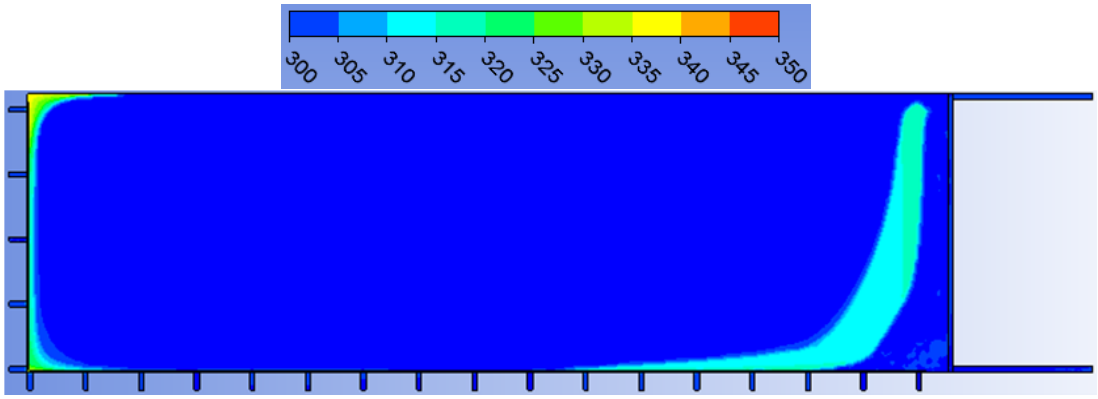

Day 20

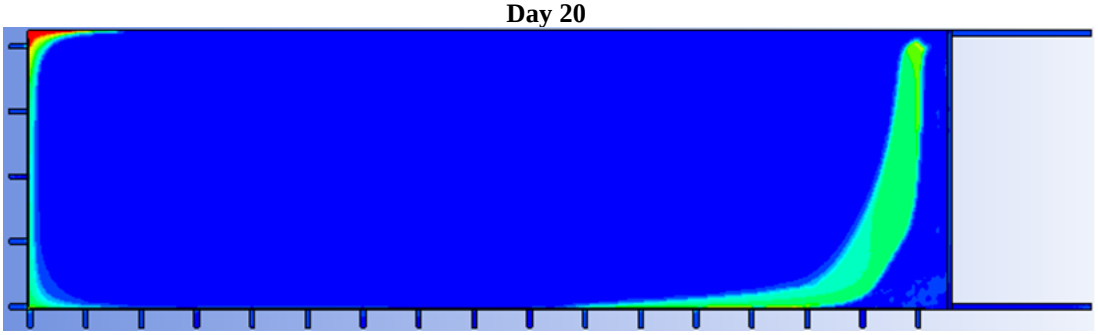

Day 25

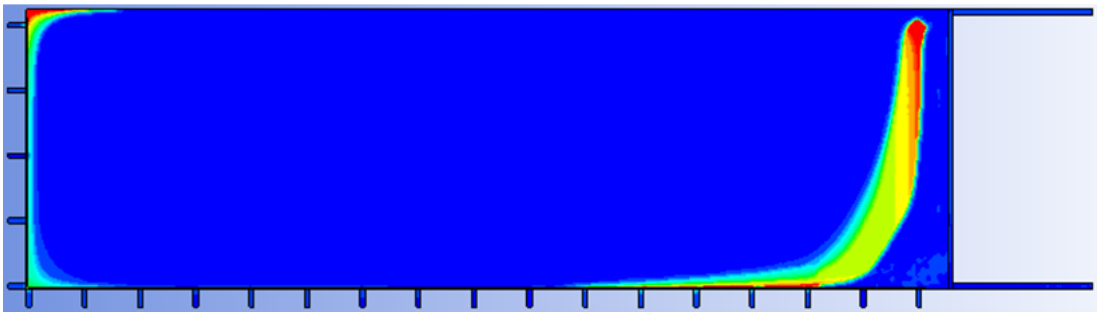

Day 30

Figure 5.41 Temperature distribution in coal layer with nitrogen injection behind seal cafter different periods

5.8.3.2 Nitrogen injection behind two seals

Figure 5.42illustrates dilution of oxygen with nitrogen injection behind seals b and c after different periods. It takes only three days to fully dilute high oxygen gas mixture in start-up area. Figure 5.43provides the heating development with reactive nitrogen injection behind two seals. It can be seen the heating can be totally suppressed and further development of oxidation is stopped. Figure 5.44 shows cooling effect of inertisation for an extended period. It can be seen the temperature can be slowly brought down. Therefore nitrogen injection at least behind two seals is able to completely suppress heating development in start-up area with air leakage from mining induced cracks.

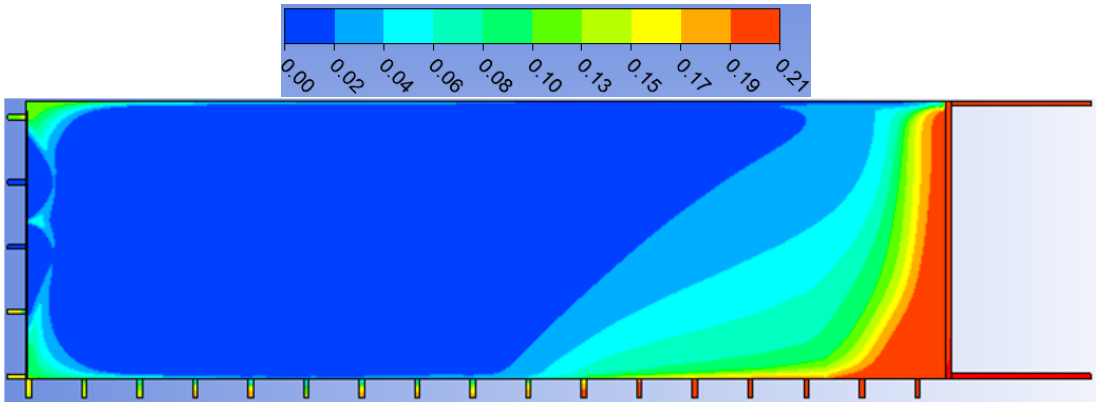

Day 16

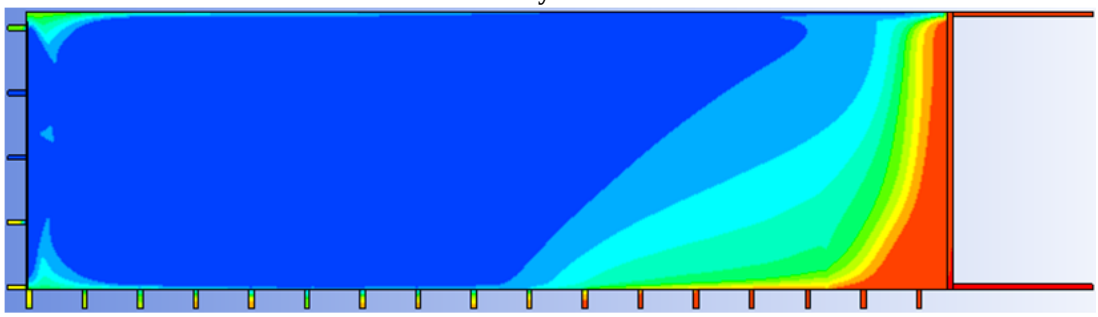

Day 17

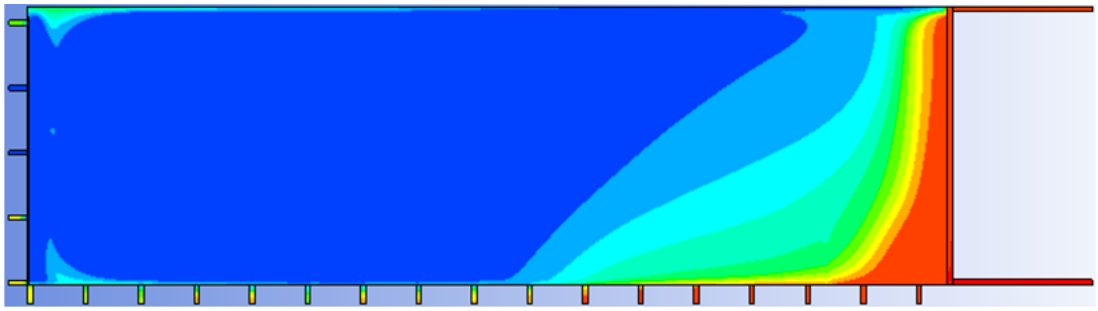

Day 18

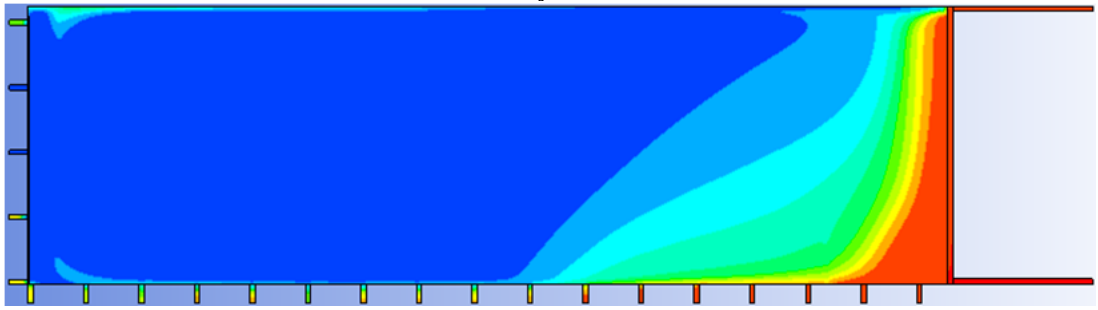

Day 19

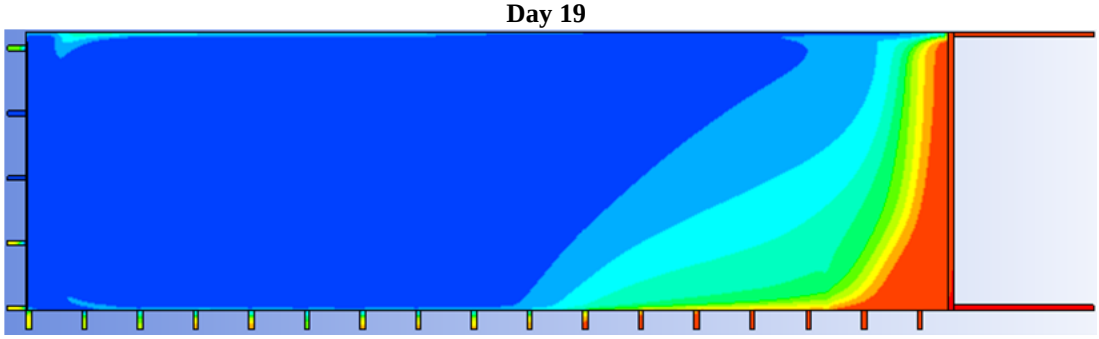

Day 20

Figure 5.42 Oxygen level in coal layer with nitrogen injection behind sealsb and cafter different periods

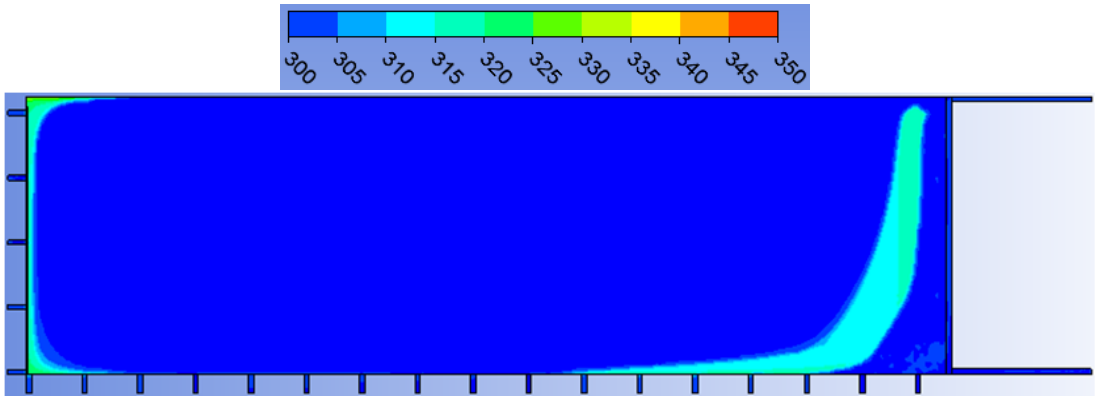

Day 20

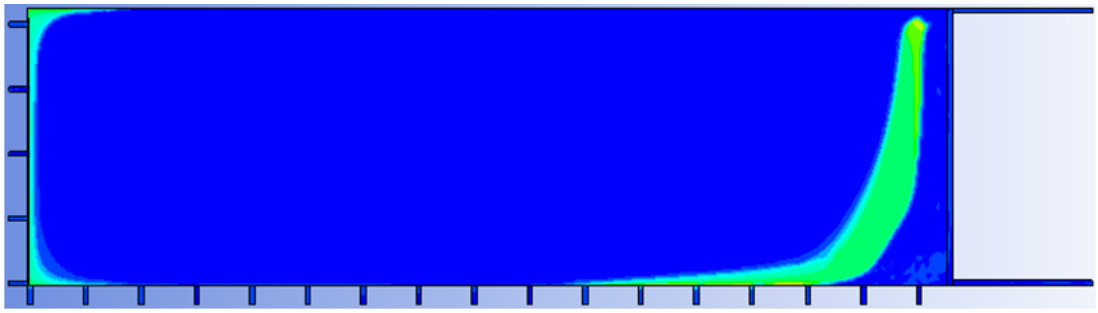

Day 25

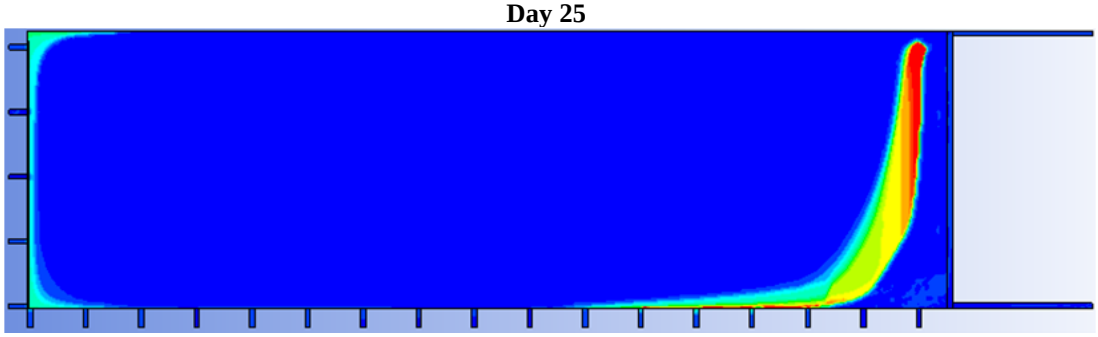

Day 30

Figure 5.43 Temperature distribution in coal layer with nitrogen injection behind seals b and cafter different periods

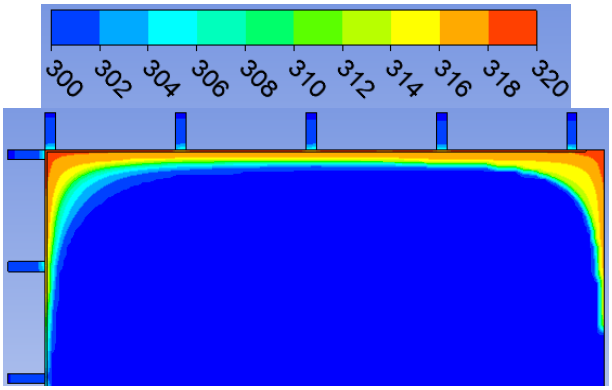

Day 15

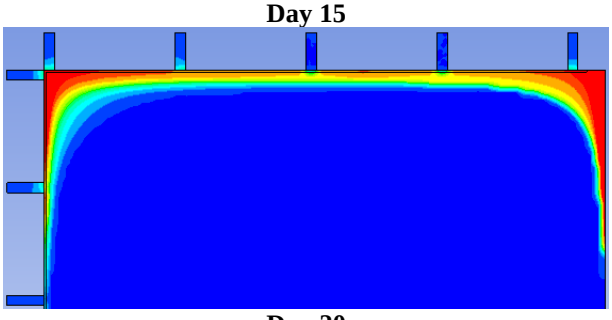

Day 20

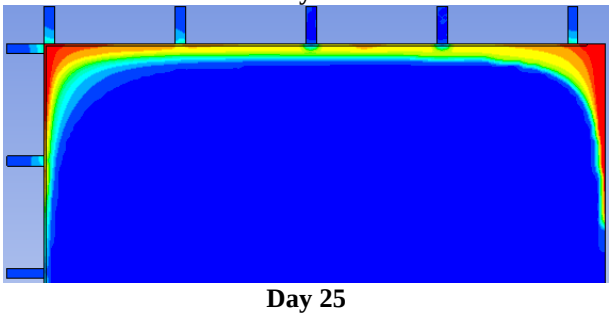

Day 25

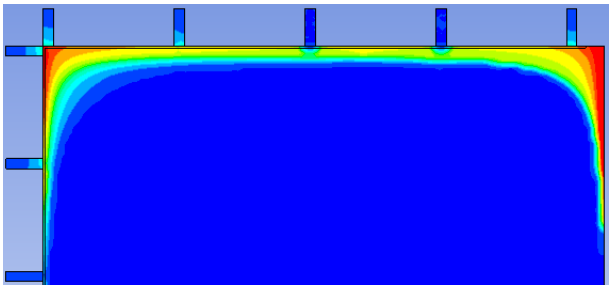

Day 30

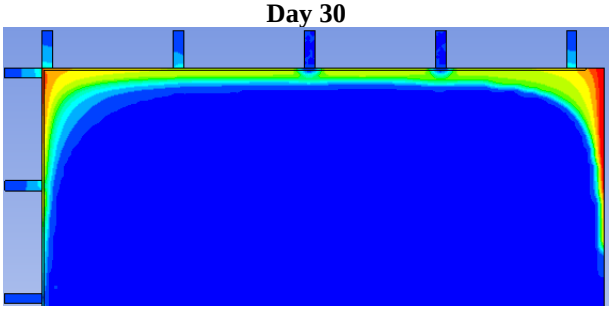

Day 35

Figure 5.44 Cooling effect of nitrogen injection behind seals b and c during an extended period

5.9 Summary

This chapter develops a three-dimensional CFD model to study heating evolution and gas dispersion in a Shendong goaf. The model is developed based on real on-site conditions with a few simplifications though. The theoretical model is composed of a number of governing equations including low temperature kinetics of coal oxidation, energy and mass conservation, momentum balance, and continuity equation. The base model is validated and calibrated via field gas monitoring data. Main findings are as listed:

Findings from results of base model:

- High velocity airflow is able to travel 30~100m deep into coal layer and more airflow is present around perimeter of goaf rather than centre of goaf due to high porosity and permeability on goaf fringe.
- High concentration oxygen can migrate into goaf approximately 500m behind face at maingate side and only about 100m at return side.
- Heating is evolved in an intermediate zone where airflow stream is able to supply enough oxygen to sustain continuous oxidation reaction and meanwhile, heat dissipated by convection is less effective than heat generated by oxidation. Incubation period of the heating is roughly 29 days.

- Most carbonic gas is generated at intake side due to presence of high oxygen gas mixture. Liberated carbonic gas is unable to flow around the entire goaf perimeter and starts to divert to return side in middle of goaf.
- CO make profile correlates well with the maximum temperature profile.
- With normal advance rate of longwall face and without air leakage from other sources, serious heating in goaf is unlikely to occur.

Findings from results of 500m model:

- High velocity gas stream is able to travel to deep goaf and high oxygen level gas is present at start-up area.
- Heating is developed at start-up area and behind longwall face. The incubation period of heating at start-up area is 25 days, which is shorter than that behind longwall face.
- CO make profile correlates well with temperature profile.
- The best locations for nitrogen injection are behind seal D, E, or F with at least 244m^3/h nitrogen injection for a proactive inertisation plan.
- Heating can be suppressed in start-up area with reactive inertisation behind seal C only. Nine days are required for nitrogen to fully disperse to heating area and the temperature is brought down very slowly.
- It needs about five days for nitrogen to fully disperse to heating area behind seals C and c. Temperature is brought down more quickly than nitrogen injection from only one seal.

Findings from results of 1000m model with air leakage from mining induced cracks:

- Due to leakage of fresh airflow, oxygen rich gas mixture is present at start-up area.
- Heating is developed in start-up area and the heating evolves quickly than that behind longwall face.
- CO make is unable to correctly indicate the severity of the heating because high level CO is generated at a very confined zone.
- The best locations for nitrogen injection are behind seal a, b, or c with at least 122m^3/h nitrogen injection for a proactive inertisation plan.

- It takes roughly 10 days to dilute gas mixture to a safe level for a reactive inertisation from only seal c. Most of the heating can be suppressed but it is not able to bring down the temperature at localised area.
- Only three days are required to fully exclude high oxygen gas from start-up area with nitrogen injection from seals b and c. The heating can be totally suppressed by nitrogen injection behind the two seals.

6 APPLICATION OF VENTILATION SIMULATION TO SPONTANEOUS COMBUSTION CONTROL: A CASE STUDY FROM BULIANTA COLLIERY

6.1 Chapter Introduction

Coal, as a carbonaceous material, is capable of being oxidised and generating heat from ambient temperatures [17, 37, 271, 272]. Self-heating or even spontaneous combustion of coal mass is likely to outbreak under favourable circumstances during many processes of coal extraction and utilisation [36, 37, 273, 274].Especially underground coal mine fires have been identified as one of the most devastating mining hazards for posing a great threat to miners, burning out valuable coal mine assets, and giving off toxic and greenhouse gases [25, 275].

Generally several internal and external factors can contribute to spontaneous combustion of coal in underground coal mine [276]. Intrinsic factors like coal properties and geological conditions are beyond control of coal operators. While Extrinsic factors like LW panel layout, ventilation deployment, and mine planning can be managed by coal operators. Among those external factors ventilation arrangement is possibly of the utmost importance because airflow leakage into goaf from ventilation in LW working is a necessary element of fire. The primary duties of mine ventilation are to dilute hazardous accumulation of gas and dust, to dissipate heat primarily produced by mining machines, and to supply respirable air to underground working force [277-279]. A proper ventilation network is capable of fulfilling this duty in an economical means while a poorly managed ventilation system is very likely to fail the duty and even worse, to facilitate development of some mining hazards. Spontaneous combustion is one of them as coal mine ventilation is inevitably feeding oxygen rich air into longwall goaf where a significant amount of coal is left. Today there is a strong move to longer panels, wider faces, greater extraction heights, increased production rates, more efficient ventilation and decreased personnel in longwall coal mine [280]. The coal seams in newly developed mines or sections are generally thick and the risk of spontaneous combustion increases significantly during longwall mining due to the large quantities

of broken coal left behind the chocks and its exposure to high oxygen levels in the goaf [228]. Due to depletion of the first coal seam many coal mines in China have extracted the second seam or mined multi-seams simultaneously. The trending can now be found in Australian mining industry as well. It undoubtedly will pose more complexities to ventilation circuits and difficulties to manage coal spontaneous combustion because mining-induced cracks are more developed and more likely to propagate to surface to draw more air leakage for multi-seam LW operations. In exhaust ventilation system fresh air is drawn from surface to LW working face through the interconnected mining-induced cracks and vice versa for the force ventilation system. The pressure differential between LW working and surface is the major driver for the leakage so minimising the pressure differential is another important duty of ventilation for LWs operated in multiple coal seams and under shallow cover. A rational philosophy in dealing with spontaneous combustion hazard is prevention is always better than cure. Although many advances in gas monitoring techniques, sealing and stopping construction, and proactive inertisation plan have been achieved, a more competent ventilation system which can reduce the leakage into goaf is the first and also the most important shield to the hazard. To quantify the pressure differential and investigate the issue with more details, a ventilation simulation program called "Ventsim" is used to perform a case study based on a real ventilation network of Bulianta colliery. The colliery is one of the most productive LW operations in China and also a very representative LW operated in multiple coal seams and under shallow cover.

6.2 Project description

6.2.1 General introduction

Bulianta colliery is situated 13km south to Ordos city of Inner Mongolia Autonomous Region of northern China. The colliery is operated in Shendong coalfield which is featured with flat and thick coal seam under shallow cover. Mining area of the colliery is approximately 34km^2 and the total proven reserve exceeds 506 million tons of coal. Due to recent upgrade of mining technology and equipment, extraction height of LW working face has increased to 7m and annual production of the coal mine has exceeds 15 million tons of coal. Bulianta colliery

and several other coal mines in Shendong coalfield have become the most productive underground LW operations in China.

Figure 6.1 Location of Bulianta colliery

6.2.2 Geological conditions

Combine the following information: data interpretation of drilling core, outcrop of strata and proven geological information of the coalfield, stratigraphy of the colliery is estimated. Figure 6.2 shows a simplified distribution of the strata. Five broad groups of strata are identified, from top to bottom they are: (a) Holocene Series Quaternary System loose bed consisting of aeolian sand, alluviation sand and loess with 28m average thickness in total; (b) Upper Jurassic to lower Cretaceous System Zhidan Group with 52m thick sandstone and conglomerate; (c) MesozoicErathem middle Jurassic System Zhiluo Formation composed by 112m thick sandstone and sand shale; (d) Mesozoic Erathem lower-middle Jurassic System Yanan Formation consisting of sandstone, shale, siltstone, sand shale, and coal seams with total thickness of 182m; (e) Mesozoic Erathem Triassic System upper series Yanchang Formation with 137m thick sandstone and coal seams. The strata (d) is further divided into three parts in which main extraction coal seam 1^{-2} seam is located in upper part and the other two main seam 2^{-2} and 3^{-1} seam are distributed in middle part. The average thicknesses of three coal seams are 4.1m, 6.8m, and 3.2m respectively. Spacing of them are approximately 32m between 1^{-2} and 2^{-2} seam and 28m between 2^{-2} and 3^{-1} seam, respectively. The mining region is part of the Ordos early-middle Jurassic coal bearing basin and no big faults are found in the basin. The

basin is developed in the platform on the basis of inheriting type basin in which the strata lies towards the N20 °to 30 ℃W and the tendency is S60 ℃~70 ℃W. The incline of the strata varies slightly from 0 ° to 3 ° and the floor of coal seam has slight fluctuation with gentle lift in the east. It is noticeable coal seams in this colliery are closely distributed and operated under very shallow cover.

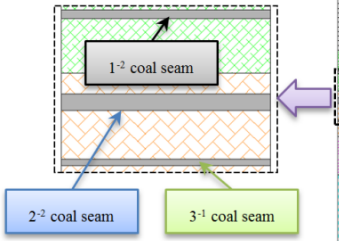

Strata	Lithology	Average thickness (m)
Holocene Series Quaternary System loose bed	Aeolian sand, alluviation sand, loess etc.	28
Upper Jurassic to lower Cretaceous System Zhidan Group	Sandstone, conglomerate	52
Mesozoic Erathem middle Jurassic System Zhiluo Formation	Sand shale, sandstone	112
Upper part of Mesozoic Erathem lower-middle Jurassic System Yanan Formation	Sandstone, siltstone, shale, coal	60
Middle part of Mesozoic Erathem lower-middle Jurassic System Yanan Formation	Sandstone, shale, siltstone, sand shale, coal	66
Lower part of Mesozoic Erathem lower-middle Jurassic System Yanan Formation	Sandstone, shale, siltstone, sand shale, coal	56
Mesozoic Erathem Triassic System upper series Yanchang Formation	Sandstone, coal	137

Figure 6.2 A simplified stratigraphy of Bulianta colliery

6.2.3 Problem identification

Currently the coal mine is extracting two coal seams, namely 1^{-2} coal seam and 2^{-2} coal seam. 3^{-1} Seam is on standby. Figure 6.3shows the overall layout of Bulianta coal mine. Real mine plan map can be seen in Appendix B. The whole mine is divided into five sections with several longwall panels within each of section. 1^{-2}Seam and 2^{-2} seam has been totally extracted in section one and two. At present section four and section five are mining 1^{-2} seam and section three is mining 2^{-2} seam as 1^{-2} seam has been extracted and it is believed overlying goaf has been interconnected via mining-induced cracks. Contaminated air is taken out of pit via two main exhaust fans. One is installed in north exhaust shaft and another one is installed in south exhaust incline. Fresh air is mainly taken from intake incline and intake shaft, refer Figure 6.3. Intake shaft serves to section five and main intake inclines serves to section three. Fresh air is supplied from both intake shaft and intake incline for section four.

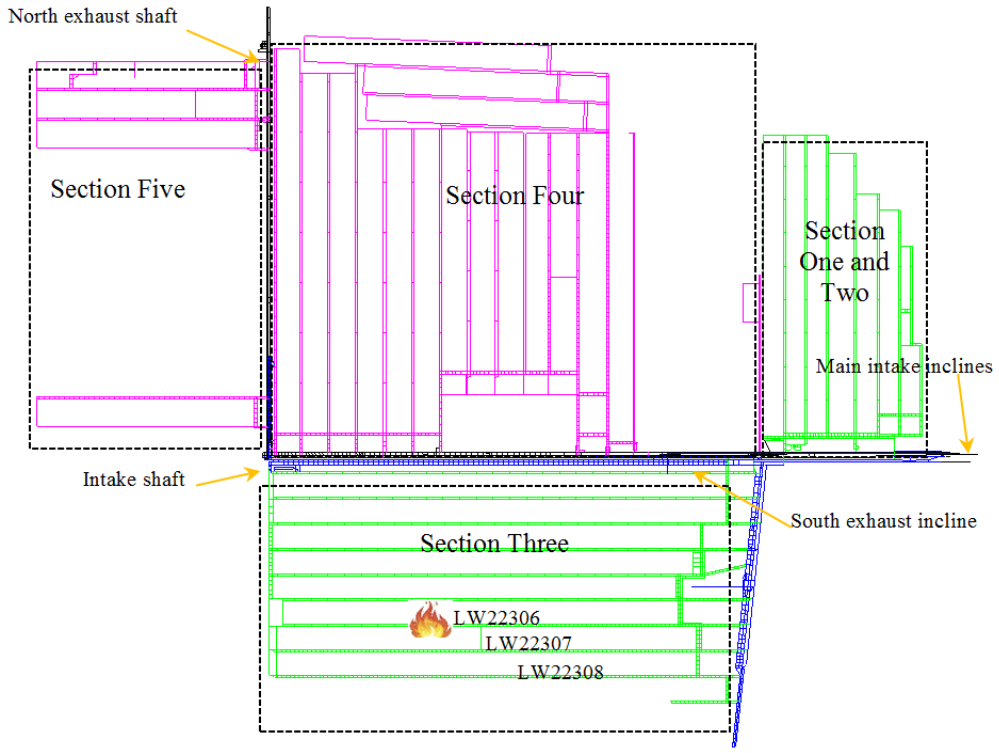

Figure 6.3 Overall layout and ventilation network of Bulianta colliery

Since the commencement of extraction of panels in section three several, serious coal oxidation and self-heating incidents have occurred and culminated in one open fire incident at LW22306 working panel, refer Figure 6.3. It was found the fire originated from overlying 1^{-2} coal seam goaf because high concentration of CO (exceeds 10000ppm) was initially detected from several boreholes drilled to overlying 1^{-2} coal seam goaf. The fire caused more than six months closure of the panel and costed hundreds of millions of dollars to quench it by slurry injection through hundreds of downholes. After undertaking investigation and incident review, the possible reason of the occurrence of the fire incident was revealed and can be illustrated in Figure 6.4. As is widely accepted, a major consequence of coal extraction is ground subsidence and creation of factures and cracks to the overlying or underlying strata. In this case after 1^{-2}seam was mined, the induced cracks may have already developed to surface due to shallow cover of the coal seam. As 2^{-2} seam was further extracted, more developed and wider cracks were likely to be induced because of higher mining height of this coal seam. These channels are very likely to become interconnected and propagate to surface, refer Figure 6.5which are real images of mining-induced cracks developed to surface. These channels can function as air leakage path from surface to active working face if any pressure differential

presents. As this mine is currently using an exhaust ventilation method, the pressure of the airflow in working face is possibly much lower than surface atmospheric pressure. Therefore the pressure differential is very likely to draw a certain amount of fresh air from surface to active longwall face through these channels. In addition the immediate roof of Shendong coalfield is very fragile and as a result, approximately 0.5m top coal is reserved to facilitate chock support and will be left in goaf as LW advances. With continual supply of fresh air, smouldering of coal developed to an open fire as the heat generated from coal oxidation is not sufficiently dissipated. The pressure differential not only aggravates the self-heating process of coal but also promotes the ingress of goaf gas into the working face. The ingress of oxygen deficient and high concentration of CO gas poses a great threat to the safety of working crew at LW face. Many practices have been exercised to control the problem. One direct solution is to seal these cracks with grout or slurry injection. However the solution is still prohibitive for two reasons. One is cost would be substantial as there are a large number of cracks required to be treated. Another difficulty is many concealed cracks are hard to be detected. Therefore minimising the pressure differential between surface and ventilation circuit by improving ventilation performance would be a promising solution and this is also an important initiative of this project.

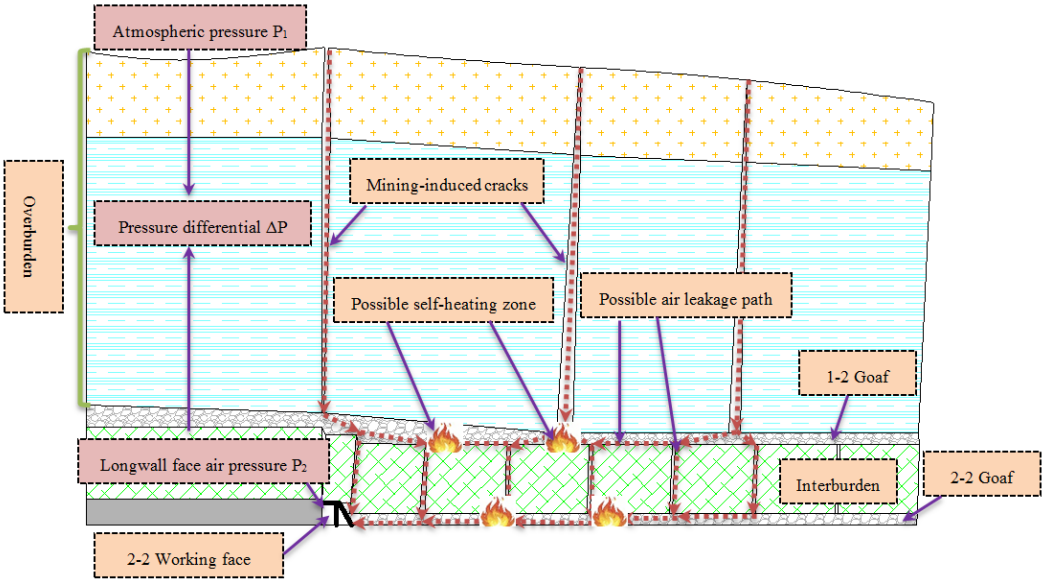

Figure 6.4 A schematic illustration of the occurrence of fire incident at Bulianta colliery

Figure 6.5 Two photographic views of mining-induced cracks developed to surface of Bulianta colliery

6.3 Development and validation of "Ventsim" model

As discussed a rational solution to the air leakage through mining-induced cracks is to minimise the pressure differential between surface and ventilation circuit. To quantify the pressure differential and to investigate this issue more critically, a ventilation simulation program "Ventsim" is used to conduct the case study. "Ventsim" is one of the most sophisticated software packages in underground mine ventilation simulation and is widely used in many Australian underground mining operations. "Ventsim" can be utilised to assist a range of mine ventilation related operations including mine ventilation design, mine network analysis and optimisation, prediction of recirculated ventilation, and economical analysis on mine ventilation.

6.3.1 A brief introduction of "Ventsim"

Ventilation is an important element in mining operation as not only fresh air required to be transported to workings but also contaminated gas needs to be diluted and dispersed. A proper ventilation network is capable of doing this job in an economical means while a poorly managed ventilation system is very likely to fail the required duty or even induce airflow to undesirable locations. Ventilation has been a primary concern in underground mines since commencement of underground mining industry. Prior to the introduction of computerized model analysis, the planning and modelling of ventilation network mainly relied on experience, blind guesswork and extensive calculations. Ventsim aims to make ventilation simulation and design more accessible to any mine engineer, ventilation related researcher and Ventilation Officer (VO) on site, even those without sufficient ventilation experience. Ventsim can be utilised to assist a range of mine ventilation related operations including mine

ventilation design, mine network analysis and optimisation, dust and heat suppression, prediction of recirculated ventilation, and economical analysis on mine ventilation. Ventsim can also help ventilation related decision making process and enable mine operators to more properly run the on-site ventilation system. The program is applicable in simulating complex ventilation model which may incorporate multi-fan operations. Ventsim has been designed as a tool which can operates independently of other mine planning packages but somehow remains a certain level a compatibility which ensures data from other mine planning packages [281]. Ventsim Classic version was firstly released in 1993 only capable of building models in two dimensions. In spite of limitations such as incompressible flow and lack of heat simulation, a large number of mines adopted Ventsim Classic for design optimisation and modification purpose. Ventsim Classic was kept improving, however all development on this program was ceased in 2007 with a major breakthrough bring the program to a 3D displaying version. Figure 6.6shows the major difference of interfaces display, particularly on presence of airways, menu bar and tool bar, and interpretation of the results.

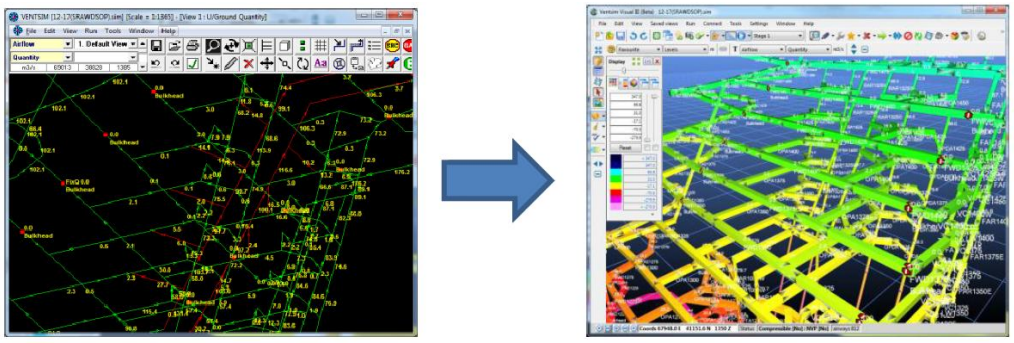

Figure 6.6 Ventsim from classic (2D) to visual (3D)

6.3.2 Model development

6.3.2.1 Create single line DXF file

In Autocad drawing obtained from mine site double-line is primarily used to represent airway. However Ventsim is only capable of identifying single line as airway so redraw the single line and convert to DXF file is the first task before any further work to be done in Ventsim. Figure 6.7 shows how single line drawing is created. Appendix B shows Bulianta single line roadway system in three dimensions.

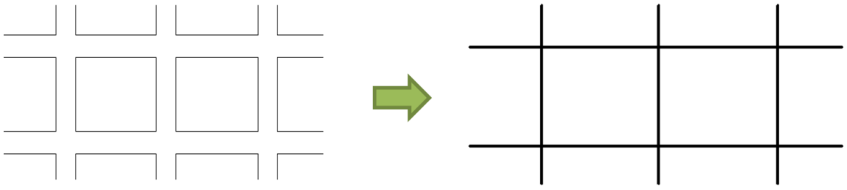

Figure 6.7 Convert double-line roadway to single line

6.3.2.2 Pre-setting and import DXF file to Ventsim

Before importing DXF drawing to Ventsim pre-settings like roadway resistance, ventilation regulator leakages, and cross sectional profile of roadway can be changed or added, refer Figure 6.8.

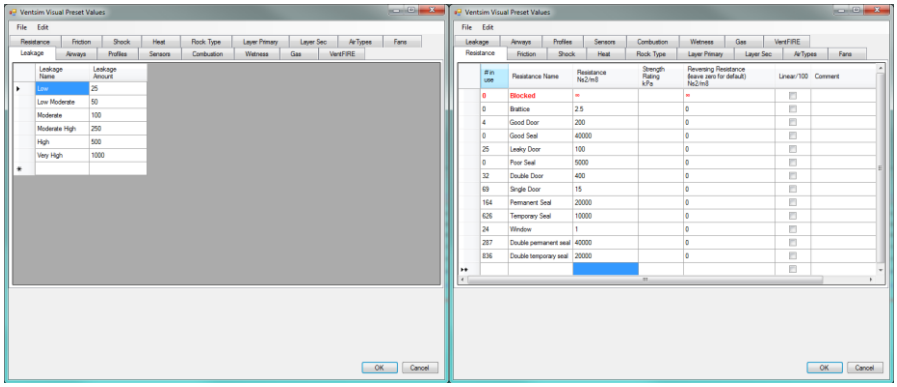

(a) Leakage rate setting (b) Door and seal resistance setting

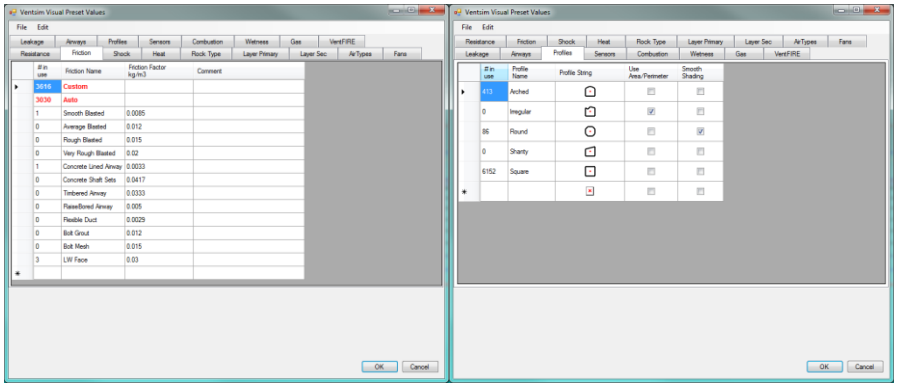

(c) Friction factor (d) Airway profiles

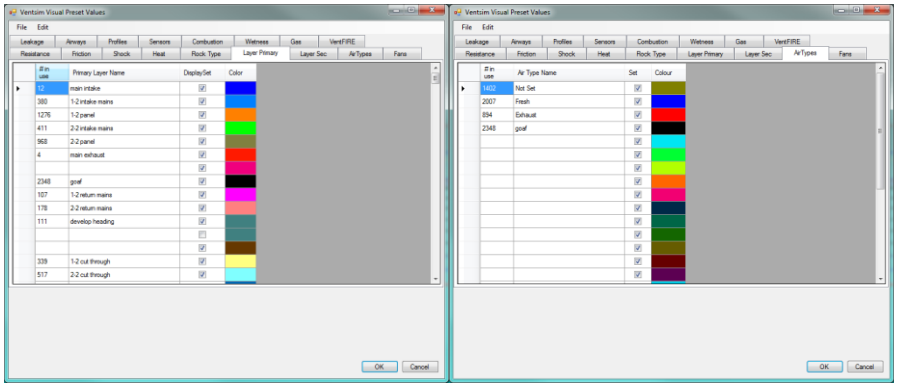

(e) Primary layer colour legend (f) Air type colour legend

Figure 6.8 Main pre-setting parameters

6.3.2.3 Geometric model clean-up and simplification

When a complex DXF drawing is imported to Ventsim, it is very likely disconnected or overlapping airways are incorporated within fresh model data. It is necessary to run geometry repair or simplification before editing any airway. Filtering tools run in three functions: (1) simplify (this function allows the user to reduce the number of airways to a more efficient number without damaging the overall model analysis), (2) binding (this function connects disconnected airways ends or intersections.), and (3) duplicate (this function allows searching for airways which have duplicates in the same positions). Filter tools can run simultaneously as a group, or individually, refer Figure 6.9.

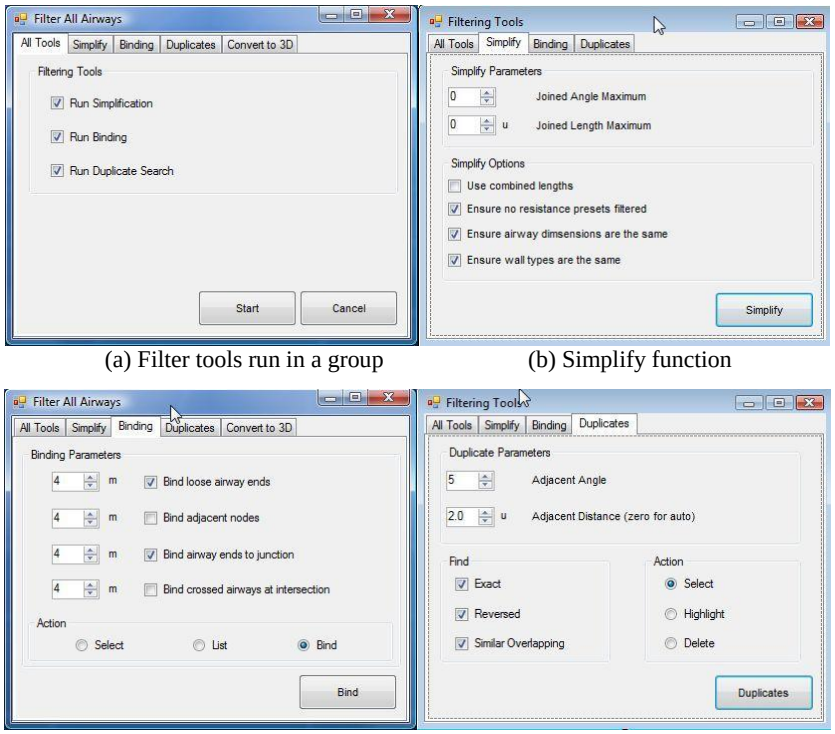

(a) Filter tools run in a group (b) Simplify function

(c) Binding function (d) Duplicate function

Figure 6.9 Filter tools to clean and simplify geometry

6.3.2.4 Airway parameter setting and edit

Next step is to set airway parameters including airway profile and geometric dimension, frictional factor, and resistance if any etc.. The length of airway is not required to be specified because it is in real scale when sketching the single line DXF file. Editing of airway can be accomplished by accessing into edit box, refer Figure 6.10.

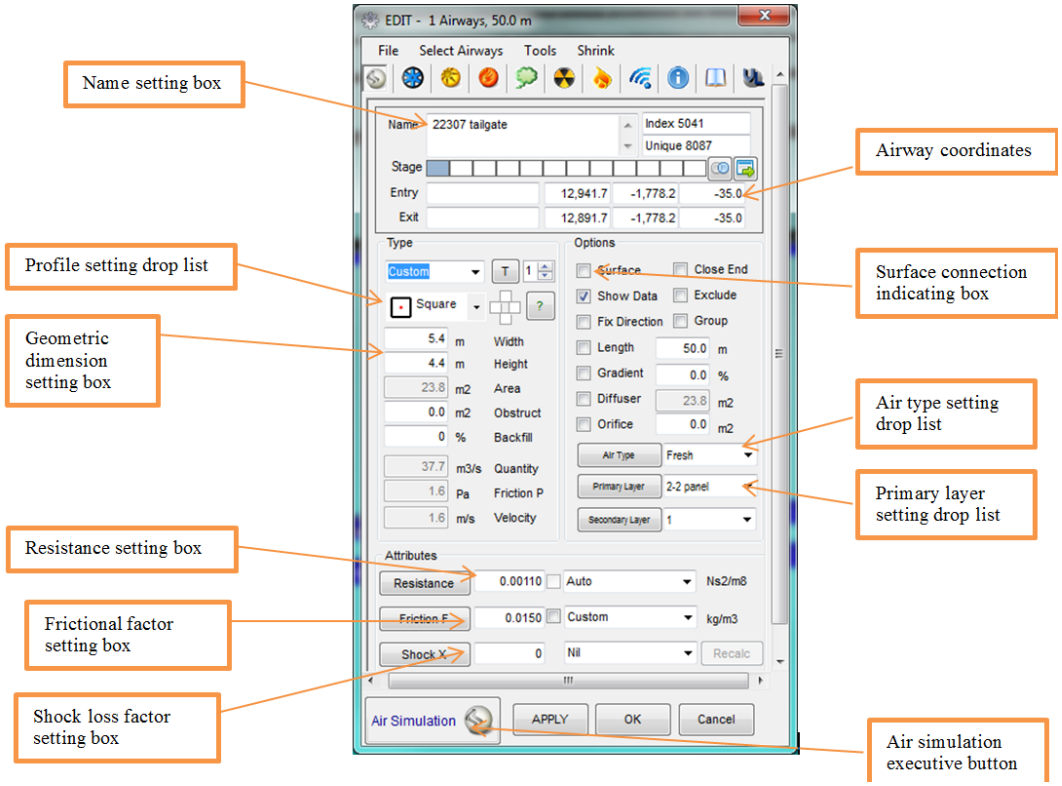

Figure 6.10 Airway parameter setting dialog box

According to mine real conditions set airway parameters one by one. The main input parameters of main airways are summarised in Table 6.1.

Table 6.1 Main input parameters of main airways

Item	Cross section profile	Support type	Height/Diameter	Width	Resistance factor	Airtype	Primary layer
			m	m	Ns^2/m^4		
Main drift	Rectangle	Concrete Lined	4.5	5	0.0077	fresh	main intake
2^{-2} Auxiliary Heading	Arched	Bolt&Grout	4	5.2	0.01725	fresh	2^{-2} mains
Section 3 Intake Heading	Rectangle	Bolt&Grout	4	5.4	0.00532	fresh	2^{-2} mains
LW22307 Maingate	Rectangle	Bolt&Mesh	4.5	6	0.03	fresh	2^{-2} panel
LW22307	Rectangle	Bolt&Mesh &Chock	5.5	5	0.04	exhaust	2^{-2} panel
LW22307 Tailgate	Rectangle	Bolt&Mesh	4.4	5.4	0.015	exhaust	2^{-2} panel
LW22308 Maingate	Rectangle	Bolt&Mesh	4.5	6	0.015	exhaust	2^{-2} panel
LW22308 Start-up	Rectangle	Bolt&Mesh	4.5	6	0.02	exhaust	2^{-2} panel
LW22308 Tailgate	Rectangle	Bolt&Mesh	4.6	5.4	0.015	fresh	2^{-2} panel
LW22309 Maingate	Rectangle	Bolt&Mesh	4.5	6	0.015	exhaust	2^{-2} panel
LW22309 Tailgate	Rectangle	Bolt&Mesh	4.6	5.4	0.015	exhaust	2^{-2} panel
LW22310 Tailgate	Rectangle	Bolt&Mesh	4.6	5.4	0.015	fresh	2^{-2} panel

2^{-2} Cut through	Rectangle	Bolt&Mesh	4	5	0.015		2^{-2} panel
Section 3 Exhaust Main	Rectangle	Bolt&Mesh	4	5.2	0.015	exhaust	2^{-2} mains
2^{-2} Exhaust Main	Rectangle	Bolt&Mesh	4	5	0.00854	exhaust	2^{-2} mains
2^{-2} Total Exhaust&1055 main	Rectangle	Bolt&Grout	4	5	0.025	exhaust	2^{-2} mains
#2 South exhaust incline	Arched	Bolt&Grout	3.4	4.3	0.00808	exhaust	main exhaust
1^{-2} Main Heading	Arched	Bolt&Grout	3.8	5.3	0.00247	fresh	1^{-2} mains
LW12411 Maingate	Rectangle	Bolt&Mesh	3.7	5.6	0.013	fresh	1^{-2} panel
LW12411	Rectangle	Bolt&Mesh &Chock	3.5	4	0.04	exhaust	1^{-2} panel
LW12411 Tailgate	Rectangle	Bolt&Mesh	3.8	5.6	0.0129	exhaust	1^{-2} panel
Face recovery roadway	Rectangle	Bolt&Mesh	4	5	0.01	exhaust	1^{-2} panel
Section 4 Exhaust Heading	Rectangle	Bolt&Mesh	3.5	5.3	0.01032	exhaust	1^{-2} mains
#1 South exhaust incline	Arched	Bolt&Grout	3.2	4.2	0.0244	exhaust	main exhaust
Huhewusu intake shaft	Round	Concrete Lined	5		0.01123	fresh	main intake
Section 5 Auxiliary Heading	Rectangle	Bolt&Mesh	3.5	7.2	0.0021	fresh	1^{-2} mains
LW12510 Maingate	Rectangle	Bolt&Mesh	3.8	5.7	0.02729	fresh	1^{-2} panel
LW12510	Rectangle	Bolt&Mesh &Chock	3.6	5	0.04	exhaust	1^{-2} panel
LW12510 Tailgate	Rectangle	Bolt&Mesh	3.9	5.5	0.02297	exhaust	1^{-2} panel
Section 5 Exhaust Heading	Rectangle	Bolt&Grout	3.7	6.1	0.02038	exhaust	1^{-2} mains
North Exhaust shaft roadway	Rectangle	Bolt&Grout	4.5	6.4	0.04356	exhaust	1^{-2} mains
North Exhaust shaft	Round	Concrete Lined	5.6		0.0033	exhaust	main exhaust
Old main intake incline	Arched	Bolt&Grout	3	3.8	0.00247	fresh	main intake
#1 main incline	Arched	Bolt&Grout	2.4	3.4	0.00247	fresh	main intake
#2 main incline	Arched	Bolt&Grout	3.2	4.1	0.00247	fresh	main intake
Auxiliary incline	Arched	Bolt&Grout	2.7	3.7	0.00247	fresh	main intake
2^{-2} main incline	Arched	Bolt&Grout	3.5	4.5	0.00247	fresh	main intake

After setting parameters to each airway, airway can be displayed in two modes, namely air type mode and primary layer mode, refer Figure 6.11, Figure 6.12, Figure 6.13, and Figure 6.14.

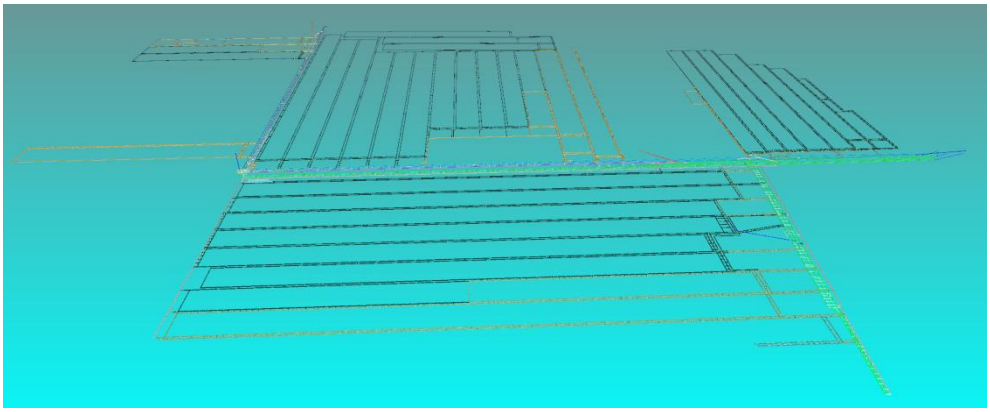

Figure 6.11 An overview of airway displayed in primary layer mode

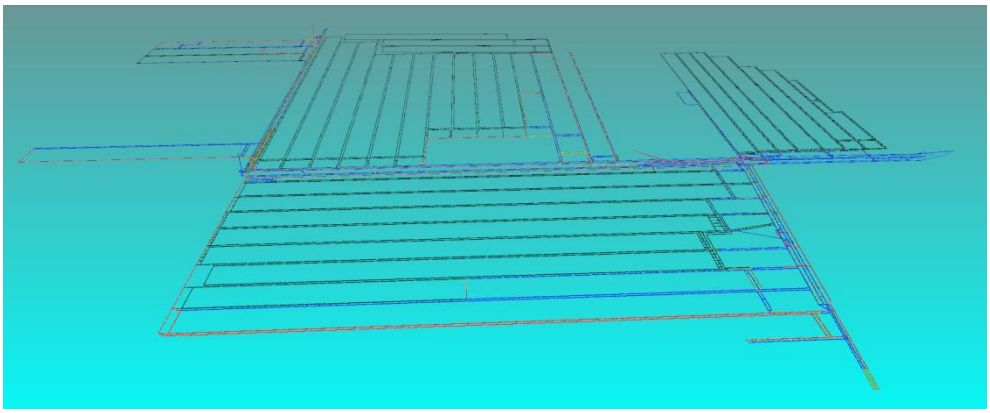

Figure 6.12 An overview of airway displayed in air type mode

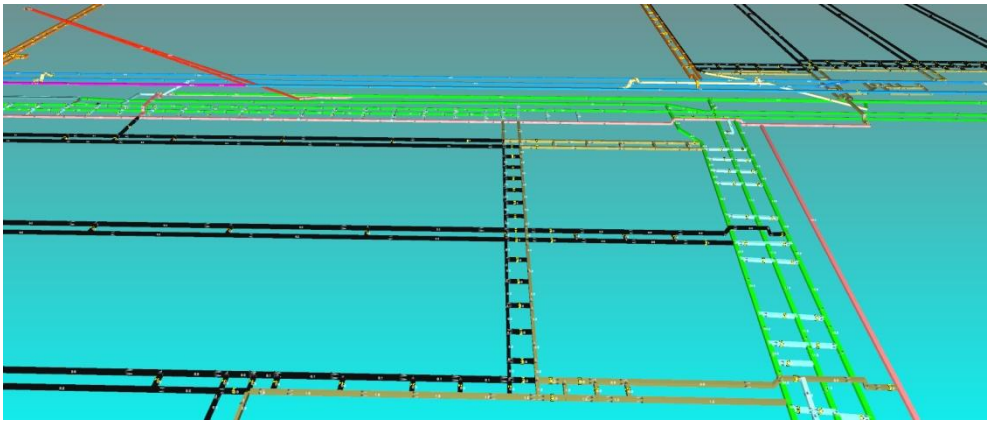

Figure 6.13 A close-up view of airway displayed in primary layer mode

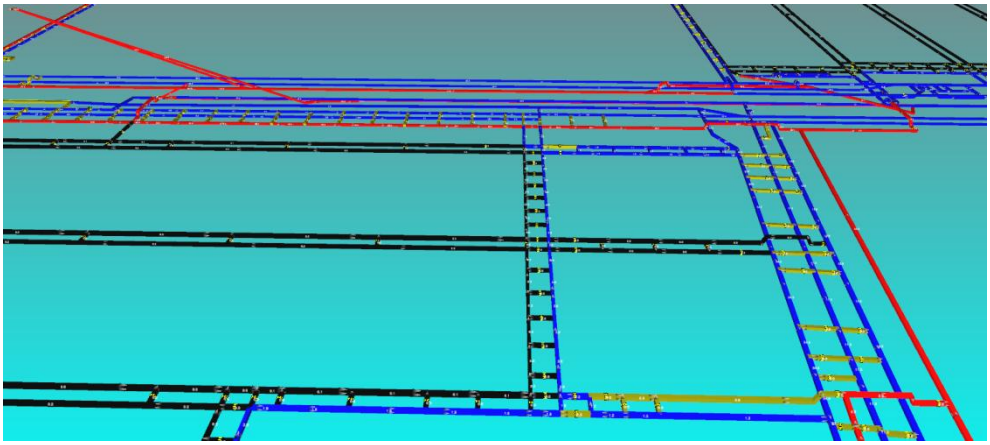

Figure 6.14 A close-up view of airway displayed in air type mode

In addition airway can be displayed with detailed information like air quantities, airway name, direction of airflow and ventilation regulator, refer Figure 6.15.

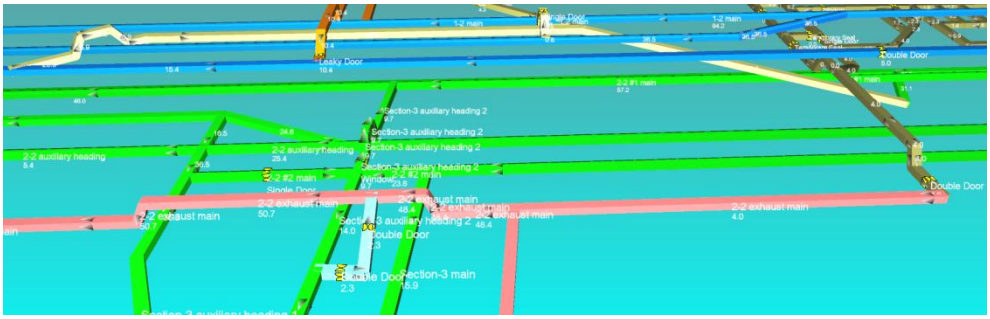

Figure 6.15 Airway detailed information displayed by Ventsim

6.3.2.5 Fan installation

A fan can be installed by exporting from a fan database which allows editing, adding and deleting of all fans. Up to one thousand fans and the associated fan curves can be imported into the fan database. A display for each fan curve will be presented when a fan is selected from the database. A customised fan can be developed following steps below:

a) Identify the fan configuration, the type of fan pressure curve, and the airflow density;
b) Divide the curve into up to ten points and exclude the stall region of the curve. Enter the curve points and fan information in the Fan Database edit form;
c) To assign a fan within the model, ensure the Fan Total Pressure method is activated and use the Edit Box to place the fan within an airway.

In this application two main exhaust fans curve were created in seven points based on site measured fan curve data, refer Figure 6.16, Figure 6.17, Figure 6.18, and

Figure 6.19. Note that fan curve can be estimated in both cubic and linear methods. Site measured fans curve data are shown in Appendix C and Appendix D.

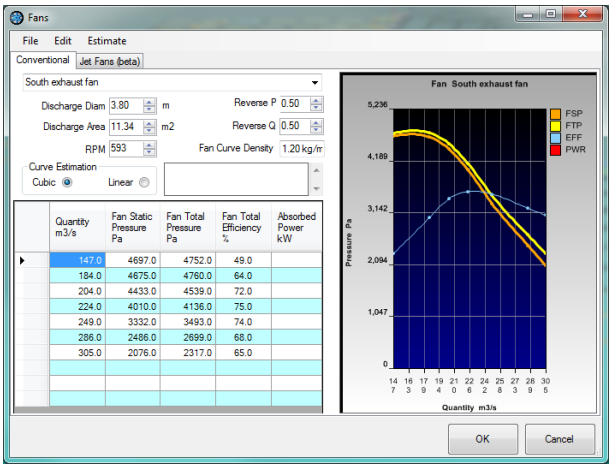

Figure 6.16 South exhaust fan curve with cubic interpolation

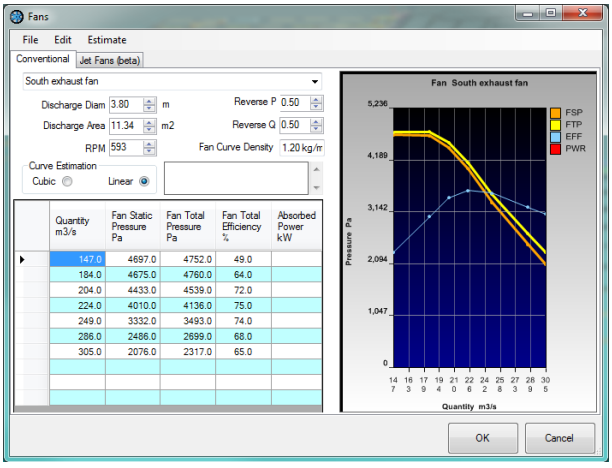

Figure 6.17 South exhaust fan curve with linear interpolation

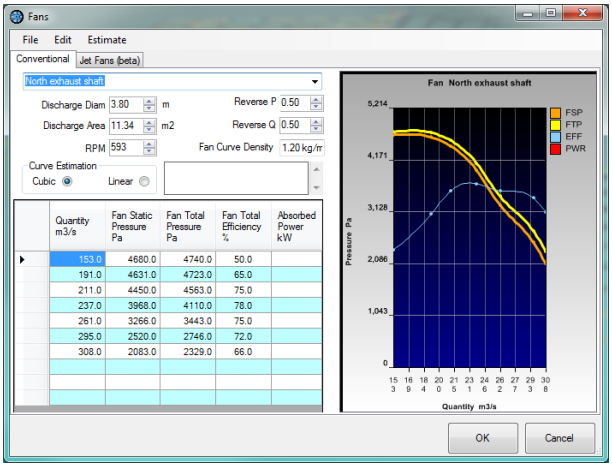

Figure 6.18 North exhaust fan curve with cubic interpolation

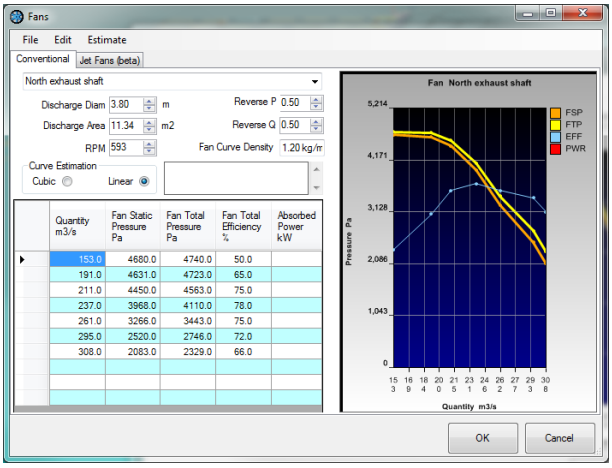

Figure 6.19 North exhaust fan curve with linear interpolation

After on site fan curve is created in fun database, fan can be installed by accessing EDIT box when the mine portal is being selected, refer Figure 6.20. When a particular fan is selected and operating power is set, the edit box will also display fan install point, power and efficiency. Figure 6.21 is fan icon displayed in Ventsim.

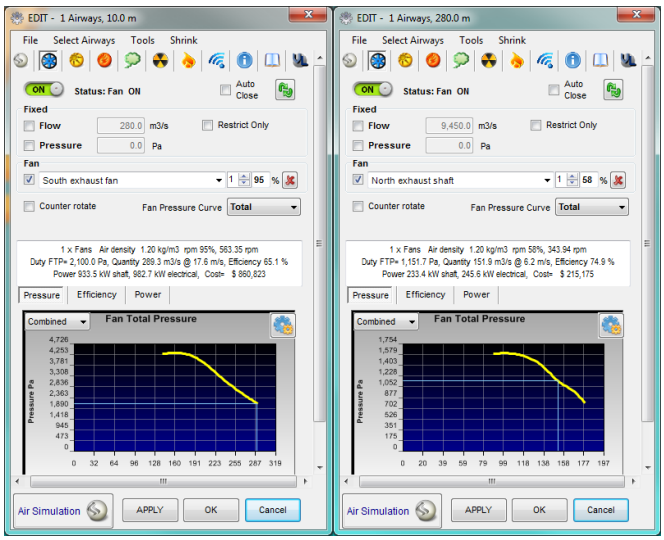

(a) South exhaust fan (b) North exhaust fan

Figure 6.20 Fan installation edit box

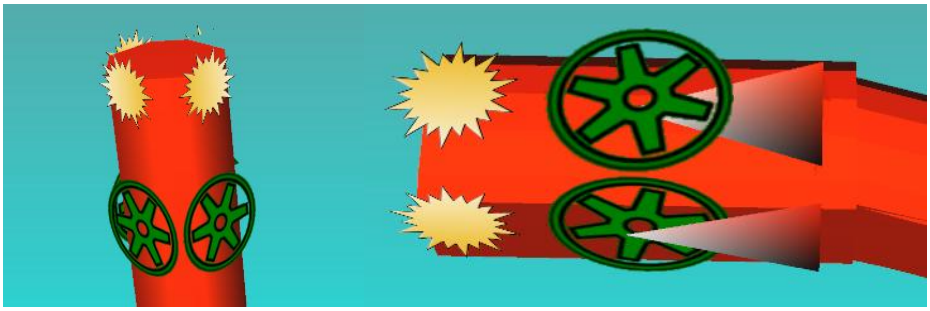

(a) South exhaust fan (b) North exhaust fan

Figure 6.21 Fan icon displayed in Ventsim

Ventsim also enables users to add auxiliary ventilation model to bring fresh air to blind headings or for other purposes. The auxiliary ventilation duct building function provides an opportunity to model complex auxiliary duct arrangements in a mine model. Auxiliary duct in mines is essential to ensure quality fresh air reaches areas of the mine without flow through ventilation, which in most cases will be blind headings. Construction of ventilation duct is available by hitting airway drawing button when a flow path is being selected, refer Figure 6.22. In the edit box parameters like duct diameter, frictional factor within duct, spatial location and leakage rate can be edited.

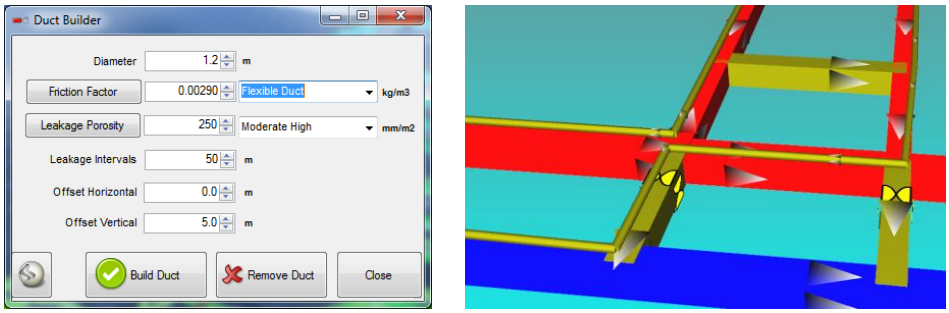

(a) Edition and construction of duct (b) Duct built in Ventsim

Figure 6.22 Construction of ventilation duct

When duct is created, a pathway will be built into the duct to allow it to draw and deliver airflow to the underlying airway. To ventilate a duct, simply EDIT the start of the duct airway with the EDIT toolbar button and then use the FAN tab to place a fan in the duct. Ventsim has two built auxiliary fans with different ventilation capacities, refer Figure 6.23.

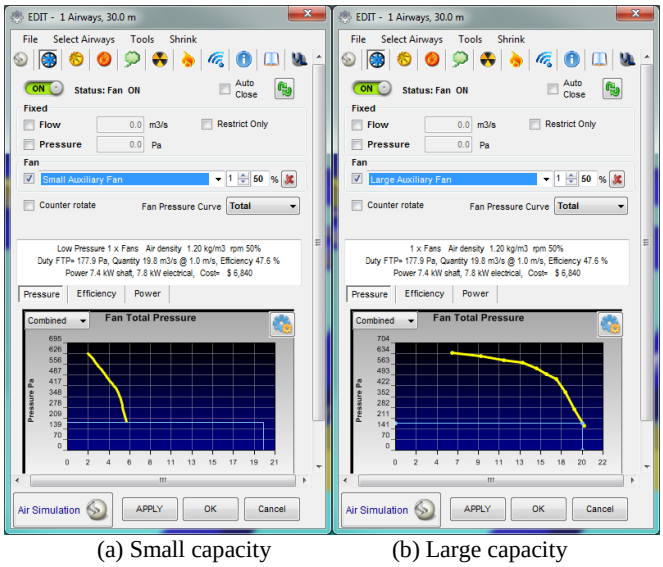

(a) Small capacity (b) Large capacity

Figure 6.23 Auxiliary fan in Ventsim

Following above procedures, Ventsim model for Bulianta colliery was developed. Figure 6.24 shows an overview of the established base model in which airways in blue colour represent fresh airflow intake, red colour stands for exhaust airflow, and black colour denotes sealed airways or virtual fringe of LW goaf.

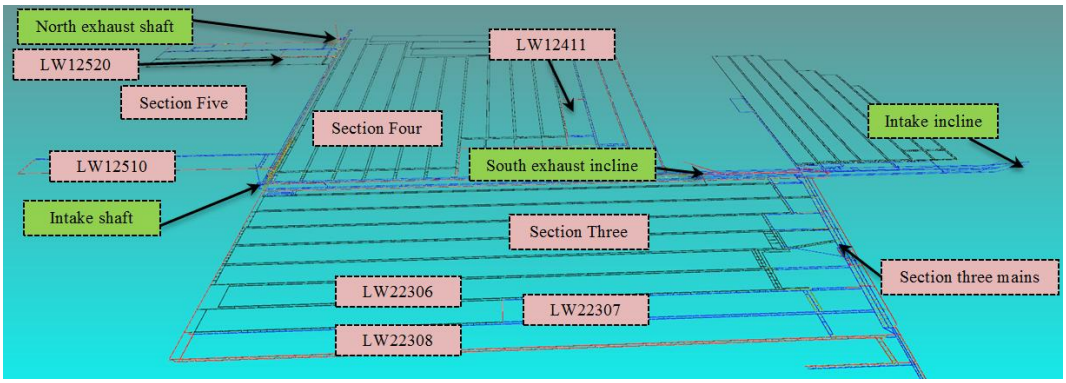

Figure 6.24 An overview of the base model in "Ventsim"

6.3.3 Model validation

The base model is validated through two steps: one is via quantity of airflow at most of the important locations and another one is to check pressure loss along critical ventilation paths. Figure 6.25 compares the site measured air flow quantity of critical locations with the computed data and it can be seen the differential is marginal. Bulianta colliery undertook a comprehensive ventilation survey in 2013 and the survey was performed along three airflow paths, namely LW22305 path, LW12409 path, and LW12519 path. The three paths represented three panel sections (section three, section four, and section five, respectively) and the pressure loss is validated through the three paths. The detail of the validation is only presented at section three as LWs in section three is the most risky area in terms of coal spontaneous combustion and ingress of goaf gas. The follow-up studies will focus on LW22307 path as well. Figure 6.26is a simplified airflow path through LW22307. Most fresh air is taken from main intake incline and then directs to 2^{-2} seam intake main. Part of the fresh airflow in 2^{-2} seam intake main is taken to section three longwalls via section three intake main. Then fresh air in LW22307 is supplied through both LW22307 maingate and LW22308 tailgate. Contaminated air is drawn to section three exhaust main via LW22307 tailgate and it is then delivered to 1055 level exhaust main before the contaminated air is discharged through fan at south exhaust incline. Figure 6.27shows the validation of pressure loss along LW22307 path. It can be seen the overall trend of it resembles that of measured LW22305 path. It

underwent a slight increase of pressure loss comparing to that of LW22305 path due to its longer flow path and the major of pressure loss occurs at exhausting airways. It can be also observed at working face the pressure loss exceeds 200Pa and as a result, the pressure differential between working face and surface is more than 200Pa. A large amount of fresh air will be attracted into LW working face once mining-induced channels propagate to surface due to presence of the 200Pa pressure differential. This pressure differential also provokes migration of goaf gas into working face and poses immediate danger to underground miners.

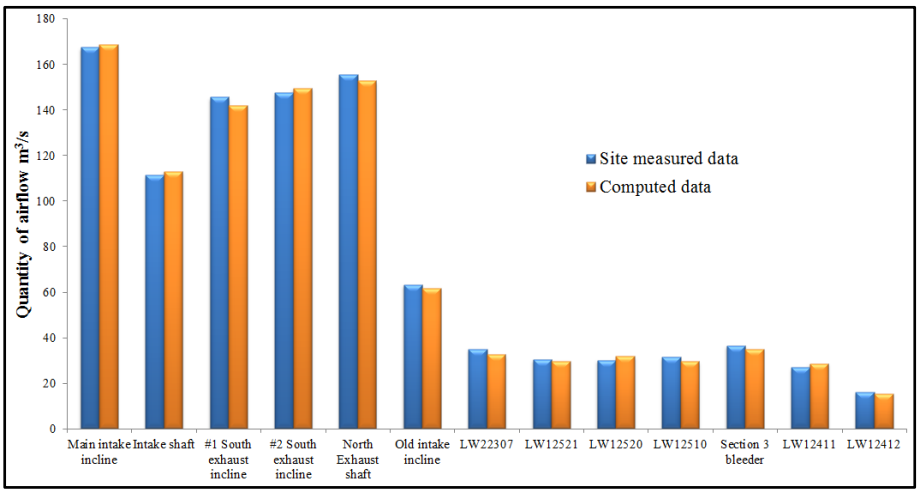

Figure 6.25 A comparison of site measured airflow quantity with computed data at critical airways

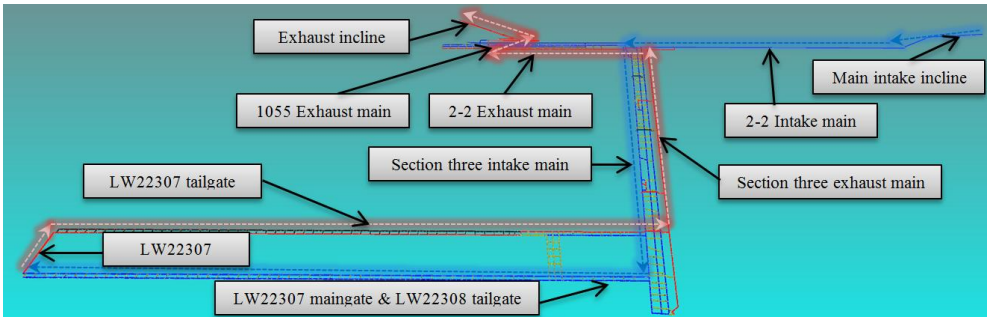

Figure 6.26 A simplified airflow path of LW22307

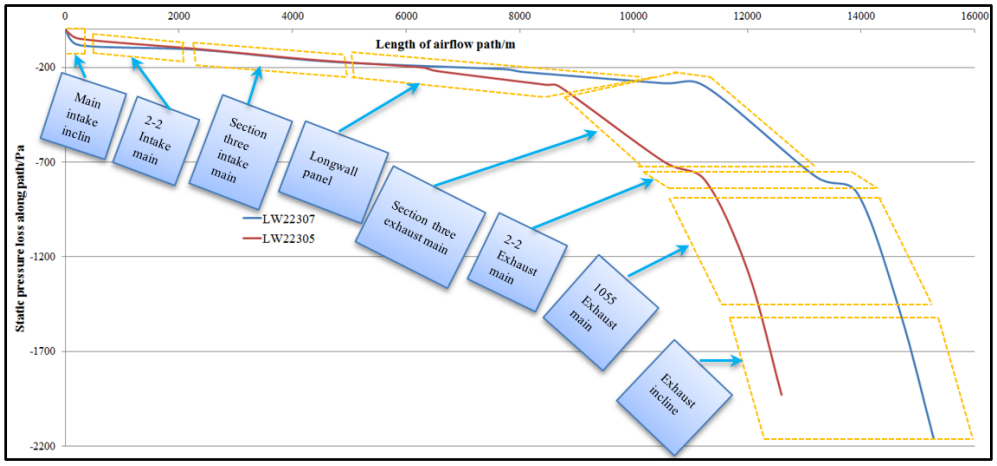

Figure 6.27 Pressure loss validation along LW22307 airflow path

6.4 Solutions and discussion

6.4.1 Possible solution one: modify ventilation network within panel

It has been studied different ventilation mode within LW panel may induce different pressure differential across LW face and therefore affect air leakage into goaf [280, 282]. To reduce pressure differential along LW22307 face, the first possible measure is to modify ventilation network within panel. In this study total seven scenarios are proposed and analysed, refer Table 6.2. The results of the simulation are presented in Figure 6.28 and Figure 6.29.

Table 6.2 Different ventilation modes of LW22307

Scenario	Illustration	Notes
On-site U	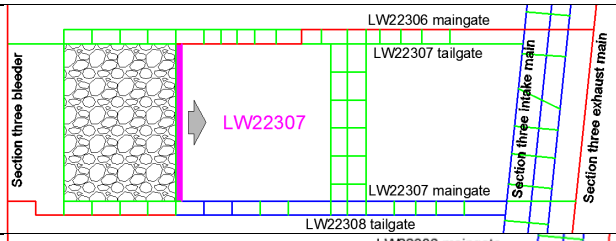	Fresh air is taken from both LW22307 maingate and LW22308 tailgate while contaminated air return to LW22307 tailgate and then LW22306 maingate.
Homotropal U	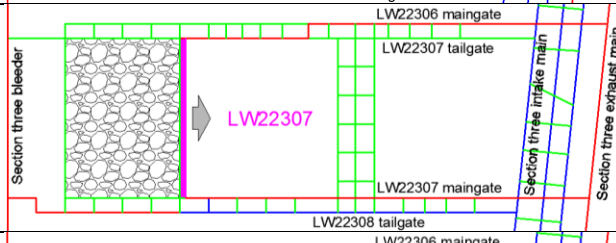	Fresh air is taken from LW22308 tailgate and allows for a split of air return to LW22307 maingate. The rest of the air returns to LW22307 tailgate after passing working face.
Reverse U	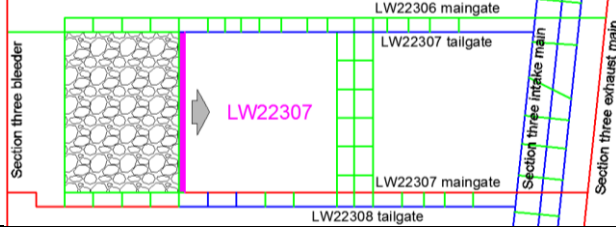	Inverse to the on-site U mode, fresh airs is taken from LW22307 tailgate and polluted air returns to LW22307maingate.

Bleederless on-site U	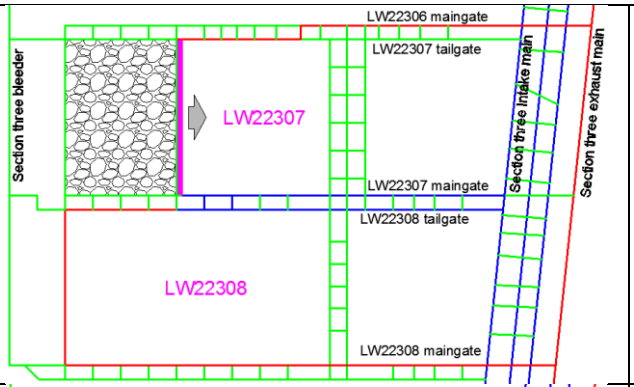	Section three bleeder is sealed. Fresh air is provided from LW22307 maingate and LW22308 tailgate. Most of the contaminated air returns to section three exhaust main through LW22307 tailgate and rest of the polluted air returns through LW22308 panel.
Bleederless homotropal U	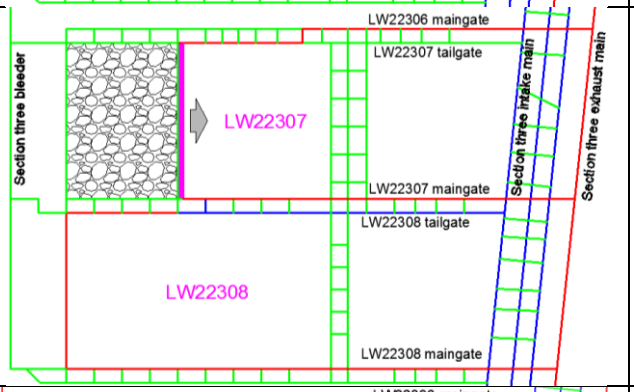	Section three bleeder is still sealed and fresh air is taken to LW22307 via LW22308 tailgate. A part of air is directed to return at the inby split location and another part of fresh air flow through LW22307 face to LW22307 tailgate and LW22306 maingate.
Bleeder return	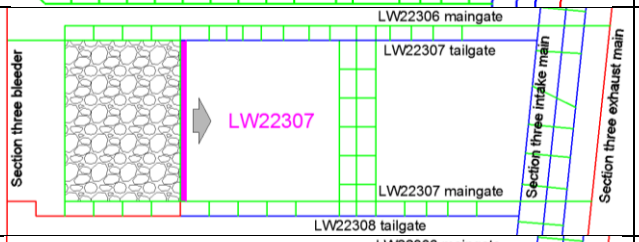	Fresh air is taken from LW22307 tailgate and dusty air is directed to LW22308 tailgate and back return to section through bleeder.
Double return	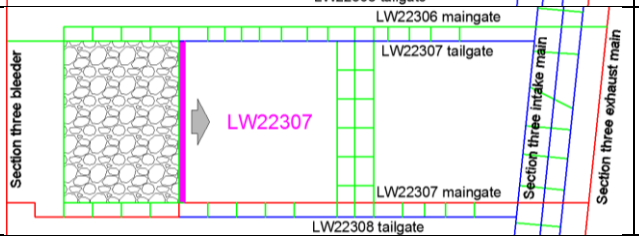	Similar to bleeder return mode, fresh air is taken from LW22307 tailgate. Air return both from LW22307 maingate and section three bleeder.

***Blue lines denote fresh airflow, red lines denote contaminated air flow, and green lines denote isolated or sealed airways**

Figure 6.28 depicts the pressure loss paths of various ventilation modes within panel. It can be seen the pressure differential is not able to be eliminated. The pressure differential at face shows little difference except for two bleederless ventilation modes.

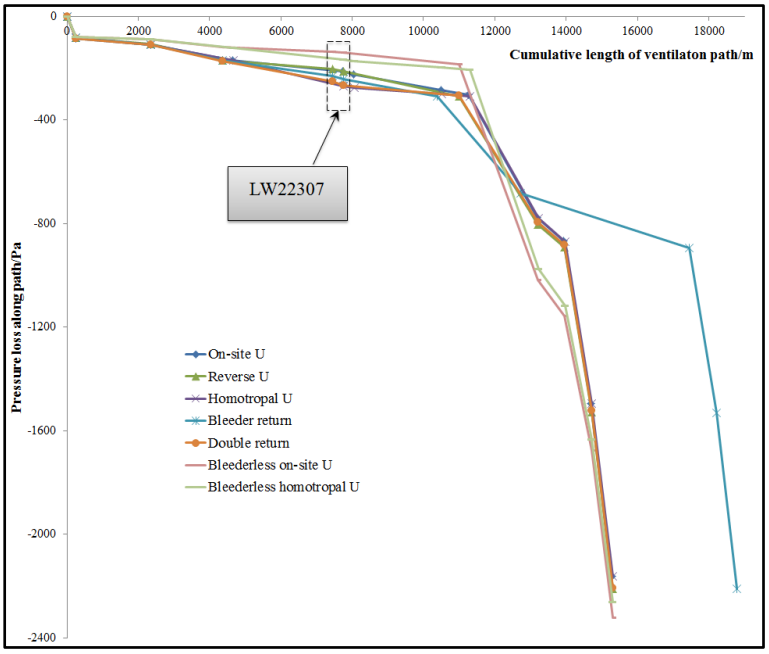

Figure 6.28 Ventilation pressure loss paths of various ventilation modes

To meet comfortable working conditions at LW face, no less than 30m^3/s fresh air is required in this colliery. As can be seen from Figure 6.29, “Homotropal U” and “Bleederless homotropal U” is clearly not suitable due to low quantity of airflow across LW22307 even though “Bleederless homotropal U” can slightly reduce the pressure differential. “Bleeder return” and “Double return” ventilation mode are able to supply sufficient air to working face but the pressure differentials become greater than that of on-site ventilation mode. “Bleederless on-site U” can considerably reduce the pressure differential but the airflow quantity is slightly less than the requirement. In addition Bleederless ventilation network would increase overall resistance and therefore it is inappropriate to be used for a long period of time. No matter how the mode of network is modified, the pressure differential would not be eliminated. It is an intrinsic flaw for exhausting ventilation network. Once mining-induced cracks develop to surface, fresh air will always be drawn to working face and vice versa for a forcing ventilation system.

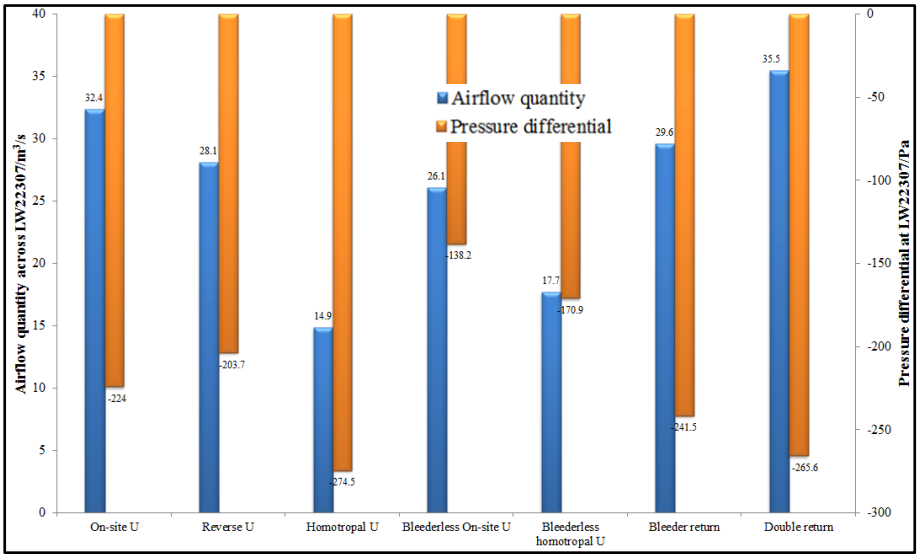

Figure 6.29 Pressure differentials and airflow quantities across LW22307 of different ventilation modes

6.4.2 Possible solution two: pressurise LW panel

To decrease pressure differential and meanwhile to deliver sufficient fresh air to LW working face, a solution called pressurising LW panel is proposed. The essence of the solution is to provide a positive pressure at the start of panel intake to offset the pressure lost in the past airways. To achieve the positive pressure, an auxiliary fan and several ventilation control devices are required, refer Figure 6.30 which is a possible deployment plan to pressurise LW22307. At the start of the panel intake, an auxiliary fan is installed at one LW22308 recovery roadway and a ventilation regulator is installed at one cut-through between LW22306 maingate and LW22307 tailgate to adjust the pressure and airflow. The ventilation regulator is essentially a ventilation door with adjustable opening. Figure 6.31shows the pressure loss trend along ventilation path with varying resistance factor and fan duty. It is noticeable pressurising LW22307 working face would considerably reduce pressure differential and in addition, ideally true balance could be acquired by adjusting the resistance factor or fan duty. Figure 6.32shows pressure differential and airflow quantity across LW222307 with varying resistance factor (R) and auxiliary fan duty (F). It is obvious airflow quantity across LW22307 would increase with more powerful fan and/or less resistance from ventilation regulator. The pressure differential evolves from negative to positive with more powerful fan and/or more resistance from ventilation regulator and therefore ideally a neutral point where there is no pressure differential can be extrapolated. However maintaining LW panel pressure slightly

positive is conducive to contain toxic gas within goaf hence improving working conditions at LW working face.

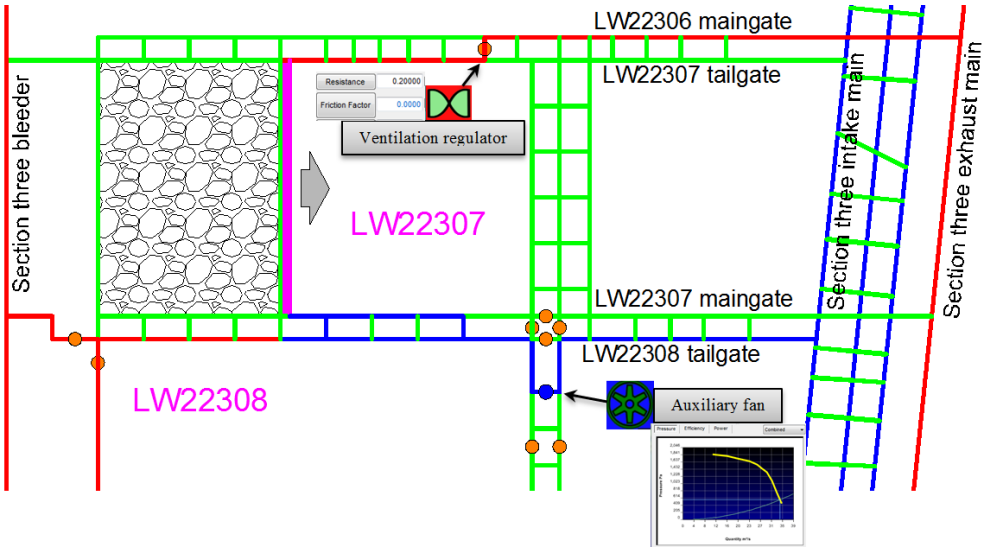

Figure 6.30 A schematic illustration of isolating LW22307 panel with positive pressure

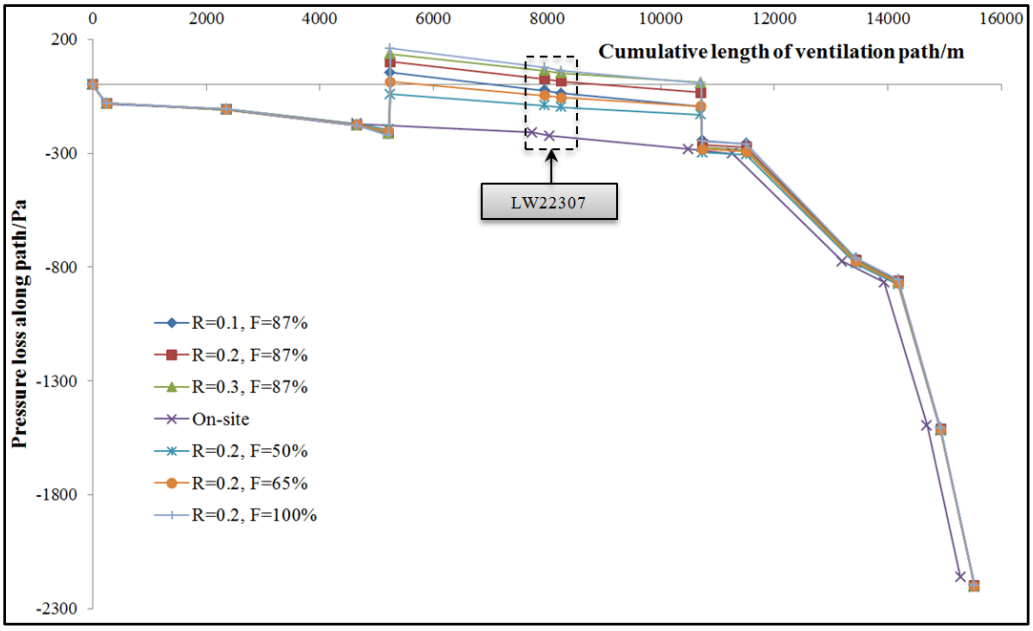

Figure 6.31 Pressure loss paths with varying resistance factors and auxiliary fan duties

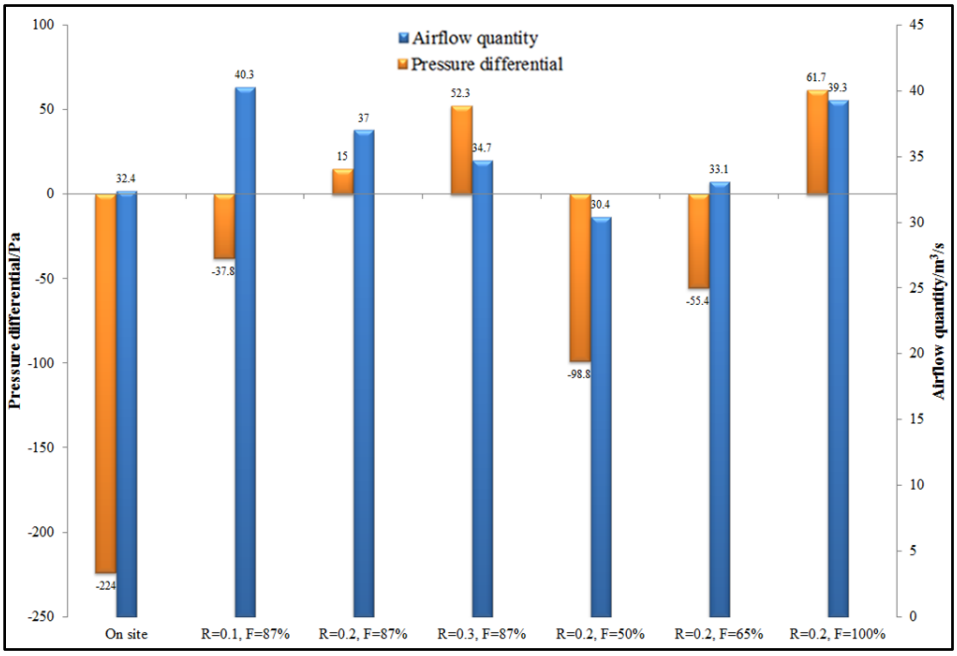

Figure 6.32 Pressure differential and airflow quantity across LW22307 with varying resistance factors and auxiliary fan duties

6.4.3 Possible solution three: a hybrid ventilation system

Rather than locally isolating and pressurising LW22307 panel, utilisation of a hybrid ventilation system (Force-Exhaust) can initially provide airflow a positive pressure to overcome the pressure loss along ventilation path before airflow arrives at LW22307 working face. The mechanism can be explained by Figure 6.33. For an exhaust ventilation system, neutral point locates at start of the intake opening and the negative pressure grows along path and peaks at fan. While for a force system, at intake fan provides airflow a positive pressure to overcome the pressure loss along path and neutral point lies at the end of the ventilation path. The hybrid ventilation system takes advantages of the two previous systems and the neutral point can be adjusted to any point in the middle of the ventilation path. By this way the pressure differential between LW workings and surface can be significantly reduced. Therefore the performance of a hybrid ventilation system is simulated with varying fan duties and the results are shown in Figure 6.34 and Figure 6.35.

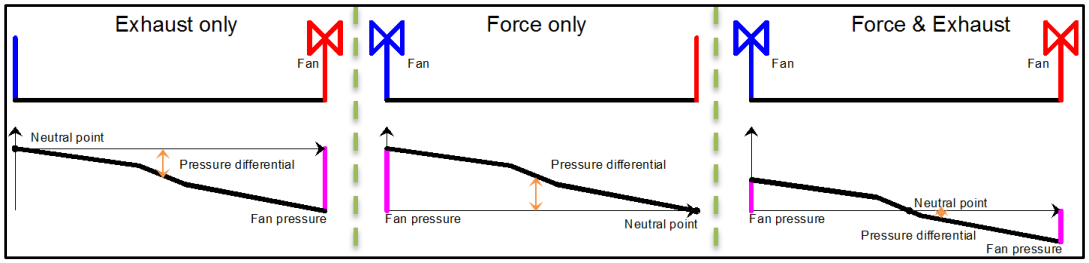

Figure 6.33 A schematic view of pressure loss along path of three ventilation systems

A forcing fan with similar capacity is installed at intake incline and several other openings are regulated with air locks by increasing magnitude of resistance factor. The solution is demonstrated by various duties of two fans and the result is illustrated in Figure 6.34 and Figure 6.35. From Figure 6.34 it can be observed airflow is given a positive pressure initially by the forcing fan to offset the pressure loss along path. The pressure differential is significantly decreased if fan dust is adjusted properly. The neutral point can move to any point by manipulating fan duties. As can be seen in Figure 6.35, it is quite obvious the airflow quantity reduces slightly with fan duty dropping but the pressure differential is very sensitive to fan duty. Ten percent alteration of fan duty may have dramatically changed the pressure differential across LW workings.

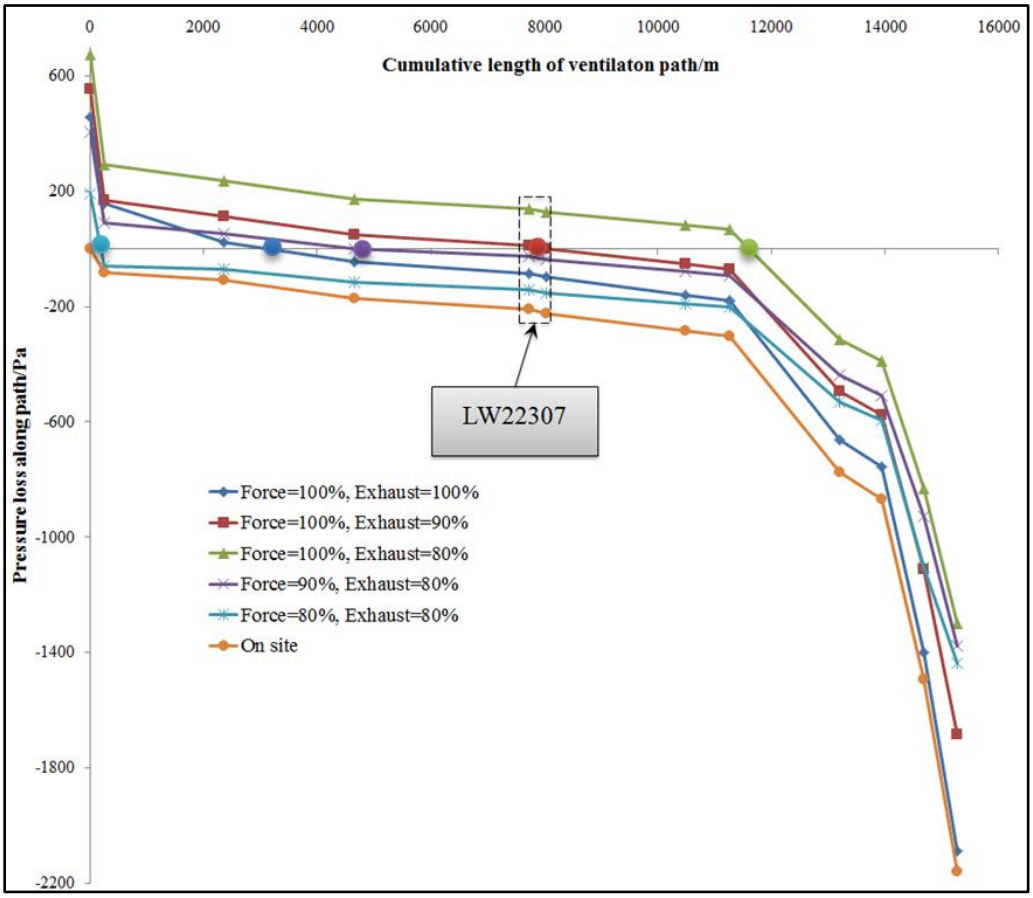

Figure 6.34 Pressure loss paths with varying fan duties of the hybrid ventilation system

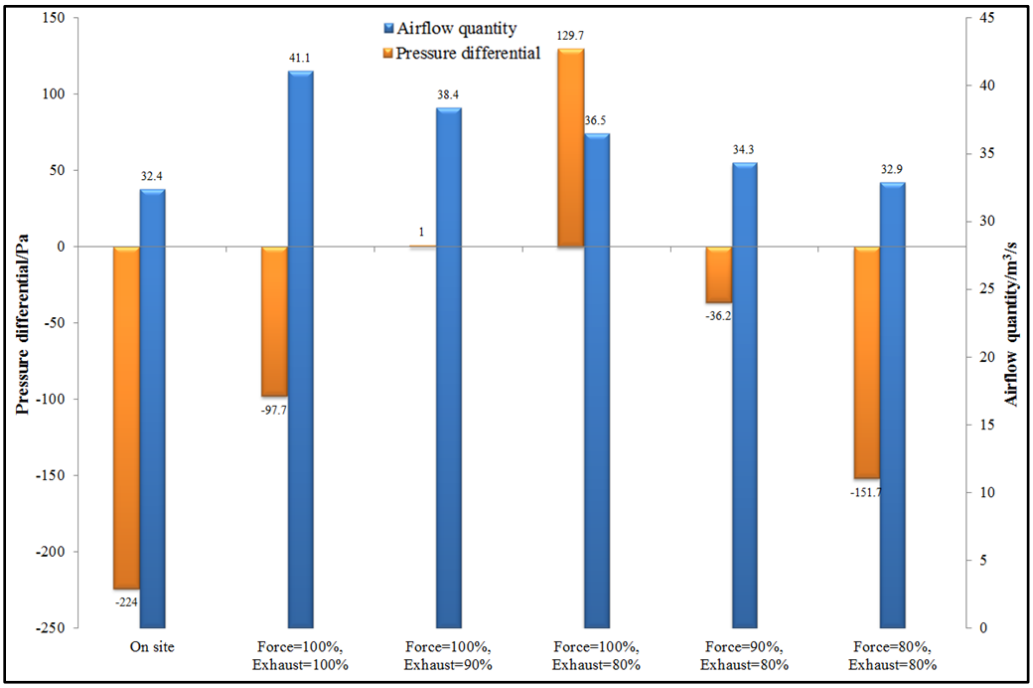

Figure 6.35 Pressure differential and airflow quantity across LW22307 with varying fan duties of the hybrid ventilation system

6.4.4 Discussion

If whole mine ventilation mode is governed by only exhausting or forcing system, the pressure differential would not be eliminated no matter how the network is modified. “Bleederless” ventilation mode may improve the problem but increase difficulty of ventilation and may cause even more pressure differential at other return airways. Hence solution one is not suitable at least for long term operation. Pressurising LW panel can tackle both the problems: sufficient air supply and less pressure differential at LW workings. The two parameters are adjustable with varying auxiliary fan duty and resistance factor of ventilation control device. The major flaw of this method is: in case auxiliary fan fails, goaf toxic gas would migrate instantly to working face and pose a great danger to working crew. Therefore extra precautions and sufficient risk assessments must be put in place before the implementation of this solution. With more and more LWs trending to be operated in underlying coal seams, a hybrid ventilation system may find its rationale because it is less complex than locally isolating and pressurising a LW panel. In addition this system has fewer disturbances to production operation comparing to balancing pressure differential of LW panel one by one. However additional capital and operational cost is incurred by installing and running extra fans and in addition, all mine accesses need to install airlocks or conveyor seals. For an on-going LW operation in multi-seam, pressurising LW panel might be a better option to minimise pressure differential and air leakage to goaf. A hybrid ventilation system should receive more considerations upon planning an underground mining operation as this system has less interference to production operations.

6.5 Field demonstration

LW22307 of Bulianta colliery commenced the operation at July, 2014. Initially the ventilation mode used within the panel is purely exhausting and no measures have been taken to mitigate potential fire occurrence although a fire incidence has occurred in adjacent goaf. With the detection of several possible self-heating developments and growing severity of ingress of oxygen deficient gas into working face, the mine determined to pressurise the LW panel (solution two) to reduce the air leakage at the end of 2014. After reviewing the failure modes and conducting risk assessments, an auxiliary fan was employed to provide the positive pressure and

associated ventilation regulators were also constructed to adjust the pressure and airflow across working face, refer Figure 6.30. Quantity of air leakage and gas composition at LW workings was continually monitored after excising this control measure. As can be seen from Figure 6.36, quantity of airflow across working face underwent a slight growth and the airflow leakage from goaf was substantially reduced after balancing the pressure differential. Figure 6.37shows gas monitoring data of a sampling point at conjunction of working face and LW22307 tailgate. The oxygen concentration increased considerably and an inverse trend was found for the nitrogen concentration. Goaf gas ingress was constrained and the working conditions were greatly improved after the control was exercised. Therefore locally pressurising LW panel is concluded as an effective measure to control pressure differential and spontaneous combustion hazard for an on-going LW operation with exhausting ventilation system.

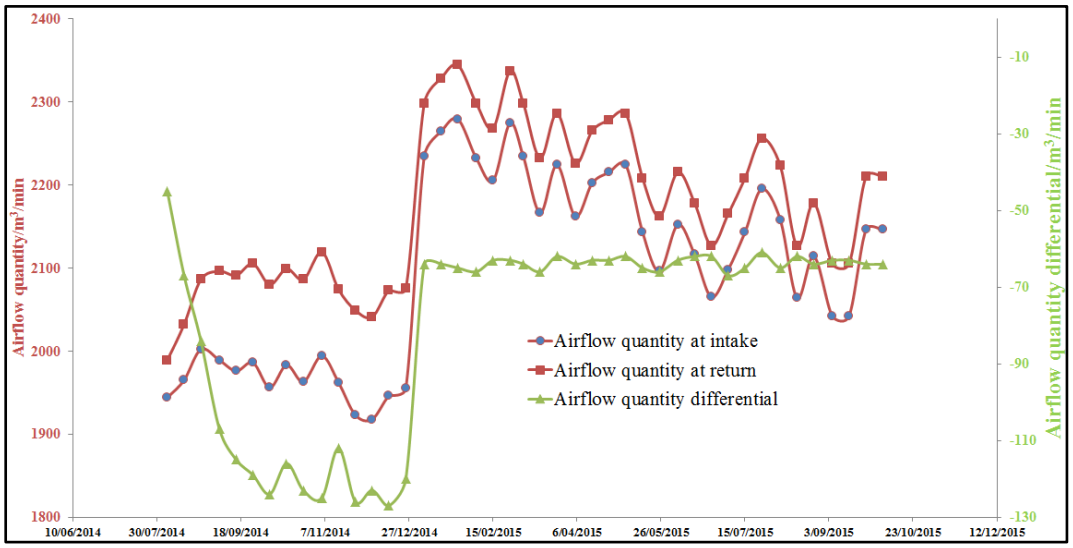

Figure 6.36 Comparison of airflow leakage before and after pressurising LW22307 at Bulianta colliery

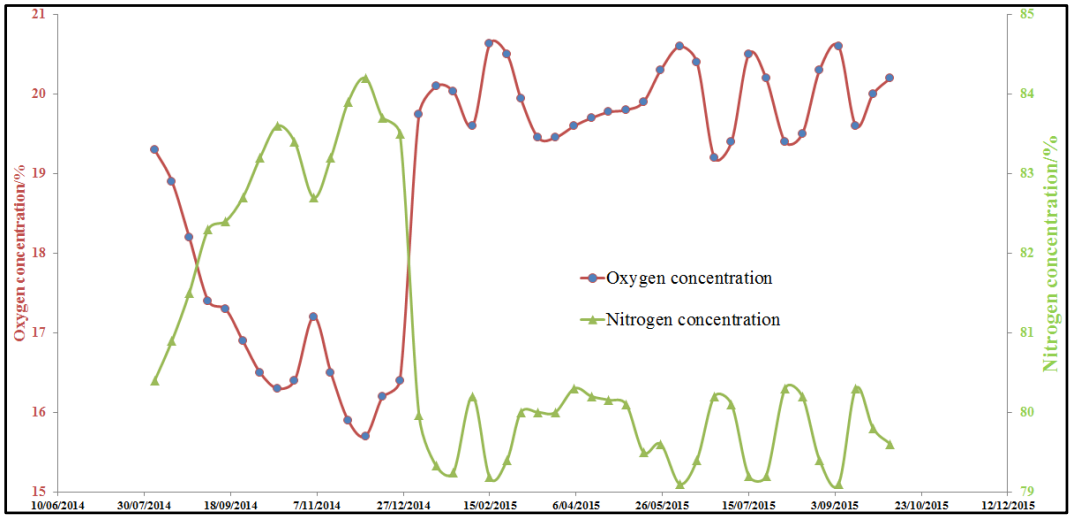

Figure 6.37 Comparison of oxygen and nitrogen concentration at conjunction of LW and return before and after pressurising LW22307 at Bulianta colliery

As this mine is an on-going operation, the large ventilation system is unlikely to be changed during extraction of LW22307 panel. Therefore, demonstration of solution three in Bulianta colliery is impossible to be accomplished. However, this method has been successfully used in a LW operation in Hunter Valley, Australia [27]. This coal mine is also operated in multi-seam and shallow cover, which resembles the LW operation in Bulianta colliery. Hence if LWs are operating under alike conditions (shallow cover or multiple coal seams which are closely distributed), a hybrid ventilation system could be a better solution as it is less complex and more flexible to adjust the neutral point. Clearly this requires more demonstrations and field trials to benchmark the solution.

6.6 Summary

Spontaneous combustion of residual coal in LW goaf is a serious hazard which causes loss of mine assets and poses a threat to underground working crew. If LWs are operating in multi-seam and under shallow cover, overlying strata undergoes multi-destruction and mining-induced cracks may propagate to surface. It is also very likely these channels become interconnected and function as air leakage path due to presence of pressure differential between LW workings and surface. Fresh air leakage into goaf aggravates the spontaneous combustion issue and adversely promotes the migration of goaf toxic gas into LW workings. To quantitatively study this issue and to investigate it with more details, a ventilation simulation package "Ventsim" is used to undertake a case study. The case scenario is selected based on

Bulianta colliery which is a very representative LW operation in multi-seam and under shallow cover in China. After development and calibration of the base model, three solutions are proposed attempting to mitigate the pressure differential issue. A few findings are listed:

- Pressure differential between LW workings and surface is an intrinsic flaw if a purely exhausting ventilation system is used in a mine. The pressure differential is not able to be eliminated no matter how the ventilation circuit is modified.
- Isolating and pressurising active LW panel can provide working face sufficient amount of fresh airflow and meanwhile reduce pressure differential. This is accomplished by deployment of an auxiliary fan and several ventilation regulators. Ideally the pressure differential can be removed if the resistance factors of ventilation control devices and duty of auxiliary fan are adjusted properly. This solution was justified in Bulianta colliery.
- Extra precautions and sufficient risk assessments must be put in place before locally pressurising LW panel because a large amount of goaf toxic gas would instantly strike working face and pose a great danger to working crew in case auxiliary fan fails. This solution is more suitable to an on-going LW operation.
- A hybrid ventilation system (Force-Exhaust) can also reduce the pressure differential by adjusting duties of the two main fans. Theoretically the neutral point can be distributed any location along the pressure loss path by manipulating performances of two fans. The solution has been demonstrated in a LW operation in Australia.
- The hybrid ventilation solution is more recommended for LW operations in planning as this system has fewer disturbances to production operation comparing to solution two. However additional capital and operational cost is imposed by installing and running extra fans and in addition, all mine accesses need to install ventilation control devices.
- No doubt ventilation simulation is a powerful tool to study spontaneous combustion issues in underground coal mines.

7 CFD MODELLING OF SELF-HEATING ON MULTIPLE COAL STOCKPILES CONSTRUCTEDIN ADJACENT

7.1 Chapter Introduction

A number of large open cut coal mining operations in Queensland of Australia are expected to commence in the near future. High volume of coal requires temporarily stored as one or multiple stockpiles in a storage yard of a coal mine site or a port before they can be transported to other destinations. Coal, as a carbonaceous material, is able to be oxidised and to liberate heat at ambient temperature with the presence of oxygen rich air [7, 9, 17, 283]. Self-heating of coal stockpile will occur if the heat generated by coal oxidation is not adequately dissipated. The accumulated heat will result in a slow rising of temperature at the initial stage of coal oxidation. Once the temperature reaches a critical value which was widely reported to be 60~120^{o}C, thermal runaway would occur and the self-heating rate of coal is very likely to take off in a relatively short period of time[3, 26, 174, 175, 284-286]. Therefore low-temperature coal oxidation is a very critical stage with concern of preventing coal spontaneous combustion. Self-heating of coal in stockpiles has long been regarded as a safety concern and additionally, pre-oxidation of coal would incur considerable loss of coal calorific value and seriously affect caking property [33, 38, 39]. More recently the liberation of large amounts of greenhouse-relevant gases and hazardous substances, such as arsenic, mercury, and lead from coal stockpile combustion or oxidation has raised considerable concerns from global communities [41, 42, 44, 287]. Despite the long history of the problem, it has also been accepted that the physical and chemical processes responsible for this problem is extremely complex[33]. Derivation of an analytical solution to the problem would be a formidable or even impossible task and consequently, the problem is often addressed numerically. Prior to the availability of high performance fluid-thermodynamics computation code, several preliminary mathematical models have been developed to investigate the issue numerically [50-64]. These studies provided valuable insights into this problem but the accuracy and applicability is questioned because these models were derived with many simplifications and limitations.

To date with the advance of Computational Fluid Dynamics (CFD) modelling techniques, predictable interpretation of self-heating of piled carbonaceous material within reasonable engineering accuracy becomes more approachable [24, 26, 35, 38, 72, 73, 97, 98, 104, 115]. Among these works, numerical solutions to self-heating of coal stockpile usually only deal with a single coal stockpile scenario but practically, multiple stockpiles are probably required to be stacked in storage yard of a coal mine or a port to increase storage capacity. Coal stockpiles stacked in these places may be subject to long period of exposure of wind flow which has been demonstrated to have significant influences on self-heating behaviour of stockpiled coal [26, 35, 97]. Therefore self-heating behavior of multiple stockpiles which are packed in proximity requires to be studied especially at low temperature range with prevailing wind conditions. The purpose of this work is to investigate the low-temperature self-heating characteristics of multiple coal stockpiles under wind flow condition and with validation, to perform variable analysis to gain more understandings of the problem in multi-stockpile scenario.

7.2 Brief mechanism of spontaneous heating of coal stockpile

A coal stockpile is essentially a porous medium consisting of heterogeneous coal particles and the voids between coal pellets are filled with mixture of fresh air and gaseous products liberated by coal oxidation. Interaction of coal with oxygen including coal oxidation and oxygen adsorption at low temperature is exothermic as a whole although it could be endothermic at some steps [17, 22]. Several studies demonstrated that the interaction of coal with water like wetting can also generate heat and it reaches to a general consensus that moisture exhibits either promoting or inhibiting effects on coal oxidation rate but fundamental mechanism especially to a kinetic sense is scarce [17, 215-217, 288]. As chemical effects of moisture were not understood completely, a few numerical models were developed to investigate only physical effect of moisture on self-heating of coal stockpile and it was indicated interaction of coal with moisture is an efficient heat transfer mechanism in which the vaporisation and diffusion of water from a hot region, followed by condensation in a cooler region, is accompanied by a considerably higher effective rate of heat transfer than that which can occur by conduction alone [52, 57, 75, 115]. The efficient heat transfer mechanism was also termed as “heat pipe” effect in some literatures and the

“heat pipe” effect usually manifested itself by leading to a levelling of temperature (80~90^{o}C) in a coal stockpile [52, 57]. It was also reported the heat generated by coal oxidation would dominate with progressive drying of coal and hence it is safe to argue that the major heat generation mechanism responsible for self-heating is coal oxidation[33]. Therefore it is plausible to ignore effects of moisture within temperature ranges below the levelling temperature exerted by “heat pipe” effect.

The generated heat is transported into and out of the stockpile by conduction, convection, and radiation. If the rate of heat generation is greater than the rate at which heat can be dissipated in the external environment, it will lead to localised temperature rise and even smouldering/open flame for a long run. Heat conduction occurs between gas-to-gas, gas-to-coal, and coal-to-coal. The low thermal conductivity of coal is the main reason why thermal energy can be well contained in the deep stockpile and cause temperature rising. Heat convection occurs between coal to gas and the efficiency of heat convection is mainly determined by velocity of gas advection within inter-particle channels. Whilst heat radiation could be a major contributor in the surface of stockpile because of solar energy it absorbed but in deep stockpile heat radiation can be negligible [74].

The air stream inside of stockpile can be constantly replaced through wind advection and diffusion caused by oxygen consumption of coal because oxygen consumption reduced the concentration resulting in diffusion if reaction rate is not the same everywhere. Convective movement can be caused by both natural convection and forced convection due to presence of pressure gradient and it has been indicated airflow driven be pressure gradient is a major transport mechanism in porous coal [76]. Diffusive movement is also capable of dispersing gas molecules in or out of coal intra-particle pores. Irrespective of complex pore structure of coal, this study adopts a global surface reaction mechanism so gas transport mechanism in micro-structures like gas diffusion into inner pores is not considered. Besides the main features described above, self-heating process of coal stockpile is also affected by exterior conditions through wind, rain, snow, ambient temperature and solar radiation[33]. Due to the extremely irregularity of meteorological conditions, effects of extrinsic factors except for wind flow are not scope of this study.

7.3 The mathematical model

On basis of the mechanistic understanding of self-heating of coal stockpile, the core constituents of the mathematical model should include description of low-temperature coal oxidation kinetics, energy conservation, species transport, momentum balance and continuity equations for fluid flow in porous medium. For the simplicity of the solution, terms of heat radiation and effect of moisture are not included in the model.

7.3.1 Low-temperature coal oxidation kinetics

The most intriguing puzzle would be the low-temperature interaction of coal with oxygen because of complex nature of coal. Despite of the mechanism of coal oxidation having not been completely solved, briefly two parallel interaction sequences were identified: one is direct burn-off and another one is adsorption sequence[17]. Solid and gaseous products are also concomitant during the two sequences and details of them are omitted here. To define coal-oxygen reaction rate with elevated temperature to a mathematical sense, a simple finite rate Arrhenius reaction mechanism is often used[24, 26, 72, 97, 98, 104], which is given,

$$r = A[C_{\mathrm{o}}]^{n}\exp(-E_{\mathrm{a}}/RT) \tag{7.1}$$

It is assumed that oxygen can penetrate throughout the coal without diffusional limitation and the reaction mechanism between gas and solid phases is deemed as a homogenous gas phase reaction [3]. The value of the reaction order in low temperature oxidation of coal and other carbonaceous materials has been indicated to vary from 0.5 to 1 [33, 75]. This model approximates first order of coal oxidation. It has also been reported that the value of apparent activation energy of different coals can vary between 12 and 95 kJ/mol [24] and more specific values of activation energy for low temperature coal oxidation can be found in the review work conducted by Wang and co-workers [17]. Taraba and Michalec [104] discussed the pre-exponential factor is of the greatest uncertainty giving ordinarily values differing over several orders and another study also indicated the pre-exponential factor has a typical value between 1 and 7×10^{5}/s [72]. It can be also seen the rate of coal oxidation is not only affected by the Arrhenius constants but also by partial pressure of oxygen at a given reaction order and temperature. Therefore any solid coal-oxygen complex produced during low-temperature coal oxidation would not affect

the rate of oxidation if Arrhenius-rate reaction mechanism is assumed. Based on experimental data, Yuan and Smith [24, 72]generalised that consuming one mole of oxygen by coal would generate one mole carbon dioxide and roughly 0.1 mole carbon monoxide plus heat at the early stage of coal oxidation, which yields a very simplified stoichiometric scheme of low-temperature coal oxidation:

$$\mathrm{Coal} + \mathrm{O_2} \rightarrow \mathrm{CO_2} + 0.1\mathrm{CO} + \mathrm{Heat} \tag{7.2}$$

This model also employs this coal oxidation reaction scheme at low temperature range. Kaji *et al*. [9] measured the rates of heat liberation and oxygen consumption due to coal oxidation at low temperature range using coals ranging from subbituminous to anthracite and 300~379kJ heat evolved per mole of oxygen at steady state was reported. Many works [24, 54, 59, 60, 98] used 300 kJ/mol oxygen as coal oxidation reaction heat so this model also uses such a value as reaction heat at low temperature range.

7.3.2 Energy conservation

Normally heat of chemical reaction is liberated due to variation of enthalpy between reactants and products. It is usually the case when modeling extremely drastic reaction like fuel combustion. Coal oxidation rate at low-temperature is however very slow and therefore the heat generated by coal oxidation is modeled as a source term and written as a User Defined Function (UDF). To be more realistic to describe heat interaction inside coal stockpile, heat transfer between coal particles should be treated in a non-equilibrium approach. The temperature differential between the solid coal particle and gas stream is important in the thermal behaviour and it is thus necessary to represent the energy stored in each individual phase as well as the exchange of thermal energy between them, which gives energy conservation for solid coal pellet:

$$(1-\varepsilon)\rho_{\mathrm{c}} C_{\mathrm{pc}} \frac{\partial T_{\mathrm{c}}}{\partial t} = (1-\varepsilon)\lambda_{\mathrm{c}} \nabla^2 T_{\mathrm{c}} + \frac{6(1-\varepsilon)}{d\varepsilon} h\left(T_{\mathrm{g}} - T_{\mathrm{c}}\right) + r\Delta H \tag{7.3}$$

In which the successive terms represent internal energy growth of coal particle, heat diffusion in solid coal, heat convection interacted with gas stream, and heat generated by coal oxidation which is a source term. In view of temperature variation is not significant in low-temperature self-heating of coal stockpile and to produce a faster convergence, many models assumed the validity of the Boussinesq approximation [26, 52, 56-58, 61]. This approximation essentially states that the

temperature variation of the fluid properties can be ignored except for the density, and that the density dependence is only considered when it gives rise to buoyancy convection in natural convection driven flows [33]. However Boussinesq approximation is not suggested to be used with species calculation and reacting flow involved otherwise accuracy of result is very likely to become inacceptable [289]. Therefore ideal compressible gas flow is considered and energy balance for the gas stream is written as:

$$\varepsilon \frac{\partial}{\partial t}\left(T_{\mathrm{g}} \rho_{\mathrm{g}} C_{\mathrm{pg}}\right)+\nabla\left[\vec{v}\left(T_{\mathrm{g}} \rho_{\mathrm{g}} C_{\mathrm{pg}}+P\right)\right]=\varepsilon \lambda_{\mathrm{g}} \nabla^{2} T_{\mathrm{g}}-\frac{6(1-\varepsilon)}{d \varepsilon} h\left(T_{\mathrm{g}}-T_{\mathrm{c}}\right) \tag{7.4}$$

In which the successive terms represent transient energy rise of gas stream, heat convection of gas stream, heat diffusion in gas stream, and heat convection interacted with solid coal.

7.3.3 Species conservation

Nitrogen is neither consumed nor produced during whole process of self-heating so species conservation is mainly focused on oxygen, carbon dioxide, and carbon monoxide in gas stream according to the assumed reaction scheme, which give rise to the species conservation:

$$\begin{cases} \text{For oxygen: } \varepsilon \frac{\partial\left(\rho C_{\mathrm{o}}\right)}{\partial t}+\varepsilon \nabla\left(\rho \vec{v} C_{\mathrm{o}}\right)-\nabla\left(\rho D_{\mathrm{o}} \nabla C_{\mathrm{o}}+D_{\mathrm{T,o}} \frac{\nabla T}{T}\right)+r=0 \\ \text{For carbon dioxide: } \varepsilon \frac{\partial\left(\rho C_{\mathrm{i}}\right)}{\partial t}+\varepsilon \nabla\left(\rho \vec{v} C_{\mathrm{i}}\right)-\nabla\left(\rho D_{\mathrm{i}} \nabla C_{\mathrm{i}}+D_{\mathrm{T,i}} \frac{\nabla T}{T}\right)-r=0 \\ \text{For carbon monoxide: } \varepsilon \frac{\partial\left(\rho C_{\mathrm{j}}\right)}{\partial t}+\varepsilon \nabla\left(\rho \vec{v} C_{\mathrm{j}}\right)-\nabla\left(\rho D_{\mathrm{j}} \nabla C_{\mathrm{j}}+D_{\mathrm{T,j}} \frac{\nabla T}{T}\right)-0.1 r=0 \end{cases} \tag{7.5}$$

In which the successive terms represent the local accumulation of species, the convective transport of species, the diffusion term of species caused by variation of species concentration and temperature, and the fraction consumed or produced by coal oxidation.

7.3.4 Momentum balance in porous medium

Navier-Stokes equation is normally used to describe momentum balance for compressible flow as density of fluid varies with temperature and elapsing of time in this case. Revise Navier-Stokes equation by adding viscous term (last term in Equation 6) to solve flow momentum balance in porous stockpile, which produces:

$$\frac{\partial}{\partial t}\left(\rho_{\mathrm{g}} \vec{v}\right)+\nabla\left(\rho_{\mathrm{g}} \vec{v} \vec{v}\right)=-\nabla P+\nabla(\vec{\tau})+\vec{F}-\varepsilon \frac{\mu}{k} \vec{v} \tag{7.6}$$

The permeability *k* of coal matrix is approximated by the Carmen–Kozeny equation for laminar flow in packed beds [133]:

$$k = \frac{\varepsilon^3 d^2}{150(1-\varepsilon)^2} \tag{7.7}$$

7.3.5 Continuity in porous medium

Mass change of bulk coal due to coal oxidation at low temperature is ignored. This model also assumes isotropic porous medium and therefore for single phase flow in isotropic porous medium, the continuity equation can be written as:

$$\frac{\partial \rho}{\partial t} + \nabla(\rho \vec{v}) = 0 \tag{7.8}$$

7.4 Numerical modelling and validation

7.4.1 Numerical model

The geometry of the stockpile is considered to be a truncated pyramid. Three identical stockpiles, namely A, B, C, are constructed with a specific height & side slope and they are located within a certain distance. The length of the stockpile is 40m. The effects of wind velocity, stockpile height, side slope, porosity, and spacing will be comparatively studied. A base model is selected with details: 4m/s wind velocity, 10m high, 50^o side slope, 0.2 porosity and 20m spacing. The model consists of two domains: (i) coal stockpile is treated as porous domain and, (ii) the remaining domain is considered as a farfield representing the open space around the stockpiles. The upper and lower boundaries are deemed as adiabatic and no-slip walls. To minimize the limitation of upper wall and outlet boundaries on the flow field around the stockpile, the farfield domain must be sufficiently large. Based on the rule of thumb of large model simulation, the dimension of the farfield domain is decided to be 50m high and 400m long, referFigure 7.1.

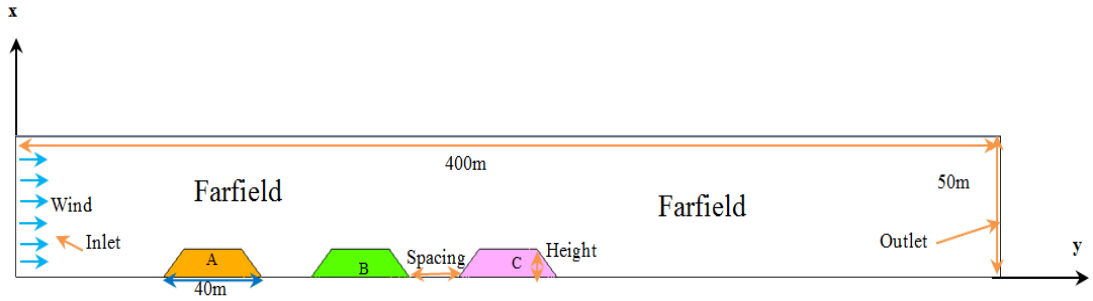

Figure 7.1 A schematic overview of the simulation

The geometries of the two domains and mesh of the model is generated via ANSYS 15.0 workbench design modeler and mesh tool, respectively. To utilize non-equilibrium thermal model in porous zone, mesh must be created in very high

standard. When activate this model, a fake solid zone which overlaps the porous fluid zone is created, and this solid zone only thermally interacts with the fluid. The discretized mesh generated for the base model via the described method is shown inFigure 7.2. Quadrilateral mesh with 1m global sizing is used to fill farfield region as show in Figure 7.2(a). As can be observed in Figure 7.2(b), down to near surface of stockpile, 40 thin layers (each layer is 0.1m thick) are inflated because this area is expected to be the preferable location of self-heating. Further deep into stockpile 0.5 m local sizing trilateral mesh is used to fill irregular region to meet high standard mesh requirement, otherwise connectivity between fluid zone and fake solid zone will result in immediate error once non-equilibrium thermal model is activated.

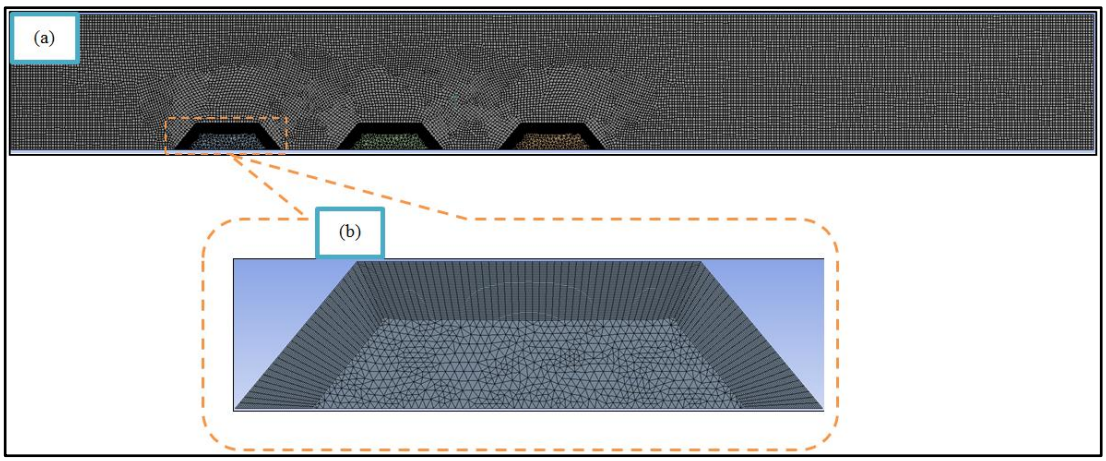

Figure 7.2 Mesh used in the simulation: (a) an overview; (b) a close-up view of stockpile A

Inlet wind profile is modelled as wind power law (refer Equation 7.9), which essentially states wind velocity progressively approaches to zero at ground surface. Wind velocity of any height can be determined via wind velocity at a reference height. In this study reference height is 10m and wind velocity refers to the wind velocity at reference height. Wind velocity profile of the farfield of the base model is shown in Figure 7.3, from which it can be observed that wind velocity at inlet varies with the proposed power law.

$$V = V_{\mathrm{R}} \left(\frac{H}{H_{\mathrm{R}}}\right)^{1/7} \tag{7.9}$$

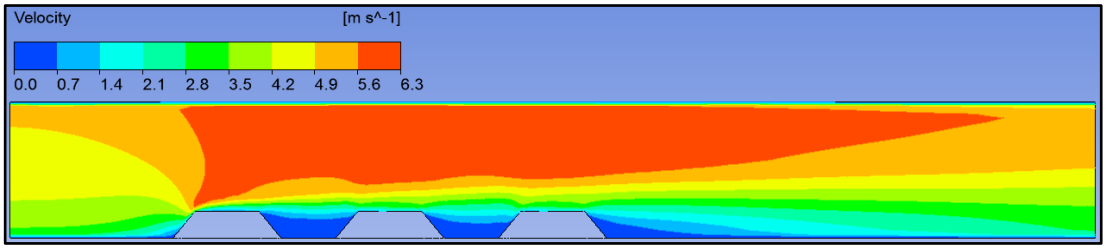

Figure 7.3 Wind velocity contour of the farfield of the base model

Wind stream is considered to be fully turbulent in farfield and thus is solved by Fluent RNG k-ε model. To suppress turbulent viscosity in porous stockpile, laminar zone option is enabled. Many works [24, 26, 53, 54, 56-58, 61, 73, 115] have also suggested natural convection is also a possible mechanism of oxygen transport so full buoyancy effect is also activated in this model. Like previous works conducted by Yuan and Smith [24, 72], two-step simulation approach is used: (i) a simulation is conducted firstly without turning on chemical reaction and heat source to obtain a steady flow in the farfield and stockpiles; (ii) the transient simulations with surface wall reaction and heat source are conducted using the steady flow field as the initial conditions.As substantial coal adiabatic testing data indicated the temperature of coal would take off after 70^{o}C [174, 175, 285] and therefore 363K is considered as the critical temperature because ambient temperature is assumed as 293K in this study. The simulation terminates once maximum temperature of any of the three stockpiles reaches 363K or alternatively, it stops running till 90days to save computation load. Important input parameters of the model are listed as Table 7.1in which low-temperature coal oxidation kinetic parameters are derived from Taraba's model [97]. The initial and boundary conditions for the model are also tabulated in Table 7.2 in which it should be noted that the initial conditions are listed in terms of steady flow field.

Table 7.1 Important input parameters in this model

Specific heat capacity of coal	1300	J kg^{-1} K^{-1}
Apparent activation energy	22	kJ mol^{-1}
Heat of coal oxidation	300	kJ mol^{-1} O_2
Apparent order of reaction	1	
Arrhenius pre-exponential factor	1.8	s^{-1}
Gravitational acceleration	9.8	m s^{-2}
Diameter of coal particle	1	cm
Heat transfer coefficient	3	W m^{-2} K^{-1}
Density of coal	1400	kg m^{-3}
Thermal conductivity of coal	0.2	W m^{-1} K^{-1}

Table 7.2 Initial and boundary conditions employed in this model

Condition		Gas flow	O_2 transport	CO_2 transport	CO transport	Temperature
Initial conditions		V=0 (m/s)	C_o=0	C_i=0	C_j=0	293K
Boundary conditions	Inlet (x=0)	Velocity inlet	C_o=0.23 (mass fraction)	C_i=0	C_j=0	293K
	Upper wall (y=50)	No flux	No flux	No flux	No flux	Adiabatic
	Lower wall (y=0)	No flux	No flux	No flux	No flux	Adiabatic
	Interface	Convection flux	Diffusion and convection flux	Diffusion and convection flux	Diffusion and convection flux	Conduction and convection
	Outlet (x=400)	Outflow	-	-	-	-

7.4.2 Model validation

This model is validated using published data [24, 35, 97]. To validate the model in more details, an additional model with similar geometric parameters to Taraba's model [97] is established, refer Figure 7.4(a). Moghtaderi *et al.* [35] and Taraba *et al.* [97] both reported that a wake region was induced right after wind passes a stockpile. This model also identifies this wake region. In addition they also suggested the greatest pressure is exerted on the front face of the pile (windward side) with a marked drop in pressure at the top of the pile before leveling off.This quantity of pressure drop is presented in non-dimensional term using the concept of a pressure coefficient [290]. The pressure coefficient, φ, is defined via

$$\varphi = \frac{2(P-P_{\mathrm{R}})}{\rho_{\mathrm{a}} V^2} \tag{7.10}$$

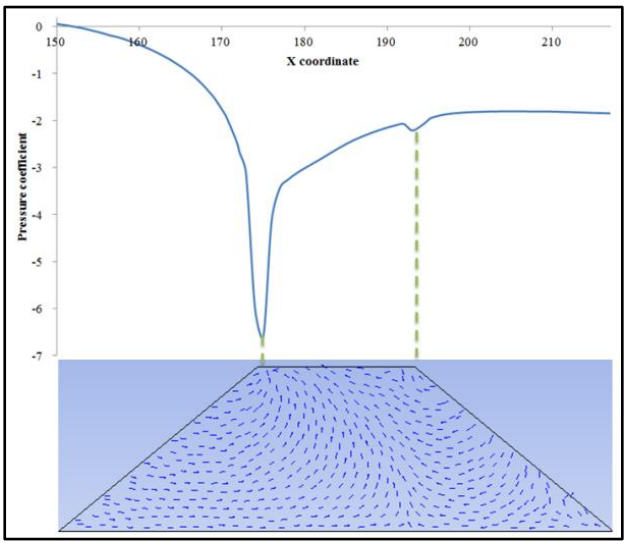

(a)Validation model

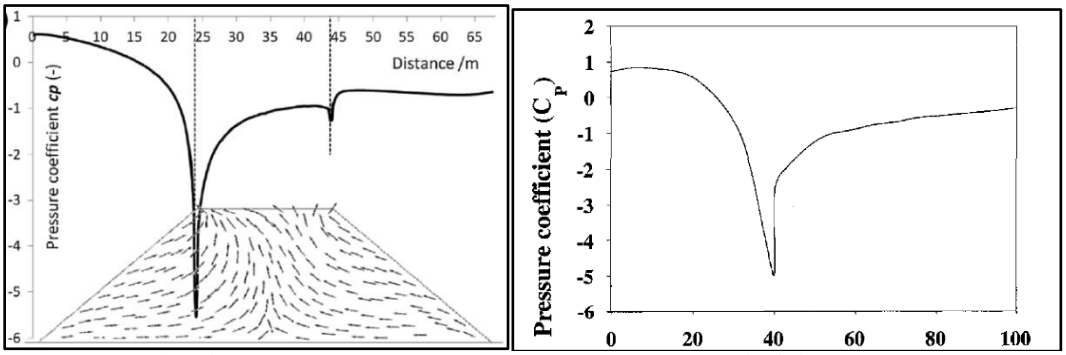

(b)Taraba's model [97] (c)Moghtaderi's model [35]

Figure 7.4 The variation of the pressure coefficient around stockpile

Figure 7.4(a) shows the distribution of the pressure coefficient around the validation stockpile at 4m/s wind velocity. As can be seen, the shape of the pressure coefficient curve of this model is very similar to those reported by Moghtaderi *et al.* [35] and Taraba *et al.* [97] and the characteristic movement of interior vectors also resembles Taraba's model. Hence it is possible to be deemed that flow field produced by the proposed model is viable.

To examine validity of transient temperature rising of the model, an appropriate time step must be selected. Yuan and Smith [24] used one minute time step to simulate self-heating of coalbed and the result was validated by real experimental data in a testing chamber. Based on the previous experience, various time steps (30 seconds, one minute, two minutes, five minutes, and one hour) are studied in this model. It is reconfirmed one minute time step would produce a rational result without incurring too much computation load. In addition various meshing sizes are studied and the mesh independence check suggests that the proposed mesh setting is able to produce a rational result. Slightly more than two thousand iterations are required to reach a convergence of the first-step steady flow field. For the subsequent transient calculation, one thousand iterations were conducted for each time step to render less residual errors for next time step and after running a few initial steps the result reaches convergence for all the remaining time steps. Figure 7.5 shows the comparison of maximum temperature rising profile between Taraba's model and the validation model at low-temperature range. It is found the two models report alike and almost linear maximum temperature rising rate at low temperature range. The validation model indicates a slightly slower temperature rising rate and the difference might attribute to the non-equilibrium thermal approach and slightly

different model setting. In this regard the model is considered to be robust and viable in simulating both steady wind flow field and unsteady heat transfer field.

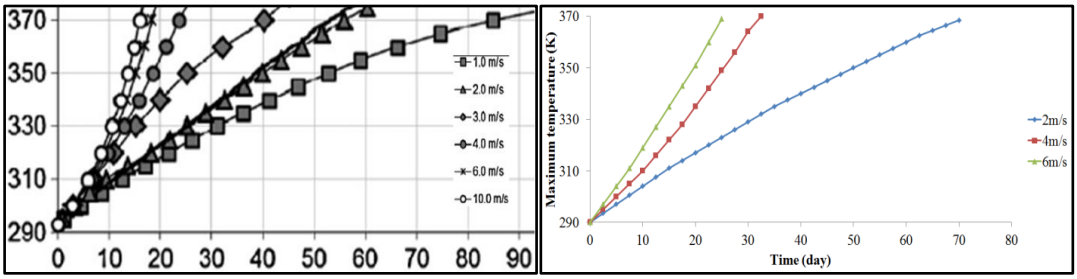

(a) Taraba's model [97] (b)Validation model

Figure 7.5 Validation of maximum temperature rising profile

7.5 Results and parametric analysis

7.5.1 Base model result

Figure 7.3has reported the wind velocity contour of farfield domain of the base model. It can be seen velocity builds up as wind encounters the first stockpile and then significantly drops after wind passes each stockpile especially at the regions between two stockpiles. It is suspected stockpile A will have the largest quantity of interior airflow than that of the other two stockpiles due to the direct confrontation to wind of stockpile A and a wake region will be induced at the leeward of each stockpile. Figure 7.6 illustrates the wind stream vector in both farfield and stockpiles. Three wake regions, namely wake region 1, 2, and 3, at the leeward of each stockpile are identified and it appears they are becoming increasingly confined. Figure 7.7 shows exterior pressure drop around the three stockpiles. It can be observed pressure drops as long as wind stream encounters or leaves a stockpile and the magnitude of the pressure drop follows the order: A>C>B. Greater pressure drop normally signifies more availability of airflow inside stockpile and it can thus be postulated the order of maximum temperature rising rate will follows the same order. To examine airflow travel path inside coal stockpile more fundamentally, interior pressure distribution must be well studied because airflow inside stockpile is greatly driven by pressure gradients. Figure 7.8 illustrates gauge pressure distribution and velocity vectors inside of the stockpiles and main air flow travel paths (dash black line) are also sketched based on the pressure gradients. In stockpile A (Figure 7.8(a)), a very low pressure zone is induced at upper-left corner of the stockpile and the largest pressure exerts at the bottom of windward side. Therefore most of the air would travel along path 1 and a hot spot is more readily to evolve along this path due

to the significant pressure gradient. Air can also migrate to stockpile along path 2a and 2b due to back flow induced by wake region 1. The low pressure zone is also able to suck air from top surface of the stockpile, which created airflow travel path 3. Hot spot hardly evolves along path 2a due to long travel distance but coal locates at path 3 and 2b can be seriously oxidised because of short travel distance. Interestingly a converged airflow is created where airflow along path 1 encounters airflow along path 2a and the phenomena was termed as "chimney" effect which was reported to be ascribed to natural convection [54] but in this case it appears the phenomena is mainly generated by forced convection. In stockpile B (Figure 7.8(b)), two slightly low pressure zones (zone A and zone B) are induced at both upper corners of the stockpile. The easiest flow path is path 1a due to more appreciable pressure gradient and shorter travelling distance and therefore hot zone is expected to develop along this path. Likewise weak airflow can transport along path 2a while moderate airflow can permeate along path 3 and 2b and coal located at these zones is likely to be deteriorated. The "chimney" effect airflow is likely to locate at centre of the stockpile due to more balanced pressure gradients present at both sides. In stockpile C (Figure 7.8(c)), the airflow behaviour resembles that of stockpile B except that the "chimney" airflow moves towards to leeward side because more appreciable pressure gradients exerted at windward side. It is postulated that location of hot spot and deteriorated coal of stockpile C is similar to that of stockpile B.

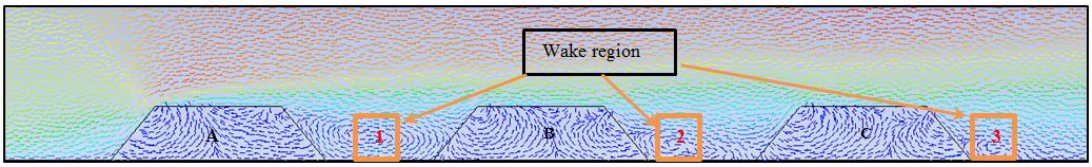

Figure 7.6 Airflow vector of the base model

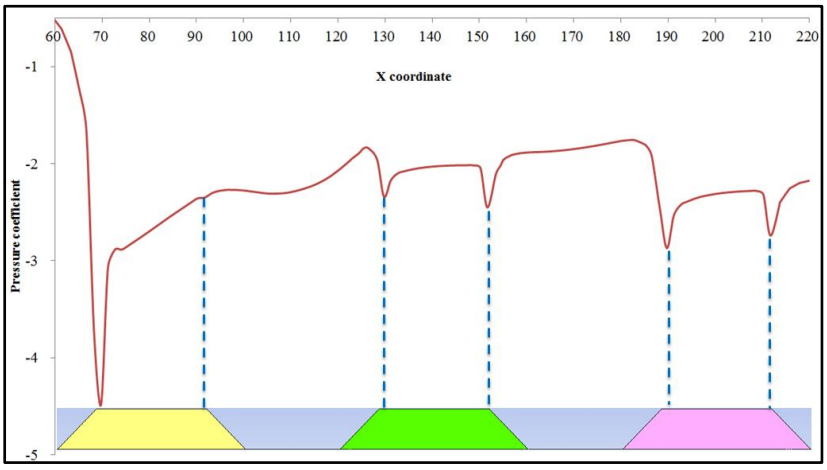

Figure 7.7 Distribution of the pressure coefficient around the three stockpiles for the base model

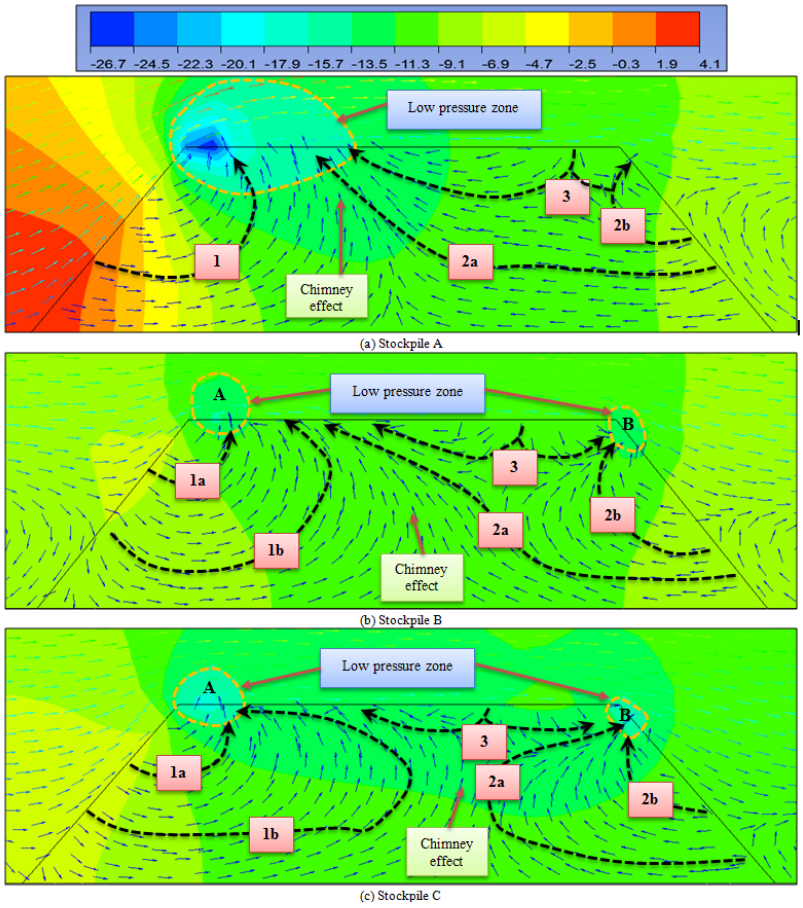

Figure 7.8 Pressure distribution and airflow travel paths inside the three stockpiles

Figure 7.9 depicts the progressive consumption of oxygen of the three stockpiles of the base model at 5, 10, 15, and 20 days respectively. There is very low concentration of oxygen in deep region of stockpiles due to the high resistance of oxygen ingress. The high oxygen concentration zone of stockpile A locates at windward side because of direct confrontation to wind. For stockpiles B and C, high oxygen ingress region favours the two upper corners which are also the low pressure zones from Figure 7.8. It is postulated self-heating hazard would develop at these high oxygen concentration zone. As can be seen from Figure 7.10, the self-heating favourable zones of the three stockpiles indeed all locates at high oxygen concentration zone and the volume of coal being oxidised of stockpile A is much larger than the other two stockpiles. The maximum temperature rising rates of the three stockpiles are also plotted, refer Figure 7.11 in which the overall trend of temperature rising rate, as predicted, is A>C>B but the rising rate of stockpile C

overlaps with that of stockpile B after 40 days as a possible result of oxygen depletion. To further examine the transport pattern of gaseous product liberated from coal oxidation inside the stockpiles, the contours of CO_2 are also captured, refer Figure 7.12. It is noticeable high concentration of this carbonic gas is retained in the interior of the stockpiles. A possible explanation is the production rate of the gaseous product outweighs its dissipation rate due to weak airflow inside of stockpiles. Additionally it can be found the highest accumulation of CO_2 develops at leeward side for stockpile A due to the insufficient dilution of weak backflow, while at windward side and beneath top for stockpile B and C, which implies the air leakage along path 1b and 3 (Figure 7.8-b, c) is not sufficiently strong to disperse the high concentration of CO_2 and the "chimney" effect would induce a high concentration of CO_2 zone beneath the top of stockpiles. Considering the emission of greenhouse effect gases contributed from low-temperature oxidation and spontaneous combustion of coal stockpile has been recently regarded as a highly concerned issue [41], the characteristic flow pattern of CO_2 dispersion and transport at exterior of stockpiles is also investigated, refer Figure 7.13. It is not hard to observe that more CO_2 is generated as self-heating of coal stockpile advances and CO_2 tends to accumulate at regions between two stockpiles. The high concentration of carbonic gases may raise another safety issue if coal operators were under exposure of such concentrated carbonic gas for a long period of time.

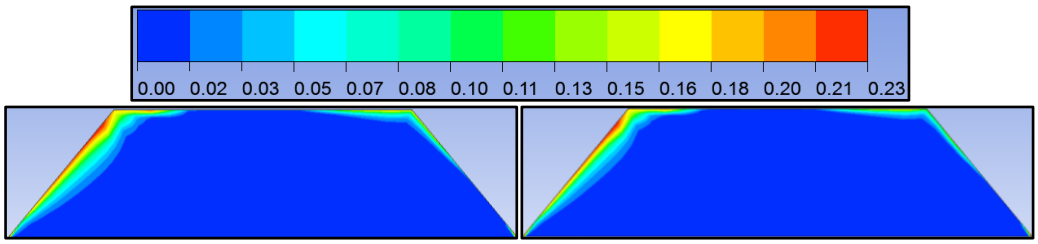

(1) 5 days (2) 10 days

(3) 15 days (4) 20 days

(a) Stockpile A

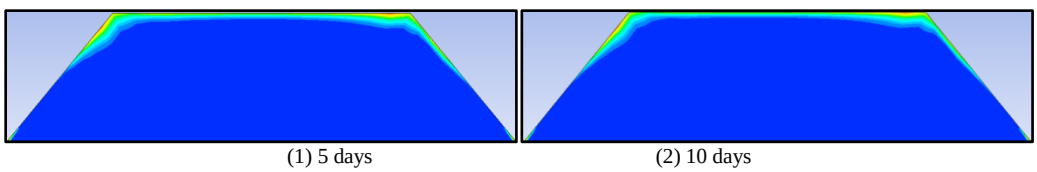

(1) 5 days (2) 10 days

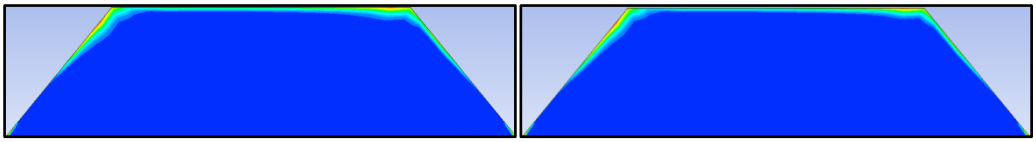

(3) 15 days (4) 20 days

(b) Stockpile B

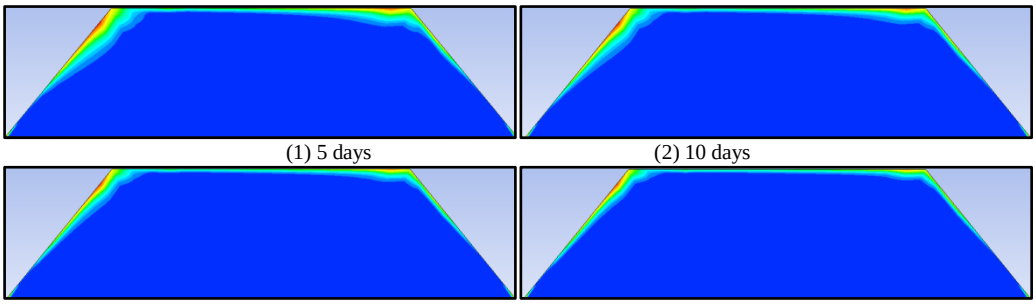

(1) 5 days (2) 10 days

(3) 15 days (4) 20 days

(c) Stockpile C

Figure 7.9 Oxygen contours (mass fraction) of three stockpiles of the base model for various periods

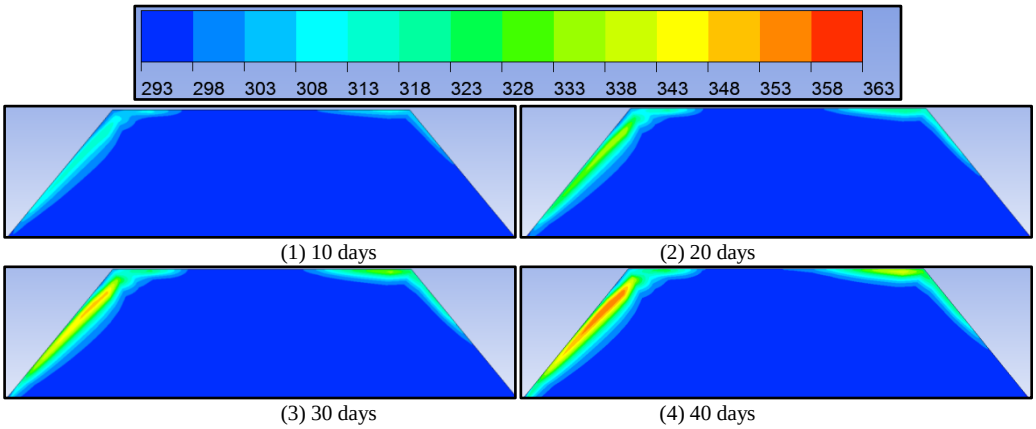

(1) 10 days (2) 20 days

(3) 30 days (4) 40 days

(a) Stockpile A

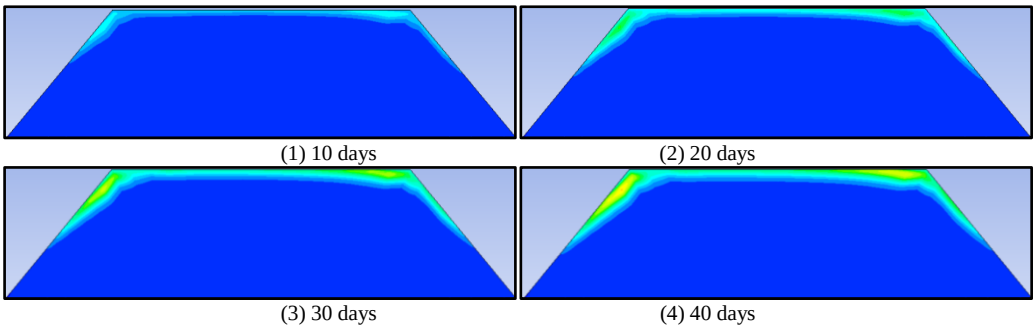

(1) 10 days (2) 20 days

(3) 30 days (4) 40 days

(b) Stockpile B

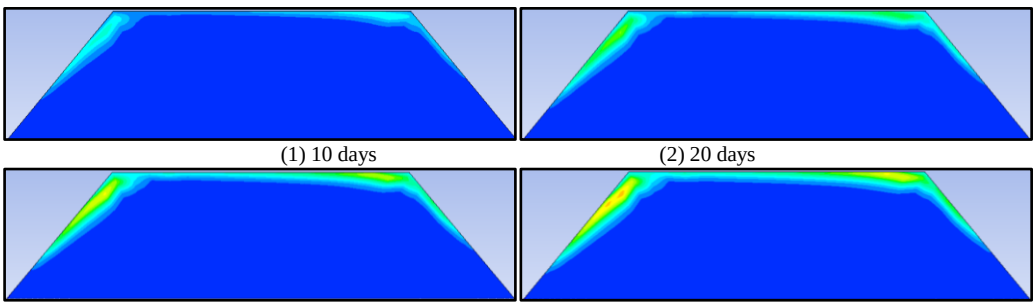

(1) 10 days (2) 20 days

(3) 30 days (4) 40 days

(c) Stockpile C

Figure 7.10 Temperature distribution of the three stockpiles of the base model after various periods

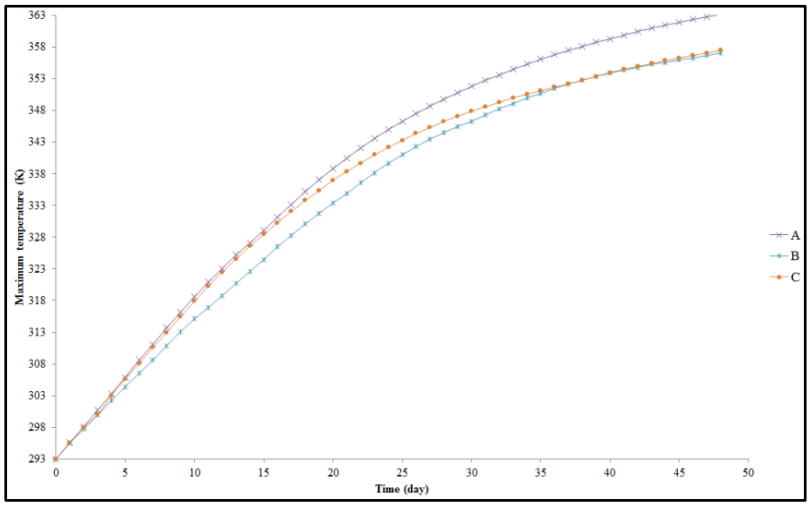

Figure 7.11 The highest temperature rising profiles of the three stockpiles of the base model

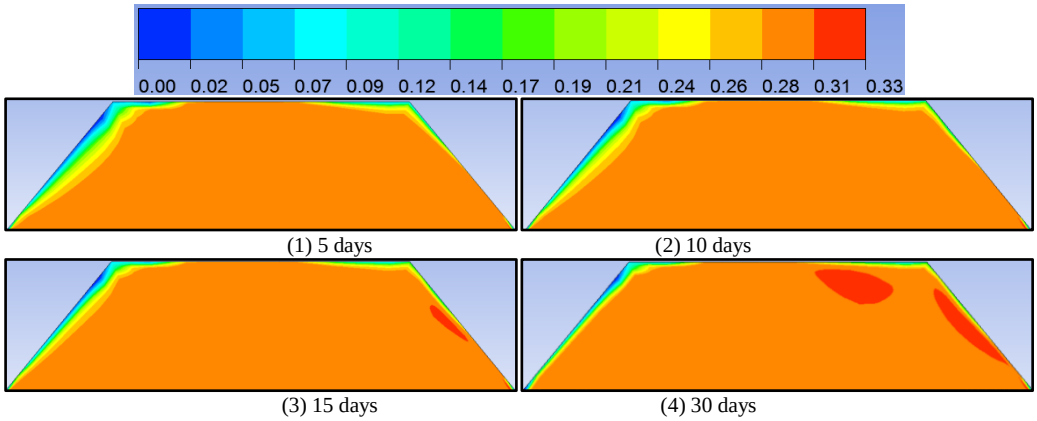

(1) 5 days (2) 10 days

(3) 15 days (4) 30 days

(a) Stockpile A

(1) 5 days (2) 10 days

(3) 15 days (4) 30 days

(b) Stockpile B

(1) 5 days (2) 10 days

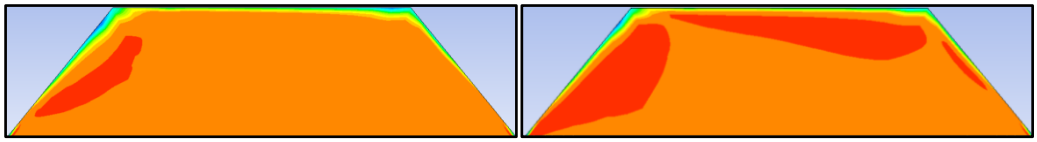

(3) 15 days (4) 30 days

(c) Stockpile C

Figure 7.12 CO_2 contours (mass fraction) of three stockpiles of the base model after various periods

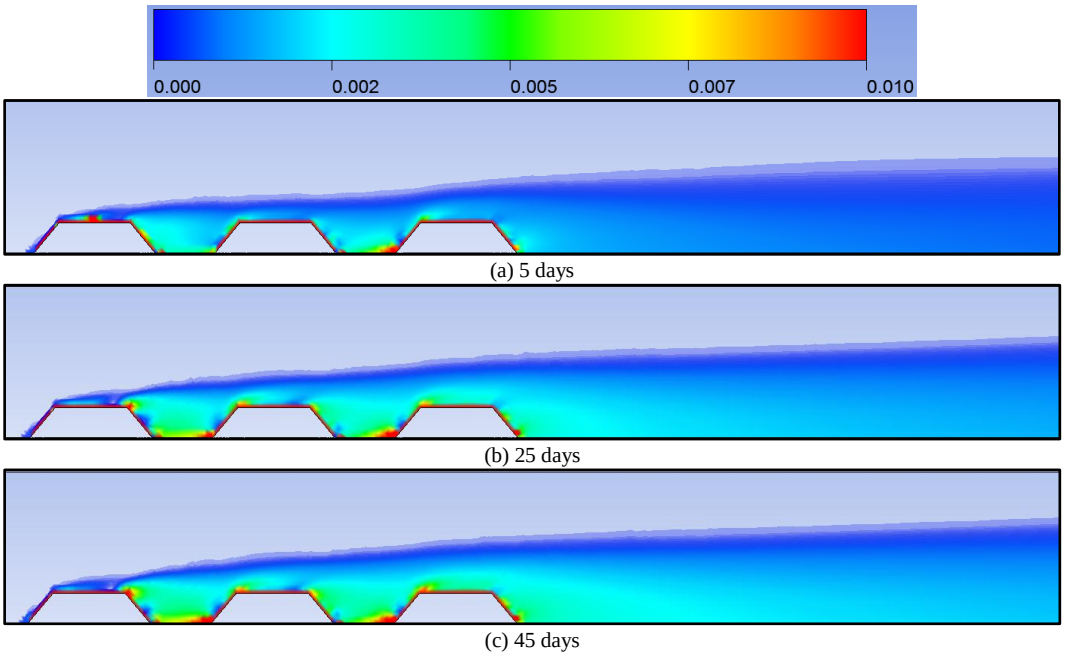

(a) 5 days

(b) 25 days

(c) 45 days

Figure 7.13 CO_2 dispersion (mass fraction) in farfield after various periods

7.5.2 Parametric study

7.5.2.1 Wind velocity

Figure 7.14 shows temperature contours of the three stockpiles after 30 days at different wind velocities and Figure 7.15 shows maximum temperature rising profiles of the three stockpiles at various wind velocities. It can be seen wind velocity has significant influences on spontaneous heating process and volume of coal being seriously oxidised of the three stockpiles especially stockpile A. Both maximum temperature rising rate and volume of deteriorated coal considerably increase ata higher wind velocity. For example, if wind velocity is as low as 2m/s, maximum temperatures of the three stockpiles are not able to reach critical value in 90 days. For the highest wind velocity 6m/s, maximum temperature of stockpile A reaches 363K in one month; whilst for medium wind velocity 4m/s, the incubation period prior to the critical temperature for stockpile A is 48 days. As previously discussed stockpile A stands like a wind barrier to stockpiles behind it, it is not surprised to notice maximum temperature rise rate of stockpile B and C is slower

than that of stockpile A even at various wind velocities. In practical, wind barrier has been proposed as a possible control to coal stockpile spontaneous combustion hazard [291]. The coal oxidation at low wind velocity might give off less amount of carbonic gas but it would be more difficult to dilute the gases product, refer Figure 7.16. It can be found the increased wind velocity can disperse the generated CO_2 more effectively and high wind velocity therefore might be a favourable parameter in this regard.

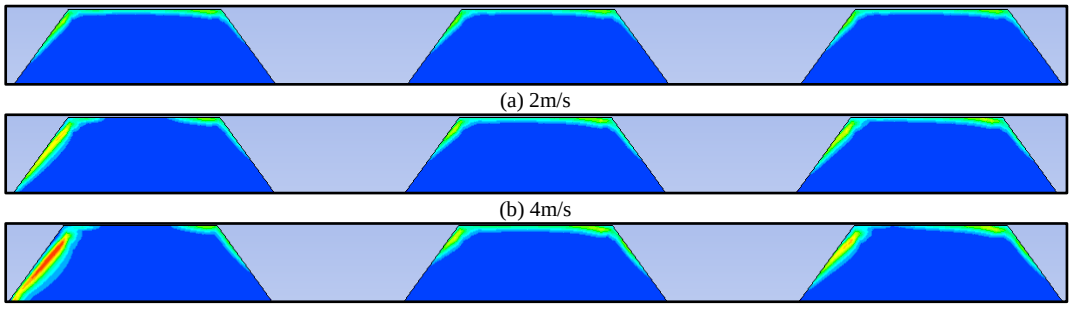

(a) 2m/s

(b) 4m/s

(c) 6m/s

Figure 7.14 Temperature contours of the three stockpiles of base model with various wind velocities at 30 days

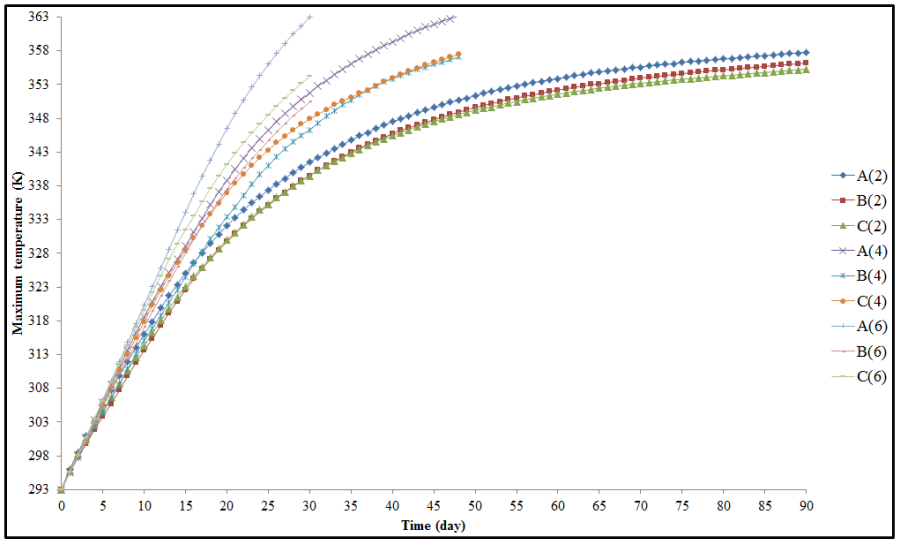

Figure 7.15 Maximum temperature rising profiles of base model with various wind velocities

***A(2) denotes stockpile-A with 2m/s wind velocity**

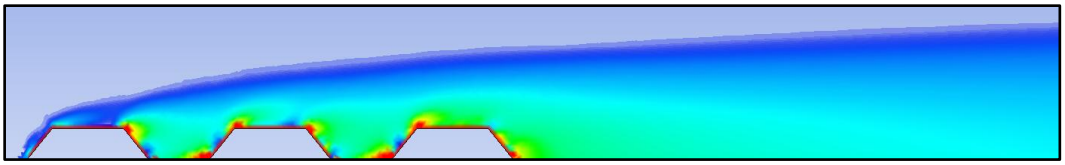

(a) 2m/s

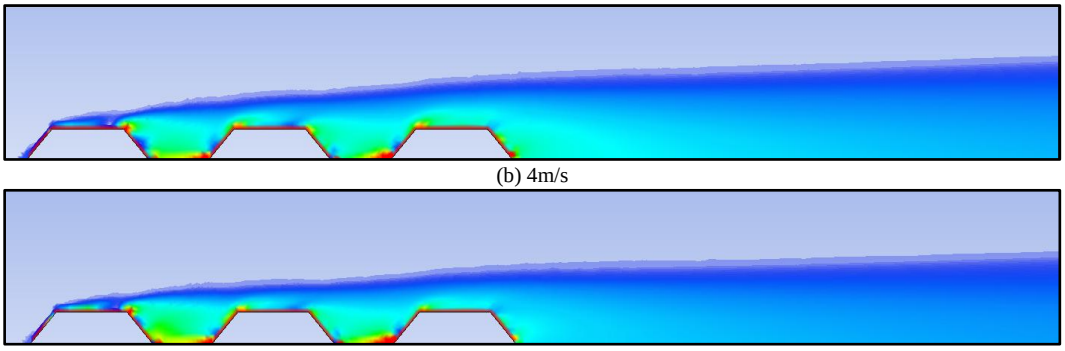

(b) 4m/s

(c) 6m/s

Figure 7.16 CO_2 dispersion (mass fraction) in farfield after 30 days at various wind velocities

7.5.2.2 Spacing

As stockpile A is essentially a wind barrier to stockpile B and C, if stockpiles stacked behind stockpile A are located within wake region of stockpile A, it is postulated the maximum temperature rising rate will always lag behind stockpile A. Flow field for a single stockpile is performed and it is found the wake region is approximately 70m in length as wind velocity is 4m/s, side slope is 50^o, and height of stockpile is 10m. Therefore spacing 5m, 20m, and 40m are chosen to examine effects of spacing within wake region and 80m is selected to compare wide spacing out of wake region. To acquire more understandings of effects of different positions of coal stockpiles, pressure profile around them must be well studied because pressure drop is the main driver of the airflow advection. The pressure coefficient profiles of different spacing of stockpiles are plotted, refer Figure 7.4 and Figure 7.17. It is indicated that different spacing almost have no effects on pressure coefficient distribution of stockpile A and it is plausible to predict that the self-heating behaviour of stockpile A will remain unchanged. It is also found pressure drops increasingly steeper with wider spacing when wind encounters stockpile B and C, which implies more airflow would be introduced to the stockpiles and more heat would be generated. Figure 7.18 shows the maximum temperature rising rates of the three stockpiles with various spacing. It is obvious spacing has little influence on stockpile A and maximum temperature develops more rapidly of stockpile B and C with wider spacing due to larger pressure variation. The maximum temperature rising profiles of stockpile B and C gradually approach to stockpile A with increasingly wider spacing. It appears stockpiles B and C lose most of the "protection" of stockpile A with wider spacing. Inversely, maximum temperature

rising profiles of stockpile B and C gradually separate with stockpile A as geometrically approach to stockpile A. Figure 7.19 shows temperature contour of stockpile B with different spacing at 30 day. It is quite clear the hot spot zone (350K) is gradually enlarged with wider spacing and the volume of deteriorated coal slightly grows as well. Stacking stockpiles in very proximity may reduce risk of self-heating hazard but would result a high concentration of carbonic gases zone at areas between two stockpiles, refer Figure 7.20. If the three stockpiles were closely stacked in 5m spacing, very high concentration CO_2 would be present at these zones. Therefore more assessments should be implemented upon final decision of how wide the stockpiles should be located at a given context.

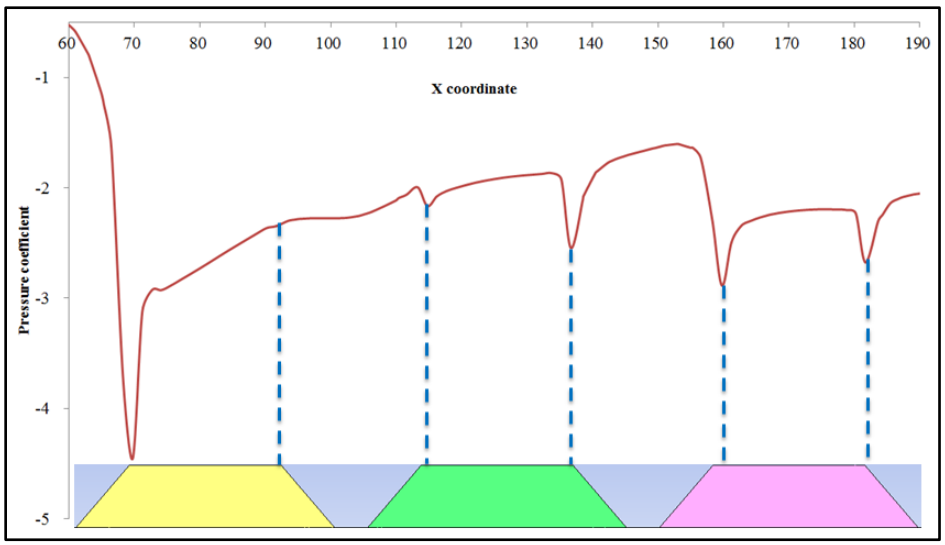

(a) Spacing=5m

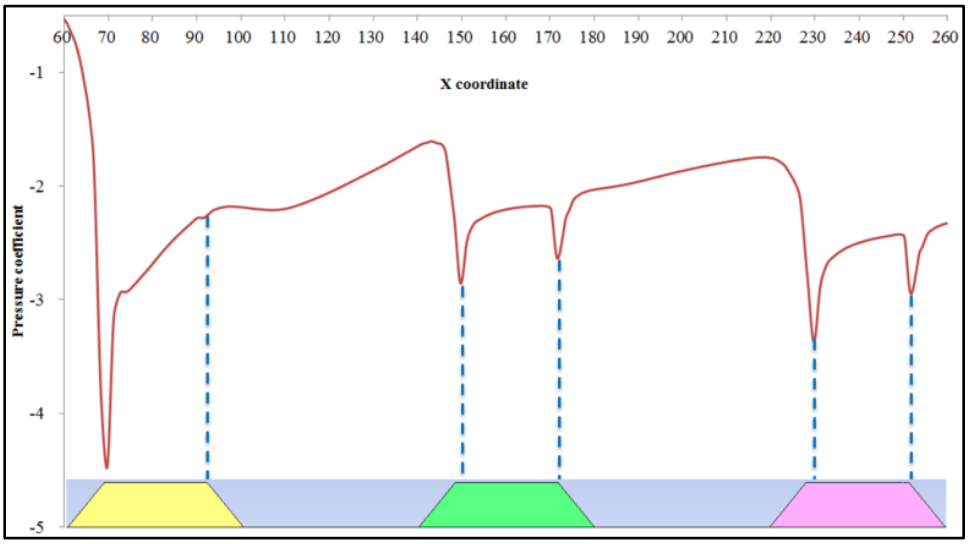

(b) Spacing=40m

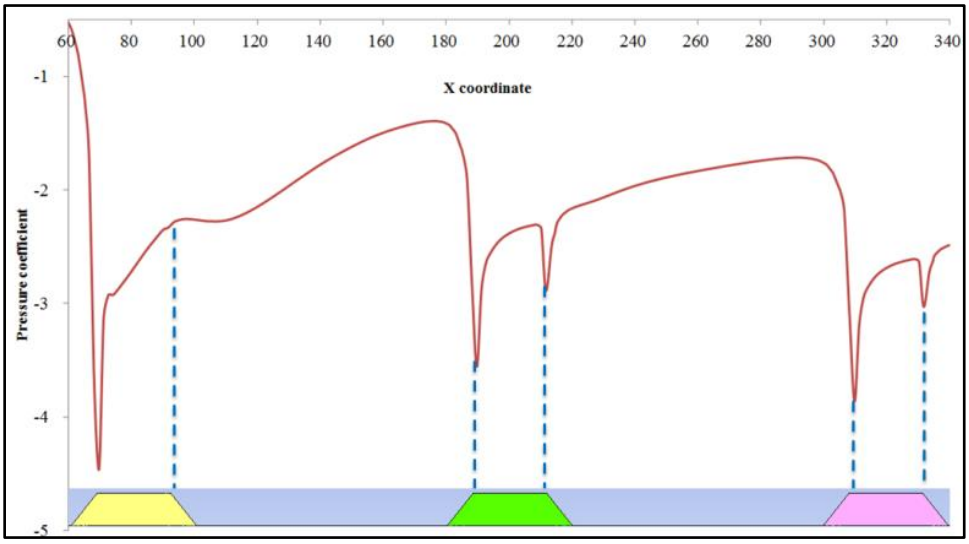

(c) Spacing=80m

Figure 7.17 Distribution of the pressure coefficient around the three stockpiles with various spacings (wind velocity=4m/s, porosity=0.2, height=10m, and side slope=50^{o})

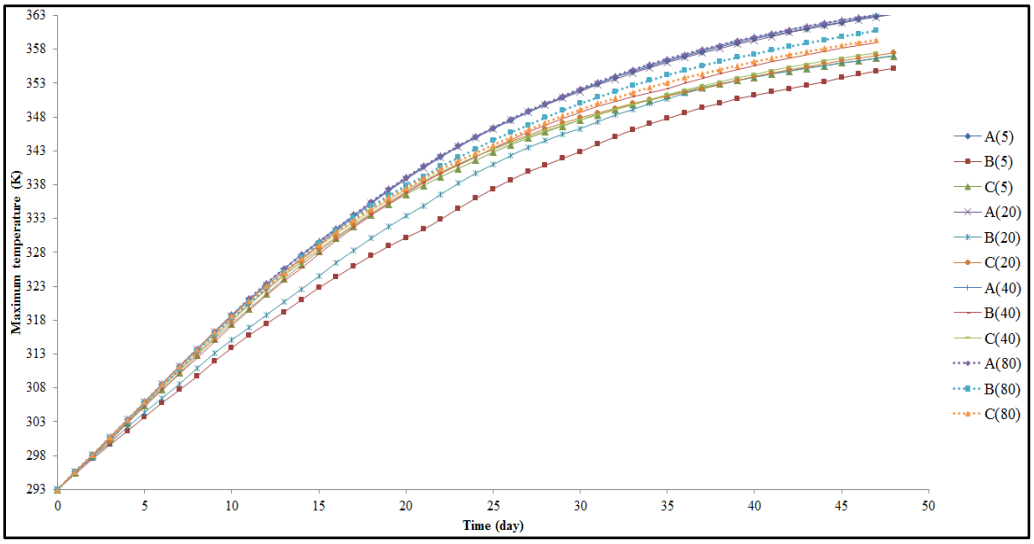

Figure 7.18 Maximum temperature rising profiles with various spacings (wind velocity=4m/s, porosity=0.2, side slope=50^{o}, and height=10m)

***A(5) denotes stockpile-A with 5m spacing**

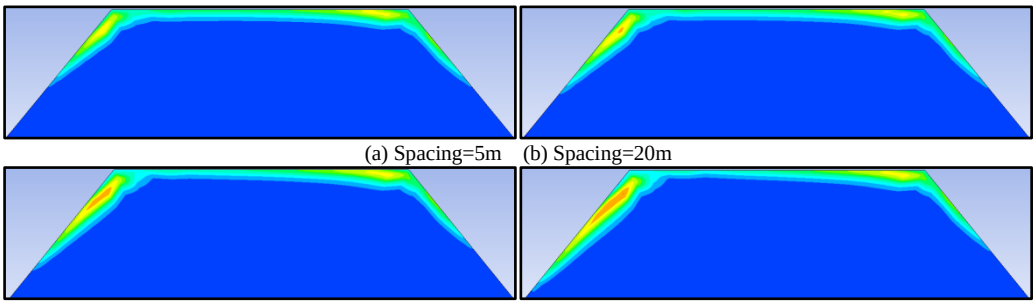

(a) Spacing=5m (b) Spacing=20m

(c) Spacing=40m (d) Spacing=80m

Figure 7.19 Temperature contour of stockpile B with various spacings (time=30 days, wind velocity=4m/s, porosity=0.2, side slope=50^{o}, and height=10m)

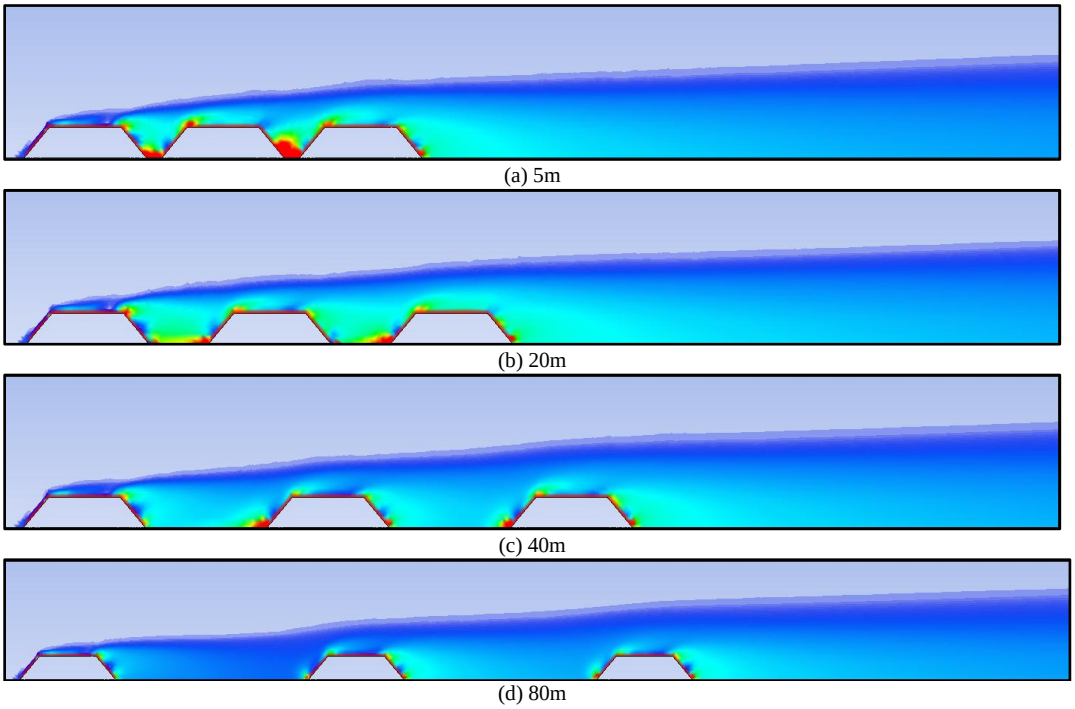

(a) 5m

(b) 20m

(c) 40m

(d) 80m

Figure 7.20 CO_2 dispersion (mass fraction) in farfield with various spacing (wind=4 m/s, time=30 days)

7.5.2.3 Porosity or compaction

Three porosity (i.e. 0.1, 0.2, 0.3) are selected to represent three compaction extents of coal stockpile, namely densely packed, slightly packed, and loosely packed. Figure 7.21 illustrates the maximum temperature rising profiles of the three stockpiles with the three compaction degrees. It is found the temperature rate significantly drops if stockpiles are densely packed due to high resistance to oxygen ingress. It spends 85 days to reach the critical temperature for stockpile A and it only reaches 340K for stockpile B. Whilst for porosity 0.2, it spends only 48 days for stockpile A to reach 363K and only 21 days for stockpile B reach 340K. Interestingly maximum temperature rising rate of slightly packed stockpile is slower than that of loosely packed stockpile at the initial stage of coal oxidation. However after roughly one month the highest temperature of slightly packed stockpile surpasses that of loosely packed stockpile. A possible explanation is available oxygen of loose stockpile is more abundant than a slightly packed stockpile initially but with consumption and depletion of oxygen, it appears convective heat dissipation becomes dominant. This can be possibly demonstrated by Figure 7.22 in which hot spot is moving deeper in more porous stockpile because of more heat being dissipated by convection while in deep stockpile oxygen concentration becomes too

low to sustain a high rate of oxidation reaction. The abnormal effect of high porosity has been reported previously but at a slightly higher temperature [58]. In addition it can be seen the volume of oxidised coal substantially increases with more loosely packed stockpile. Therefore porosity less than 0.2 is recommended if coal is expected to be stored for a long run and porosity less than 0.3 is recommended if caking property and calorific value of coal needs to be retained. Densely packed stockpile has additional benefit due to its low emission of greenhouse effect gas, refer Figure 7.23. The accumulation of CO_2 is much alleviated between stockpile A and B, and slightly diluted between stockpile B and C.

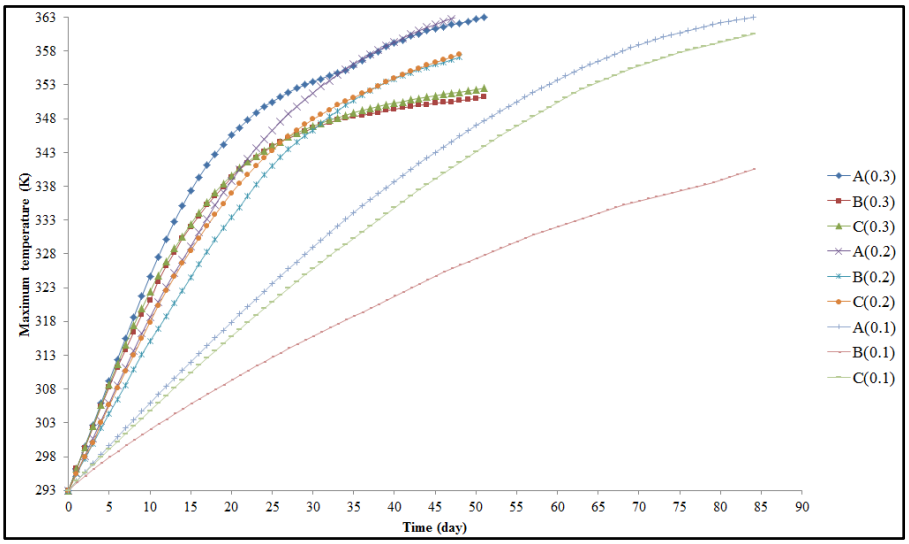

Figure 7.21 Maximum temperature rising profiles with different porosities (wind velocity=4m/s, spacing=20m, side slope=50^o, and height=10m)

***A(0.3) denotes stockpile-A with 0.3 porosity**

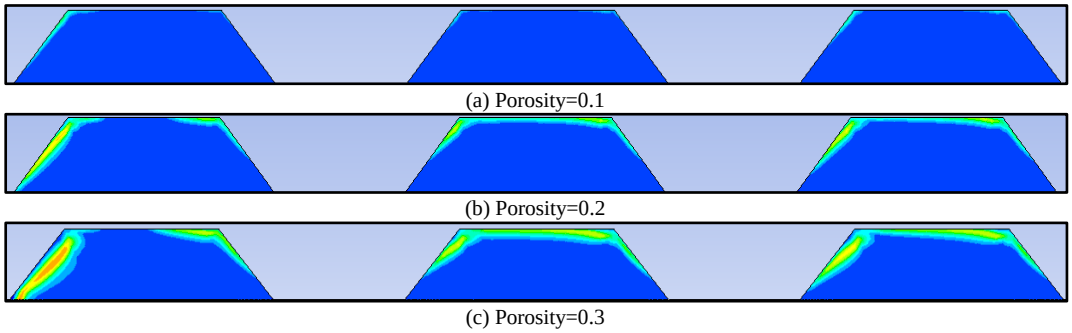

(a) Porosity=0.1

(b) Porosity=0.2

(c) Porosity=0.3

Figure 7.22 Temperature contours of the three stockpiles with different porosities (time=30 days, height=10m, side slope=50^o, and spacing=20m)

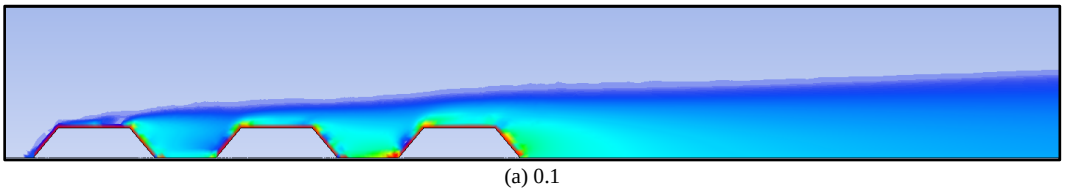

(a) 0.1

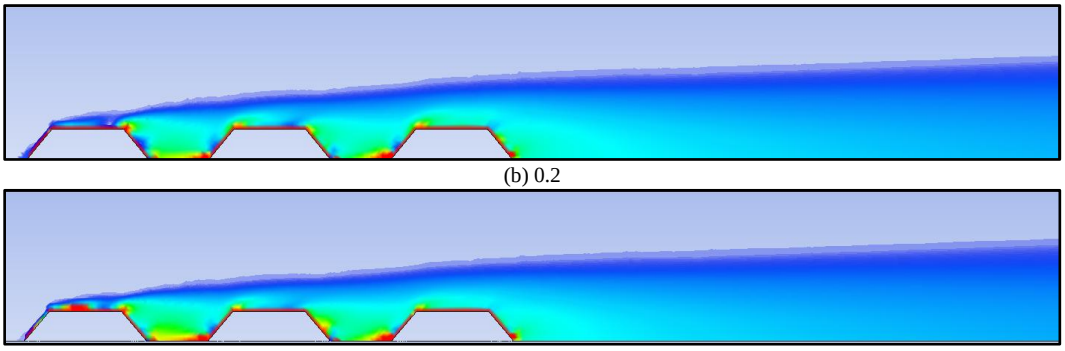

(b) 0.2

(c) 0.3

Figure 7.23 CO_2 dispersion (mass fraction) in farfield with various porosities (wind=4 m/s, time=30 days)

7.5.2.4 Height

In Australia Hunter Valley power station pile height lower than 4.5m is suggested for long run storage. To maintain the discreetness of the study, higher stockpiles (5m, 7.5m, 10m) will be studied because it has been indicated higher stockpile is less safe in terms of coal spontaneous combustion [26, 39, 58]. As can be seen fromFigure 7.24, maximum temperature rising rate of stockpile A slightly slows down with greater height but the effects are limited. Maximum temperature rising rate of stockpile B and C also slightly slow down with lower height for a long run but initially lower stockpile may have faster temperature rising rate. For example, maximum temperature of 10m high stockpile B falls behind both 5m and 7.5m high stockpile B in the first 20 days. A possible reason is lower stockpile A weakens the "protection" to stockpile B and more air is attracted into stockpile B. With progress of self-heating, it becomes increasingly hard for lower stockpile B to contain the interior thermal energy and cause slow temperature rising rate after an initial period. From Figure 7.25 it can be known the effects of different heights of stockpile on temperature contour and volume of deteriorated coal are very limited at low temperature range. The dispersion of CO_2 in farfield with various stockpile heights is also studied. As can be seen from Figure 7.26 CO_2 is more readily to be diluted for lower stockpile because more airflow is introduced towards stockpile B and C due to less obstruction of stockpile A. Through above analysis it can be deducted lower stockpile can have two benefits: (i) reduce self-heating risk; (ii) facilitate dispersion of carbonic gases. However, lowering packing height of stockpile will meanwhile reduce the storage capacity of single stockpile so more comprehensive evaluation requires to be conducted.

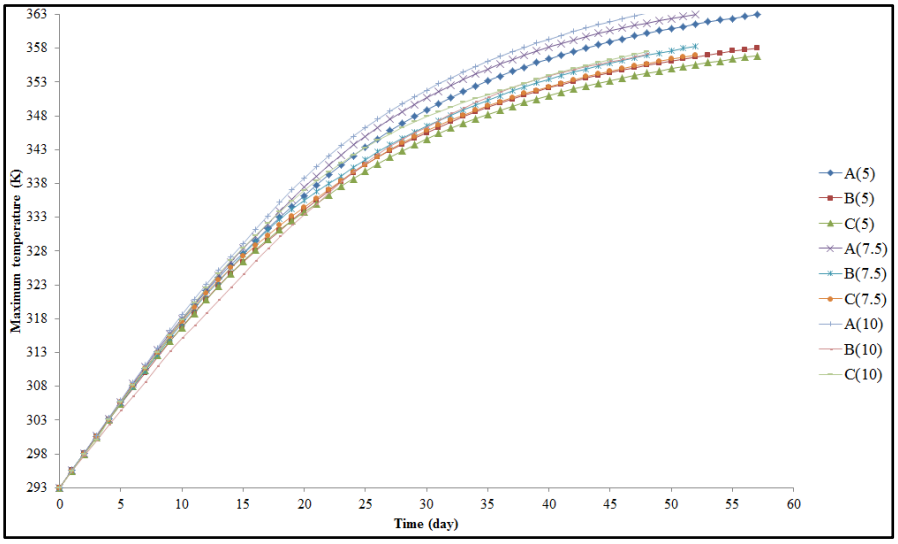

Figure 7.24 Maximum temperature rising profiles with different heights (wind velocity=4m/s, spacing=20m, side slope=50^o, and porosity=0.2)

***A(5) denotes stockpile-A with 5m height**

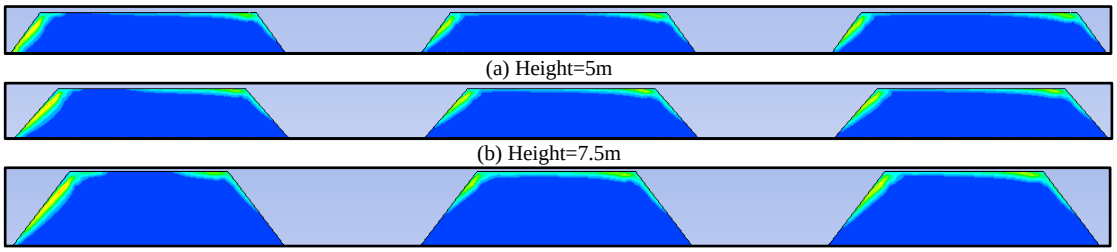

(a) Height=5m

(b) Height=7.5m

(c) Height=10m

Figure 7.25 Temperature contours of the three stockpiles with different heights (time=30 days, porosity=0.2, side slope=50^o, and spacing=20m)

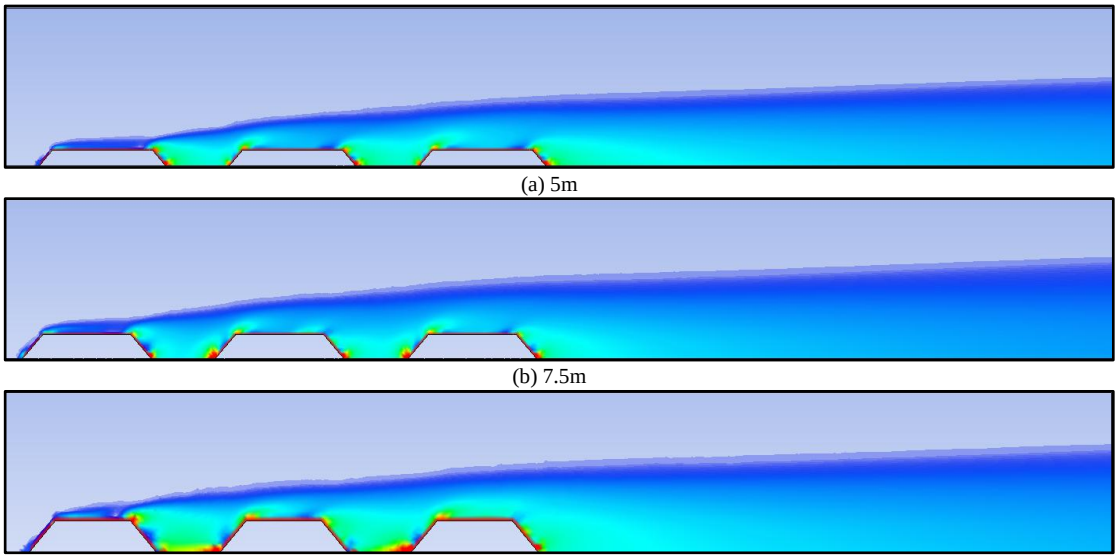

(a) 5m

(b) 7.5m

(c) 10m

Figure 7.26 CO_2 dispersion (mass fraction) in farfield with various heights (wind=4 m/s, time=30 days)

7.5.2.5 Slope

Three slopes are studied in this work, namely 35^o, 50^o (the base model), and 65^o representing gentle, normal, and steep stockpile respectively. It has been reported the self-heating problem can be alleviated when the slope is made gentler [58, 61]. This study indicates a similar finding but merely for the first stockpile at low temperature range. As can be seen from Figure 7.27, side slope has a strong effect on maximum temperature rising rate of stockpile A but has limited influence on stockpile B and C. Self-heating rate of stockpile A significantly reduces with gentler side slope. When stockpile is 35^o, it is found initial self-heating rate of gentle stockpile B is faster than its steep stockpile but slows down for a long run. A possible reason is "protection" of stockpile A is considerably weakened with gentle slope and as a result of it, more air is directed to stockpile B. Figure 7.28shows the evolution of hot spot with different slopes at 30 day. It can be seen hot zone of stockpile A is enlarged with steeper slope and little difference can be observed for stockpile B and C. In addition it appears volume of coal being oxidised slightly increases with steep side slope for stockpile A and little difference can be identified for stockpile B and C. The dispersion pattern of CO_2 with different stockpile slopes is also investigated. As can be seen from Figure 7.29, the high concentration of CO_2 gas mixture can be better flushed with steep slope stockpile and therefore it needs to be further evaluated upon employing a gentle slope to alleviate the self-heating problem.

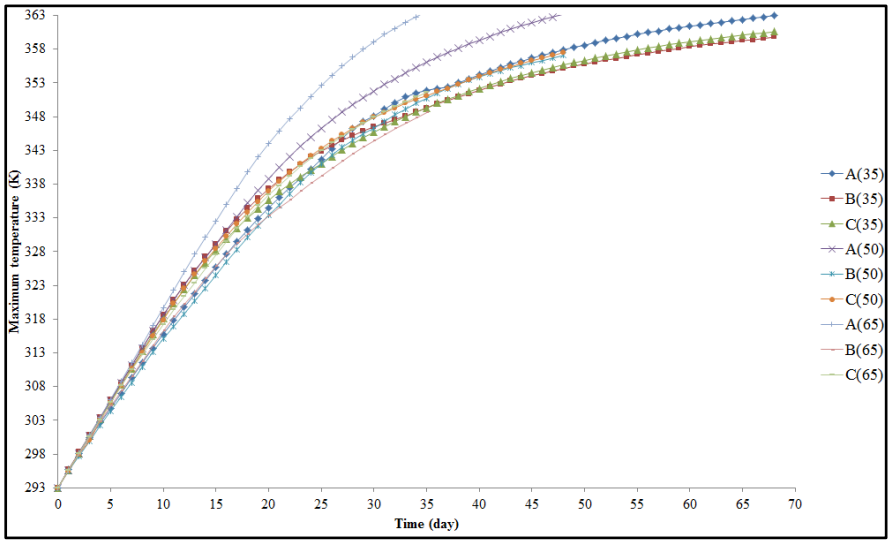

Figure 7.27 Maximum temperature rising profiles with different side slopes (wind velocity=4m/s, spacing=20m, height= 10m, and porosity=0.2)

***A(35) denotes stockpile-A with 35^o side slope**

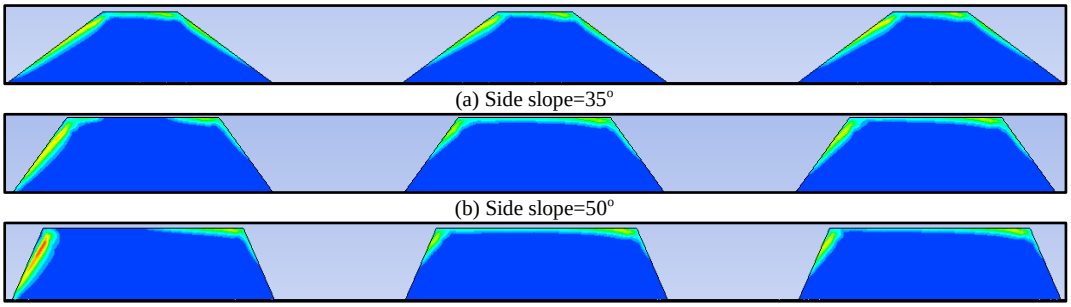

(a) Side slope=35°

(b) Side slope=50°

(c) Side slope=65°

Figure 7.28 Temperature contours of the three stockpiles with different side slopes (time=30 days, porosity=0.2, height=10m, and spacing=20m)

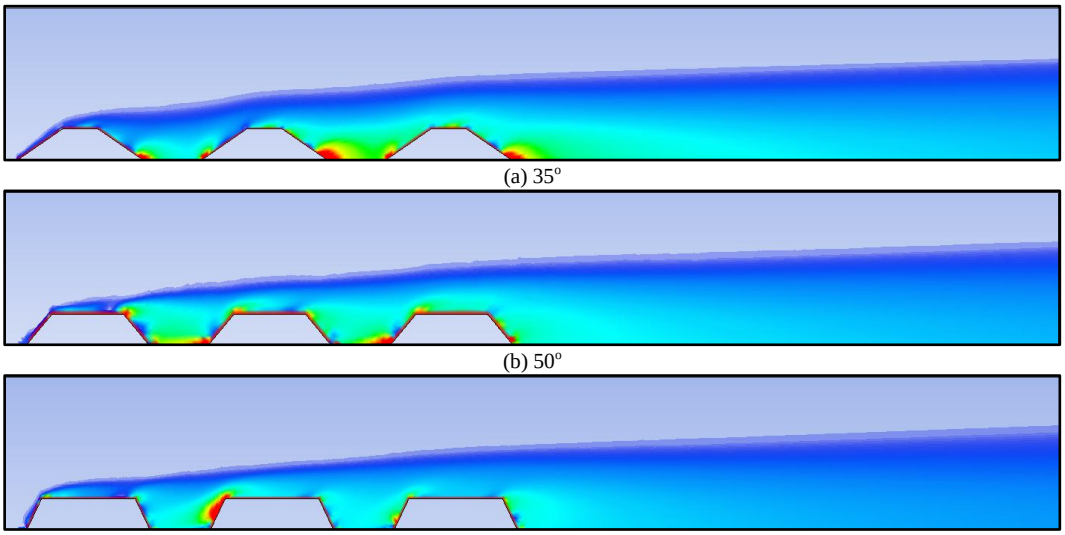

(a) 35°

(b) 50°

(c) 65°

Figure 7.29 CO_2 dispersion (mass fraction) in farfield with various slopes (wind=4 m/s, time=30 days)

7.6 Summary

The phenomenon of self-heating of coal stockpile is a result of complex physical and chemical processes. Although this is a long-standing problem, complete understanding has never been fully grasped. To gain more insights of self-heating hazard on coal stockpile especially for the scenario where multiple stockpiles need to be constructed in proximity, a non-equilibrium thermal model is developed with assistance of CFD code under conditions of wind flow. After validation of the proposed model a base model is selected and investigated in many details. It was found wind velocity builds up as it encounters the first stockpile and then significantly drops at the regions between two stockpiles where a wake region is expected to be induced. Exterior pressure drop around the three stockpiles is studied to provide more understanding of fluid dynamics involved in this problem. Interior pressure gradients distribution for the three stockpiles is further investigated to

estimate the possible travel path of airflow in a more fundamental way. All the evidence indicates more airflow will be introduced into stockpile A than the other two stockpiles and therefore it is postulated stockpile A is like a wind barrier and very likely to lead the evolution of self-heating. The conjecture was then confirmed by maximum temperature rising profiles of the three stockpiles. The progressive consumption of oxygen and accumulation of gaseous products are also analysed to gain more insights in coal oxidation process. Liberation of carbonic gas and its flow pattern in the farfield is investigated to grasp more knowledge as greenhouse effect gas emission contributed from low temperature and spontaneous combustion of coal stockpile has attracted intensive attentions recently. Last not the least parametric analysis was conducted and several meaningful findings are listed:

a) Stronger wind would promote evolution of self-heating hazard and increase volume of deteriorated coal but meanwhile facilitate dilution of the gaseous products;
b) Different spacing has little influence on self-heating behaviour of the first stockpile and more closely stacked stockpiles has a slower temperature rising rate for the other two stockpiles but would result in undesirable accumulation of carbonic gases in the zones between two stockpiles;
c) Porosity has significant influences on spontaneous heating process of the three stockpiles. Compaction might not always slow down maximum temperature rising rate but would considerably reduce volume of oxidised coal. Porosity less than 0.1 is recommended for long time storage of coal and porosity less than 0.2 is recommended for prevention of large volume of degraded coal; densely compaction of coal stockpile has another benefit in low emission of greenhouse effect gas;
d) Lower coal stockpile is capable of prolonging induction period but the effect is very limited at low temperature range. Lower stockpile also facilitates dispersion of gaseous product of coal oxidation but storage capacity will be considerably reduced so more assessments required to be implemented;
e) Gentle stockpile would slow down development of self-heating for stockpile A but initial temperature rising rate of behind stockpiles may increase because of weakened “protection” of stockpile A. High concentration of CO_2 gas mixture can be better flushed with steep slope stockpile and thus

comprehensive evaluations needs to be conducted upon using a gentle slope to alleviate the problem.

8 CONCLUSIONSAND RECOMMENDATIONS

8.1 Conclusions

8.1.1 Conclusions from the investigation of spontaneous combustion in Shendong coal mines

- Shendong coalfield is the largest coalfield in China and the most important energy supplier in China. Since 2000 increasing numbers of spontaneous combustion incidents have been reported due to a variety of reasons such as increasing intensity of mining operations and lack of monitoring and control practices.
- Key features of longwall operations in Shendong coal mines are identified: (1) Shendong coals are intrinsically liable to heating; (2) chain pillars are allowed to be crushed with full strata caving; (3) 0.3~0.5m top/floor coal is reserved to protect the immediate roof/floor during longwall cutting; (4)closely distributed coal seams are extracted under shallow overburden; (5) more auxiliary roadways are driven and cut-through seals are often poorly constructed; (6) longwall panels are usually several kilometer's long and longwall faces are 240~360m wide; (7) several longwall goafs become interconnected after failure of coal pillars.
- From the key features of Shendong coal mines, the spontaneous combustion related problems are critically investigated: (1) air leakage into goaf is severe especially the leakage sourcing from mining induced cracks; (2) a significant amount of coal which contains top coal above gateroads, crushed coal pillars, and a layer of top/floor coal in longwall face is left in goaf; (3) drainage of upper longwall goaf draws fresh airflow and cause heating of flooded coal that is more liable to spontaneous combustion; (4) goaf gas ingress (oxygen depletion and high CO concentration) into longwall face especially at return corner of the tailgate. These problems are not isolated and one problem may have great impacts to another one.

8.1.2 Conclusions from experimental tests of Shendong coals

- Four Shendong coals were collected from fresh exposed longwall face and proximate and ultimate compositions of these coal samples were

immediately determined upon receiving them. Flooded and oxidised coal samples were also prepared.

- Ignition temperatures of the four coal samples were relatively low and all below 300^{o}C. Ignition temperatures of oxidised coal samples were 8~15^{o}C lower than fresh coal samples. Ignition temperatures of flooded coal samples were close to or slightly lower to that of fresh coals.
- CO_x (CO and CO_2) gases of all coal samples were produced starting from low temperature oxidation and the concentrations increased rapidly with temperature especially for temperature higher than 130^{o}C. Less CO_x gases were produced for all oxidised coal samples than that of fresh coal samples and flooded coal samples. More CO_x gases were liberated by fresh coal samples than that of flooded coal samples at low temperature while with coal temperature passing a critical value between 130^{o}C and 170^{o}C, the trend was reversed. Production rates of C_xH_y (CH_4 and C_2H_4) gases of oxidised coal samples were also lower than that of fresh and flooded coal samples especially at a high temperature. Initial amount of produced CH_4 of fresh coal samples was larger than that of flooded coal samples while the trend was reversed after a critical temperature. Unlike production trend of CH_4, C_2H_4evolution of flooded coal samples was more than that of fresh coal samples across the whole tests.
- A new adiabatic oxidation rig was designed, assembled and commissioned at the University of Wollongong to determine low temperature heating behaviour of Shendong coals. Based on the latest ISCP classification, adiabatic testing results indicated all coal samples even with a pre-oxidation history exhibit high risk of spontaneous combustion and the flooded coal samples present a higher risk.

8.1.3 Conclusions from CFD model of heating evolution and gas migration in a Shendong goaf

A three-dimensional CFD model was developed to study heating evolution and gas migration in a Shendong goaf. The geometric model was developed based on real on-site conditions and the theoretical model incorporated a set of governing equations including low temperature kinetics of coal oxidation, energy and mass conservation, momentum balance, and continuity equation. The base model was

validated and calibrated via field gas monitoring data. After that more studies were conducted and inertisation plans were proposed. Main findings are summarised as following:

Base model:

- High velocity airflow was able to travel 30~100m deep into layer of residual coal and more airflow was present around perimeter of goaf rather than centre of goaf due to high porosity and permeability in goaf perimeter.
- High concentration oxygen can migrate into goaf approximately 500m behind face at maingate side and only about 100m at return side.
- Heating was evolved in an intermediate zone where airflow stream was able to supply enough oxygen to sustain continuous oxidation reaction and meanwhile, heat dissipated by convection was less effective than heat generated by oxidation. Incubation period of the heating was roughly 29 days.
- Most carbonic gas was generated at intake side due to presence of high oxygen gas mixture. Liberated carbonic gas was unable to flow around the entire goaf perimeter and started to divert to return side in middle of the goaf.
- CO make profile correlated well with the maximum temperature profile.
- With normal advance rate of longwall face and without air leakage from other sources, serious heating in the goaf was unlikely to occur.

500m model:

- High velocity gas stream was able to travel to deep goaf and high oxygen level gas was present at start-up area.
- Heatings were able to be developed at start-up area and behind longwall face. The incubation period of heating at start-up area was 25 days, which is shorter than that behind longwall face.
- CO make profile correlated well with temperature profile.
- The best locations for nitrogen injection were behind seal D, E, or F with at least 244m^3/h nitrogen injection for a proactive inertisation plan.
- Heating can be suppressed in start-up area with reactive inertisation behind seal C only. Nine days were required for nitrogen to fully disperse to heating area and the temperature was brought down very slowly though.

- It needed about five days for nitrogen to fully disperse to heating area behind seals C and c. Temperature was brought down more quickly than nitrogen injection from only one seal.

1000m model with air leakage from mining induced cracks:

- Due to leakage of fresh airflow, oxygen rich gas mixture was present at start-up area.
- Heating was developed in start-up area and the heating evolvedfaster than that behind longwall face.
- CO make was unable to correctly indicate the severity of the heating because high level CO was generated at a very confined zone.
- The best locations for nitrogen injection were behind seal a, b, or c with at least 122m^3/h nitrogen injection for a proactive inertisation plan.
- It took roughly 10 days to dilute gas mixture to a safe level for a reactive inertisation from only seal c. Most of the heating can be suppressed but it was not able to bring down the temperature at localised area.
- Only three days were required to fully exclude high oxygen gas from start-up area with nitrogen injection from seals b and c. The heating can be totally suppressed by nitrogen injection behind the two seals.

8.1.4 Conclusions from ventilation simulation of Bulianta colliery

- Presence of differential pressure between longwall face and surface was the root cause of air leakage into goaf in a mining scenario where mining induced cracks propagated to surface. The differential pressure was not able to be eliminated no matter how the ventilation circuit is modified if an exhausting ventilation system is used.
- Isolating and pressurising active longwall panel was likely to reduce the differential pressure. This was accomplished by deployment and cooperation of an auxiliary fan and several ventilation regulators. The differential pressure can be eliminated if the resistance factors of ventilation control devices and duty of auxiliary fan are adjusted properly.
- A hybrid ventilation system (Force-Exhaust) can also reduce the differential pressure by adjusting duties of the two main surface fans. The neutral point can be ideally distributed at any point along the pressure loss path by adjusting performances of the two fans.

8.1.5 Conclusions from CFD model of heating evolution in coal stockpiles

- Incoming wind with a higher velocity would promote evolution of heating hazard and increased volume of oxidised coal but meanwhile facilitated dilution of the gaseous products.
- Different spacing of coal stockpiles had little influence on heating behaviour of the first stockpile. More closely stacked stockpiles had a slower temperature rising rate for the two stockpiles behind but would resulted in undesirable accumulation of carbonic gases between two stockpiles.
- Porosity had significant influences on heating process of the three stockpiles. Compaction might not always slow down maximum temperature rising rate but would considerably reduce volume of oxidised coal. Densely compaction of coal stockpile had another benefit in significantly low emission of greenhouse effect gases.
- Lower coal stockpile was capable of prolonging induction period but the effect was very limited at low temperature range. In addition lower stockpile promoted dispersion of gaseous product of coal oxidation.
- Gentle stockpile would slow down development of self-heating for the first stockpile but initial temperature rising rate of adjacent stockpiles may increase due to weakened "protection" of the first stockpile. High concentration of CO_2 gas mixture can be better dispersed with steeper slope stockpile.

8.2 Recommendations

Further research is recommended to be conducted within following directions:

- To date different apparatus and testing methods for gas evolution test and adiabatic test have been developed and used but the variations of both inter and intra laboratories indicate that a standard testing method including experimental apparatus, coal sample preparation and storage, testing procedures, and data interpretation method should be developed.
- Coal oxidation kinetics study still remains not fully understood especially at low temperature between interaction of the Elovich dependence and Arrhenius correlation. Therefore more investigations should be conducted either experimentally or numerically.

- To fully understand oxidation behaviour of Shendong coals, in-situ FTIR test is recommended to capture information of solid oxidation products with elevated temperatures. Such information is expected to be very useful to facilitate interpretation of gas evolution especially with influence of moisture.
- Pore structure and pore volume distribution of flooded coal needs more studies to demonstrate whether long time water immersion affects pore structure of coal.
- As a longwall is keeping advancing and thus in reality, volume of the longwall goaf is gradually increasing. Meanwhile due to periodic caving of roof, permeability of goaf also varies within such a dynamic process. As permeability of goaf has an impact to gas flow pattern and evolution of heating in goaf, the variation of permeability and dimension of goaf needs to be considered. This may involve utilisation of dynamic mesh.
- To maintain simplicity and to save computational load, most models for heatings of coal stockpile were developed in one or two dimensions. Whilst a three dimensional model may capture more information of self-heating and mass transfer behaviour of a coal stockpile and thus development of a three dimensional model is also a direction of future work.
- Moisture may considerably affect self-heating behaviour of coal mass in many aspects. The previous models mainly considered additional heat transport mechanism arisen from evaporation and recondensation of moisture. However, there are two effects of moisture should be worthy of more inspections: inclusion of heat of ‘‘wetting” and how oxidation rate varies with progressive drying. Therefore a model with considering those effects of moisture needs to be developed.
- To enhance applicability of the proposed spontaneous combustion model, more validation works need to be conducted. In underground model monitoring gas data at more locations can be used to calibrate the model. For surface coal stockpile a possible validation method would be the erection of wind, rain, solar radiation, and varying ambient temperature profiles accompanied with scattered temperature monitoring sensors inside a stockpile.

- In some warm regions like Queensland, Australia, apart from oxidation, solar radiation is another important source of heating in coal stockpile. Therefore heat exchange via solar radiation must be incorporated when modelling self-heating of coal stockpile in such a region. Development of coal heating model with heat transfer via radiation could be another future work.

APPENDICES

Appendix A-Summary of parametric studies of various numerical models of coal mass self-heating

Reference	*Examined variables and assigned values*										
	Coal reactivity	Particle size (m)	Moisture content (% by mass)	Stockpile height (m)	Stockpile slope (o)	Packing porosity	Airflow velocity (m/s)	Bed length (m)	Thermal conductivity(W m-1 K-1)	Initial temperature (K)	Oxygen concentration (%)
[50]	-	-	-	-	-	0.1, 0.125, 0.15, 0.175	-	-	-	-	-
[51]	Various values of activation energy (8, 20, 40, 60) and rate constants, Elovich effect	-	-	-	-	-	0, 1×10^{-5}, 2×10^{-5}, 5×10^{-5}, 2×10^{-4}	3.4, 4.5, 4.6, 8	-	-	-
[52]	Various values of pre-exponential factor (1.2×10-10, 4.2×10-10, 1.2×10-9), deterioration effect	-	0, 8	-	-	0.05, 0.2, 0.3	2×10^{-7}, 2×10^{-6}, 6×10^{-6}, 2×10^{-5}, 2×10^{-4}	-	0.12, 0.2	283, 293	-
[54]	Various values of activation energy (53, 62, 71) and pre-exponential factor (1, 10, 100)	-	-	-	-	0.2, 0.3, 0.4	-	1, 5, 10	-	-	-
[59]	-	5.625×10^{-5}, 1.125×10^{-4}, 2.25×10^{-4}	-	-	-	0.165, 0.33	2.2, 4.4	-	-	-	-
[57]	-	0.01, 0.02, 0.03	Dry, moist	-	-	-	0.5×10^{-5}, 1×10^{-5}, 2×10^{-5},	-	-	-	-
[61]	Two values of pre-exponential factors (8.83×10^{7},8.83×10^{5})	0.0023,0.0096	-	-	11.3, 14, 18.4, 20, 21.8, 26.6, 39.8	0.06, 0.12, 0.18, 0.24, 0.3, 0.36	0.45, 2.23, 4.46, 6.69, 8.93	-	-	-	-
[64]	Varying values of pre-exponential factors	0.003~0.015	0~30	-	-	-	-	-	-	293~333	-
[39]	-	-	-	0.85, 1, 1.2, 1.8, 2.4, infinite	-	-	-	-	-	-	-
[58]	Three coals with different Arrhenius constants	-	16.81, 1.81, 35.4	1, 1.5, 2, 3, 4, 5	26, 34, 45, 63	0.2, 0.3, 0.4	-	-	-	-	-
[74]	Various values	-	-	-	-	0.2,	-	-	-	-	-

	of activation energy (40, 26.88, 58, 30.64) and pre-exponential factor (10, 6, 8.83×10^{6}, 1485)					0.3, 0.35, 0.4					
[107]	-	-	-	-	-	0.1, 0.13, 0.15, 0.17, 0.2, 0.25, 0.3	0, 5, 10	-	-	-	-
[26]	-			3, 4, 5, 6, 7.5, 9	45, 56.3, 71.6, 80.5	0.1, 0.15, 0.2, 0.25, 0.3, 0.35, 0.4	0.001, 0.05, 0.5, 1	-	-	-	5, 8, 10, 15, 18, 21
[97]	-	-	-	-	-	-	1, 2, 3, 4, 6, 10	-	-	-	-

Appendix B-Allocation of Shendong coal mines

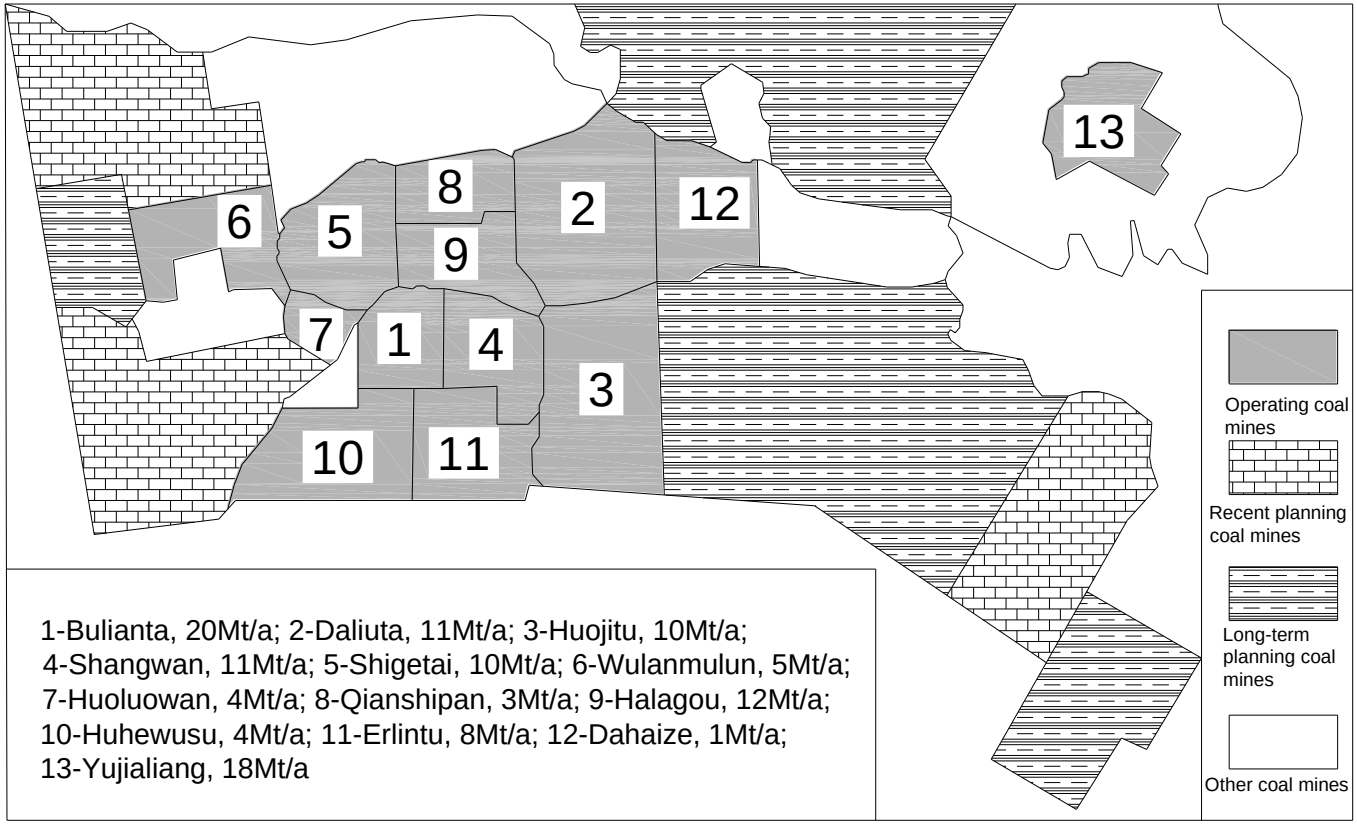

Appendix C-Intrinsic spontaneous combustion propensity rating standard used in China coal industry

For volatile content (dry ash free)>18%

Class	Propensity rating	Oxygen adsorption/mL g^{-1}
I	Very liable	>0.7
II	Liable	0.4~0.7
III	Not liable	<=0.4

For volatile content (dry ash free)<=18%

Class	Propensity rating	Oxygen adsorption/mL g^{-1}	Total sulphur content
I	Very liable	>=1	>=2
II	Liable	<1	
III	Not liable		<2

Appendix D-Original results of ignition temperature test

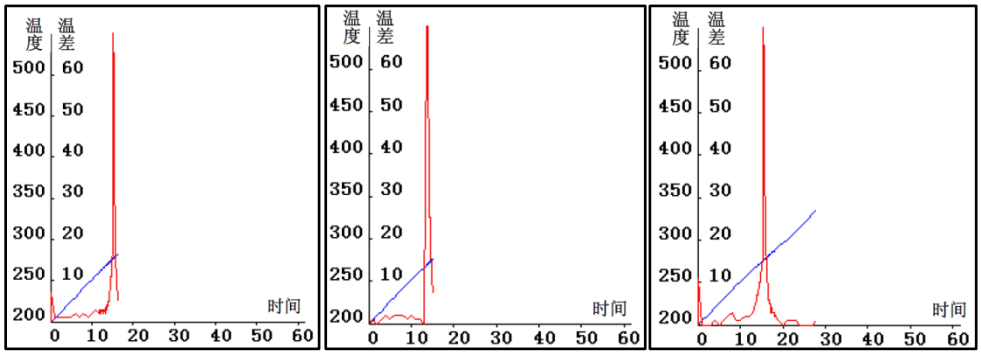

(a) Fresh coal(b) Oxidised coal(c) Flooded coal

BLT1-2 coal sample

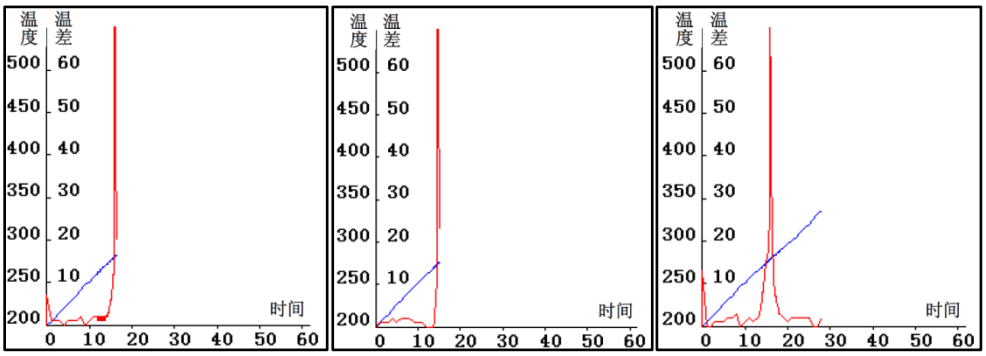

(a) Fresh coal(b) Oxidised coal(c) Flooded coal

BLT2-2 coal sample

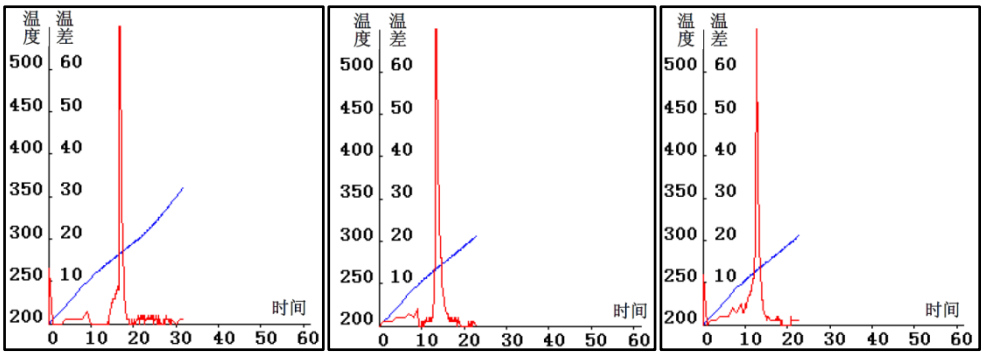

(a) Fresh coal(b) Oxidised coal(c) Flooded coal

SGT2-2 coal sample

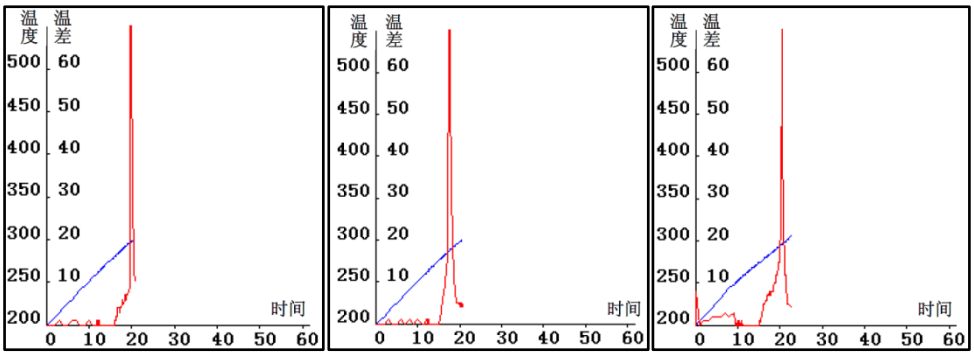

(a) Fresh coal(b) Oxidised coal(c) Flooded coal

SGT3-1 coal sample

Appendix E-Bulianta coal mine layout

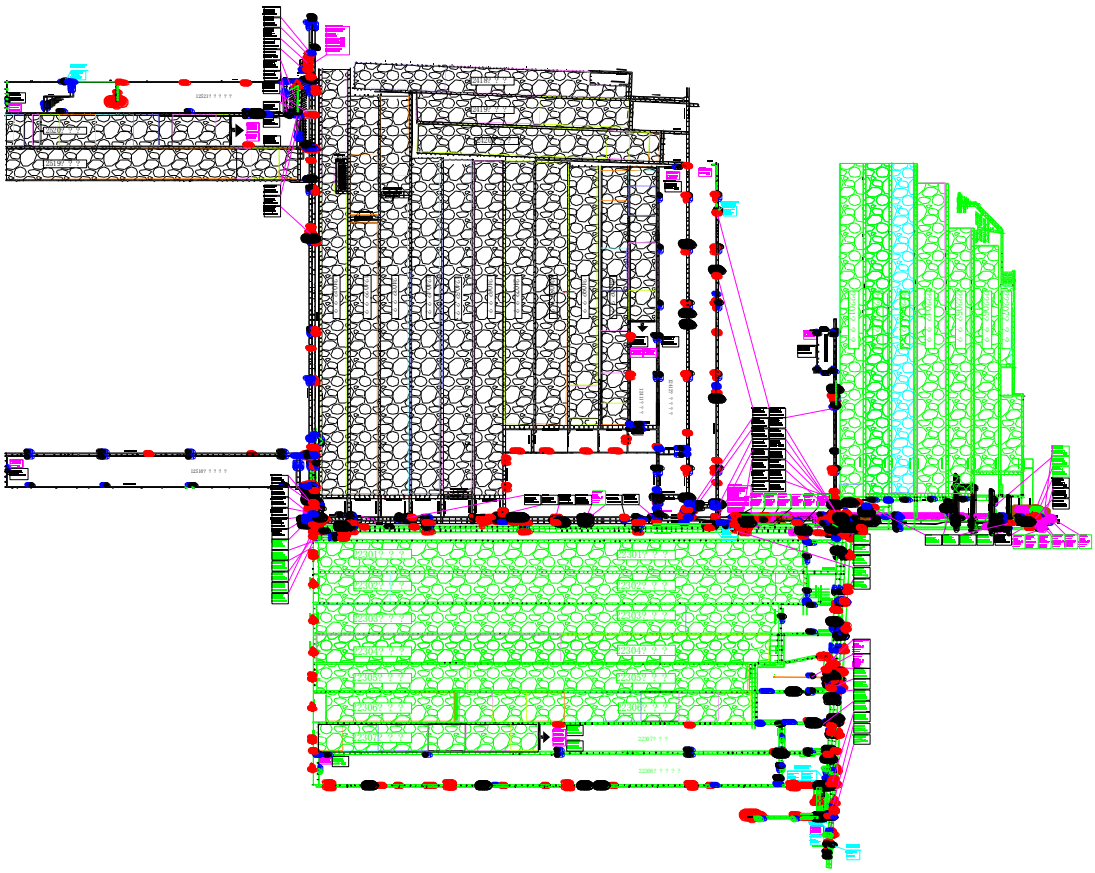

Appendix F-Huojitu coal mine layout

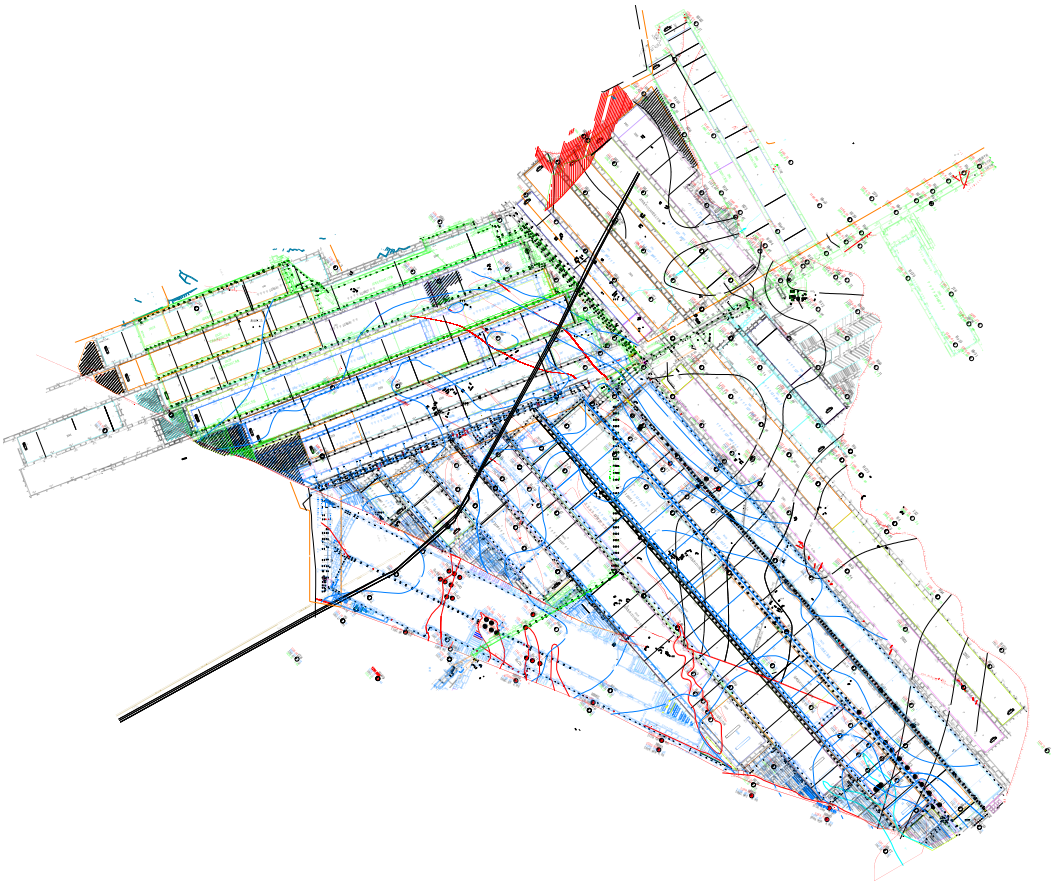

Appendix G-Shigetai coal mine layout

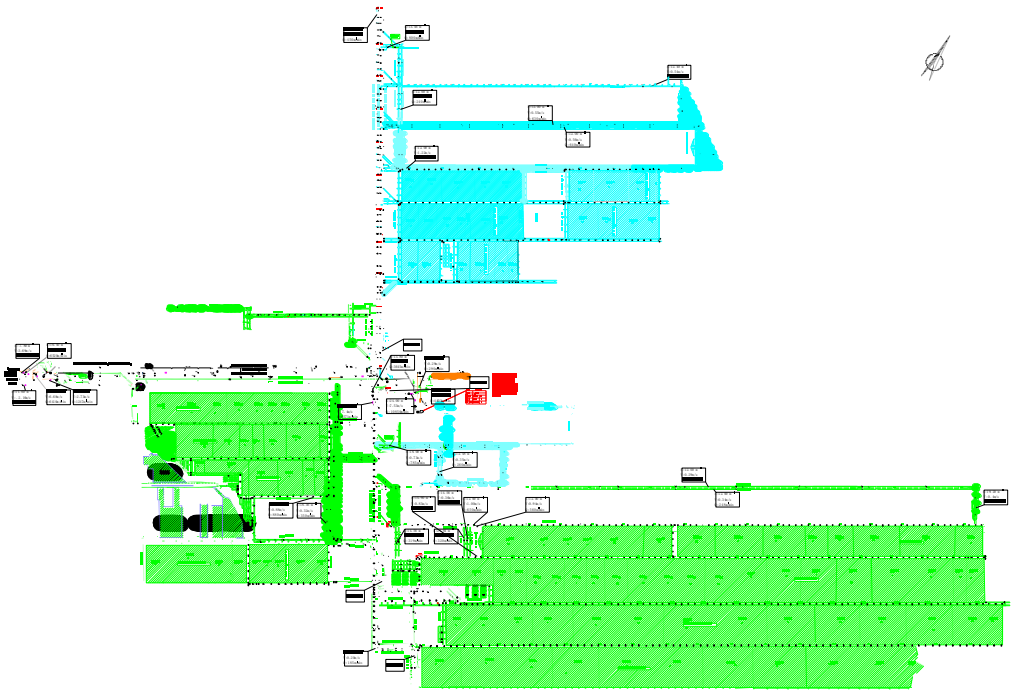

Appendix H-Single line layout of Bulianta coal mine

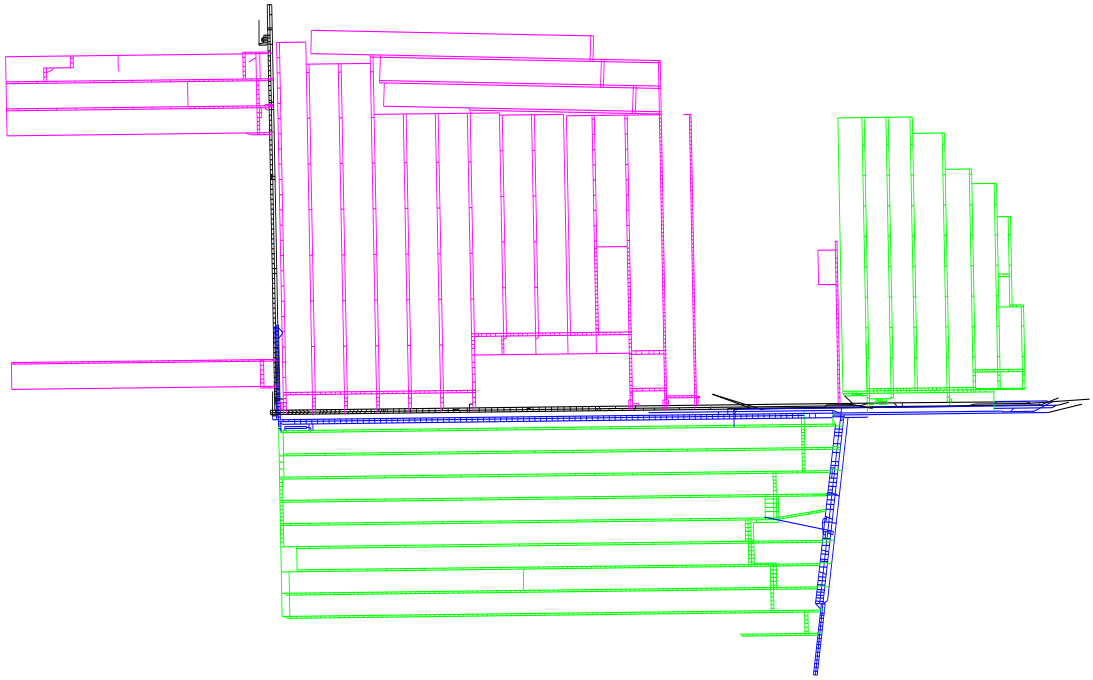

Appendix I-Field measured fan curve data of south exhaust fan

Item	Field measured data											
	Air temperature ℃	Relative moisture %RH	Barometric pressure kPa	Gauge static pressure Pa	Averaged air velocity m/s	Motor input power kW		Motor efficiency %		Rotate speed r/min	Fan noise dB	Diffuser noise dB
						1	2	1	2			
1	19.8	82.5	83.9	1930	21.0	480.2	482.1	93.5	93.5	593	71	69
2	20.0	82.3	83.9	2240	19.7	499.3	503.6	93.5	93.5	593	72	72
3	20.0	82.4	83.9	2890	17.1	532.3	518.6	93.5	93.5	593	74	73
4	20.2	82.1	83.9	3420	15.4	565.4	532.3	93.5	93.5	593	75	74
5	20.2	82.1	83.9	3750	14.0	588.6	550.1	93.5	93.5	593	76	76
6	20.2	82.0	83.9	3930	12.6	620.1	589.2	93.5	93.5	593	78	77
7	20.2	81.9	83.9	3920	10.1	650.2	620.1	93.5	93.5	593	78	79
Cross section area/m^2		14.5					Diffuser outlet area/m^2		15.2	Transmissionefficiency %		99.0

Item	Computed data									
	Air quantity m^3/s	Velocity pressure	Static pressure Pa	Total pressure Pa	Shaft power kW	Output power kW		Efficiency %		Air density kg/m^3
						Static pressure	Total pressure	Static pressure	Total pressure	
1	304.6	218.3	1711.6	1910.6	890.7	521.4	582.0	58.5	65.3	0.9894
2	285.8	192.0	2047.9	2222.9	928.4	585.3	635.3	63.0	68.4	0.9885
3	248.8	145.5	2744.4	2877.0	972.8	682.8	715.8	70.2	73.5	0.9885
4	223.5	117.5	3302.4	3406.6	1016.1	738.4	761.7	72.6	74.9	0.9884
5	204.3	98.1	3651.8	3738.8	1054.0	746.1	763.8	70.7	72.4	0.9884
6	183.7	79.3	3850.6	3921.0	1119.4	707.4	720.3	63.2	64.3	0.9884
7	147.3	51.0	3868.9	3914.2	1175.9	569.9	576.6	48.4	49.0	0.9884
Stall point	304.6	218.3	1711.6	1910.6	890.7	521.4	582.0	58.5	65.3	0.9894

Item	Density conversion factor kρ	Rotate speed conversion factor kn	Standardised data							
			Air quantity m^3/s	Fan static pressure /Pa	Total pressure Pa	Shaft power kW	Output power/kW		Efficiency %	
							Static pressure	Total pressure	Static pressure	Total pressure
1	1.2129	1.0000	304.6	2076.0	2317.3	1080.4	632.4	705.9	58.5	65.3
2	1.2140	1.0000	285.8	2486.2	2698.6	1127.0	710.5	771.2	63.0	68.4
3	1.2140	1.0000	248.8	3331.7	3492.7	1180.9	829.0	869.0	70.2	73.5
4	1.2141	1.0000	223.5	4009.5	4136.0	1233.7	896.5	924.7	72.6	74.9

5	1.2141	1.0000	204.3	4433.7	4539.3	1279.7	905.8	927.4	70.7	72.4
6	1.2141	1.0000	183.7	4675.0	4760.4	1359.1	858.9	874.6	63.2	64.3
7	1.2141	1.0000	147.3	4697.3	4752.2	1427.6	692.0	700.1	48.4	49.0
Stall point	1.2129	1.0000	304.6	2076.0	2317.3	1080.4	632.4	705.9	58.5	65.3

Appendix J-Field measured fan curve data of north exhaust fan

Item	Field measured data											
	Air temperature ℃	Relative moisture %RH	Barometric pressure kPa	Gauge static pressure Pa	Averaged air velocity m/s	Motor input power kW		Motor efficiency %		Rotate speed r/min	Fan noise dB	Diffuser noise dB
						1	2	1	2			
1	19.8	82.5	83.9	1940	21.2	479.2	482.1	93.5	93.5	593	70	68
2	20.0	82.3	83.9	2280	20.3	496.6	505.2	93.5	93.5	593	72	72
3	20.0	82.4	83.9	2850	17.9	541.1	522.3	93.5	93.5	593	73	73
4	20.2	82.1	83.9	3400.	16.3	576.3	539.2	93.5	93.5	593	75	74
5	20.2	82.1	83.9	3770	14.5	592.6	554.3	93.5	93.5	593	76	75
6	20.2	82.0	83.9	3900	13.1	631.2	597.4	93.5	93.5	593	77	77
7	20.2	81.9	83.9	3910	10.5	659.7	626.3	93.5	93.5	593	78	78
Cross section area/m^2		14.5				Diffuser outlet area/m^2		15.2		Transmission efficiency %		99.0

Item	Computed data									
	Air quantity m^3/s	Velocity pressure	Static pressure Pa	Total pressure Pa	Shaft power kW	Output power kW		Efficiency %		Air density kg/m^3
						Static pressure	Total pressure	Static pressure	Total pressure	
1	307.8	222.9	1717.0	1920.2	889.8	528.5	591.1	59.4	66.4	0.9894
2	294.5	203.8	2076.1	2261.9	927.4	611.4	666.1	65.9	71.8	0.9885
3	260.7	159.7	2690.2	2835.8	984.4	701.3	739.3	71.2	75.1	0.9885
4	236.7	131.7	3268.2	3385.0	1032.6	773.8	801.5	74.9	77.6	0.9884
5	210.9	104.6	3665.3	3758.1	1061.6	773.3	792.8	72.8	74.6	0.9884
6	190.9	85.7	3814.2	3890.2	1137.3	728.4	742.9	64.0	65.3	0.9884
7	153.5	55.4	3854.5	3903.7	1190.4	591.9	599.4	49.7	50.3	0.9884
Stall point	307.8	222.9	1717.0	1920.2	889.8	528.5	591.1	59.4	66.4	0.9894

Item	Density conversion	Rotate speed conversio	Standardised data					
			Air quantity	Fan static pressure/	Total pressur	Shaft powe	Output power/kW	Efficiency %

	factor kρ	n facto kn	m ³/s	Pa	e Pa	r kW	Static pressur e	Total press ure	Static pressure	Total pressu re
1	1.2129	1.0000	307.8	2082.5	2329.0	1079 .3	641.1	716.9	59.4	66.4
2	1.2140	1.0000	294.5	2520.4	2745.9	1125 .8	742.2	808.6	65.9	71.8
3	1.2140	1.0000	260.7	3265.9	3442.6	1195 .0	851.4	897.5	71.2	75.1
4	1.2141	1.0000	236.7	3967.9	4109.7	1253 .7	939.5	973.1	74.9	77.6
5	1.2141	1.0000	210.9	4450.1	4562.7	1289 .0	938.8	962.6	72.8	74.6
6	1.2141	1.0000	190.9	4630.9	4723.1	1380 .8	884.3	901.9	64.0	65.3
7	1.2141	1.0000	153.5	4679.8	4739.4	1445 .3	718.6	727.8	49.7	50.3
Stall point	1.2129	1.0000	307.8	2082.5	2329.0	1079 .3	641.1	716.9	59.4	66.4

REFERENCES

1. *BP Statistical Review of World Energy June 2016. BP Global*. 2016.
2. *International Energy Statistics* 2016; Available from: https://www.eia.gov/cfapps/ipdbproject/iedindex3.cfm?tid=1&pid=7&aid=1&cid=AS,&syid=2000&eyid=2012&unit=TST.
3. Arisoy, Ahmet and Basil Beamish, *Reaction kinetics of coal oxidation at low temperatures.* Fuel, 2015. **159**: p. 412-417.
4. Banerjee, S. C., B. D. Banerjee, and R. N. Chakravorty, *Rate studies of aerial oxidation of coal at low temperatures (30–170 ℃).* Fuel, 1970. **49**(3): p. 324-331.
5. Baris, K., S. Kizgut, and V. Didari, *Low-temperature oxidation of some Turkish coals.* Fuel, 2012. **93**: p. 423-432.
6. Clemens, Anthony H., Trevor W. Matheson, and Donald E. Rogers, *Low temperature oxidation studies of dried New Zealand coals.* Fuel, 1991. **70**(2): p. 215-221.
7. Itay, Michael, Cavan R. Hill, and David Glasser, *A study of the low temperature oxidation of coal.* Fuel Processing Technology, 1989. **21**(2): p. 81-97.
8. Kaji, Ryuichi, Yukio Hishinuma, and Yoichi Nakamura, *Low temperature oxidation of coals: Effects of pore structure and coal composition.* Fuel, 1985. **64**(3): p. 297-302.
9. Kaji, Ryuichi, Yukio Hishinuma, and Yoichi Nakamura, *Low temperature oxidation of coals—a calorimetric study.* Fuel, 1987. **66**(2): p. 154-157.
10. Krishnaswamy, Srinivasan, Saurabh Bhat, Robert D. Gunn, and Pradeep K. Agarwal, *Low-temperature oxidation of coal. 1. A single-particle reaction-diffusion model.* Fuel, 1996. **75**(3): p. 333-343.
11. Krishnaswamy, Srinivasan, Robert D. Gunn, and Pradeep K. Agarwal, *Low-temperature oxidation of coal. 2. An experimental and modelling investigation using a fixed-bed isothermal flow reactor.* Fuel, 1996. **75**(3): p. 344-352.
12. Nugroho, Y. S., A. C. McIntosh, and B. M. Gibbs, *Low-temperature oxidation of single and blended coals.* Fuel, 2000. **79**(15): p. 1951-1961.
13. Petit, J. C., *A calorimetric investigation of the low temperature oxidation of coal and activated carbon.* Fuel, 1990. **69**(7): p. 861-866.
14. Pietrzak, R. and H. Wachowska, *Low temperature oxidation of coals of different rank and different sulphur content ☆.* Fuel, 2003. **82**(6): p. 705-713.
15. Polat, S. and I. J. Harris, *Low-temperature oxidation of Victorian brown coal.* Fuel, 1984. **63**(5): p. 669-672.
16. van der Plaats, G., H. Soons, and H. A. G. Chermin, *Low-temperature oxidation of coal.* Thermochimica Acta, 1984. **82**(1): p. 131-136.
17. Wang, Haihui, Bogdan Z. Dlugogorski, and Eric M. Kennedy, *Coal oxidation at low temperatures: oxygen consumption, oxidation products, reaction mechanism and kinetic modelling.* Progress in Energy and Combustion Science, 2003. **29**(6): p. 487-513.
18. Zhang, Yulong, Jianming Wu, Liping Chang, Junfeng Wang, and Zhengfeng Li, *Changes in the reaction regime during low-temperature oxidation of coal*

in confined spaces. Journal of Loss Prevention in the Process Industries, 2013. **26**(6): p. 1221-1229.
19. Zhang, Yulong, Jianming Wu, Liping Chang, Junfeng Wang, Sheng Xue, and Zhengfeng Li, *Kinetic and thermodynamic studies on the mechanism of low-temperature oxidation of coal: A case study of Shendong coal (China).* International Journal of Coal Geology, 2013. **120**: p. 41-49.
20. Wang, Haihui, Bogdan Z. Dlugogorski, and Eric M. Kennedy, *Low-temperature oxidation of coal at elevated pressures.* Journal of Loss Prevention in the Process Industries, 1998. **11**(6): p. 373-381.
21. Yuan, Liming and Alex C. Smith, *Experimental study on CO and CO_2 emissions from spontaneous heating of coals at varying temperatures and O_2 concentrations.* Journal of Loss Prevention in the Process Industries, 2013. **26**(6): p. 1321-1327.
22. Shi, Ting, Xiaofang Wang, Jun Deng, and Zhenyi Wen, *The mechanism at the initial stage of the room-temperature oxidation of coal.* Combustion and Flame, 2005. **140**(4): p. 332-345.
23. Bhat, Saurabh and Pradeep K. Agarwal, *The effect of moisture condensation on the spontaneous combustibility of coal.* Fuel, 1996. **75**(13): p. 1523-1532.
24. Yuan, Liming and Alex C. Smith, *CFD modeling of spontaneous heating in a large-scale coal chamber*. Journal of Loss Prevention in the Process Industries, 2009. **22**(4): p. 426-433.
25. Song, Zeyang and Claudia Kuenzer, *Coal fires in China over the last decade: A comprehensive review.* International Journal of Coal Geology, 2014. **133**: p. 72-99.
26. Zhu, Hong-qing, Ze-yang Song, Bo Tan, and Yu-ze Hao, *Numerical investigation and theoretical prediction of self-ignition characteristics of coarse coal stockpiles.* Journal of Loss Prevention in the Process Industries, 2013. **26**(1): p. 236-244.
27. MDG-1006, *Technical reference for MDG 1006 spontaneous combustion management guideline*, I.I. NSW, Editor. 2011, Mine Safety Operations Branch.
28. De Rosa, Maria I, *Analysis of Mine Fires for All US Underground and Surface Coal Mining Categories: 1990-1999*. 2004: US Department of Health and Human Services, Public Health Service, Centers for Disease Control and Prevention, National Institute for Occupational Safety and Health, Pittsburgh Research Laboratory.
29. Singh, RVK and VK Singh, *Status of mine fire of jharia coalfield and suggestions for prevention & control.* Coal Mining Technology & Management, 2004. **9**(6-8): p. 38-44.
30. Zhou, Fubao, Wanxing Ren, Deming Wang, Tiliang Song, Xiang Li, and Yuliang Zhang, *Application of three-phase foam to fight an extraordinarily serious coal mine fire.* International Journal of Coal Geology, 2006. **67**(1–2): p. 95-100.
31. Gouws, M. J. and T. P. Knoetze, *Coal self-heating and explosibility.* Journal of the South African Institute of Mining and Metallurgy, 1995. **95**(1): p. 37-44.
32. Carras, J. N., S. Day, A. Saghafi, and O. C. Roberts, *Spontaneous Combustion in Open Cut Coal Mines -- Recent Australian Research*. 2005: Research Online.

33. Carras, John N. and Brian C. Young, *Self-heating of coal and related materials: Models, application and test methods.* Progress in Energy and Combustion Science, 1994. **20**(1): p. 1-15.
34. Carres, J. N. and A. Saghafi, *Predicting spontaneous combustion in spoil piles from open cut coal mines*. 1998: Research Online.
35. Moghtaderi, B., B. Z. Dlugogorski, and E. M. Kennedy, *Effects of Wind Flow on Self-Heating Characteristics of Coal Stockpiles.* Process Safety and Environmental Protection, 2000. **78**(6): p. 445-453.
36. Zhang, Jian, Yuntao Liang, Ting Ren, Zhongwei Wang, and Gongda Wang, *Transient CFD modelling of low-temperature spontaneous heating behaviour in multiple coal stockpiles with wind forced convection.* Fuel Processing Technology, 2016. **149**: p. 55-74.
37. Zhang, Jian, Ting Ren, Yuntao Liang, and Zhongwei Wang, *A review on numerical solutions to self-heating of coal stockpile: Mechanism, theoretical basis, and variable study.* Fuel, 2016. **182**: p. 80-109.
38. Yang, Yongliang, Zenghua Li, Yibo Tang, Zhen Liu, and Huaijun Ji, *Fine coal covering for preventing spontaneous combustion of coal pile.* Natural Hazards, 2014. **74**(2): p. 603-622.
39. Arisoy, Ahmet and Fehmi Akgün, *Effect of Pile Height on Spontaneous Heating of Coal Stockpiles.* Combustion Science and Technology, 2000. **153**(1): p. 157-168.
40. Swann, Philip D., David J. Allardice, and David G. Evans, *Low-temperature oxidation of brown coal. 1. Changes in internal surface due to oxidation.* Fuel, 1974. **53**(2): p. 85-87.
41. Carras, John N., Stuart J. Day, Abou Saghafi, and David J. Williams, *Greenhouse gas emissions from low-temperature oxidation and spontaneous combustion at open-cut coal mines in Australia.* International Journal of Coal Geology, 2009. **78**(2): p. 161-168.
42. Day, Stuart, John Carras, Robyn Fry, and David Williams, *Greenhouse gas emissions from Australian open-cut coal mines: contribution from spontaneous combustion and low-temperature oxidation.* Environmental Monitoring & Assessment, 2010. **166**(1-4): p. 529-541.
43. Kuenzer, Claudia and Glenn B. Stracher, *Geomorphology of coal seam fires.* Geomorphology, 2012. **138**(1): p. 209-222.
44. Chen, Gang, Xiaoqian Ma, Musong Lin, Xiaowei Peng, and Zhaosheng Yu, *Pollutant emission characteristics and interaction during low-temperature oxidation of blended coal.* Journal of the Energy Institute, 2016. **89**(1): p. 40-47.
45. Liang, Yanci, Handong Liang, and Shuquan Zhu, *Mercury emission from coal seam fire at Wuda, Inner Mongolia, China.* Atmospheric Environment, 2014. **83**: p. 176-184.
46. Deng, Jun, Yang Zhang, Chenghui Li, Qingwei Li, Liji Wu, and Yongjun He, *Research of limit parameters and oxidation kinetics of water-logging coal self-ignition.* Coal Technology, 2016(3): p. 152-154.
47. Wen, Hu, Dong Wang, Yanhui Zhao, Qinghua Meng, and Huawei Zhang, *Experimental study on coal spontaneous combustion characteristics of soaked.* Coal Technology, 2015(1): p. 261-263.

48. Qin, Xiaowen, *Study on characteristics of low temperature oxidation of air-dried coal soaked in water*. Master Thesis, 2015, China University of Mining & Technology.
49. Sun, Xuming, *Research on dissolved substances from coal and influence on propensity of coal to spontaneous combustion in the long-term soak.* Master Thesis, 2015, China University of Mining & Technology.
50. Sondreal, Everett A and Robert C Ellman, *Laboratory determination of factors affecting storage of North Dakota lignite: computer simulation of spontaneous heating.* 1974, Bureau of Mines, Grand Forks, N. Dak.(USA). Grand Forks Energy Research Lab.
51. Nordon, Peter, *A model for the self-heating reaction of coal and char.* Fuel, 1979. **58**(6): p. 456-464.
52. Schmal, Dick, Jan H. Duyzer, and Jan Willem van Heuven, *A model for the spontaneous heating of coal.* Fuel, 1985. **64**(7): p. 963-972.
53. Brooks, Kevin, Steven Bradshaw, and David Glasser, *Spontaneous combustion of coal stockpiles - an unusual chemical reaction engineering problem.* Chemical Engineering Science, 1988. **43**(8): p. 2139-2145.
54. Brooks, Kevin and David Glasser, *A simplified model of spontaneous combustion in coal stockpiles.* Fuel, 1986. **65**(8): p. 1035-1041.
55. Young, B. D., D. F. Williams, and A. W. Bryson, *Two-dimensional natural convection and conduction in a packed bed containing a hot spot and its relevance to the transport of air in a coal dump.* International Journal of Heat and Mass Transfer, 1986. **29**(2): p. 331-336.
56. Bradshaw, Steven, David Glasser, and Kevin Brooks, *Self-ignition and convection patterns in an infinite coal layer.* Chemical Engineering Communications, 1991. **105**(1): p. 255-278.
57. Arisoy, Ahmet and Fehmi Akgün, *Modelling of spontaneous combustion of coal with moisture content included.* Fuel, 1994. **73**(2): p. 281-286.
58. Akgun, F. and R. H. Essenhigh, *Self-ignition characteristics of coal stockpiles: theoretical prediction from a two-dimensional unsteady-state model.* Fuel, 2001. **80**(3): p. 409-415.
59. Edwards, John C., *Mathematical modeling of spontaneous heating of a coalbed*, ed. M. United States. Bureau of. 1990, Washington, D.C. : U.S. Dept. of the Interior, Bureau of Mines.
60. Salinger, Andrew G., Rutherford Aris, and Jeffrey J. Derby, *Modeling the spontaneous ignition of coal stockpiles.* AIChE Journal, 1994. **40**(6): p. 991-1004.
61. Krishnaswamy, Srinivasan, Pradeep K. Agarwal, and Robert D. Gunn, *Low-temperature oxidation of coal. 3. Modelling spontaneous combustion in coal stockpiles.* Fuel, 1996. **75**(3): p. 353-362.
62. Hull, Ashley, Jennifer L. Lanthier, and Pradeep K. Agarwal, *The role of the diffusion of oxygen in the ignition of a coal stockpile in confined storage.* Fuel, 1997. **76**(10): p. 975-983.
63. Hull, Ashley S., Jennifer L. Lanthier, Zumao Chen, and Pradeep K. Agarwal, *The role of the diffusion of oxygen and radiation on the spontaneous combustibility of a coal pile in confined storage.* Combustion and Flame, 1997. **110**(4): p. 479-493.

64. Monazam, Esmail R, Lawrence J Shadle, and Abolghasem Shamsi, *Spontaneous combustion of char stockpiles.* Energy & fuels, 1998. **12**(6): p. 1305-1312.
65. Zambra, C. E., N. O. Moraga, and M. Escudey, *Heat and mass transfer in unsaturated porous media: Moisture effects in compost piles self-heating.* International Journal of Heat and Mass Transfer, 2011. **54**(13–14): p. 2801-2810.
66. Aganetti, R., A. Lamorlette, E. Guilbert, D. Morvan, and G. R. Thorpe, *Advection and the self-heating of organic porous media.* International Journal of Heat and Mass Transfer, 2016. **93**: p. 1150-1158.
67. Chen, X. D., *On the mathematical modeling of the transient process of spontaneous heating in a moist coal stockpile.* Combustion and Flame, 1992. **90**(2): p. 114-120.
68. Lohrer, C., U. Krause, and J. Steinbach, *Self-Ignition of Combustible Bulk Materials Under Various Ambient Conditions.* Process Safety and Environmental Protection, 2005. **83**(2): p. 145-150.
69. Lohrer, C., M. Schmidt, and U. Krause, *A study on the influence of liquid water and water vapour on the self-ignition of lignite coal-experiments and numerical simulations.* Journal of Loss Prevention in the Process Industries, 2005. **18**(3): p. 167-177.
70. Gómez, M. A., D. Patiño, R. Comesaña, J. Porteiro, M. A. Álvarez Feijoo, and J. L. Míguez, *CFD simulation of a solar radiation absorber.* International Journal of Heat and Mass Transfer, 2013. **57**(1): p. 231-240.
71. Ashwin, T. R., G. S. V. L. Narasimham, and Subhash Jacob, *CFD analysis of high frequency miniature pulse tube refrigerators for space applications with thermal non-equilibrium model.* Applied Thermal Engineering, 2010. **30**(2–3): p. 152-166.
72. Yuan, Liming and Alex C. Smith, *Numerical study on effects of coal properties on spontaneous heating in longwall gob areas.* Fuel, 2008. **87**(15–16): p. 3409-3419.
73. Kim, Chul Jin and Chae Hoon Sohn, *A novel method to suppress spontaneous ignition of coal stockpiles in a coal storage yard.* Fuel Processing Technology, 2012. **100**: p. 73-83.
74. Krajčiová, M., L. Jelemenský, M. Kiša, and J. Markoš, *Model predictions on self-heating and prevention of stockpiled coals.* Journal of Loss Prevention in the Process Industries, 2004. **17**(3): p. 205-216.
75. Bowes, P. C., *Self-heating : evaluating and controlling the hazards*. 1984, Dept. of the Environment, Building Research Establishment ;: Garston, Merseyside :.
76. Wang, Gongda, Ting Ren, Kai Wang, and Aitao Zhou, *Improved apparent permeability models of gas flow in coal with Klinkenberg effect.* Fuel, 2014. **128**: p. 53-61.
77. Wang, H., B. Z. Dlugogorski, and E. M. Kennedy, *Theoretical analysis of reaction regimes in low-temperature oxidation of coal.* Fuel, 1999. **78**(9): p. 1073-1081.
78. Wang, Haihui, Bogdan Z. Dlugogorski, and Eric M. Kennedy, *Thermal decomposition of solid oxygenated complexes formed by coal oxidation at low temperatures.* Fuel, 2002. **81**(15): p. 1913-1923.

79. Wang, H., B. Z. Dlugogorski, and E. M. Kennedy, *Kinetic modeling of low-temperature oxidation of coal.* Combustion and Flame, 2002. **131**(4): p. 452-464.
80. Wang, H., B. Z. Dlugogorski, and E. M. Kennedy, *Analysis of the mechanism of the low-temperature oxidation of coal.* Combustion and Flame, 2003. **134**(1–2): p. 107-117.
81. Wang, Haihui, Bogdan Z Dlugogorski, and Eric M Kennedy, *Pathways for production of CO2 and CO in low-temperature oxidation of coal.* Energy & fuels, 2003. **17**(1): p. 150-158.
82. Wang, De-ming, Hai-hui Xin, Xu-yao Qi, Guo-lan Dou, Guan-sheng Qi, and Li-yang Ma, *Reaction pathway of coal oxidation at low temperatures: a model of cyclic chain reactions and kinetic characteristics.* Combustion and Flame, 2016. **163**: p. 447-460.
83. Wang, Haihui, Bogdan Z Dlugogorski, and Eric M Kennedy, *Experimental study on low-temperature oxidation of an Australian coal.* Energy & fuels, 1999. **13**(6): p. 1173-1179.
84. Karsner, Grant G and Daniel D Perlmutter, *Model for coal oxidation kinetics. 1. Reaction under chemical control.* Fuel, 1982. **61**(1): p. 29-34.
85. Karsner, Grant G and Daniel D Perlmutter, *Model for coal oxidation kinetics. 2. An effectiveness factor interpretation.* Fuel, 1982. **61**(1): p. 35-43.
86. Swann, Philip D and David G Evans, *Low-temperature oxidation of brown coal. 3. Reaction with molecular oxygen at temperatures close to ambient.* Fuel, 1979. **58**(4): p. 276-280.
87. Harris, John A and David G Evans, *Low-temperature oxidation of brown coal. 2. Elovich adsorption kinetics and porous materials.* Fuel, 1975. **54**(4): p. 276-278.
88. Kam, AY, AN Hixson, and DD Perlmutter, *The oxidation of bituminous coal—I Development of a mathematical model.* Chemical Engineering Science, 1976. **31**(9): p. 815-819.
89. Kam, AY, AN Hixson, and DD Perlmutter, *The oxidation of bituminous coal—II experimental kinetics and interpretation.* Chemical Engineering Science, 1976. **31**(9): p. 821-834.
90. Gethner, Jon S., *Kinetic study of the oxidation of Illinois No. 6 coal at low temperatures.* Fuel, 1987. **66**(8): p. 1091-1096.
91. Gethner, Jon S., *Thermal and oxidation chemistry of coal at low temperatures.* Fuel, 1985. **64**(10): p. 1443-1446.
92. Nelson, Charles R., *Chemistry of coal weathering*. 1989, Amsterdam; New York; New York, N.Y., U.S.A.: Elsevier ; Distributors for the U.S. and Canada, Elsevier Science Pub. Co.
93. Jensen, EJ, N Melnyk, JC Wood, and N Berkowitz, *The dry oxidation of subbituminous coal*. 1966.
94. Khan, M. Rashid, C. Elaine Everitt, and Alain P. Lui, *Modeling of oxygen chemisorption kinetics on coal char.* Combustion and Flame, 1990. **80**(1): p. 83-93.
95. McLintock, IS, *The Elovich equation in chemisorption kinetics.* Nature, 1967. **216**: p. 1204-1205.
96. Nordon, Peter, Brian C. Young, and Norman W. Bainbridge, *The rate of oxidation of char and coal in relation to their tendency to self-heat.* Fuel, 1979. **58**(6): p. 443-449.

97. Taraba, Boleslav, Zdeněk Michalec, Vladimíra Michalcová, Tomáš Blejchař, Marian Bojko, and Milada Kozubková, *CFD simulations of the effect of wind on the spontaneous heating of coal stockpiles.* Fuel, 2014. **118**: p. 107-112.
98. Xia, Tongqiang, Xinxin Wang, Fubao Zhou, Jianhong Kang, Jishan Liu, and Feng Gao, *Evolution of coal self-heating processes in longwall gob areas.* International Journal of Heat and Mass Transfer, 2015. **86**: p. 861-868.
99. Moore, Walter J., *Physical chemistry*. 1963, London: Longman.
100. Peleg, Micha, Mark D Normand, and Maria G Corradini, *The Arrhenius equation revisited.* Critical reviews in food science and nutrition, 2012. **52**(9): p. 830-851.
101. Jones, J. C. and S. C. Newman, *Non-Arrhenius behaviour in the oxidation of two carbonaceous substrates.* Journal of Loss Prevention in the Process Industries, 2003. **16**(3): p. 223-225.
102. Nugroho, Yulianto S, Andrew C McIntosh, and Bernard M Gibbs, *On the prediction of thermal runaway of coal piles of differing dimension by using a correlation between heat release and activation energy.* Proceedings of the Combustion Institute, 2000. **28**(2): p. 2321-2327.
103. Akgun, F. and A. Arisoy, *Effect of particle size on the spontaneous heating of a coal stockpile.* Combustion and Flame, 1994. **99**(1): p. 137-146.
104. Taraba, Boleslav and Zdeněk Michalec, *Effect of longwall face advance rate on spontaneous heating process in the gob area – CFD modelling.* Fuel, 2011. **90**(8): p. 2790-2797.
105. Taraba, Boleslav, *Reversible and irreversible interaction of oxygen with coal using pulse flow calorimetry.* Fuel, 1990. **69**(9): p. 1191-1199.
106. Schmidt, LD and JL Elder, *Atmospheric oxidation of coal at moderate temperatures.* Industrial & Engineering Chemistry, 1940. **32**(2): p. 249-256.
107. Fierro, V., J. L. Miranda, C. Romero, J. M. Andrés, A. Arriaga, and D. Schmal, *Model predictions and experimental results on self-heating prevention of stockpiled coals.* Fuel, 2001. **80**(1): p. 125-134.
108. Karsner, GG and DD Perlmutter, *Reaction regimes in coal oxidation.* AIChE Journal, 1981. **27**(6): p. 920-927.
109. Gouws, MJ, GJ Gibbon, Li Wade, and HR Phillips, *An adiabatic apparatus to establish the spontaneous combustion propensity of coal.* Mining Science and Technology, 1991. **13**(3): p. 417-422.
110. Ertunc, Goker and Mustafa Versan Kok, *Determination of kinetic parameters of different origin coals using software.* Journal of Thermal Analysis and Calorimetry, 2015. **119**(2): p. 1407-1413.
111. Li, Bo, Gang Chen, Hui Zhang, and Changdong Sheng, *Development of non-isothermal TGA–DSC for kinetics analysis of low temperature coal oxidation prior to ignition.* Fuel, 2014. **118**: p. 385-391.
112. Jones, J. C., P. S. Chiz, R. Koh, and J. Matthew, *Kinetic parameters of oxidation of bituminous coals from heat-release rate measurements.* Fuel, 1996. **75**(15): p. 1755-1757.
113. Brooks, Kevin, Vemuri Balakotaiah, and Dan Luss, *Effect of natural convection on spontaneous combustion of coal stockpiles.* AIChE Journal, 1988. **34**(3): p. 353-365.
114. Rosema, A., H. Guan, and H. Veld, *Simulation of spontaneous combustion, to study the causes of coal fires in the Rujigou Basin.* Fuel, 2001. **80**(1): p. 7-16.

115. Ejlali, A., D. J. Mee, K. Hooman, and B. B. Beamish, *Numerical modelling of the self-heating process of a wet porous medium.* International Journal of Heat and Mass Transfer, 2011. **54**(25–26): p. 5200-5206.
116. Semenov, N. N. and Ia I. Frenkel', *Chemical kinetics and chain reactions*. 1935, Oxford: Clarendon Press.
117. Semenov, Nikolaĭ Nikolaevich, *Thermal Theory of Combustion and Explosion. 3; Theory of Normal Flame Propagation.* 1942.
118. Frank-Kamenetskii, David Albertovich, *Diffusion and heat exchange in chemical kinetics*. 1955: Princeton University Press.
119. Hoff, J. H. van't, *Etudes de dynamique chimique*. Landmarks of science. 1884, Amsterdam: Frederik Muller.
120. Thomas, PH, *On the thermal conduction equation for self-heating materials with surface cooling.* Transactions of the Faraday Society, 1958. **54**: p. 60-65.
121. Thomas, PH, *Some approximations in the theory of self-heating and thermal explosion.* Trans. Faraday Soc., 1960. **56**: p. 833-839.
122. Thomas, PH. *Effect of reactant consumption on the induction period and critical condition for a thermal explosion*. in *Proceedings of the Royal Society of London A: Mathematical, Physical and Engineering Sciences*. 1961: The Royal Society.
123. Thomas, PH, *Self-heating and thermal ignition-a guide to its theory and application.* Ignition, Heat Release and Noncombustibility of Materials, ASTM STP, 1972. **502**: p. p56.
124. Thomas, PH and PC Bowes, *Some aspects of the self-heating and ignition of solid cellulosic materials.* British Journal of Applied Physics, 1961. **12**(5): p. 222.
125. Bowes, P. C., *Thermal ignition in two-component systems, theoretical model.* Combustion and Flame, 1969. **13**(5): p. 521-530.
126. Bowes, P. C. and P. H. Thomas, *Ignition and extinction phenomena accompanying oxygen-dependent self-heating of porous bodies.* Combustion and Flame, 1966. **10**(3): p. 221-230.
127. Gray, BF and SK Scott, *The influence of initial temperature-excess on critical conditions for thermal explosion.* Combustion and Flame, 1985. **61**(3): p. 227-236.
128. Gray, BF and GC Wake, *On the determination of critical ambient temperatures and critical initial temperatures for thermal ignition.* Combustion and Flame, 1988. **71**(1): p. 101-104.
129. Adler, J and Julius W Enig, *The critical conditions in thermal explosion theory with reactant consumption.* Combustion and Flame, 1964. **8**(2): p. 97-103.
130. Brooks, Kevin, Nicoloas Svanas, and David Glasser, *Evaluating the risk of spontaneous combustion in coal stockpiles.* Fuel, 1988. **67**(5): p. 651-656.
131. Ejlali, A. and K. Hooman, *Buoyancy Effects on Cooling a Heat Generating Porous Medium: Coal Stockpile.* Transport in Porous Media, 2011. **88**(2): p. 235-248.
132. Turner, John Stewart, *Buoyancy effects in fluids*. 1979: Cambridge University Press.
133. Bird, R. B., W. E. Stewart, and E. N. Lightfoot, *Transport phenomena, John Wiley and Sons, Inc., New York.* 1960.

134. Brinkman, HC, *A calculation of the viscous force exerted by a flowing fluid on a dense swarm of particles.* Applied Scientific Research, 1949. **1**(1): p. 27-34.
135. Miron, Y, AC Smith, and CP Lazzara, *Sealed-flask test for evaluating the self-heating tendencies of coal. Rept. of Investigations/1990*. 1990, Bureau of Mines, Pittsburgh, PA (USA). Pittsburgh Research Center.
136. Ponec, Vladim ír, Zlatko Knor, and Slavoj Cerny, *Adsorption on solids [by] Vladimir Ponec, Zlatko Knor [and] Slavoj Cerny; English translation [from the Czech] edited by D. Smith and NG Adams*. 1974.
137. Young, Brian C and Peter Nordon, *Method for determining the rate of oxygen sorption by coals and chars at low temperatures.* Fuel, 1978. **57**(9): p. 574-575.
138. Hitchcock, W, DI Cliff, and BB Beamish. *A study of the gases produced by the oxidation of bulk coal under laboratory conditions*. in *12th US/North American Mine Ventilation Symposium 2008*. 2008: The University of Nevada, Reno.
139. Lu, P., G. X. Liao, J. H. Sun, and P. D. Li, *Experimental research on index gas of the coal spontaneous at low-temperature stage.* Journal of Loss Prevention in the Process Industries, 2004. **17**(3): p. 243-247.
140. Yuan, Liming and Alex C. Smith, *CO and CO2 emissions from spontaneous heating of coal under different ventilation rates.* International Journal of Coal Geology, 2011. **88**(1): p. 24-30.
141. Chamberlain, Eric A. C., Gordon Barrass, and John T. Thirlaway, *Gases evolved and possible reactions during low-temperature oxidation of coal.* Fuel, 1976. **55**(3): p. 217-223.
142. Marinov, Vassil N, *Self-ignition and mechanisms of interaction of coal with oxygen at low temperatures. 2. Changes in weight and thermal effects on gradual heating of coal in air in the range 20–300 °C.* Fuel, 1977. **56**(2): p. 158-164.
143. Marinov, Vassil N, *Self-ignition and mechanisms of interaction of coal with oxygen at low temperatures. 3. Changes in the composition of coal heated in air at 60 °C.* Fuel, 1977. **56**(2): p. 165-170.
144. Clemens, AH, TW Matheson, and DE Rogers, *DTA studies of the low temperature oxidation of low rank coals.* Fuel, 1990. **69**(2): p. 255-256.
145. Ismail, IMK and PL Walker, *DSC and TGA measurements of O2 interaction with coal chars.* Fuel, 1989. **68**(11): p. 1456-1460.
146. Mu ñoz-Guillena, MJ, A Linares-Solano, and C Salinas-Martinez de Lecea, *Determination of calorific values of coals by differential thermal analysis.* Fuel, 1992. **71**(5): p. 579-583.
147. Pis, Jos éJ, G de La Puente, E Fuente, A Mor án, and F Rubiera, *A study of the self-heating of fresh and oxidized coals by differential thermal analysis.* Thermochimica Acta, 1996. **279**: p. 93-101.
148. Beall, Herbert, Bradley J. Howard, and John T. Vaughey, *X-ray studies of coal oxidation.* Energy & fuels, 1988. **2**(5): p. 721-722.
149. Bend, Stephen L and Dawn M Kosloski, *A petrographic examination of coal oxidation.* International Journal of Coal Geology, 1993. **24**(1-4): p. 233-243.
150. Bruening, FA and AD Cohen, *Measuring surface properties and oxidation of coal macerals using the atomic force microscope.* International Journal of Coal Geology, 2005. **63**(3): p. 195-204.

151. Hou, Lei, George D. Cody, Patrick G. Hatcher, Samuel Gravina, and Mark A. Mattingly, *Imaging the microstructure of low rank coals.* Fuel, 1994. **73**(2): p. 199-203.
152. Huai, Huaying, Alec F. Gaines, and Colin D. Flint, *Scanning electron microscopy of treated bituminous coals.* Fuel Processing Technology, 1992. **32**(1): p. 25-37.
153. Huggins, FE, GP Huffman, and MC Lin, *Observations on low-temperature oxidation of minerals in bituminous coals.* International Journal of Coal Geology, 1983. **3**(2): p. 157-182.
154. Anderson, Ken B and RB Johns, *Oxidation studies of Australian coals—I. Aliphatic and aromatic hydrocarbon centres of oxidative attack.* Organic Geochemistry, 1986. **9**(5): p. 219-224.
155. Calemma, V., R. Rausa, R. Margarit, and E. Girardi, *FT-i.r. study of coal oxidation at low temperature.* Fuel, 1988. **67**(6): p. 764-770.
156. Deming, Wang, Xiaoxing ZHONG, Gu Junjie, and QI Xuyao, *Changes in active functional groups during low-temperature oxidation of coal.* Mining Science and Technology (China), 2010. **20**(1): p. 35-40.
157. Gethner, Jon S, *Kinetic study of the oxidation of Illinois No. 6 coal at low temperatures: evidence for simultaneous reactions.* Fuel, 1987. **66**(8): p. 1091-1096.
158. Grzybek, Teresa and Krystyna Kreiner, *Surface Changes in Coals after Oxidation. 1. X-ray Photoelectron Spectroscopy Studies.* Langmuir, 1997. **13**(5): p. 909-912.
159. Supaluknari, S, FP Larkins, P Redlich, and WR Jackson, *An FTIR study of Australian coals: characterization of oxygen functional groups.* Fuel Processing Technology, 1988. **19**(2): p. 123-140.
160. Xu, T, D-M Wang, H-H Xin, G-L Dou, X-X Zhong, and X-Y Qi, *In-situ Series Diffuse Reflection FTIR Used in Studying the Oxidation Process of Coal.* Energy Sources, Part A: Recovery, Utilization, and Environmental Effects, 2014. **36**(16): p. 1756-1763.
161. Yürüm, Yuda and Nurşen Altuntaş, *Air oxidation of Beypazari lignite at 50 C, 100 C and 150 C.* Fuel, 1998. **77**(15): p. 1809-1814.
162. Zhang, Yulong, Junfeng Wang, Sheng Xue, Jianming Wu, Liping Chang, and Zhengfeng Li, *Kinetic study on changes in methyl and methylene groups during low-temperature oxidation of coal via in-situ FTIR.* International Journal of Coal Geology, 2016. **154**: p. 155-164.
163. Martin, Ronald R., J. Anthony MacPhee, Mark Workinton, and Elizabeth Lindsay, *Measurement of the activation energy of the low temperature oxidation of coal using secondary ion mass spectrometry.* Fuel, 1989. **68**(8): p. 1077-1079.
164. Martin, R. R., N. S. McIntyre, C. G. Winder, D. C. Sanders, D. D. Johnston, and J. A. McPhee, *Detection of low temperature oxidation of coal on a microscopic scale using secondary ion mass spectrometry.* Fuel, 1986. **65**(9): p. 1313-1314.
165. MacPhee, J. Anthony and Biswanath N. Nandi, *13C n.m.r. as a probe for the characterization of the low-temperature oxidation of coal.* Fuel, 1981. **60**(2): p. 169-170.

166. Dack, Stuart W, Malcolm D Hobday, Thomas D Smith, and John R Pilbrow, *Free radical involvement in the oxidation of Victorian brown coal.* Fuel, 1983. **62**(12): p. 1510-1512.
167. Dack, Stuart W., Malcolm D. Hobday, Thomas D. Smith, and John R. Pilbrow, *Free-radical involvement in the drying and oxidation of victorian brown coal.* Fuel, 1984. **63**(1): p. 39-42.
168. Kudynska, J. and H. A. Buckmaster, *Low-temperature oxidation kinetics of high-volatile bituminous coal studied by dynamic in situ 9 GHz c.w. e.p.r. spectroscopy.* Fuel, 1996. **75**(7): p. 872-878.
169. Carr, R Melville, Haruo Kumagai, Barrie M Peake, Brian H Robinson, Anthony H Clemens, and Trevor W Matheson, *Formation of free radicals during drying and oxidation of a lignite and a bituminous coal.* Fuel, 1995. **74**(3): p. 389-394.
170. Kudynska, J. and H. A. Buckmaster, *Third International Symposium on the Biological Processing of CoalThe low temperature oxidation process in an Alberta hv bituminous coal as monitored using the 9GHz CW-EPR Mn2+ hfs spectral parameter.* Fuel, 1993. **72**(12): p. 1733-1738.
171. Kim, AG, *Laboratory studies on spontaneous heating of coal. A summary of information in the literature.[45 references]*. 1977, Bureau of Mines, Pittsburgh, Pa.(USA). Pittsburgh Mining and Safety Research Center.
172. Sevenster, PG, *STUDIES ON THE INTERACTION OF OXYGEN WITH COAL IN THE TEMPERATURE RANGE 0-DEGREES-C TO 90-DEGREES-C. 1.* Fuel, 1961. **40**(1): p. 7-17.
173. Smith, Alex C and Charles P Lazzara, *Spontaneous combustion studies of US coals.* 1987.
174. Beamish, B. Basil, Modher A. Barakat, and John D. St George, *Adiabatic testing procedures for determining the self-heating propensity of coal and sample ageing effects.* Thermochimica Acta, 2000. **362**(1–2): p. 79-87.
175. Beamish, B. Basil, Modher A. Barakat, and John D. St. George, *Spontaneous-combustion propensity of New Zealand coals under adiabatic conditions.* International Journal of Coal Geology, 2001. **45**(2–3): p. 217-224.
176. Qi, Xuyao, Haihui Xin, Deming Wang, and Guansheng Qi, *A rapid method for determining the R70 self-heating rate of coal.* Thermochimica Acta, 2013. **571**: p. 21-27.
177. Ren, T. X., J. S. Edwards, and D. Clarke, *Adiabatic oxidation study on the propensity of pulverised coals to spontaneous combustion.* Fuel, 1999. **78**(14): p. 1611-1620.
178. Vance, W. E., X. D. Chen, and S. C. Scott, *The rate of temperature rise of a subbituminous coal during spontaneous combustion in an adiabatic device: The effect of moisture content and drying methods.* Combustion and Flame, 1996. **106**(3): p. 261-270.
179. Zubíček, V. and A. Adamus, *Susceptibility of coal to spontaneous combustion verified by modified adiabatic method under conditions of Ostrava–Karvina Coalfield, Czech Republic.* Fuel Processing Technology, 2013. **113**: p. 63-66.
180. Bowes, PC and A Cameron, *Self‐heating and ignition of chemically activated carbon.* Journal of Applied Chemistry and Biotechnology, 1971. **21**(9): p. 244-250.

181. Sherman, Ralph A, JM Pilcher, and HN Ostborg, *A laboratory test for the ignitibility of coal.* Fuel, 1941. **20**(8): p. 194-202.
182. Chamberlain, EAC and DA Hall, *The liability of coals to spontaneous combustion.* Colliery Guardian, 1973. **221**(2): p. 65-72.
183. Mikula, RJ, VA Munoz, KL Kasperski, and OI Ogunsola. *Laboratory techniques for assessing susceptibility to spontaneous combustion*. in *ANNUAL INTERNATIONAL PITTSBURGH COAL CONFERENCE*. 1992: UNIVERSITY OF PITTSBURGH SCHOOL OF ENGINEERING CENTRE FOR ENERGY.
184. Xuyao, Qi, Deming Wang, James A. Milke, and Xiaoxing Zhong, *Crossing point temperature of coal.* Mining Science and Technology (China), 2011. **21**(2): p. 255-260.
185. Li, Zhengfeng, Yulong Zhang, Xiaoxia Jing, Yanli Zhang, and Liping Chang, *Insight into the intrinsic reaction of brown coal oxidation at low temperature: Differential scanning calorimetry study.* Fuel Processing Technology, 2016. **147**: p. 64-70.
186. Slovák, Václav and Boleslav Taraba, *Effect of experimental conditions on parameters derived from TG-DSC measurements of low-temperature oxidation of coal.* Journal of Thermal Analysis and Calorimetry, 2010. **101**(2): p. 641-646.
187. Cliff, D., D. Rowlands, and J. Sleeman, *Spontaneous combustion in Australian underground coal mines*. 1996.
188. Huang, Xinyan and Guillermo Rein, *Smouldering combustion of peat in wildfires: Inverse modelling of the drying and the thermal and oxidative decomposition kinetics.* Combustion and Flame, 2014. **161**(6): p. 1633-1644.
189. Zipf Jr, R Karl, W Marchewka, K Mohamed, J Addis, and F Karnack, *Tube bundle system: for monitoring of coal mine atmosphere.* Mining engineering, 2013. **65**(5): p. 57.
190. Timko, Robert J and RL Derick, *Methods to determine the status of mine atmospheres–an overview.* Journal of the Mine Ventilation Society of South Africa (SAUS), 2006: p. 1-9.
191. Singh, Ashok K, RVK Singh, Mahendra P Singh, Hem Chandra, and NK Shukla, *Mine fire gas indices and their application to Indian underground coal mine fires.* International Journal of Coal Geology, 2007. **69**(3): p. 192-204.
192. Sajimon, J. *AMSA Floxal Nitrogen Generator In Underground Inerting Applications*. in *Proceedings of the 31st International Conference of Safety in Mines Research Institutes, Brisbane*. 2005.
193. Gillies, ADS and HW Wu, *Inertisation and mine fire simulation using computer software.* Australian Coal Association Research Program, 2007.
194. Lynn, KP, J Maitland, H Jones, K Ross, and BA Kathage, *Report on an accident at Moura No. 4 Underground Mine on Wednesday, 16th July, 1986 (pp. 34).* Brisbane: Queensland State Government, 1987.
195. Bell, S, D Cliff, P Harrison, and C Hester, *Recent developments in coal mine inertisation in Australia.* Coal Operators' Conference, University of Wollongong & the Australasian Institute of Mining and Metallurgy, 1998.
196. Prebble, S and A Self, *Spontaneous combustion at the Blair Athol coal mine.* Proceed. Queensland Mining, 2000.

197. Mucho, TP, IR Houlison, AC Smith, and MA Trevits, *Coal mine inertisation by remote application.* Proceedings of the 2005 US National Coal Show. Pittsburgh, PA, h ttp://www. mining-media. com/ncs/papers/4-B% 20Mucho-Smith Trevits. pdf, 2005: p. 1-14.
198. Sujanti, Wiwik and Dong-ke Zhang, *A laboratory study of spontaneous combustion of coal: the influence of inorganic matter and reactor size.* Fuel, 1999. **78**(5): p. 549-556.
199. Taraba, Boleslav, Rudolf Peter, and Václav Slovák, *Calorimetric investigation of chemical additives affecting oxidation of coal at low temperatures.* Fuel Processing Technology, 2011. **92**(3): p. 712-715.
200. Colaizzi, Gary J, *Prevention, control and/or extinguishment of coal seam fires using cellular grout.* International Journal of Coal Geology, 2004. **59**(1): p. 75-81.
201. Xiao-wei, Zhai, Deng Jun, Wen Hu, and Ma Wei, *Research of the air leakage law and control techniques of the spontaneous combustion dangerous zone of re-mining coal body.* Procedia Engineering, 2011. **26**: p. 472-479.
202. Xue, Sheng and Hua Cui, *Innovative Techniques for Detection and Control of Underground Spontaneous Combustion of Coal*, in *Coal Operators' Conference 2004*. 2004: University of Wollongong. p. 161-167.
203. Ray, S. K. and R. P. Singh, *Recent Developments and Practices to Control Fire in Undergound Coal Mines.* Fire Technology, 2007. **43**(4): p. 285-300.
204. Zhou, Fubao, Wanxing Ren, Deming Wang, Tiliang Song, Xiang Li, and Yuliang Zhang, *Application of three-phase foam to fight an extraordinarily serious coal mine fire.* International Journal of Coal Geology, 2006. **67**(1): p. 95-100.
205. Wang, An and Wenshun You, *Mechanism analysis and prevention measures for spontaneous combustion firing in seam of Shenfu Dongsheng mining area.* Coal Science and Technology, 2002. **30**(B01): p. 58-64.
206. HU, Zhen-Qi, Xin-Jing WANG, and An-Min HE, *Distribution characteristic and development rules of ground fissures due to coal mining in windy and sandy region.* Journal of China Coal Society, 2014. **39**(1): p. 11-18.
207. Kan, Wu, Hu Zhenqi, and Chang Jiang, *Distribution law of ground crack induced by coal mining.* Journal of China University of Mining & Technology, 1997. **26**(2): p. 56-59.
208. FAN, Gang-wei, Dong-sheng ZHANG, and Li-qiang MA, *Overburden movement and fracture distribution induced by longwall mining of the shallow coal seam in the Shendong coalfield [J]*. Journal of China University of Mining & Technology, 2011. **2**: p. 007.
209. Xu, JL, WB Zhu, and XZ Wang, *Study on water-inrush mechanism and prevention during coal mining under unconsolidated confined aquifer.* Journal of Mining & Safety Engineering, 2011. **3**: p. 002.
210. Wang, Haihui, Bogdan Z Dlugogorski, and Eric M Kennedy, *Role of inherent water in low-temperature oxidation of coal.* Combustion Science and Technology, 2003. **175**(2): p. 253-270.
211. Allardice, DJ and DG Evans, *The brown-coal/water system: Part 1, The effect of temperature on the evolution of water from brown coal.* Fuel, 1971. **50**(2): p. 201-210.

212. Allardice, DJ and DG Evans, *The-brown coal/water system: Part 2. Water sorption isotherms on bed-moist Yallourn brown coal.* Fuel, 1971. **50**(3): p. 236-253.
213. Yu, Jianglong, Arash Tahmasebi, Yanna Han, Fengkui Yin, and Xianchun Li, *A review on water in low rank coals: The existence, interaction with coal structure and effects on coal utilization.* Fuel Processing Technology, 2013. **106**: p. 9-20.
214. Stott, JB, *Influence of moisture on the spontaneous heating of coal.* 1960.
215. Nordon, P. and N. W. Bainbridge, *Heat of wetting of a bituminous coal.* Fuel, 1983. **62**(5): p. 619-621.
216. Clemens, Anthony H. and Trevor W. Matheson, *The role of moisture in the self-heating of low-rank coals.* Fuel, 1996. **75**(7): p. 891-895.
217. Chen, X. Dong and James B. Stott, *The effect of moisture content on the oxidation rate of coal during near-equilibrium drying and wetting at 50 ℃.* Fuel, 1993. **72**(6): p. 787-792.
218. Banerjee, Sudhish Chandra, *Spontaneous combustion of coal and mine fires*. 1985: Balkema Rotterdam.
219. Suuberg, Eric M, Yoshinobu Otake, Yongseung Yun, and Seetharama C Deevi, *Role of moisture in coal structure and the effects of drying upon the accessibility of coal structure.* Energy & fuels, 1993. **7**(3): p. 384-392.
220. Deevi, SC and EM Suuberg, *Physical changes accompanying drying of western US lignites.* Fuel, 1987. **66**(4): p. 454-460.
221. Nelson, Charles R, *Chemistry of coal weathering.* 1989.
222. Liu, Chao, *Study and application on the technique of preventing and extinguishing spontaneous combustion hazards in mining compound seam of Daliuta*. Master Thesis, 2009, Taiyuan University of Technology.
223. Wang, Xinyu, *Research on CO migration rules and control technologies in the huge goaf of fully mechanized coal face of spontaneous combustion coal seam*. Master Thesis, 2013, Taiyuan University of Technology.
224. Yang, Guangwen and Xing Ai, *Origin and contro of CO at LW250 of Dayaner coal mine.* Safety in coal mines, 2003. **34**(10): p. 41-43.
225. WANG, Xin-yu, Jian-ming WU, and Yu-guo WU, *Source Analysis and Overrun Control Measures of CO at Working Face in Shendong Mining Area.* Safety in coal mines, 2013. **8**: p. 044.
226. Zhai, Xiaowei, Lingjun Ma, and Jun Deng, *Study and application of CO content prediction model to upper corner of coal mining face.* Coal Science and Technology, 2011. **39**(11): p. 59-62.
227. Zhang, Duo, *Study on the mining working face co source and accumulation of close distance coal seams*. Master Thesis, 2014, Xi án University of Science and Technology.
228. Ren, Ting Xiang and Rao Balusu, *Proactive goaf inertisation for controlling longwall goaf heatings.* Procedia Earth & Planetary Science, 2009. **1**(1): p. 309.
229. Fuertes, A. B., E. Hampartsoumian, and A. Williams, *Direct measurement of ignition temperatures of pulverized coal particles.* Fuel, 1993. **72**(9): p. 1287-1291.
230. Gupta, R. P., V. S. Gururajan, J. A. Lucas, and T. F. Wall, *Ignition temperature of pulverized coal particles: Experimental techniques and coal-related influences.* Combustion and Flame, 1990. **79**(3–4): p. 333-339.

231. Gouws, M. J., G. J. Gibbon, L. Wade, and H. R. Phillips, *An adiabatic apparatus to establish the spontaneous combustion propensity of coal.* Mining Science and Technology, 1991. **13**(3): p. 417-422.
232. Jones, J. C., K. P. Henderson, J. Littlefair, and S. Rennie, *Kinetic parameters of oxidation of coals by heat-release measurement and their relevance to self-heating tests.* Fuel, 1998. **77**(1–2): p. 19-22.
233. Ozbas, K, M Kök, and C Hicyilmaz, *DSC study of the combustion properties of Turkish coals.* Journal of Thermal Analysis and Calorimetry, 2003. **71**(3): p. 849-856.
234. Wang, Hai-Hui, *Kinetic analysis of dehydration of a bituminous coal using the TGA technique.* Energy & fuels, 2007. **21**(6): p. 3070-3075.
235. Kaljuvee, Tiit, Merli Keelman, Andres Trikkel, and Vilma Petkova, *TG-FTIR/MS analysis of thermal and kinetic characteristics of some coal samples.* Journal of Thermal Analysis and Calorimetry, 2013. **113**(3): p. 1063-1071.
236. Kissinger, Homer E, *Reaction kinetics in differential thermal analysis.* Analytical chemistry, 1957. **29**(11): p. 1702-1706.
237. Wang, Qingsong, Jinhua Sun, and Song Guo, *Spontaneous combustion identification of stored wet cotton using a C80 calorimeter.* industrial crops and products, 2008. **28**(3): p. 268-272.
238. Zhao, Xuejuan, Qingsong Wang, Huahua Xiao, Zhanli Mao, Peng Chen, and Jinhua Sun, *Prediction of coal stockpile autoignition delay time using micro-calorimeter technique.* Fuel Processing Technology, 2013. **110**: p. 86-93.
239. Ren, Ting and Rao Balusu, *The use of CFD modelling as a tool for solving mining health and safety problems*, in *2010 Underground Coal Operators' Conference*. 2010: University of Wollongong. p. 339-349.
240. Xu, Guang, Kray D Luxbacher, Saad Ragab, Jialin Xu, and Xuhan Ding, *Computational fluid dynamics applied to mining engineering: a review.* International Journal of Mining, Reclamation and Environment, 2016: p. 1-25.
241. Wala, AM, S Vytla, CD Taylor, and G Huang, *Mine face ventilation: a comparison of CFD results against benchmark experiments for the CFD code validation.* Mining engineering-new york then littleton colorado, 2007. **59**(10): p. 49.
242. Wala, AM, JC Yingling, J Zhang, and R Ray. *Validation study of computational fluid dynamics as a tool for mine ventilation design*. in *Proceedings of the Sixth International Mine Ventilation Congress (Pittsburgh, PA*. 1997.
243. Wala, AM, JC Yingling, and J Zhang, *Evaluation of the face ventilation systems for extended cuts with remotely operated mining machines using three-dimensional numerical simulations.* Preprints-society of mining engineers of AIME, 1998.
244. Jade, RK and BS Sastry. *An experimental and numerical study of two-way splits and junctions in mine airways*. in *12th US/North American Mine Ventilation Symposium*. 2008.
245. Aminossadati, Saiied M and Kamel Hooman. *Numerical simulation of ventilation air flow in underground mine workings*. in *12th US/North American Mine Ventilation Symposium*. 2008.

246. Zhang, Xichen, Yutao Zhang, and Jerry C Tien, *The efficiency study of the push-pull ventilation system in underground mine.* 2011.
247. Ray, RE, MJ Gilbey, and P Kumar. *The application of vertically-mounted jet fans in ventilation shafts for a rail overbuild*. in *12th US/North American Mine Ventilation Symposium*. 2008.
248. Kelsey, Adrian, J Kidger, and M Ivings, *CFD modelling of methane movement in mines*. 2002: Health and Safety Laboratory.
249. Ren, TX, JS Edwards, and RR Jozefowicz. *CFD modeling of methane flow around longwall coal faces*. in *Proceedings of the 6th International Mine Ventilation Congress*. 1997: Pittsburgh.
250. Balusu, R, N Tuffs, D White, and T Harvey, *Surface goaf gas drainage strategies for highly gassy longwall mines [J]*. Journal of the Mine Ventilation Society of South Africa, 2006. **59**(3): p. 78-84.
251. Tanguturi, K and R Balusu, *CFD modeling of methane gas distribution and control strategies in a gassy coal mine.* The Journal of Computational Multiphase Flows, 2014. **6**(1): p. 65-77.
252. Karacan, CÖ, TX Ren, and R Balusu. *Advances in grid-based numerical modeling techniques for improving gas management in coal mines*. in *Proceeding of 12th US/North American Mine Ventilation Symposium*. 2008.
253. Toraño, Javier, Susana Torno, Mario Menendez, Malcolm Gent, and Judith Velasco, *Models of methane behaviour in auxiliary ventilation of underground coal mining.* International Journal of Coal Geology, 2009. **80**(1): p. 35-43.
254. Edwards, JC and CC Hwang. *CFD modeling of fire spread along combustibles in a mine entry*. in *Proceedings of the SME Annual Meeting*. 2006.
255. Edwards, John C, Robert A Franks, Gene F Friel, and Liming Yuan, *Experimental and modeling investigation of the effect of ventilation on smoke rollback in a mine entry.* Transactions-society for mining metallurgy and exploration incorporated, 2007. **320**: p. 53.
256. Huang, Jiejie, J Bruining, and K-HAA Wolf, *Modeling of gas flow and temperature fields in underground coal fires.* Fire Safety Journal, 2001. **36**(5): p. 477-489.
257. Trevits, Michael A, Michael P Valoski, and John E Urosek, *Understanding mine fires by determining the characteristics of deep-seated fires.* NIOSH Document, 2009.
258. Edwards, JC and CC Hwang, *CFD analysis of mine fire smoke spread and reverse flow conditions.* 1999.
259. Hwang, CC and JC Edwards. *CFD Modeling of smoke reversal*. in *Proceeding of the International Conference of Engineering Fire Protection Design. Bethesda, Maryland, USA: Society of Fire Protection Engineers*. 2001.
260. Mossad, Ruth, Anthony Vella, and Rao Balusu. *Inertisation of highwall mining to control methane concentrations at the Moura Mine*. in *Proceedings of the 7th International Conference on Computational Fluid Dynamics in the Minerals and Process Industries (CFD2009)*. 2009: CSIRO Publishing.
261. Morla, Ramakrishna, Rao Balusu, Krishna Tanguturi, and Ren Ting, *Inertisation options for BG method and optimisation using CFD*

*modelling.*International Journal of Mining Science and Technology, 2015. **25**(3): p. 401-405.
262. Trevits, Michael A, L Yuan, M Thibou, and G Hatch. *Use of CFD modeling to study inert gas injection into a sealed mine area*. in *SME Annual Meeting*. 2010.
263. Heerden, J and Peter Sullivan. *The application of CFD for evaluation of dust suppression and auxiliary ventilation systems used with continuous miners*. in *Proceedings of the Sixth US Mine Ventilation Symposium (Salt Lake City, UT*. 1993.
264. Toraño, J, S Torno, M Menéndez, and M Gent, *Auxiliary ventilation in mining roadways driven with roadheaders: Validated CFD modelling of dust behaviour*. Tunnelling and Underground Space Technology, 2011. **26**(1): p. 201-210.
265. Ren, TX and Rao Balusu. *Innovative CFD modeling to improve dust control in longwalls*. in *8th Underground Coal Operators' Conference, University of Wollongong, Wollongong*. 2008.
266. Kurnia, Jundika Candra, Agus Pulung Sasmito, and Arun Sadashiv Mujumdar, *Dust dispersion and management in underground mining faces.* International Journal of Mining Science and Technology, 2014. **24**(1): p. 39-44.
267. Xu, Guang, Kray D Luxbacher, Saad Ragab, and Steve Schafrik, *Development of a remote analysis method for underground ventilation systems using tracer gas and CFD in a simplified laboratory apparatus.* Tunnelling and Underground Space Technology, 2013. **33**: p. 1-11.
268. Zheng, Y and Jerry C Tien. *DPM dispersion study using CFD for underground metal/nonmetal mines*. in *Proceedings of the 12th US/North America mine ventilation symposium, Reno*. 2008.
269. Collecutt, Greg, David Humphreys, and David Proud. *CFD simulation of underground coal dust explosions and active explosion barriers*. in *Seventh International Conference on CFD in the Minerals and Process Industries CSIRO, Melbourne, Australia*. 2009.
270. Ardejani, Faramarz Doulati, Behshad Jodeiri Shokri, Ernest Baafi, Kumars Seif Panahi, and Raghu Nath Singh, *Application of Computational Fluid Dynamics (CFD) for simulation of acid mine drainage generation and subsequent pollutants transportation through groundwater flow systems and rivers*. 2011: INTECH Open Access Publisher.
271. Liang, Yuntao, Fuchao Tian, Haizhu Luo, and Hui Tang, *Characteristics of coal re-oxidation based on microstructural and spectral observation.* International Journal of Mining Science and Technology, 2015. **25**(5): p. 749-754.
272. Chen, Peng, Fujun Huang, and Yue Fu, *Performance of water-based foams affected by chemical inhibitors to retard spontaneous combustion of coal.* International Journal of Mining Science and Technology, 2016. **26**(3): p. 443-448.
273. Wang, Longkang, Tingxiang Ren, Baisheng Nie, Yang Chen, Changqing Lv, Haoyang Tang, and Jufeng Zhang, *Development of a spontaneous combustion TARPs system based on BP neural network.* International Journal of Mining Science and Technology, 2015. **25**(5): p. 803-810.

274. Yang, Yongliang, Zenghua Li, Shisong Hou, Fanjun Gu, Siyuan Gao, and Yibo Tang, *The shortest period of coal spontaneous combustion on the basis of oxidative heat release intensity.* International Journal of Mining Science and Technology, 2014. **24**(1): p. 99-103.
275. Stracher, Glenn B and Tammy P Taylor, *Coal fires burning out of control around the world: thermodynamic recipe for environmental catastrophe.* International Journal of Coal Geology, 2004. **59**(1): p. 7-17.
276. Morris, R and T Atkinson, *Seam factor and the spontaneous heating of coal.* Mining Science and Technology, 1988. **7**(2): p. 149-159.
277. Bascompta Massanés, Marc, Lluís Sanmiquel Pera, and Josep Oliva Moncunill, *Ventilation management system for underground environments.* Tunnelling and Underground Space Technology, 2015. **50**: p. 516-522.
278. Kursunoglu, Nilufer and Mustafa Onder, *Selection of an appropriate fan for an underground coal mine using the Analytic Hierarchy Process.* Tunnelling and Underground Space Technology, 2015. **48**: p. 101-109.
279. Ren, Ting, Zhongwei Wang, and Graeme Cooper, *CFD modelling of ventilation and dust flow behaviour above an underground bin and the design of an innovative dust mitigation system.* Tunnelling and Underground Space Technology, 2014. **41**: p. 241-254.
280. Gillies, Stewart and Hsin Wei Wu, *Australian longwall panel ventilation practices.* 13th Coal Operators' Conference, University of Wollongong, 2013.
281. Wei, Feng, Zhu Fangping, and Lv Huiqing, *The Use of 3D Simulation System in Mine Ventilation Management.* Procedia Engineering, 2011. **26**: p. 1370-1379.
282. Smith, AC, WP Diamond, TP Mucho, and JA Organiscak, *Bleederless ventilation systems as a spontaneous combustion control measure in US coal mines.* Pittsburgh, PA: US Department of the Interior, Bureau of Mines, IC, 1994. **9377**.
283. Shamsi, Abolghasem, Lawrence J. Shadle, and Kalkunte S. Seshadri, *Study of low-temperature oxidation of buckskin subbituminous coal and derived chars produced in ENCOAL process.* Fuel Processing Technology, 2004. **86**(3): p. 275-292.
284. Yuan, Liming and Alex C. Smith, *The effect of ventilation on spontaneous heating of coal.* Journal of Loss Prevention in the Process Industries, 2012. **25**(1): p. 131-137.
285. Beamish, B. Basil and Darren G. Blazak, *Relationship between ash content and R70 self-heating rate of Callide Coal.* International Journal of Coal Geology, 2005. **64**(1–2): p. 126-132.
286. Arisoy, Ahmet and Basil Beamish, *Mutual effects of pyrite and moisture on coal self-heating rates and reaction rate data for pyrite oxidation.* Fuel, 2015. **139**: p. 107-114.
287. Kuenzer, Claudia, Jianzhong Zhang, Anke Tetzlaff, Paul van Dijk, Stefan Voigt, Harald Mehl, and Wolfgang Wagner, *Uncontrolled coal fires and their environmental impacts: Investigating two arid mining regions in north-central China.* Applied Geography, 2007. **27**(1): p. 42-62.
288. McCutcheon, Alan L. and Michael A. Wilson, *Low-Temperature Oxidation of Bituminous Coal and the Influence of Moisture.* Energy & fuels, 2003. **17**(4): p. 929-933.
289. ANSYS FLUENT 15.0, *Users' guide, ANSYS Inc.* 2014.

290. McCaughey, M. and D. F. Fletcher, *Calculations of the wind-induced pressure distribution on a model building.* Fire Safety Journal, 1993. **21**(3): p. 189-205.
291. Fierro, V., J. L. Miranda, C. Romero, J. M. Andrés, A. Arriaga, D. Schmal, and G. H. Visser, *Prevention of spontaneous combustion in coal stockpiles: Experimental results in coal storage yard.* Fuel Processing Technology, 1999. **59**(1): p. 23-34.